A BOND-VALENCE APPROACH TO THE STRUCTURE, CHEMISTRY AND PARAGENESIS OF COMPLEX HYDROXY-HYDRATED PHOSPHATE OXYSALT MINERALS

BY

DANIELLE M. C. HUMINICKI

A Thesis submitted to the Faculty of Graduate Studies
in Partial Fulfilment of the Requirements
for the Degree of

Masters of Science

Department of Geological Sciences
University of Manitoba
Winnipeg, Manitoba

National Library of Canada
Acquisitions and Bibliographic Services
395 Wellington Street
Ottawa ON K1A 0N4
Canada

Bibliothèque nationale du Canada
Acquisitions et services bibliographiques
395, rue Wellington
Ottawa ON K1A 0N4
Canada

Your file Votre référence

Our file Notre référence

0-612-76778-7

Canada

THE UNIVERSITY OF MANITOBA

FACULTY OF GRADUATE STUDIES

*****

COPYRIGHT PERMISSION PAGE

A BOND-VALENCE APPROACH TO THE STRUCTURE, CHEMISTRY AND PARAGENESIS OF COMPLEX HYDROXY-HYDRATED PHOSPHATE OXYSALT MINERALS

BY

DANIELLE M. C. HUMINICKI

A Thesis/Practicum submitted to the Faculty of Graduate Studies of The University of Manitoba in partial fulfillment of the requirements of the degree of

Master of Science

ABSTRACT

Phosphate minerals are widespread and occur in many geological systems. Although they are of minimal economic significance, they are environmentally important. As paragentic mineral sequences of phosphates occur in complex systems, there is an interest in evaluating changes in their crystal structure rather than just their chemical variation for evolving systems. Studies have shown that there are relations between the chemical compositions of hydroxy-hydrated minerals and their position in paragentic sequences. Moreover, studies have also shown that there are relations between the atomic arrangements of minerals to their position in paragenetic sequences, which has lead to the development of structural hierarchy classifications of minerals (Moore 1965,1973). It is of interest to develop a comprehensive method of classifying hydroxy-hydrated oxysalt minerals based on their structure in order to evaluate evolving systems where not just the chemical composition but the structure of the minerals changes.

This new approach has been developed to look at the chemical compositions and paragenesis of complex hydroxy-hydrated phosphate minerals from a crystal-structure perspective. Combining a hierarchical ordering scheme for oxysalt structures with bond-valence theory and the valence-matching principle allows for the ability to understand the factors that control the chemical compositions of interstitial complexes and to predict which chemical compositions tend to be stable in Nature.

As phosphate minerals occur in a wide variety of environments, the focus of this thesis has been on first classifying all phosphate minerals based on their crystal structure. Minerals can be divided into (1) the *structural unit*, which is defined by strong bonds between atoms, and (2) the *interstitial complex*, which links structural units into a continuous structure. The interstitial complex is usually cationic and is characterized by its *Lewis acidity* or electrophilic strength. The structural unit is usually anionic and is

characterized by its *Lewis basicity*. The *valence-matching principle* examines the interaction between these structural components, and a stable structure forms when the Lewis acidity of the interstitial complex closely matches the Lewis basicity of the structural unit. Therefore, it is useful to develop a structural hierarchy classification of complex minerals (*i.e.* phosphate minerals) based on the connectivity of polyhedra with higher bond-valence (structural units). This structural classification scheme enables investigations of structural interactions of different components within a mineral.

The Lewis acidity of a generalized interstitial complex $\{^{[m]}M^{+}_{a}\,^{[n]}M^{2+}_{b}\,^{[l]}M^{3+}_{c}\,(H_2O)_d\,(H_2O)_e\,(OH)_f\,(H_2O)_g\}^{(a+2b+3c-f)+}$ may be expressed graphically in terms of the coordination numbers [*m*], [*n*] and [*l*] of the cations *M* of amounts *a, b* and *c*, the amounts of transformer, *d*, non-transformer, *e*, and hydrogen-bonded, *g*, (H_2O) groups, and the amount of (OH), *f*. The intersection of this function with the range of Lewis basicity of a specific structural unit defines the values of the coefficients *m, n, l, a, b, c, d, e, f* that are possible for a stable structure.

It has already been shown for the sulfate and borate minerals that the range in Lewis basicity for a structural unit corresponds to the range of pH over which a mineral is stable. Thus a correlation can be made directly for the change in polymerization of structural units as a function of pH. There is a reasonable correlation between the average basicity of the structural unit and the pH of the parent aqueous solution. Thus it is possible to make a connection between the details of a crystal structure and there conditions of formation. Here, this approach has been applied to the phosphate minerals, providing the groundwork for future work on paragenetic sequences of phosphate minerals based on the details of a crystal structure.

ACKNOWLEDGEMENTS

I would like to thank my advisor Dr. Frank C. Hawthorne for introducing me to this work, though tedious at times it has been very rewarding. I believe beyond a doubt his work is truly great and that he is a profound teacher. I have found that although much has been accomplished in terms of the information presented it is the encouraging images of the suspected impossibilities becoming possible that truly inspire great science.

As for twin B (Michelle Ann Elizabeth Huminicki), although you have not been with me physically the past two years you have never left my side. You have always been there for me when I needed you the most, whether it be the surprise visits or the phone calls from other countries. I would also like to thank my parents (Patrick and Carol Huminicki) for their support and most of all Dave C. Benson thank-you, my love. Yes, and you too Micky my pet!

TABLE OF CONTENTS

LIST OF FIGURES

FIGURE

LIST OF TABLES

TABLE

CHAPTER 1

Introduction

1.1 Premise

Understanding why anything occurs as it does in Nature has been a major question for Science for the last few hundred years. Scientists are constantly revising theories in order to explain what is going on, and use models to extract information from our surroundings. In the geological sciences, the value of minerals is important in all areas, from mining and economic development to paleoenvironmental investigation. The information tied up in minerals lays out a foundation for Geology, whether it is on how to explore for copper or where the most valuable gemstone is most likely to be found.

Far more is known about the compositionally simple rock forming minerals than the complex hydroxy-hydrated oxysalt minerals such as the phosphates yet there is much more information tied up in the complex minerals. For example, a simple mineral such as quartz gives less information about its history than a more complex mineral such as pyroxene or amphibole. Quartz, SiO_2, is compositionally simple, and only minimal information can be derived from its composition and structure. However, pyroxene is more complex. There are both orthorhombic $MgSiO_3$ - $FeSiO_3$ (enstatite-ferrosilite) and monoclinic pyroxenes typically of the four-component system $CaMgSi_2O_6$ - $CaFeSi_2O_6$ - $Mg_2Si_2O_6$ - $Mg_2Si_2O_6$, and both the chemical compositions and the ordering of cations over different sites in the structure are affected by their conditions of formation. Studies of pyroxene structures at high temperature and pressure give information

about exsolution, solid solution, and phase transitions, and site populations provide geothermometers and geobarameters (Deer et al.).

In the case of the even more chemically complex hydroxy-hydrated oxysalt minerals [e.g., collinsite, $Ca_2[Mg(PO_4)_2(H_2O)_2]$; vauquelinite, $Pb^{2+}_2[Cu^{2+}(PO_4)(CrO_4)(OH)]$, structural complexity and the difficulty in resolving the (OH) and (H_2O) groups preclude standard theoretical approaches to mineral stability (e.g., thermodynamic calculations, molecular orbital or molecular mechanics calculations). Moreover, additional issues arise when considering complex minerals:

(1) What controls the details of their chemical composition? For example, in collinsite and vauquelinite, why are the interstitial cations Ca_2 and Pb^{2+}_2 instead of K_4 or Na_4? Why are there no (H_2O) groups bonded to interstitial cations and two interstitial (H_2O) groups associated with the structural unit? Why are there two (H_2O) groups not bonded to interstitial cations rather than one or three (or any other number of) (H_2O) groups?

(2) Such minerals are normally stable over a small range of external conditions (e.g., Eh, pH, T, P) and are often associated with many (> 20) other complex minerals of similar composition in some paragenesis. What factors control their relative stabilities?

The principle topics in this thesis involve factors that control atomic arrangement, chemical composition and relative stability of phosphate minerals. The extended bond-valence theory and ideas developed by Hawthorne (1985a, 1990, 1994, 1992, 1997), Schindler et al. (2002) and Schindler and Hawthorne (2001a-c) can approach these questions from a structural perspective.

Common rocks consist of a small number of rock-forming minerals that will adjust their chemistry (adjust chemical composition to accommodate changes in bulk chemistry) and crystal structure (geometrically adjust to thermal expansion and elastic compression) in response to changing conditions. These mineral assemblages tend to reveal their history through changes in chemistry as a function of progressive crystallization. However, non-rock-forming minerals are typically formed in complex environments where their formation is dominated by equilibrium processes. These are a large group of complex minerals where even slight changes in environmental conditions can lead to their structure breaking down. So when looking at complex minerals during progressive evolution of a system it makes sense to monitor the progressive changes in the crystal structures of the minerals.

Hawthorne (1993) points out the important steps taken in regards to classification schemes for complex structural arrangements of minerals. Bragg introduced the hierarchy classification for silicates based on the mode of polymerization of the (alumino-) silicate part of the structure. Hawthorne (1993) shows how this scheme can be compared with Bowen's discontinuous reaction series in igneous rocks (Fig. 1.1). The classification schemes parallel each other in terms of progressive condensation of the tetrahedral component of the structure. With progressive crystallization there is progressive condensation, which in turn indicates that there is a relation between temperature and mineral topology and stability (Hawthorne, 1993).

Moore (1973) took these ideas further by creating a paragenetic hierarchy for pegmatitic phosphate minerals. The idea of creating a structural hierarchy

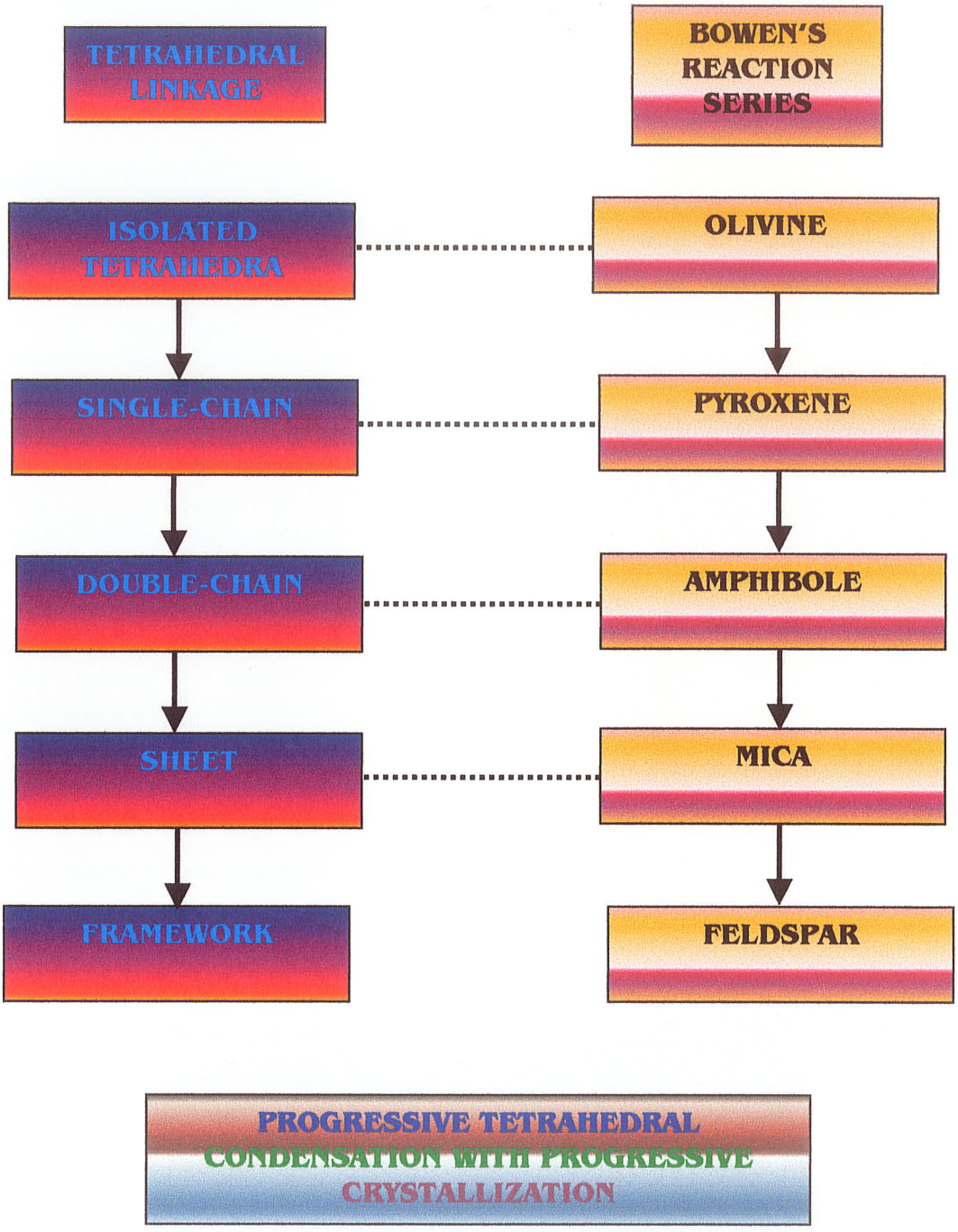

Figure 1.1. Comparision between Bragg's classification of the silicate minerals and Bowen's discontinuous reaction series for igneous rocks (after Hawthorne 1992).

based on the polymerization of structural components in complex minerals helps us to understand the implications that there is a relation in the connectivity of these complex minerals forming at different temperatures, pressures and compositions. Relating the structure and chemistry of complex hydrous minerals in terms of bond-valence requirements to the environments in which they occur and comparing them with rock-forming, high-pressure, high-temperature, anhydrous minerals is the key to solving this problem.

1.2 Main ideas

Complex oxysalt minerals are widespread and occur in many geological systems. In order to study minerals from complex environments, where the emphasis is on the change in mineral structure, rather than chemical variations with progressive evolution of the system, some type of structural hierarchal classification scheme is required. Classifying mineral groups in terms of their structure using a binary representation for even the most complex minerals, has led to advances in stoichiometric predictions for complex hydroxy-hydrated oxysalt minerals. The roles of hydroxyl and water in minerals are important factors and will have an effect on mineral stability.

The development of a bond-valence approach to evaluate complex hydroxy-hydrated oxysalt minerals from a crystal-structure perspective uses the combination of a hierarchical ordering scheme with bond-valence theory and the valence-matching principle to understand the factors that control the chemical compositions of interstitial complexes and gives the ability to predict what chemical compositions tend to be stable in Nature. A framework is then

developed in which it becomes possible to predict the chemistry from the structural characteristics of these minerals formed in complex low-temperature environments. These fundamental observations may later be applied to all aspects of mineral formation such as paragenetic sequences of minerals.

1.3 Phosphate minerals: hydroxy-hydrated oxysalts

Although phosphate minerals are only of minor economic value, they occur extensively as primary minerals (*e.g.* in pegmatites) and as secondary minerals in low-temperature hydrothermal environments. There have been previous systematic classifications of complex oxysalt minerals which are important for evaluating paragenesis of these minerals (Moore 1973, Hawthorne 1998). As paragenetic sequences of minerals occur in varied and often complex systems, it is the ultimate goal to be able to evaluate the changes in the crystal structures of the component minerals, rather than just their chemical composition. To this end, a large part of this thesis will involve the formation of a comprehensive structural hierarchy for phosphate minerals.

CHAPTER 2

Bond-valence theory and developments

2.1 Introduction

The approach developed here for evaluating crystal structures is one of an *a priori* nature. Brown (1981) introduced the idea of using bond-valence to investigate and predict the properties of complex solids and liquids. Hawthorne (1992, 1997) has extended this theory to include hydrated-hydroxy oxysalt minerals and introduced the importance of the role of water and hydrogen bonding in these complex minerals. A great deal of empirical work has been done calculating bond-lengths and atomic valences for crystal structures (Brown and Shannon 1973, Brown and Altermatt 1985, Brown 1987, Baur 1972). Schindler and Hawthorne (2001a, 2001b, 2001c) have used this approach and taken these ideas further by developing a quantitative method for predicting stable mineral structures. This method is applied to the phosphate minerals in this thesis. The definitions and basic concepts of bond-valence theory and its developments will be reviewed in this chapter.

2.2 Basic concepts of bond-valence theory

Bond-valence theory (Brown 1981) and its developments (Hawthorne 1985a, 1994, 1997) are used to consider structure topology and hierarchical classification of structures. Bond-valence theory can be considered as a simple form of molecular-orbital theory (Burdett and Hawthorne 1993; Hawthorne 1994, 1997) such that the idea of complex chemical bonding is simplified without a loss of important information. The bond-valence curves of Brown and Shannon (1973)

and Brown and Altermatt (1985) are commonly used when calculating bond-valence tables.

2.2.1 Chemical bonding

Bond-valence theory begins with the atom, which for simplicity can be considered as the most basic unit of matter to remain unchanged during a chemical reaction. A crystal can be defined as a network of atoms connected by chemical bonds. For most Earth materials, any path through this network contains alternating cations and anions, and the total network is subject to the *law of electroneutrality*: the total valence of the cations is equal to the total valence of the anions.

The chemical bond can be defined as a bond between two atoms or groups of atoms where the forces acting between them lead to the formation of an aggregate with sufficient stability to consider it as an independent molecular species (Pauling 1960). Atoms can be involved in five (ideal) types of bonds: (1) ionic, (2) covalent, (3) metallic, (4) van der Waals, and (5) hydrogen. Properties of minerals can be systemized based on these types of chemical bonds (Table 2.1).

(1) Ionic bonds usually form when electrons in the valence shell of an atom are transferred to the valence shell of another so that they both achieve an inert-gas configuration where the outer orbital is filled and the atom resides in its lowest energy-state. Ionic bonds result from the

TABLE 2.1. PROPERTIES BASED ON PRINCIPAL TYPES OF CHEMICAL BOND*

Property	Bond Type			
	Ionic (Electrostatic)	Covalent (Electron-shared)	Metallic	van der Waals (Residual)
Bond strength	Strong	Very strong	Variable strength, generally moderate	Weak
Mechanical	Hardness moderate to high, depending on interionic distance and charge; brittle	Hardness great Brittle	Hardness low to Moderate; gliding common; high plasticity; sectile; ductile; malleable	Crystals soft and somewhat plastic
Electrical	Insulators (poor conductors) in the solid state; melts and solutions conduct by ion transport	Semi-conductors	Good conductors; conduction by electron transport	Insulators in both solid and liquid state
Thermal (melting point = m.p.; coefficient of thermal expansion = coef.)	m.p. moderate to high depending on interionic distance and charge; low coef.	m.p high; low coef.; atoms and molecules in melt	Variable m.p. and coef.; atoms in melt	Low m.p.; high coef.; liquid crystal molecules in melt
Solubility	Soluble in polar solvents to yield solutions containing ions	Very low solubilities	Insoluble, except in acids or alkalis by chemical reaction	Soluble in organic solvents to yield solutions
Structure	Nondirected; gives structures of high coordination and symmetry	Highly directional; gives structures of lower coordination and symmetry	Nondirect; gives structures of very high coordination and symmetry	Nondirected; symmetry low because of shape of molecules
Examples	Halite, NaCl; Fluorite, CaF_2; most minerals	Diamond, C; Sphalerite, ZnS; molecules of O_2; organic molecules	Copper, Cu;Silver, Ag; Gold, Au; Electrum, (Au,Ag); most metals	Sulfur (weak bond); organic compounds; graphite (weak bond)

* after Klein and Hurlbut (1985)

Coulomb attraction of the excess charges of the oppositely charged ions. The atoms of metallic elements contribute outer electrons easily, whereas those of nonmetallic elements will accept electrons as they approach one another to achieve a filled outer orbital and form a stable unit.

e.g. $P([Ne]3sp^2 3p^3) \rightarrow P^{5+}([Ne]) + 5e^-$

$O(1s^2 2s^2 2p^4) + 2e^- \rightarrow O^{2-}(1s^2 2s^2 2p^6)$

The amount of ionic character of a chemical bond depends on the relative electronegativities of the elements, which is a measure of the ability of an atom to attract electrons to itself (expressed in dimensionless numbers) and is related to both the ionization energy and electron affinity. Electronegativity increases across a period and decreases down a group. Elements with low electronegativities are electron donors and elements with high electronegativities are electron acceptors (Klein and Hurlbut 1985). The greater the electronegativity difference between two atoms, the greater the ionic character of the bond between the two atoms.

(2) Covalent bonds share electrons (instead of donating or accepting electrons) in order to achieve an inert gas configuration. In the case of chlorine, it requires one electron to fill its outer orbital. Then it is highly reactive and will combine with another chlorine to share an electron pair between the two atoms, creating a strong bond between them

e.g. $\cdot\ddot{\text{Cl}}: + \cdot\ddot{\text{Cl}}: \rightarrow :\ddot{\text{Cl}}:\ddot{\text{Cl}}:$

The number of covalent bonds can be predicted for an atom by counting the number of electrons needed to obtain a stable electron configuration.

(3) Metallic bonding involves atomic nuclei and nonvalence electron orbitals joined by the electrical cloud of valence electrons that surround the nucleus. So in the case of metallic bonding, many atoms share the same electrons, the bonds may be considered fractional bonds. This type of bonding is common for transition metals such as Cu, Ag and Au. The bonding electrons hold the atoms together and the ability of these electrons to transport heat and electrical charge leads to the high thermal and electrical conductivity of metals.

(4) Van der Waals bonds are weak bonds that are involved in bonding the more strongly bonded parts of a mineral structure together.

(5) The unique nature of hydrogen in affecting structure properties in inorganic minerals is of interest here. Bonds involving hydrogen are formed between a positively charged hydrogen ion and a strongly electronegative atom such as oxygen to create polar bonds (Fig. 2.1a). Polar bonds occur when two atoms with different abilities to attract electrons are joined by a chemical bond. The positively charged hydrogen atom will also form a weak bond to another electronegative atom, called the *hydrogen bond*. A *hydrogen bond* is an intermolecular attraction in which a hydrogen atom that is bonded to an electronegative atom, and therefore has a partial positive charge, is

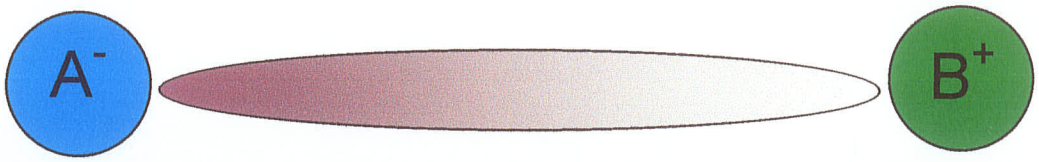

(a)

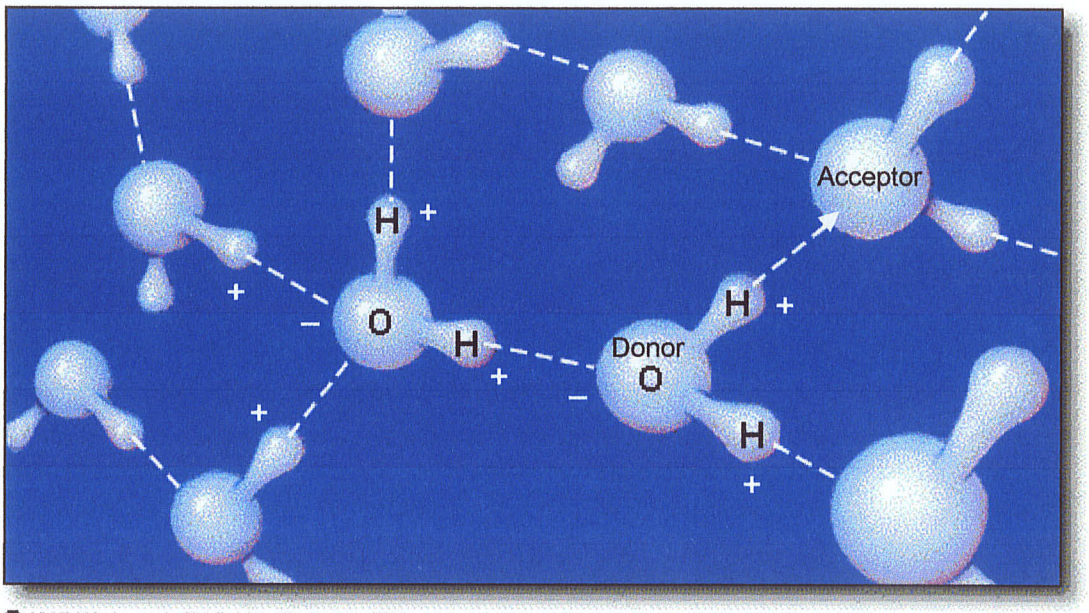

(b)

Figure 2.1. (a) If the electrons in a chemical bond are more strongly attracted to A than B, the part of the molecule with A develops a slight negative charge, while the B part develops a slight positive charge, creating a polar molecule. The magnitude of these charges is dependant on the relative abilities of these atoms to attract electrons (i.e. electonegativity). (b) The dashed lines show *hydrogen bonds*.

attracted to an unshared electron pair on another electronegative atom (Fig. 2.1b). The atom forming the strong bond to the hydrogen is called the *donor atom*, D, and the atom that receives a weak bond from the hydrogen atom is called the *acceptor* atom, A (Fig. 2.1b). The strength of hydrogen bonding is determined by the H ····· A bond length and the D–H ····· A angle. For the minerals in which we are interested, oxygen is the donor atom and (usually) the acceptor atom. The bond length between the hydrogen atom and the donor atom is about 1 Å. For a typical hydrogen bond, the H ····· A distance is dependent on the nature of the acceptor atom and is typically shorter than 3.2 Å for an oxygen atom (Brown and Altermatt 1985). Typical bond angles for D–H ····· A are ~100 to 180° with an average value of 165°.

As already mentioned, the degree of ionic versus covalent character of a bond is dependent on the electronegativity difference between two atoms. Two atoms with similar electronegativities that share electrons will still have a polar character such that there is a skewed distribution of electron density towards the slightly more electronegative atom, even thought the bond exhibits a primarily covalent character (Fig. 2.1a). The polar nature of these bonds will also be affected by the degree of electronegativity difference: atoms of lower electronegativity are cations and atoms of higher electronegativity are anions. These types of bonds will be considered when evaluating the low-temperature, low-pressure surficial minerals such as the hydrated, hydroxy-oxysalt minerals

examined in this thesis. The polar nature of (H_2O) and $(OH)^-$ strongly affects the topological properties of the structure of a mineral.

2.2.2 Coordination number [CN]

The coordination number of an atom is the number of bonds formed by that atom. Cations are coordinated by anions such that the centre of each anion lies at the apexes of an (approximately) regular polyhedron and the cation lies approximately in the centre of the coordinating polyhedron, *e.g.* P^{5+} coordinated by four O^{2-} atoms will form a (PO_4) group with P at the centre and O^{2-} at the four vertices of a tetrahedron. There are several ways that cation coordination can be determined; (1) defining a minimum bond-valence for a bond; (2) determination on the basis of any large gap that occurs in the distribution of interatomic distances around a cation; (3) geometric arrangements.

Likewise, anions may also be considered as occupying the centre of a coordinating polyhedron of cations. In the case of oxygen, the average coordination in most minerals lies between [3] and [4].

2.2.3 Bond topology and its relation to Pauling's rules

The foremost law of structure stability is one of electroneutrality; the sum of the formal charges of all elements in a crystal is equal to zero. This rule leads to strong chemical constraints for mineral compositions.

Bragg (1925) introduced the idea that atoms have a specific size and coordination number and that minerals such as silicates are formed by

polymerization of coordination polyhedra. Pauling (1929, 1960) developed these ideas further into a set of rules for the behavior of complex ionic crystals:

(1) a coordination polyhedra of anions is formed around each cation, where the cation distance is determined by the radius sum, and the coordination of the cation is determined by the radius ratio, which is the relative size of the coordinating ions. Radios ratio = R_A (radius of cation):R_X (radius of anion) e.g. the radius ratio for NaCl is Na^+ = 1.02 Å (C.N. = 6), Cl^- = 1.81Å (C.N. = 6); therefore the radius ratio = R_{Na+}:R_{Cl-} = 1.02/1.81 = 0.56. There are lower and upper limits to the radius ratio for the different geometries for various coordinating polyhedra.

(2) the electrostatic valency principle states that the strength of the bond from a cation to an anion is equal to the cation charge divided by the cation CN; in a stable ionic structure, the formal valence of each anion is approximately equal to the sum of the incident bond-strengths.

(3) The existence of shared edges and faces of polyhedra decreases mineral stability. This effects cations of high valence and small CN, and cation polyhedra with a radius ration close the lower limit for that coordinating polyhedron.

(4) In a crystal with several types of cations, those cations of high valence and small CN tend not to share edges or faces; if they do, the cation and its coordinating polyhedron tend to distort in order to reduce cation-cation repulsion.

(5) The principle of parsimony denotes the tendency for crystal structures to have only a small number of cation and anion sites.

These rules allow the following generalizations about the structure and chemistry of an inorganic crystal:

(1) the formula is electrically neutral;

(2) (weak) predictions may be made of possible coordination number based on the radius ratio;

(3) predictions can be made of mean bond-lengths by summing ionic radii.

Although these general rules can be applied to stable mineral structures, there are some important considerations that are not addressed. For example, (1) why do some chemical compositions occur and others don't, even though they are electrically neutral? (2) What is the bond connectivity (topology) for a crystal with a given stoichiometry? (3) For a given composition and bond connectivity, what controls the site occupancy? Hawthorne (1992, 1994) has addressed these questions, and the answers can now be considered further using additional quantitative bond-valence considerations for different mineral groups (Schindler & Hawthorne 2001a-c).

2.2.4 Bond strengths

The strength of a bond is the magnitude of the valence of the cation divided by its coordination number (Fig. 2.2). According to Pauling's second rule, the strength measured in valence units (*vu*) of an electrostatic bond, p, is defined as

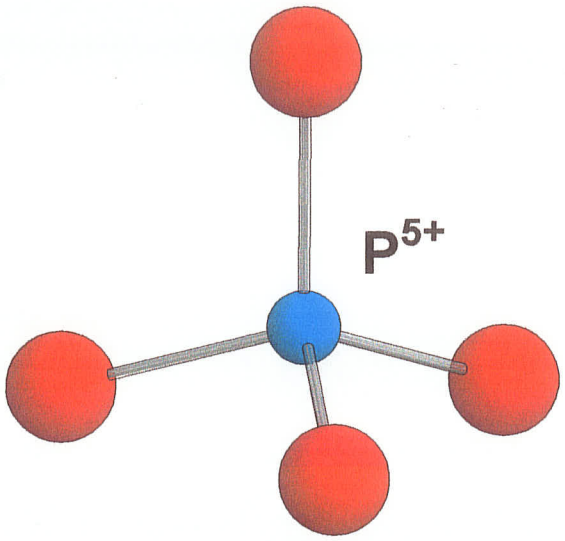

(PO_4)

b.s. = 5/4 = 1.25 *vu*

(a)

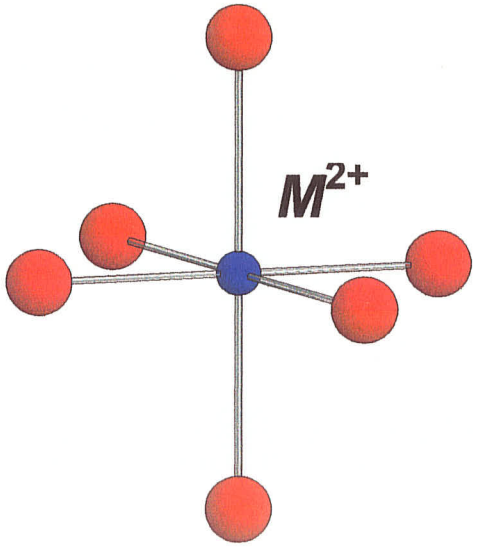

$(M^{2+}ø_6)$

b.s. = 2/6 = 0.33 *vu*

(b)

Figure 2.2. Bond-strengths in (PO_4) and $(M^{2+}ø_6)$.

$$p = \text{cation valence} / \text{cation coordination number} = Z / cn$$

e.g. Bond-strength of $^{[4]}P^{5+}$ = 5/4 = 1.25 *vu* (Table 2.2). For an ionic structure to be stable, the sum of the bond-strengths around an anion must equal the magnitude of the formal valence of that anion (Fig. 2.3).

$$\sum_{anion} p \sim |Z_{anion}|$$

2.2.5 Bond-valence relations

According to Pauling's second rule, the strength of an electrostatic bond is defined as the formal valence of the cation divided by its coordination number; the electrostatic valence principle states that the sums of the bond strengths around cations and anions are approximately equal to their formal valences. However, this rule is only a general approximation. Baur (1970) found that the bond-strength sums around anions deviated by as much as 40%, and that deviations from Pauling's second rule correlate with variations in bond-lengths in crystals. The variation in bond-strength has been characterized for specific cation-anion bonds and the term *bond-valence* is applied instead of the term *bond-strength*, used by Pauling, in order to distinguish between these two quantities.

Brown and Shannon (1973) devised empirical bond-valence – bond-length curves for specific cation – oxygen bonds. Brown (1981) determined that specific cations from many different structures have bond-valences within ~ 20% of the mean value; therefore this value is characteristic of that specific cation;

TABLE 2.2. VÄYRYNENITE, $Mn^{2+}[Be(PO_4)(OH)]$: BOND-STRENGTHS (*vu*)*

	M	*P*	*Be*	H	Σ
O(1)	1/3 1/3	5/4			2
O(2)	1/3	5/4	1/2		2
O(3)		5/4	1/2	0.2	~ 2
O(4)	1/3 1/3	5/4			2
O(5)	1/3		1/2 1/2	0.8	~ 2
Σ	2	5	2	1	

*Bond-strengths according to Pauling's second rule.

TABLE 2.3. VÄYRYNENITE, $Mn^{2+}[Be(PO_4)(OH)]$: EMPIRICAL BOND-VALENCES (*vu*)*

	M	*P*	*Be*	H	Σ
O(1)	0.31 0.45	1.25			2.01
O(2)	0.33	1.19	0.52		2.04
O(3)		1.23	0.53	0.20	1.96
O(4)	0.36 0.40	1.30			2.06
O(5)	0.21		0.46 0.48	0.80	1.95
Σ	2.06	4.97	1.99	1.00	

*Bond valences calculated using the curves of Brown & Altermatt (1985).

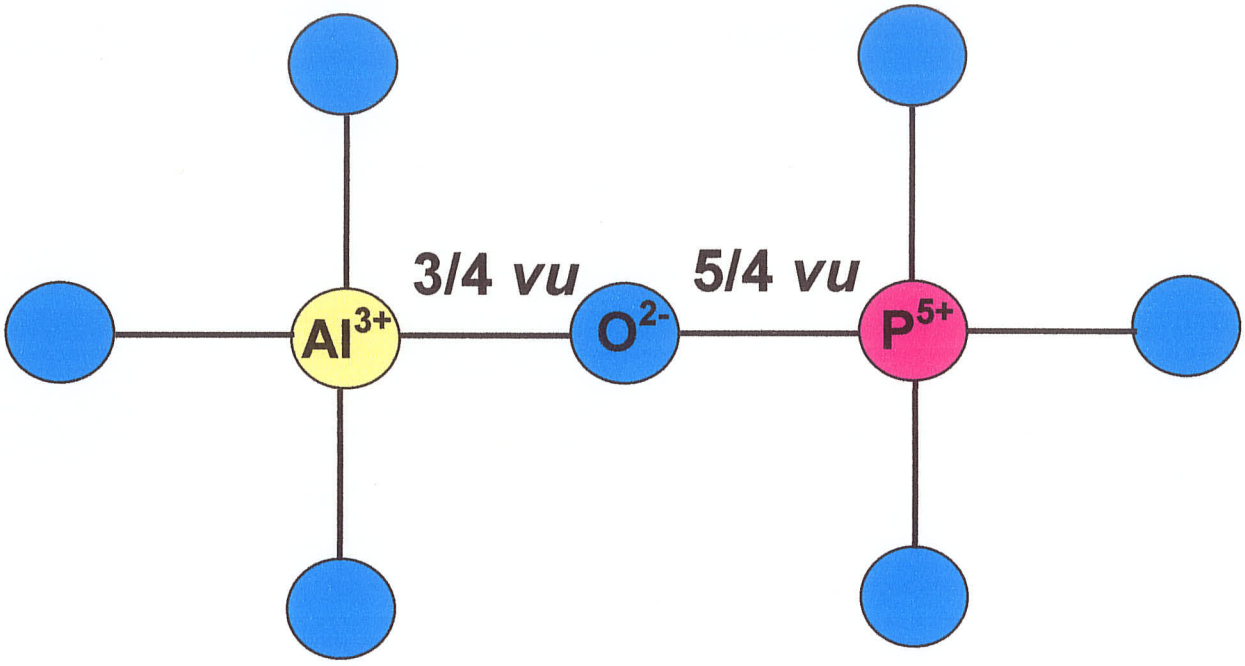

$$\Sigma_{O^{2-}} = 3/4 + 5/4 = 8/4 = 2\ vu$$

Figure 2.3. The sum of the bond strengths around the anion must equal the magnitude of the formal valence of the anion.

characteristic bond-valence = atomic (formal) valence / mean coordination number = Z / <CN>. Brown and Shannon (1973) used 417 crystals with well-known structures to derive bond-valence – bond-length relations for the bonds between oxygen and various cations using the requirement that the sums of the bond-valences around these cations be equal to their valence. The relation is $s = (R/R_o)^{-N}$; where s = bond valence (in valence units, *vu*), R = bond-length (Å), and R_o and N are fitted constants. R_o and N are parameters independent of the ionic character of the bond and the cation coordination number. These resultant bond-valences are related to the covalent character of the bond, and the sum around each cation is within 5% of its formal valence. The bond-valence – bond-length curves are useful in cases where the cation coordination is distorted; for predicting positions of hydrogen atoms, to analyze for different oxidation states and site occupancies, to calculate ionic radii, and to evaluate the accuracy of crystal-structure determinations (Brown and Shannon 1973).

Brown and Altermatt (1985) revised the expression used for the relation between bond-length (R) and bond-valence (s) using 750 atom pairs such that $s = \exp[(R_o - R)/B]$, where R_i is the observed individual bond-length and R_o and B are constants for a given element. This algorithm is more advantageous than the previous in that the variation in the B parameter between atom pairs is less than that for N and R_o can be fitted exactly for each cation environment (Brown and Altermatt 1985).

Calculated characteristic bond-valences correlate well with observed bond-lengths and other bond properties (Brown and Shannon 1973, Brown 1981,

Brown and Altermatt 1985). If the interatomic distances are known, bond-valences can be calculated from the curves of Brown (1981, 1988). If the interatomic distances are not known, bond-valences can be approximated by the Pauling bond-strengths. Calculated bond-valences for väyrynenite are compared with Pauling bond-strengths for the same mineral in Tables 2.2 and 2.3. The shorter the bond length between atoms, the higher the bond valence; likewise, the longer the bond length between atoms, the lower the bond valence (Table 2.4). Essentially, bond valence is a measure of the strength of the bond between a cation and an anion that depends on bond-length. The mean bond-valence correlates with the formal charge and cation radius, and varies smoothly across the periodic table (Hawthorne 1997).

These ideas involve an *a posteriore* approach to crystal-structure topology such that the structures of the crystals must be known in great detail in order to apply this method. In order to be able to predict any aspects of the crystal structure, an *a priori* approach is required.

2.3 Lewis theory of acids and bases

The Bronsted (or Bronsted-Lowry) definitions of acids and bases are as follows: an acid is a proton (H^+ ion) donor, and a base is a proton acceptor. On the other hand, G. N. Lewis developed a theory of acids and bases that is based upon sharing of electron pairs. A **Lewis acid** is any substance (such as the H^+ ion) that can accept a pair of nonbonding electrons to form a new bond. In other words, a Lewis acid is an **electron-pair acceptor** or **electrophile**. A **Lewis base**

TABLE 2.4. BOND-VALENCE VARIATION WITH BOND-LENGTH VARIATION

Bonds	Bond-length (Å)	Bond-valence (*vu*)
P – O(1)	1.543(1)	1.25
P – O(2)b	1.553(1)	1.19
P – O(3)	1.540(1)	1.23
P – O(4)	1.520(1)	1.30

is any substance (such as the OH^- ion) that can donate a pair of nonbonding electrons to form a new bond. A Lewis base is therefore an **electron-pair donor** or **nucleophile**. A simple example is the formation of the hydronium ion (H_3O^+) from a proton, H^+ (no electrons), and water, H_2O (which has electron pairs to donate). The product is called an adduct or complex. When one substance donates all the electrons for the bond, the bond is called a coordinate covalent bond. In this example, H^+ is the Lewis acid and H_2O is the Lewis base.

All metal cations are potential Lewis acids because their positive charge will readily attract electron pairs and they all have at least one empty orbital. The hydroxide ion is an excellent Lewis base and so it will bind readily to metal cations to give metal hydroxides.

The principal advantage of the Lewis theory is the way it expands the number of acids and therefore the number of acid-base reactions. In the Lewis theory, an acid is any ion or molecule that can accept a pair of nonbonding valence electrons; Al^{3+} ions form bonds to six water molecules to give a complex ion.

$$Al^{3+}(aq) + 6\ H_2O(l) \rightleftharpoons Al(H_2O)_6{}^{3+}(aq)$$

This is an example of a Lewis acid-base reaction. The Lewis structure of water suggests that the H_2O molecule has nonbonding pairs of valence electrons and can therefore act as a Lewis base. The electron configuration of the Al^{3+} ion suggests that this ion has empty $3s$, $3p$, and $3d$ orbitals that can be used to hold pairs of nonbonding electrons donated by neighboring H_2O molecules.

$$Al^{3+} = [Ne]\ 3s^0\ 3p^0\ 3d^0$$

Thus, the $Al(H_2O)_6^{3+}$ ion is formed when an Al^{3+} ion acting as a Lewis acid picks up six pairs of electrons from neighboring H_2O molecules acting as Lewis bases to give an **acid-base complex**, or **complex ion**.

The Lewis acid-base theory explains why BF_3 reacts with ammonia, NH_3. BF_3 is a trigonal-planar molecule because electrons can be found in only three places in the valence shell of the boron atom. As a result, the boron atom is sp^2 hybridized, which leaves an empty $2p_z$ orbital on the boron atom. BF_3 can therefore act as an electron-pair acceptor, or Lewis acid. It can use the empty $2p_z$ orbital to accept a pair of nonbonding electrons from a Lewis base, such as ammonia, to form a covalent bond. BF_3 therefore reacts with Lewis bases such as NH_3 to form acid-base complexes in which all of the atoms have a filled shell of valence electrons.

2.3.1 Lewis-acid strength of a cation

Using the Lewis definition of an acid, the Lewis-acid strength of a cation can be defined as the distribution of the charge of a cation over its coordinating bonds, or the characteristic mean bond-valence of a cation to its ligands. The value of the Lewis-acid strength (characteristic bond-valence) is the cation charge divided by the *average* coordination number of the cation. As already discussed, the bond-valence around specific cations from a range of different mineral structures have been found to vary within ~20% of the mean value, which is charateristic for that specific cation. In the case where the cation has only one coordination number; the mean bond-valence of that cation will be equal to the

Pauling bond-strength. For example, S^{6+} (sulphur) is found naturally occurring in [4]-coordination in oxysalt minerals so the mean bond-valence is 1.50 *vu*. If the cation occurs with more than one coordination number, then the mean bond-valence is equal to the weighted mean of the bond-valences in all the observed structures. An ideal mean bond-valence for Ca^{2+} in octahedral coordination is 0.33 *vu*; however, calcium can occur in [5] to [12]-coordination, and the weighted mean bond-valence (Lewis-acid strength) of Ca is 0.27 *vu* (Table 2.5).

As mean bond-valence is related to the formal charge and size (coordination) of a cation, it varies accordingly throughout the periodic table (Brown 1981). The mean bond-valence of a cation also correlates with electronegativity, which is a measure of the cations electron-accepting ability. Therefore, Lewis-acid strength is the measure of the electron-accepting ability (electrophilic strength) of the cations.

2.3.2 Lewis-base strength of a simple oxyanion

The Lewis-base strength (characteristic mean bond-valence) of an anion can be defined as the average bond-valence per bond received by that anion. The bond-valence incident at an O^{2-} atom can vary significantly, based on the type of bonds it forms with other atoms and depending on its coordination number. [12]-coordinated Na will contribute 0.08 *vu* to an O atom, and tetrahedrally coordinated S will contribute 1.50 *vu* to a coordinating O-atom. Individual bond-valences have too great a range in value for the mean bond-valence of simple anions to be of any reasonable use when predicting bond

TABLE 2.5. LEWIS-ACID STRENGTHS (*vu*) FOR CATIONS OF GEOLOGICAL INTEREST*

Li	0.22	Sc	0.50	Cu^{2+}	0.45
Be	0.50	Ti^{3+}	0.50	Zn	0.36
B	0.88	Ti^{4+}	0.75	Ga	0.50
C	1.30	V^{3+}	0.50	Ge	0.75
N	1.75	V^{5+}	1.20	As	1.02
Na	0.16	Cr^{3+}	0.50	Se	1.30
Mg	0.36	Cr^{6+}	1.50	Rb	0.10
Al	0.63	Mn^{2+}	0.36	Sr	0.24
Si	0.95	Mn^{3+}	0.50	Sn	0.66
P	1.30	Mn^{4+}	0.67	Sb	0.86
S	1.65	Fe^{2+}	0.36	Te	1.06
Cl	2.00	Fe^{3+}	0.50	Cs	0.08
K	0.13	Co^{2+}	0.40	Ba	0.20
Ca	0.27	Ni^{2}+	0.50	Pb^{2+}	0.20

* after Hawthorne (1997)

valences in structures. It is therefore more practical to consider Lewis-base strength in terms of complex oxyanions (Lewis bases) such as $(PO_4)^{3-}$ (Figure 2.4). In $(PO_4)^{3-}$, each of the O^{2-} atoms receives 1.25 *vu* from the central [4]-coordinated P^{5+}, atom and require an additional 0.75 *vu* from neighboring atoms. If the O^{2-} has an average coordination of [4], then the required bond-valence per bond to the O^{2-} atom (excluding the P–O) will be 0.75 *vu* / ([n] – 1) or 0.25 *vu* (Table 2.6). The range of Lewis-base strength for each specific oxyanion is much smaller, and therefore the prediction of bond valences is much more realistic.

2.3.3 Valence-matching principle

The valence-matching principle states that simple structures are stable when the Lewis-acid strength of the cation closely matches the Lewis-base strength of the anion. In other words, a stable chemical bond will form between two constituents that have matching properties. For example, the Lewis-base strength of $(PO_4)^{3-}$ (0.25 *vu*) does not match the Lewis-acid strength of Na (0.16 *vu*), and $Na_3(PO_4)$ is not a mineral. However, the Lewis-base strength of $(PO_4)^{3-}$ (0.25 *vu*) closely matches the Lewis-acid strength of Ca (0.27 *vu*) and calcium phosphate, $Ca_3(PO_4)_2$, does occur as a stable compound.

2.4 Binary structural representation of complex minerals

One of the problems in dealing with mineral structures is the complexity of the atom interactions; there are a large number of them, and their spatial characteristics are important. However, the same situation applies to an atom:

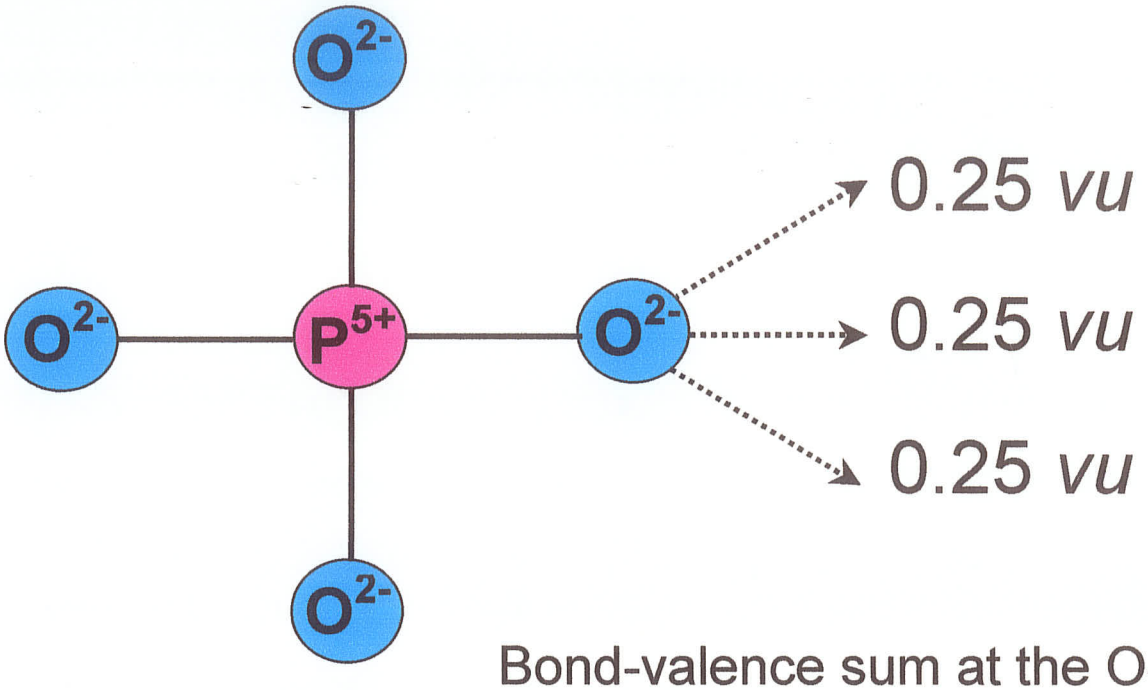

Bond-valence sum at the O-atom

1.25 *vu* + 0.75 *vu* = 2.0 *vu*

Lewis-base strength of $(PO_4)^{3-}$ based on an average coordination number [4] for the O-atom:

0.75 *vu* /3 = 0.25 *vu* = average bond-valence per bond

Figure 2.4. Lewis-base strength of a complex oxyanion (after Hawthorne 1997).

TABLE 2.6. LEWIS-BASE STRENGTHS (*vu*) FOR SPECIFIC OXYANIONS OF GEOLOGICAL INTEREST*

$(BO_3)^{3-}$	0.33	$(CO_3)^{2-}$	0.25
$(SiO_4)^{4-}$	0.33	$(NO_3)^{3-}$	0.12
$(AlO_4)^{3-}$	0.42	$(VO_4)^{3-}$	0.25
$(PO_4)^{3-}$	0.25	$(SO_4)^{2-}$	0.17
$(AsO_4)^{3-}$	0.25	$(CrO_4)^{2-}$	0.17

* after Hawthorne (1997)

there is a nucleus and numerous electrons, all interacting in a very complex manner; nevertheless, we can usefully consider an atom as a single unit with simple properties such as size, charge and electronegativity. The same approach can be taken for complex minerals such that they can be divided into (1) the *structural unit*, which is defined by strong bonds between atoms, and (2) the *interstitial complex*, which links structural units into a continuous structure *via* weak bonds (Fig. 2.5a). This *binary representation* makes dealing with the complexity of atomic interaction in a mineral structure more simple (Fig.2.5b). When this is done (Hawthorne, 1985a, 1986, 1990), a Lewis basicity can be defined for the structural unit in exactly the same way as for a more conventional oxyanion.

The interstitial components of a structure can usually be considered in a simple additive fashion to produce an aggregate structure, the *interstitial complex*, which can be characterized by its Lewis acidity. Thus a structure can be factored into two components, and this enables the use the valence-matching principle to examine the interaction of the *structural unit* with the *interstitial complex*. It is worth emphasizing here that that the development of a *binary representation* gives a simple quantitative model of even the most complicated structure, and allows quantitative insight into the weak bonding between the interstitial complex and the structural unit, interactions that control the stability of the mineral.

BINARY REPRESENTATION OF COMPLEX MINERALS

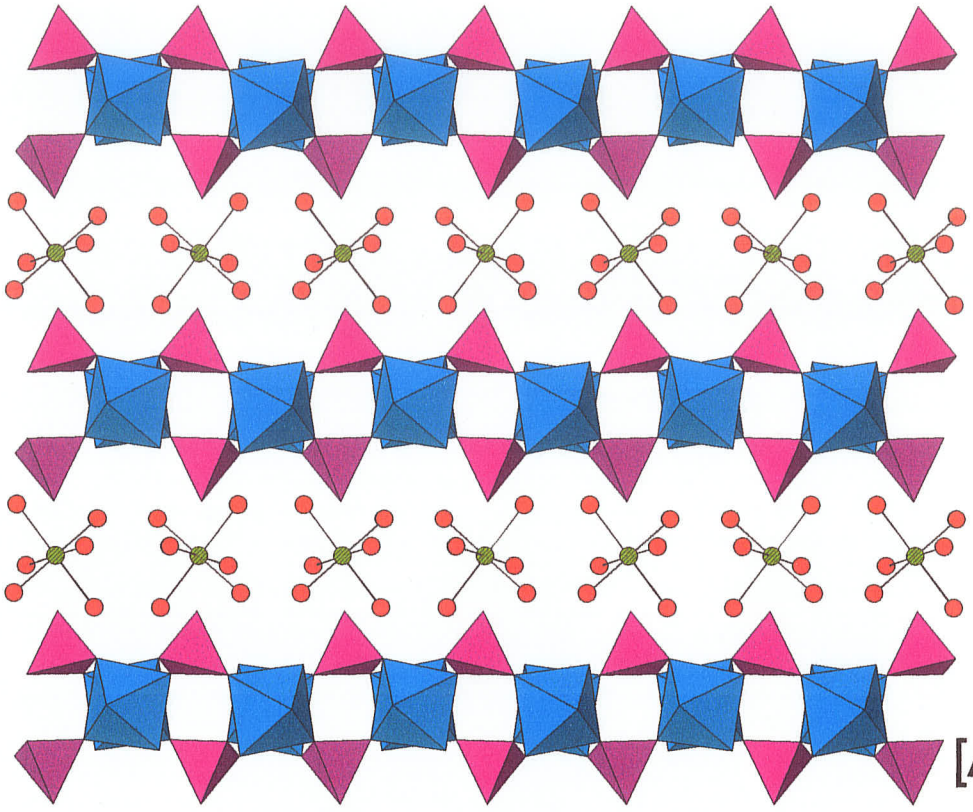

INTERSTITIAL COMPLEX: $Fe^{2+}(H_2O)_6$

STRUCTURAL UNIT: $[Al(PO_4)(OH)(H_2O)]^2$

EXAMPLE: metavauxite

$Fe^{2+}(H_2O)_6[Al(PO_4)(OH)(H_2O)]_2$

(a)

INTERSTITIAL COMPLEX defined by Lewis acidity

STRUCTURAL UNIT defined by Lewis basicity

(b)

Figure 2.5. (a) Binary representation of complex hydroxy-hydrated minerals and (b) the valence-matching principle.

2.4.1 Structural unit

Hawthorne (1985) considered the structural unit as a very complex oxyanion with intrinsic characteristic properties, and defined it formally as an array of strongly bonded polyhedra forming (usually) anion complexes (Fig 2.5a). Here, the components that are part of the structural unit can be considered to involve bond-valences greater than 0.33 *vu*.

2.4.2 Interstitial complex

The interstitial components are an array of large low-valence (alkali and alkaline-earth) cations, simple anions (e.g. OH^- or Cl^-) and (H_2O) groups that link the structural units together (Fig 2.5a). In accord with the binary structural representation the interstitial components are considered as a single unit, the interstitial complex, that typically has a net positive charge. The components of the interstitial complexes involve bond-valences less than 0.33 *vu*.

2.5 Valence-matching principle for complex phosphate minerals

Using a binary representation of a complex mineral structure, a Lewis acidity for the interstitial complex and a Lewis basicity for the structural unit can be defined, and their interaction can be considered using the valence-matching principle.

Brown (1981) introduced the use of the valence-matching principle as a useful method for indicating which acids are likely to bond to which bases and what coordination number are needed for a good match in order to predict the stability of chemical compounds. Here, this idea is applied to the interaction if an

interstitial complex and a structural unit, with the intension of examining the range of chemical composition possible for an interstitial complex, given a specific structural unit.

2.6 Classification of complex phosphate minerals

In order to examine bond topology and chemical compositions of structures (and mineral paragenesis), it is essential to have some sort of ordering scheme when examining specific mineral groups. There have been some attempts at classifying phosphate minerals and significant advances have been made classifying other major mineral groups. Bragg (1930) classified the major rock-forming silicate minerals according to the type of polymerization of $(Si,Al)O_4$ tetrahedra, and this scheme was extended by Zoltai (1960) and Liebau (1985); it is notable that this scheme parallels Bowen's reaction series (Bowen 1928) for silicate minerals in igneous rocks. Paragenetic studies have shown that there are specific relations between chemical composition and the position of minerals in paragenetic sequences (Bandy 1938; sulfates) and it has also been observed that relations exist between mineral structures and their position in a pargenetic sequences hence the development of structural hierarchies (Moore 1963, 1973). Much insight can be derived from such structural hierarchies, particularly with regard to controls on bond topology (Hawthorne 1983a, 1994), mineral chemistry (Schindler and Hawthorne 2001a,b; Schindler et al. 2002) and mineral paragenesis (Moore 1965b, 1973a; Hawthorne 1984, 1998; Hawthorne et al. 1987; Schindler and Hawthorne 2001c).

Chapter 4 deals in great detail with the classification of phosphate minerals based on the polymerization of the structural unit (after Hawthorne 1985, 1987).

CHAPTER 3

Structural Aspects of Complex Oxysalt Minerals

3.1 Introduction

The most fundamental characteristic of a mineral is its crystal structure, a complete description of which involves the identities, amounts and arrangement of atoms that constitute the mineral. The physical, chemical and paragenetic characteristics of a mineral should arise as natural consequences of its crystal structure and the interaction of that structure with the environment in which it occurs. A structural hierarchy is an arrangement of crystal structures that reflects the systematic change in the character of their bond topologies. As the bond topology is a representation of the energetic characteristics of a structure (Hawthorne 1994, 1997), an adequate structural hierarchy of minerals should provide the most useful basis for the interpretation of the role of minerals in Earth processes.

Pauling (1929) makes the statement: "Why does aluminum fluorsilicate, $Al_2SiO_4F_2$, crystallize with the structure of topaz and not with some other structure? These questions are answered formally by the statement that in each case the structure with the minimum free energy is stable. This answer, however, is not satisfying; what is desired in our atomistic and quantum theoretical era is the explanation of this minimum free energy in terms of atoms or ions and their properties." To this end, Hawthorne (1983a, 1985a, 1990, 1994, 1992, 1997), Schindler et al. (2002) and Schindler and Hawthorne (2001a, 2001b, 2001c) have created a forum for these explanations.

3.2 Structural characteristics of oxysalt minerals

Hawthorne (1983a) proposed that structures be ordered or classified according to the polymerization of those cation coordination polyhedra with higher bond-valences. The bond-valence requirements of cations are satisfied by the formation of anion coordination polyhedra around them. A structure can therefore be thought of as an array of complex anions that polymerize in order to satisfy their bond-valence requirements; the most important linkages involving the strongest bonds. Higher bond-valence polyhedra polymerize to form *homo-* or *heteropolyhedral clusters* that constitute the *fundamental building block (FBB)* of the structure. This *FBB* is repeated, often polymerized, by translational symmetry operators to form the *structural unit*, which has already been defined, the excess charge of which is balanced by the presence of *interstitial* species (Hawthorne 1985a). The *FBB* consists of tetrahedra, triangles and octahedra as the principle components.

3.3 Structural Classes based on the fundamental building block

The possible modes of *FBB* polymerization are (1) unconnected polyhedra; (2) finite clusters; (3) infinite chains; (4) infinite sheets; (5) infinite frameworks. Hawthorne (1992) described minerals based on tetrahdra and octahedra as part of the FBB's that forms the structural unit. The phosphate minerals consist mainly of structural units that have the composition $[M(T\varphi_4)\varphi_n]$ and $[M(T\varphi_4)_2\varphi_n]$ described by Hawthorne (1992). The different topologies of

these polyhedra for the different possible modes of polymerization are briefly reviewed below:

(1) Minerals of the unconnected polyhedra class are of the form $[M(T\varphi_4)\varphi_n]$ and $[M(T\varphi_4)_2\varphi_n]$ based on isolated $(M\varphi_6)$ octahedra and $(T\varphi_4)$ tetrahedra. These tetrahedra and octahedra are linked together by large low-valence interstitial cations and by hydrogen bonding. The (H_2O) groups play an important part in holding the structure together. Typically the tetrahedral cations are coordinated by oxygen atoms, whereas the octahedral cations are coordinated by (H_2O) groups. In this class of minerals the non-occluded (H_2O) groups form an important hydrogen-bonding network that hold the structures together.

(2) Minerals with finite cluster structures considered are generally of the forms $[M(T\varphi_4)\varphi_n]$ and $[M_2(T\varphi_4)_2\varphi_n]$ based on finite clusters $(M\varphi_6)$ octahedra and $(T\varphi_4)$ tetrahedra. Some of the possible types of finite clusters of the stoichiometry $[M_2(T\varphi_4)_2\varphi_n]$ ($M = 3^+, 2^+$; $T = 5^+, 6^+$) are shown in Figure 3.1. These cluster arrangements have the maximum number of anions, which have their bond-valence requirements satisfied (Hawthorne 1983). In this case, each *M*-cation contributes, 0.5 or 0.33 *vu* and each *T*-cation contribute 1.25 or 1.5 *vu*. Considering only clusters of the type where there are no linkages between tetrahedra, then the φ_n anions shared between polyhedra will have an incident valence between 1.58 and 2.0 *vu*. This is of interest when considering the idea that the clusters that have the maximum number

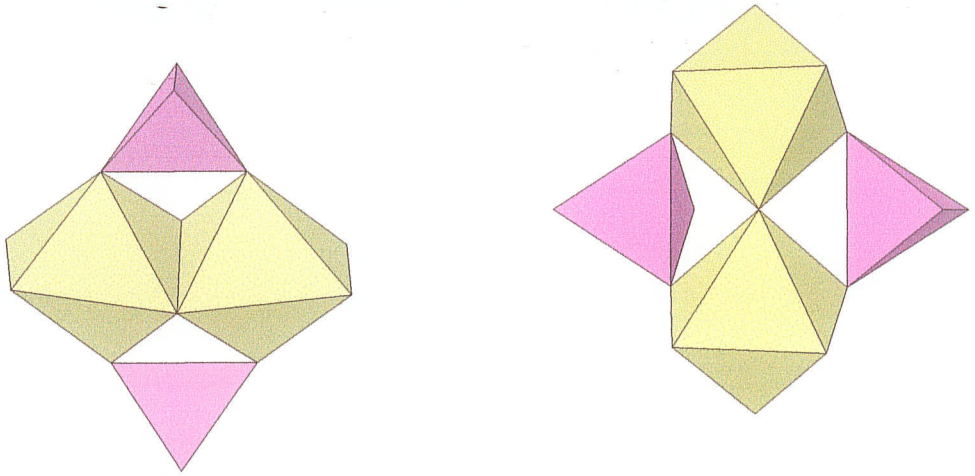

(a) $[M_2(T\varphi_4)_2\varphi_6]$ (b) $[M_2(T\varphi_4)_2\varphi_7]$

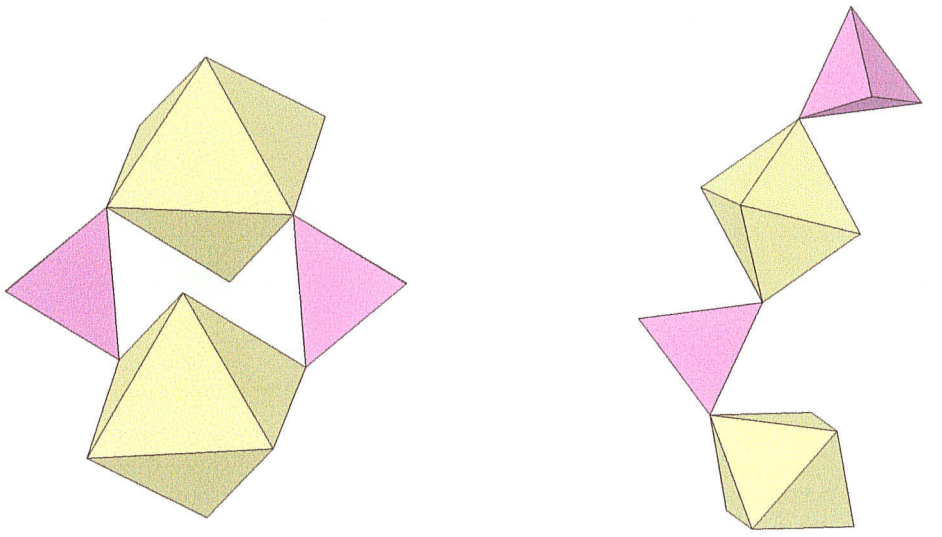

(c) $[M_2(T\varphi_4)_2\varphi_8]$ (d) $[M_2(T\varphi_4)_2\varphi_9]$

Figure 3.1. The possible $[M_2(T\varphi_4)_2\varphi_n]$ clusters (n = 6,7,8,9) for which the bond-valence requirements of Φ_n are most nearly satisfied (after Hawthorne 1983).

of anions with their bond-valence requirement satisfied, will tend to retain their stability in solution (Hawthorne 1983).

(3) There are a large number of infinite chain structures possible for minerals with a structural unit of the stoichiometries $[M(T\varphi_4)\varphi_n]$ and $[M_2(T\varphi_4)_2\varphi_n]$ that can be created from *FBB's* of tetrahedra and octahedra. Hawthorne (1983, 1992) discusses some of these *FBB* linkages that form various chains. Hawthorne (1992) pointed out that even though there a fair amount of diversity in terms of topology for $M(T\varphi_4)\varphi_n]$ and $[M_2(T\varphi_4)_2\varphi_n]$ type chains; the most common types of $[M(T\varphi_4)\varphi_n]$ and $[M_2(T\varphi_4)_2\varphi_n]$ chains tend to be the simplest. The most common chains for the phosphate minerals are discussed further in Chapter 4.

(4) For the class of minerals with infinite sheets structure, it is seen that as the structural unit becomes more polymerized the number of possible types of sheets formed based on either corner-sharing, edge-sharing or face-sharing octahedra with decorated tetrahedra becomes vast. Some of the more common and important minerals of this class are considered by Hawthorne (1992).

(5) The class of minerals based on infinite framework structures of $(M\varphi_6)$ octahedra and $(T\varphi_4)$ tetrahedra are more complex when considering polymerization patterns in three directions. Again some of the more prevalent minerals of this class are discussed in Hawthorne (1992).

It can be noted that these various modes of polymerization alone are not adequate in terms of defining mineral properties based on their crystal structure. However, it is a useful bases for classifying mineral groups and to consider the possible arrangements of structural units and determine which may be the most common/stable based on their bond-valence requirements. The hierarchy classification of the phosphates (Chapter 4) is based on these considerations of Hawthorne (1983, 1992).

CHAPTER 4

The crystal chemistry and structural hierarchy of phosphate minerals

4.1. Introduction

All phosphate minerals were systematically investigated and are classified according to the general classification discussed in Chapter 3. This structural classification leaves less onus on the genetic crystal chemistry of minerals. Structural aspects are considered first, then paragenetic sequences and their relations to the structural classification are considered (Chapter 5 and 6). The classification and mineral descriptions presented here have been accepted for publication (Huminicki and Hawthorne 2002).

4.1.1 Polymerization of ($P\varphi_4$) and other ($T\varphi_4$) tetrahedra

As already stated, bond valence is a measure of the strength of a chemical bond, and in a (PO_4) group, the mean bond-valence is 5/4 = 1.25 *vu*. The valence-sum rule (Brown 1981) states that the sum of the bond valences incident at an atom is equal to the magnitude of the formal valence of that atom. Thus any oxygen atom linked to a central P cation receives ~1.25 *vu* from that cation, and hence must receive ~0.75 *vu* from surrounding cations. An oxygen atom will unlikely link to two P atoms since it would receive, on average, 2 x 1.25 = 2.50 *vu* which would violate the valence-sum rule. Thus (PO_4) groups that polymerize to each other in a mineral (pyrophosphates) are rare with the exception of three known phosphate minerals in which (PO_4) groups do polymerize [canaphite: $Na_2Ca[P_2O_7](H_2O)_4$, wooldridgeite: $Na_2CaCu^{2+}{}_2[P_2O_7]_2(H_2O)_{10}$ and kanonerovite: $Ma_3Mn^{2+}[P_3O_{10}](H_2O)_{12}$], and

polyphosphates are common among synthetic compounds (Corbridge 1985). Therefore phosphates cannot be classified in an analogous way to silicates (*i.e.* by the polymerization characteristics of the principal oxyanion).

The simple anions of a (PO_4) group each require ~0.75 *vu* to satisfy their bond-valence requirements. So any tetrahedral oxyanion with a mean bond-valence of $\leq$ 0.75 *vu*, including (AlO_4), (BO_4), (BeO_4) and (LiO_4) groups will satisfy the bond-valence requirements for an anion of the (PO_4) group. Moreover, P–O bonds in specific structural arrangements (distortions) may have bond valences somewhat less that 1.25 *vu*, raising the possibility that (PO_4) groups might polymerize with (SiO_4) groups (mean bond-valence = 1.0 *vu*). Phosphates show all of these particular polymerizations, in accord with the valence-sum rule.

4.1.2 Polymerization of ($P\varphi_4$) tetrahedra and other ($M\varphi_n$) polyhedra

In oxysalt minerals, the coordination number of oxygen has most commonly been found to be [3] or [4]. This being the case, the *average* bond-valence (Lewis base-strength) incident at the oxygen atom bonded to one P cation would be ~0.75/3 = 0.25 *vu* or ~0.75/2 = 0.38 *vu* for other cation-oxygen bonds. The most common non-tetrahedrally coordinated cations tend to be divalent and trivalent cations (*e.g.* Mg, Fe^{2+}, Mn^{2+}, Al, Fe^{3+}) in octahedral coordination and monovalent (*e.g.* Na, K) and divalent (e.g. Ca, Sr) cations with coordination numbers of [7] and greater. The average bond-valences involved in bonds to these cations are $^{[6]}M^{2+}$ = 0.33, $^{[6]}M^{3+}$ = 0.50, $^{[7]}M^{+}$ = 0.14, $^{[7]}M^{2+}$ = 0.29 *vu*. Hence, (PO_4) groups link easily to all of these cations, particularly in hydoxy-

hydrated phosphates where hydrogen bonds commonly contribute an additional bond-valence of between 0.1 and 0.3 *vu* to the anions of the structural unit.

4.2 The Structural hierarchy of phosphate minerals

This loose polymerization suggests that we should classify the phosphates according to the types of polymerization of their principal coordination polyhedra (structural unit), as suggested by Hawthorne (1983a, 1998) and discussed briefly above. There are several possible ways in which (PO_4) may polymerize, however, the most common ways tend to be restricted in terms of bond-valence requirements and stability. The most common polymerizations in phosphate minerals are between tetrahedra and tetrahedra, between tetrahedra and octahedra, and between tetrahedra and large-cation polyhedra (*i.e.* [7]-coordinated and above). Therefore, the phosphates can be divided into these three principal groups according to:

(1) polymerization of tetrahedral and tetrahedra;

(2) polymerization of tetrahedra and octahedra;

(3) polymerization of tetrahedra and > [6]-coordinated polyhedra.

There is some overlap between these three groups such as the case with minerals that contain both M^{2+} and M^{3+} in octahedra coordination. In this situation, M^{2+} may be considered as part of the interstital complex rather than the structural unit if both are present (also depends on connectivity). This is in accord with the method of classification based on the part of the structure with higher bond-valence. A somewhat arbitrary value of 0.33 *vu* has been assigned as the minimum bond-valence requirement for bonding in the structural unit. Most other

bonds with a bond-valence of less than 0.33 *vu* are considered to be part of the interstitial complex.

The first group, involving polymerization of (PO_4) tetrahedra and other ($T\varphi_4$) tetrahedra (T = Be, Zn, B, Al, and Si), is relatively small. They can be characterized in terms of higher connectivity. The second group, involving polymerization of (PO_4) tetrahedra and ($M\varphi_6$) octahedra, is very large. The structures in this group are arranged according to Hawthorne (1983a) (Chapter 3) and similar to the classification of the sulfate minerals given by Hawthorne et al. (2000), according to the mode of polymerization of the tetrahedra and octahedra: (1) unconnected polyhedra; (2) finite clusters of polyhedra; (3) infinite chains of polyhedra; (4) infinite sheets of polyhedra; (5) infinite frameworks of polyhedra. Likewise, within each class, structures are arranged in terms of increasing connectivity of the constituent polyhedra of the structural unit. The third group are characterized by polymerization of (PO_4) tetrahedra and > [6]-coordinated polyhedra. These structures can be considered to have (PO_4) groups as there structural unit for the purpose of classification. Detailed chemical and crystallographic information and references are given in Appendix A. In all Figures, (PO_4) groups are shown as dashed-line-shaded, unless otherwise noted in the Figure.

4.3 Structures with polymerized (PO_4) and ($T\varphi_4$) groups

As noted above, (PO_4) tetrahedra can polymerize with other (PO_4) groups, and with other tetrahedrally coordinated cations such as Be, Zn, B, Al, Li and Si. However, in minerals, only the following polymerizations are observed: (PO_4)–

(PO_4), (PO_4)–$(Be\phi_4)$, (PO_4)–(ZnO_4) and (PO_4)–(AlO_4). There are several minerals containing both (PO_4) and $(B\varphi_4)$ or $(Si\varphi_4)$ groups in which the different polyhedra do not polymerize, however, minerals in which (PO_4) polymerizes with $(B\varphi_4)$ or $(Si\varphi_4)$ groups are not reported.

4.3.1 Finite clusters of (PO_4) and $(T\varphi_4)$ tetrahedra

Most of the minerals considered in this class (Table 4.1) contain polymerized (PO_4) groups; the other minerals contain (PO_4) tetrahedra that polymerize with another type of $(T\varphi_4)$ group.

In **canaphite**, $Na_2Ca(H_2O)_4[P_2O_7]$, (PO_4) tetrahedra link together to form $[P_2O_7]$ groups in the eclipsed configuration. When viewed down [100], the structure consists of layers of $(Na\varphi_6)$ and $(Ca\varphi_6)$ octahedra with intermittent $[P_2O_7]$ groups inserted in between layers (Fig. 4.1a). The layers consist of staggered chains of $(Na\varphi_6)$ octahedra that extend along *a* and are linked in the *b*-direction by $(Ca\varphi_6)$ octahedra to form a sheet of octahedral. Additional linkage within the structure consists of an extensive network of hydrogen bonds involving the (H_2O) groups of the $(CaO_5\{H_2O\})$ and $(NaO_3\{H_2O)_3)$ octahedra.

In **wooldridgeite**, $Na_2Ca(H_2O)_6[Cu^{2+}{}_2(P_2O_7)_2(H_2O)_2](H_2O)_2]$, $[P_2O_7]$ groups also occur in the eclipsed configuration. A noteworthy part of the wooldridgeite structure is the $[Cu^{2+}(P_2O_7)(H_2O)]$ chain (Fig. 4.1c) in which $(Cu\varphi_6)$ octahedra link by sharing one set of *trans* ligands (H_2O) to form a 7 Å chain (Moore 1970), decorated by $[P_2O_7]$ groups, that extends along [101] (and $[10\bar{1}]$). Each chain is flanked by a chain of corner-sharing $(Na\varphi_6)$ octahedra in which the Na–φ–Na

TABLE 4.1. Phosphate minerals* based on finite clusters of (PO_4) and ($T\Phi_4$) tetrahedra

Mineral	Cluster	Space group	Figure
Canaphite	$[P_2O_7]$	*Pc*	4.1a,b
Wooldridgeite	$[P_2O_7]$	*Fdd*2	4.1c,d,e
Kanonerovite	$[P_3O_{10}]$	$P2_1/n$	4.2a
"Pyrocoproite" **	P_2O_7	–	–
"Pyrophosphate" **	P_2O_7	–	–
"Arnhemite" **	P_2O_7	–	–
Gainesite *	$[Be(PO_4)_4]$	$I4_1/amd$	4.2b
McCrillisite	$[Be(PO_4)_4]$	$I4_1/amd$	4.2b
Selwynite	$[Be(PO_4)_4]$	$I4_1/amd$	4.2b

* For isostructural minerals, the name of the group is indicated by a * in this and all following tables;

** These names are used in the literature, but have not been approved by CNMMN of IMA.

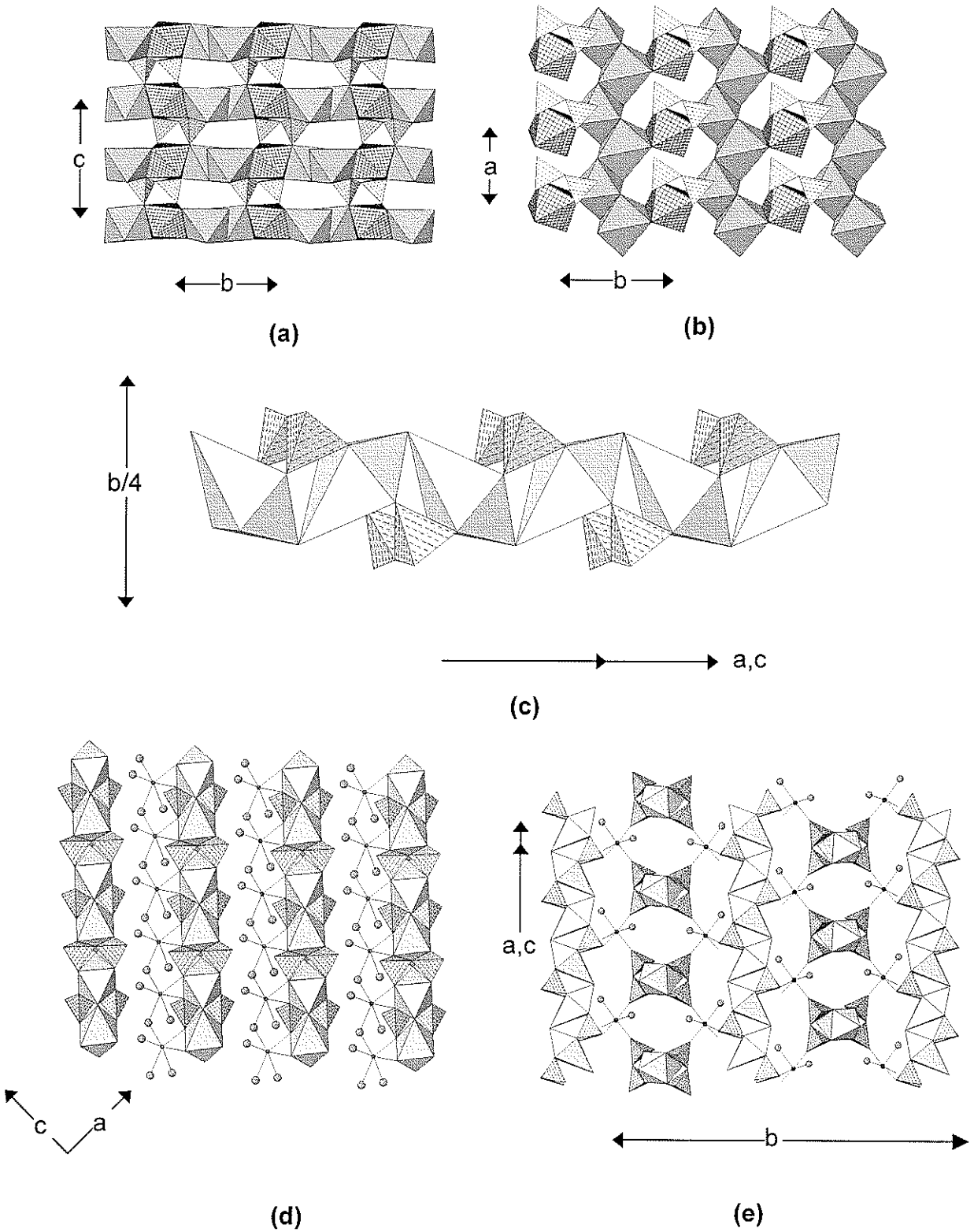

Figure 4.1. (a) canaphite projected onto (100); (b) canaphite projected onto (001); ($Ca\varphi_6$): 4^4-net-shaded, ($Na\varphi_6$): shadow-shaded; (c) $[Cu^{2+}(P_2O_7)(H_2O)]$ chain in wooldridgeite; (d) wooldridgeite projected onto (010); (e) orthogonal sets of $[Cu^{2+}(P_2O_7)(H_2O)]$ chains in wooldridgeite; ($Cu^{2+}\varphi_6$): shadow-shaded, Na atoms: small dark circles, (H_2O): large shaded circles.

linkage is through *cis* vertices and each ($Na\varphi_6$) octahedron shares an edge with a ($Cu\varphi_6$) octahedron, and these chains are linked in the [$\bar{1}$01] direction into a sheet by ($Ca\varphi_6$) octahedra (Fig. 4.1d). These sheets stack along the [010] direction (Fig. 4.1e), with each sheet rotated 90° with respect to the adjacent sheets.

In **kanonerovite**, $Na_3Mn^{2+}[P_3O_{10}](H_2O)_{12}$, three ($PO_4$) tetrahedra link together to form a $[P_3O_{10}]$ fragment. All three (PO_4) tetrahedra of this trimeric group share one vertex with the same ($Mn^{2+}\varphi_6$) octahedron (Fig. 4.2a) to form an $[Mn^{2+}(H_2O)_3P_3O_{10}]$ cluster. ($Na\varphi_6$) octahedra link by sharing vertices to form clusters that link $[Mn^{2+}(H_2O)_3P_3O_{10}]$ clusters adjacent in the *c*-direction. All other linkages involve hydrogen bonds emanating from the (H_2O) groups of the $[Mn^{2+}(H_2O)_3P_3O_{10}]$ cluster and interstitial (H_2O) groups.

In **gainesite**, $Na_2Zr_2[Be(PO_4)_4]$, and the isostructural minerals **mccrillisite**, $Cs_2Zr_2[Be(PO_4)_4]$, and **selwynite**, $Na_2Zr[Be(PO_4)_4]$, a (BeO_4) tetrahedron links to four (PO_4) tetrahedra to form the pentameric cluster $[BeP_4O_{16}]$. These clusters are linked into a continuous framework through (ZrO_6) octahedra (Fig. 4.2b). Note that the Be and P sites in the gainesite structure are only half-occupied, and in the tetrahedral-octahedral framework, tetrahedral clusters alternate with cavities occupied by interstitial Na atoms.

4.3.2 Infinite chains of (PO_4) and ($T\varphi_4$) tetrahedra

The minerals in this class can be divided into two broad groups based on the (bond valence) linkage involved in the infinite chains. Minerals of this class are listed in Table 4.2.

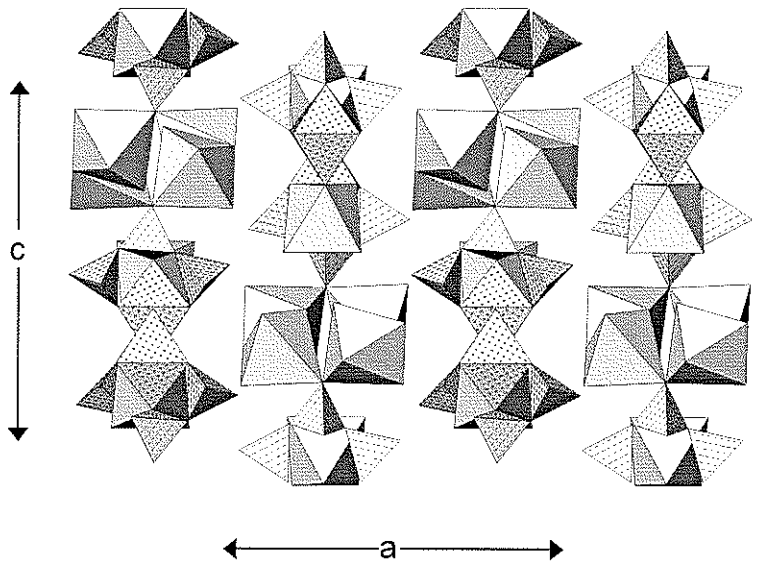

(a)

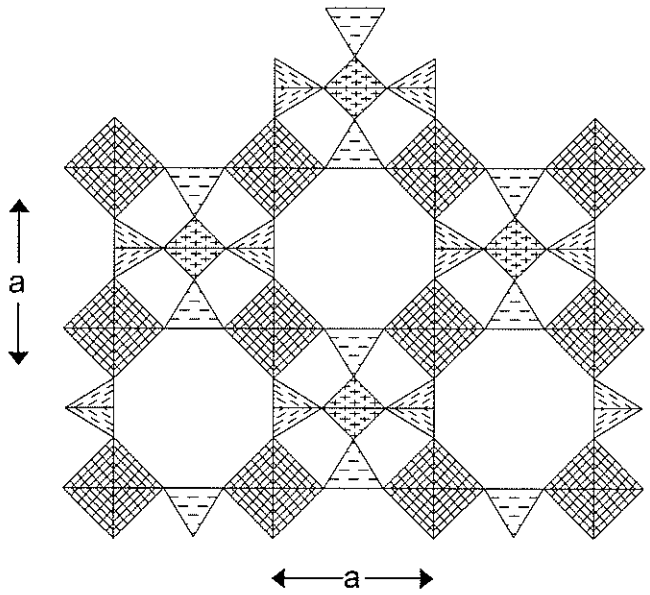

(b)

Figure 4.2. (a) kanonerovite projected onto (010), $[P_3O_{10}]$ trimers are (dashed-line shaded) linked to $(Mn^{2+}\varphi_6)$ octahedra (dot-shaded); these clusters are linked by $(Na\varphi_6)$ octahedra (shadowed) and by hydrogen bonding involving (H_2O) groups (not shown); (b) the finite tetrahedron cluster ($[BeP_4O_{16}]$ pentamer) in gainesite, linked by (ZrO_6) octahedra (line-shaded); (BeO_4): cross-shaded.

TABLE 4.2. Phosphate minerals based on infinite chains of (PO_4) and $(T\Phi_4)$ tetrahedra

Mineral	Chain	Space group	Figure
Moraesite	$[Be_2(PO_4)(OH)]$	$C2/c$	4.3a,b
Väyrynenite	$[Be(PO_4)(OH)]$	$P2_1/a$	4.3c,d
Fransoletite	$[Be_2(PO_4)_2(PO_3\{OH\})_2]$	$P2_1/a$	4.4a,b
Parafransoletite	$[Be_2(PO_4)_2(PO_3\{OH\})_2]$	$P\bar{1}$	–
Roscherite	$[Be_4(PO_4)_6(OH)_6]$	$C2/c$	4.4c,d
Zanazziite	$[Be_4(PO_4)_6(OH)_6]$	$C2/c$	4.4c,d
Spencerite	$[Zn(PO_4)(OH)(H_2O)]$	$P2_1/c$	4.4e,f

Moraesite, $[Be_2(PO_4)(OH)](H_2O)_4$, contains chains (ribbons) of (PO_4) and (BeO_4) tetrahedra. The (PO_4) tetrahedra are four-connected and the (BeO_4) tetrahedra are three-connected, and the resulting $[Be_2(PO_4)(OH)]$ ribbons extend along the *c*-direction (Fig. 4.3a). These ribbons form a face-centered array (Fig. 4.3b) and are linked by hydrogen bonds involving interstitial (H_2O) groups.

Väyrynenite, $Mn^{2+}[Be(PO_4)(OH)]$, contains chains of (PO_4) and (BeO_4) tetrahedra extending in the *a*-direction (Fig. 4.3c). (BeO_4) tetrahedra link by corner-sharing to form a pyroxenoid-like $[TO_3]$ chain that is decorated on both sides by (PO_4) tetrahedra to form a ribbon in which the (BeO_4) tetrahedra are four-connected and the (PO_4) tetrahedra are two-connected. These ribbon-like chains are linked by edge-sharing pyroxene-like chains of $(Mn^{2+}O_6)$ octahedra that also extend parallel to the *a*-axis. The resulting structural arrangement consists of modulated sheets of tetrahedra and octahedra (Fig. 4.3d).

Fransoletite and **parafransoletite** are dimorphs of composition $Ca_3[Be_2(PO_4)_2(PO_3\{OH\})_2](H_2O)_4$. The principal motif in each structure is a complex chain of tetrahedra consisting of four-membered rings of alternating (PO_4) and (BeO_4) tetrahedra that link through common (BeO_4) tetrahedra; these chains extend in the *a*-direction (Fig. 4.4a). Viewed end-on (Fig. 4.4b), the chains form a square array and are linked by [6]- and [7]-coordinated Ca atoms that form sheets parallel to {001}; further interchain linkage occurs through H-bonding involving (H_2O) groups. The fransoletite and parafransoletite structures differ only in the relative placement of the octahedrally coordinated Ca atom and the disposition of adjacent chains along their length (Kampf 1992).

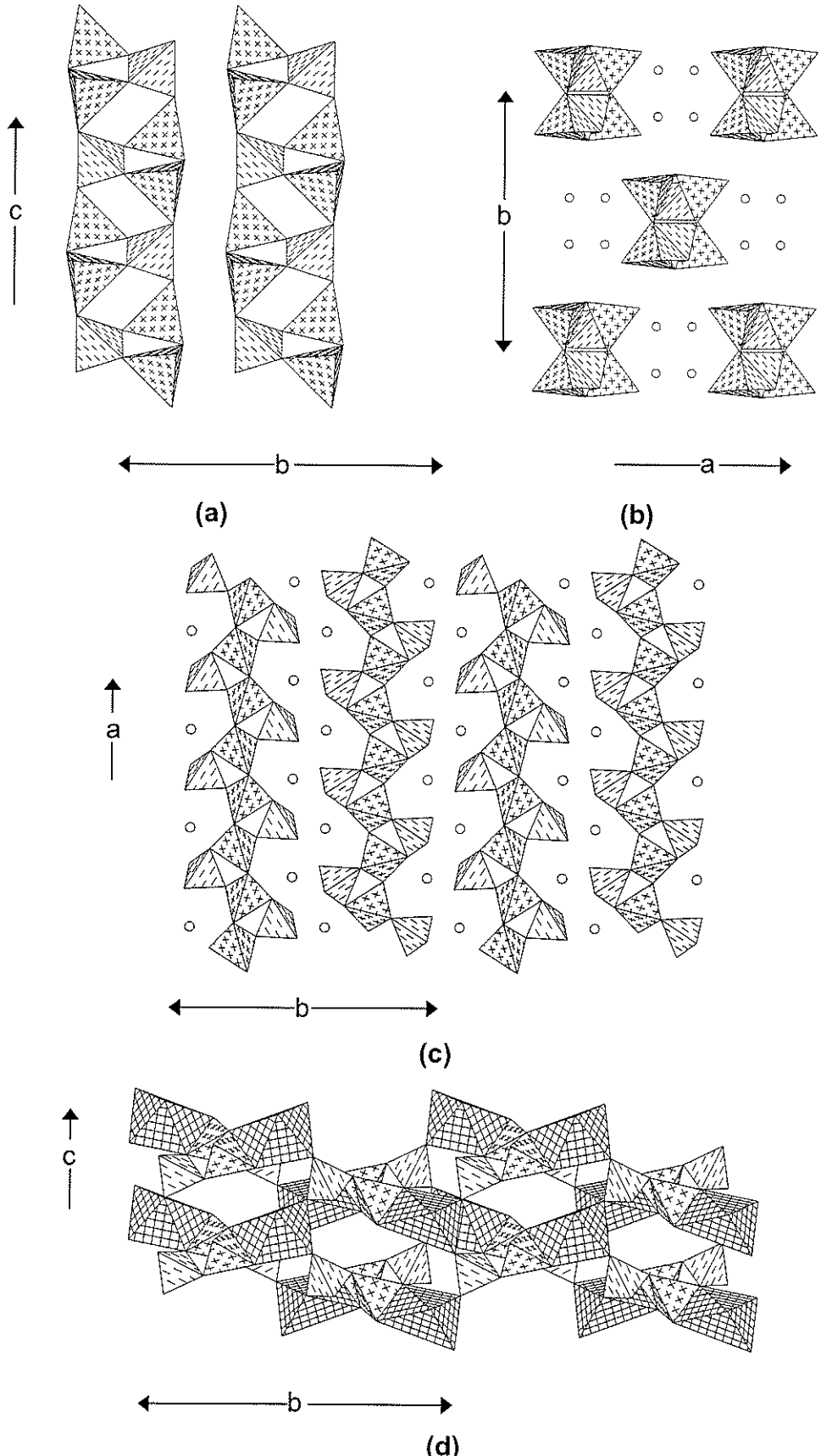

Figure 4.3. (a) moraesite projected down the *a*-axis; (PO_4): line-shaded; (BeO_4): cross-shaded; (b) moraesite projected down the *c*-axis; (H_2O) groups: unshaded circles; (c) väyrynenite projected down the *c*-axis; Al atoms: circles; (d) väyrynenite projected down the *a*-axis.

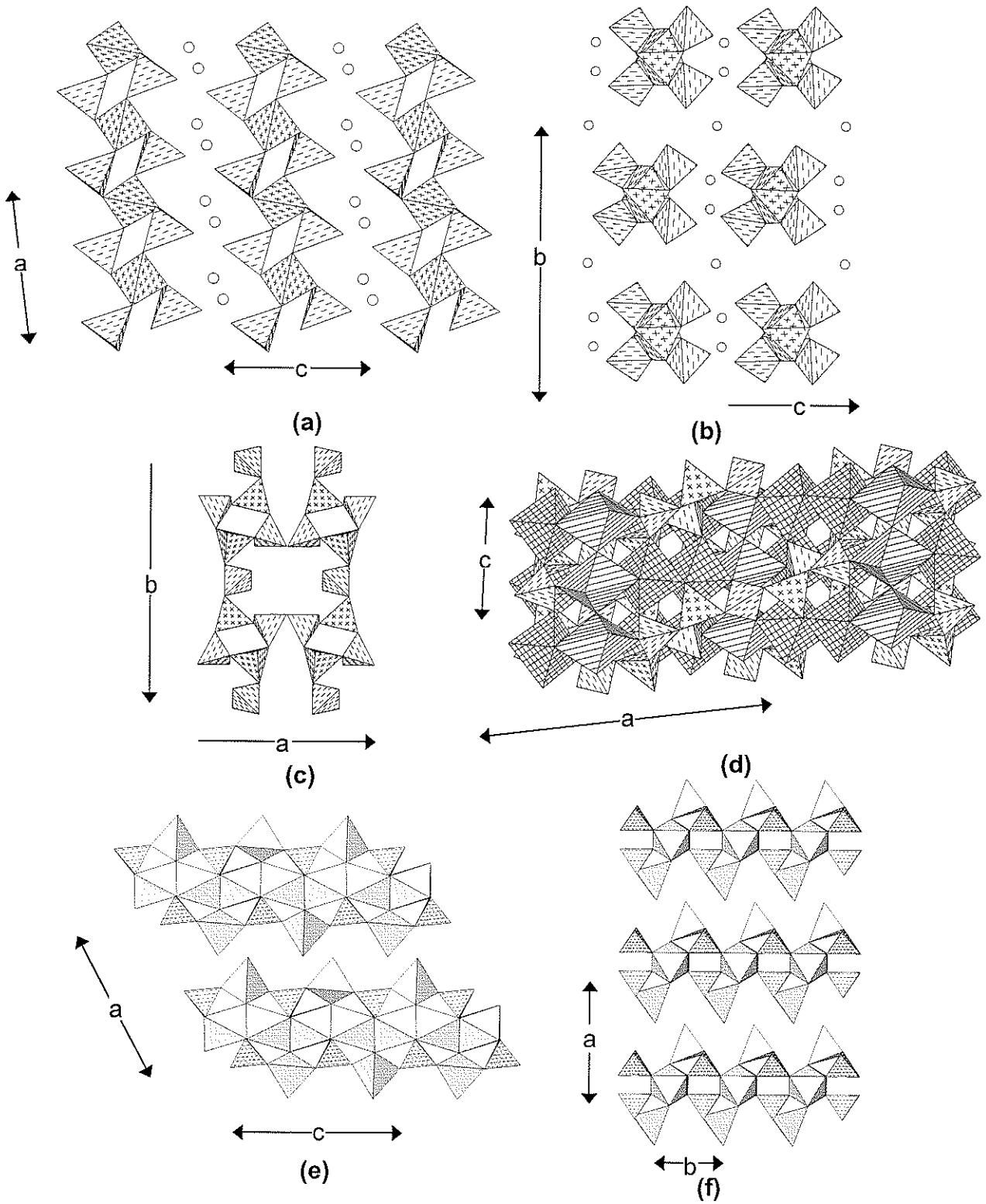

Figure 4.4. (a) fransoletite projected onto (010); Mn^{2+} atoms: circles; (b) fransoletite projected down the *a*-axis; (c) roscherite projected down the *c*-axis; (d) roscherite projected onto (010); trivalent octahedra (trellis-shaded) are only two-thirds occupied (by Al); Ca atoms are omitted; (e) spencerite projected onto (010); (f) spencerite projected onto (001); (PO_4) and (ZnO_4) chains are 'end-on'.

Roscherite and **zanazziite** are composed of very convoluted chains of $Be\varphi_4$ and (PO_4) tetrahedra extending in the [101] direction (Fig. 4.4c; note that in this view, the two chains appear to join at a mirror plane parallel to their length; however, the plane in question is a glide plane and the two chains do not join at this plane, they are displaced in the *c*-direction). The chain consists of four-membered rings of alternating $Be\varphi_4$ and (PO_4) tetrahedra linked through (PO_4) tetrahedra that are not members of these rings (Fig. 4.4c). These chains are linked by $(Al,\square)O_6$ and $(Mg,Fe^{2+})O_6$ octahedra that form edge-sharing chains parallel to [110] and $[1\bar{1}0]$; the octahedral chains link to each other in the [001] direction by sharing *trans* vertices (Fig. 4.4d). The resultant octahedral-tetrahedral framework is strengthened by [7]-coordinated Ca occupying the interstices.

The structure and composition of these minerals is not completely understood. Roscherite (Slavík 1914) is the Mn^{2+}-dominant species and zanazziite (Leavens et al. 1990) is the Mg-dominant species. Lindberg (1958) also reported an Fe^{2+}-dominant species from the Sapucaia pegmatite, Minas Gerais, that is currently unnamed. The situation is complicated by the fact that the original crystal-structure determination of roscherite (Fanfani et al. 1975) was done on a crystal of what was later determined to be *zanazziite* with the ideal end-member formula $Ca_2Mg_4(Al_{0.67}\square_{0.33})_2[Be_4(PO_4)_6(OH)_6](H_2O)_4$. Fanfani et al. (1977) report a triclinic structure for roscherite that is Mn^{2+} dominant, *i.e.* *roscherite* with the ideal end-member formula $Ca_2Mn^{2+}{}_4(Fe^{3+}{}_{0.67}\square_{0.33})(\square)[Be_4(PO_4)_6(OH)_4(H_2O)_2](H_2O)_4$. Note that the trivalent-cation content ($Al_{1.33}$ vs. $Fe^{3+}{}_{0.67}$) and type are different in the two species, and

electroneutrality is maintained by replacement of OH by H_2O: Fe^{3+} + □ (vacancy) + 3 H_2O → $Al^{3+}{}_2$ + 3 OH. Whether the monoclinic → triclinic transition is caused by the Mn^{2+} → Mg replacement or by the reaction noted above is not yet known.

Spencerite, $Zn_2[Zn(OH)(H_2O)(PO_4)]_2(H_2O)$, contains simple linear chains of alternating ($Zn\varphi_4$) [$\varphi_4 = O_2(OH)(H_2O)$] and ($PO_4$) tetrahedra extending along the *c* direction (Fig. 4.4e) and cross-linked into heteropolyhedral sheets by ($Zn\varphi_6$) octahedra. These sheets are also shown in Fig. 4.4f, where it can be seen that the ($Zn\varphi_6$) octahedra share all their vertices with ($Zn\varphi_4$) and (PO_4) tetrahedra. The heteropolyhedral sheets link solely *via* hydrogen bonding that involves one (H_2O) group (not shown in Figs. 4.4e or 4.4f) held in the structure solely by hydrogen bonding.

4.3.3 Infinite sheets of (PO_4) and ($T\varphi_4$) tetrahedra

The minerals in this class (Table 4.3) can be divided into two groups: (PO_4)–(BeO_4) linkages, and (PO_4)–(ZnO_4) linkages.

Hydroxylherderite, Ca[Be(PO_4)(OH)] and **herderite**, Ca[Be(PO_4)F], are isostructural; the structures of the first two were reported in different orientations: $P2_1/c$ and $P2_1/a$, respectively. The sheet unit consists of (PO_4) and ($Be\varphi_4$) tetrahedra at the vertices of a two-dimensional net (Fig. 4.5a). Four-membered rings of alternating (PO_4) and ($Be\varphi_4$) tetrahedra link by sharing vertices between (PO_4) and ($Be\varphi_4$) tetrahedra; thus the sheet can be considered to be constructed from chains of four-membered rings that extend in the [110] and [1$\bar{1}$0] directions (Fig. 4.5a). These sheets stack in the *c*-direction (Fig. 4.5b) and are linked by layers of [8]-coordinated Ca atoms. Note that the structure reported by Lager and

TABLE 4.3. Phosphate minerals based on infinite sheets of (PO_4) and $(T\Phi_4)$ tetrahedra

Mineral	Sheet	Space group	Figure
Herderite	$[Be(PO_4)(OH)]$	$P2_1/a$	4.5a,b
Hydroxylherderite	$[Be(PO_4)(OH)]$	$P2_1/a$	4.5a,b
Uralolite	$[Be_4P_3O_{12}(OH)_3]$	$P2_1/n$	4.5c,d
Ehrleite	$[BeZn(PO_4)_2(PO_3\{OH\})]$	$P\bar{1}$	4.5e,f
Hopeite	$[Zn(PO_4)]$	$Pnma$	4.6a,b
Parahopeite	$[Zn(PO_4)]$	$P\bar{1}$	4.6c,d
Phosphophyllite	$[Zn(PO_4)]$	$P2_1/c$	4.7a,b
Veszelyite	$[Zn(PO_4)(OH)]$	$P2_1/a$	4.7c,d
Kipushite	$[Cu^{2+}{}_5Zn(PO_4)_2(OH)_6(H_2O)]$	$P2_1/c$	4.7e,f
Scholzite	$[Zn(PO_4)]$	$Pbc2_1$	4.8a,b
Parascholzite	$[Zn(PO_4)]$	$I2/c$	4.8c,d

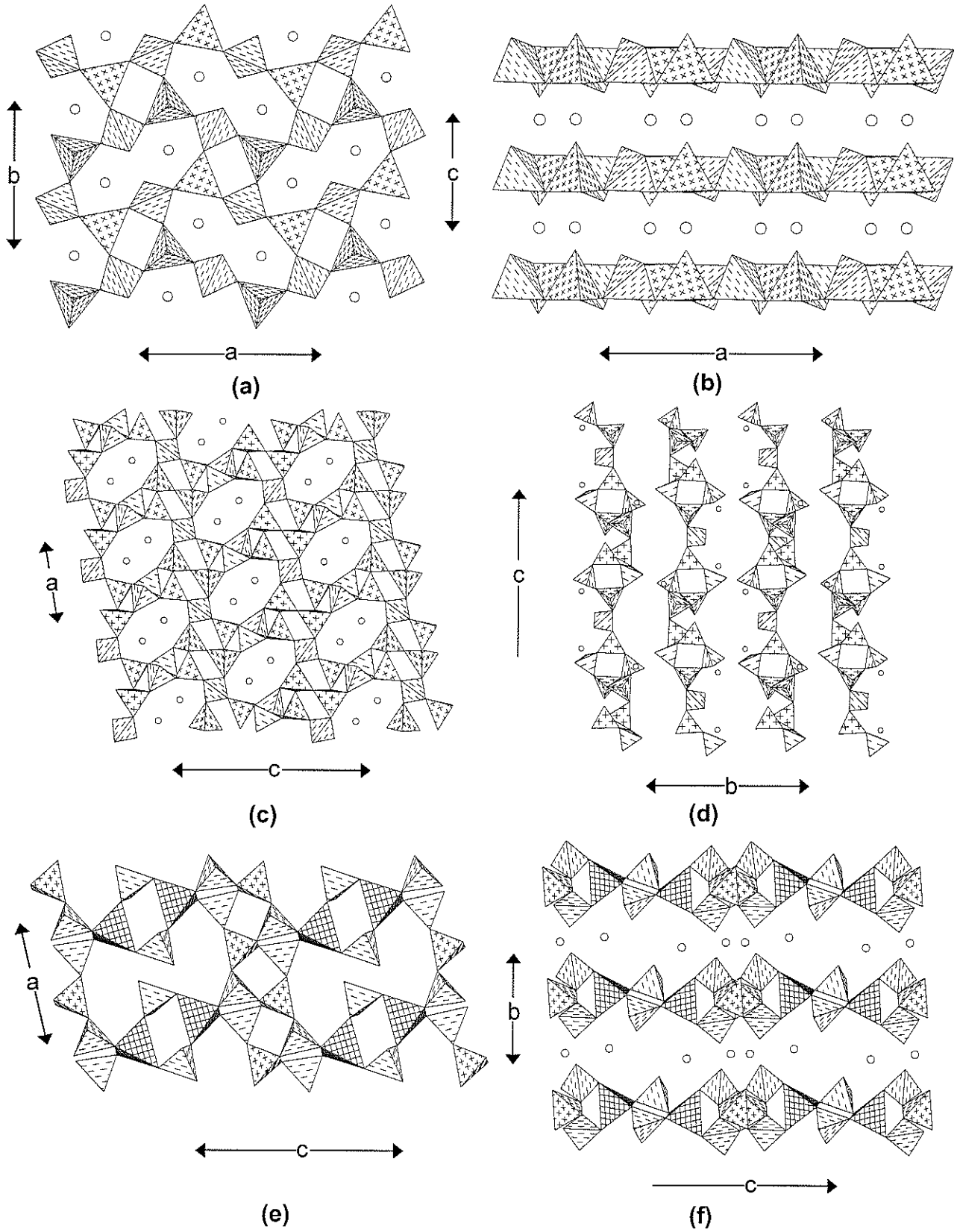

Figure 4.5. (a) herderite projected onto (001); (b) herderite projected onto (010); (c) uralolite projected onto (010); (d) uralolite projected down the *a*-axis; (e) the structural unit in ehrleite projected onto (010); (PO_4), (BeO_4) (cross-shaded) and (ZnO_4) (trellis-shaded) tetrahedra share corners to form a sheet; (f) ehrleite projected down the *a*-axis; Ca atoms: circles.

Gibbs (1974) seems to have been done on hydroxylherderite rather than herderite.

Uralolite, $Ca_2[Be_4P_3O_{12}(OH)_3](H_2O)_5$, contains ($PO_4$) and ($BeO_4$) tetrahedra linked into a sheet (Fig. 4.5c). Eight-membered rings of tetrahedra (P–Be–P–Be–P–Be–P–Be) link through common (PO_4) groups to form chains that extend along [101]. These chains link in the (010) plane via sharing of tetrahedral vertices, forming three-membered (Be–Be–Be and Be–Be–P) and four-membered (Be–Be–Be–P) rings. Interstitial [7]-coordinated Ca atoms lie within the eight-membered rings (in projection). The layers stack along the *b*-direction (Fig. 4.5d) and are linked by Ca atoms (circles) and H-bonding; in this view, the three- and four-membered rings are easily seen.

Ehrleite, $Ca_2[BeZn(PO_4)_2(PO_3\{OH\})](H_2O)_4$, has a very complicated sheet of tetrahedra, both from topological and chemical viewpoints. There is one distinct (BeO_4) tetrahedron and this links to four ($P\varphi_4$) groups (Fig. 4.5e); similarly, there is one (ZnO_4) tetrahedron and this links to four ($P\varphi_4$) groups. However, the ($P\varphi_4$) groups link only to three or two other tetrahedra. Four-membered rings of alternating (PO_4) and (BeO_4) tetrahedra link through common (BeO_4) tetrahedra to form chains in the *a*-direction (Fig. 4.5e). These chains are linked in the *c*-direction by four-membered rings of alternating (PO_4) and (ZnO_4) tetrahedra to form additional four-membered rings (Zn–P–Be–P). The result is an open sheet, parallel to (010), with buckled twelve-membered rings (Fig. 4.5e) into which project the H atoms of the acid-phosphate groups. These sheets stack along the *b*-direction (Fig. 4.5f) and are linked together by [7]-coordinated and [8]-coordinated interstitial Ca atoms.

In **hopeite**, $Zn(H_2O)_4[Zn(PO_4)]_2$, kinked chains of ($Zn\phi_4$) tetrahedra extend in the *c*-direction, and adjacent chains are linked by (PO_4) tetrahedra to form a sheet parallel to (101) (Fig. 4.6a). The (ZnO_4) tetrahedra are four-connected, but the (PO_4) tetrahedra are only three-connected; this difference in connectivity is very important as it promotes structural linkage perpendicular to the sheet. A continuous sheet with this connectivity requires unusual coordination numbers for some of the simple anions of the sheet: for the (PO_4) group, the anion coordination numbers within the sheet are [1], [2] x 2 and [3], and for the (ZnO_4) group, the anion coordination numbers within the sheet are [2] x 2 and [3] x 2. Hence the sheet is quite corrugated, as can be seen in Figure 4.6b: the (ZnO_4) tetrahedra form a central layer and the (PO_4) tetrahedra form two outer (or sandwiching) layers. The sheets are linked in the *b*-direction by ($ZnO_2\{H_2O\}_4$) octahedra (Fig. 4.6b), the [1]-coordinated anion of the phosphate group forming a ligand of the linking $^{[6]}Zn$ cation. In **parahopeite**, $Zn(H_2O)_4[Zn(PO_4)]_2$, (PO_4) and (ZnO_4) tetrahedra lie at the vertices of a 4^4 net to form a sheet in which (PO_4) tetrahedra link only to (ZnO_4) tetrahedra, and *vice versa*. Thus all tetrahedra are four-connected, and all vertices (simple anions) are two-connected within the resultant sheet (Fig. 4.6c). These sheets are parallel to (101) and are linked in the *b*-direction by ($ZnO_2\{H_2O\}_4$) octahedra in which the *trans* O-atoms belong to adjacent sheets (Fig. 4.6d).

In **phosphophyllite**, $Fe^{2+}(H_2O)_4[Zn(PO_4)]_2$, ($PO_4$) and ($Zn\varphi_4$) tetrahedra form a sheet (Fig. 4.7a) that is topologically identical to the [$Zn(PO_4)$] sheet in hopeite (Fig. 4.6a). These sheets are linked by ($Fe^{2+}O_2\{H_2O\}_4$) octahedra, similar to the linkage by ($ZnO_2\{H_2O\}_4$) octahedra in hopeite. However, in

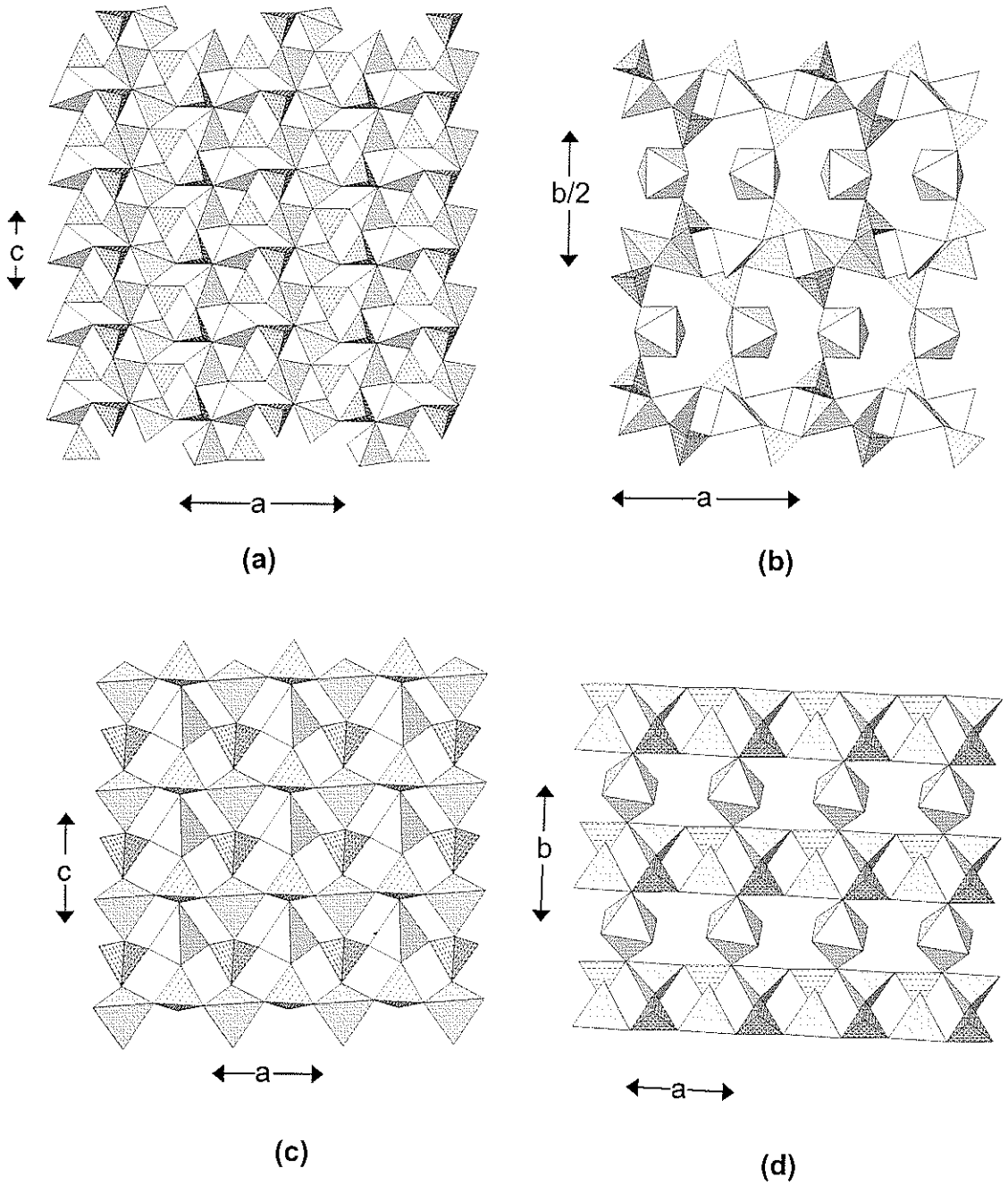

Figure 4.6. (a) hopeite projected onto (010); (b) hopeite projected onto (001); hydrogen bonds are omitted; (c) parahopeite projected onto (010); (d) parahopeite projected onto (001); (PO_4): broken-line shaded, (ZnO_4): grey-shaded, ($Zn\varphi_6$): shadow-shaded.

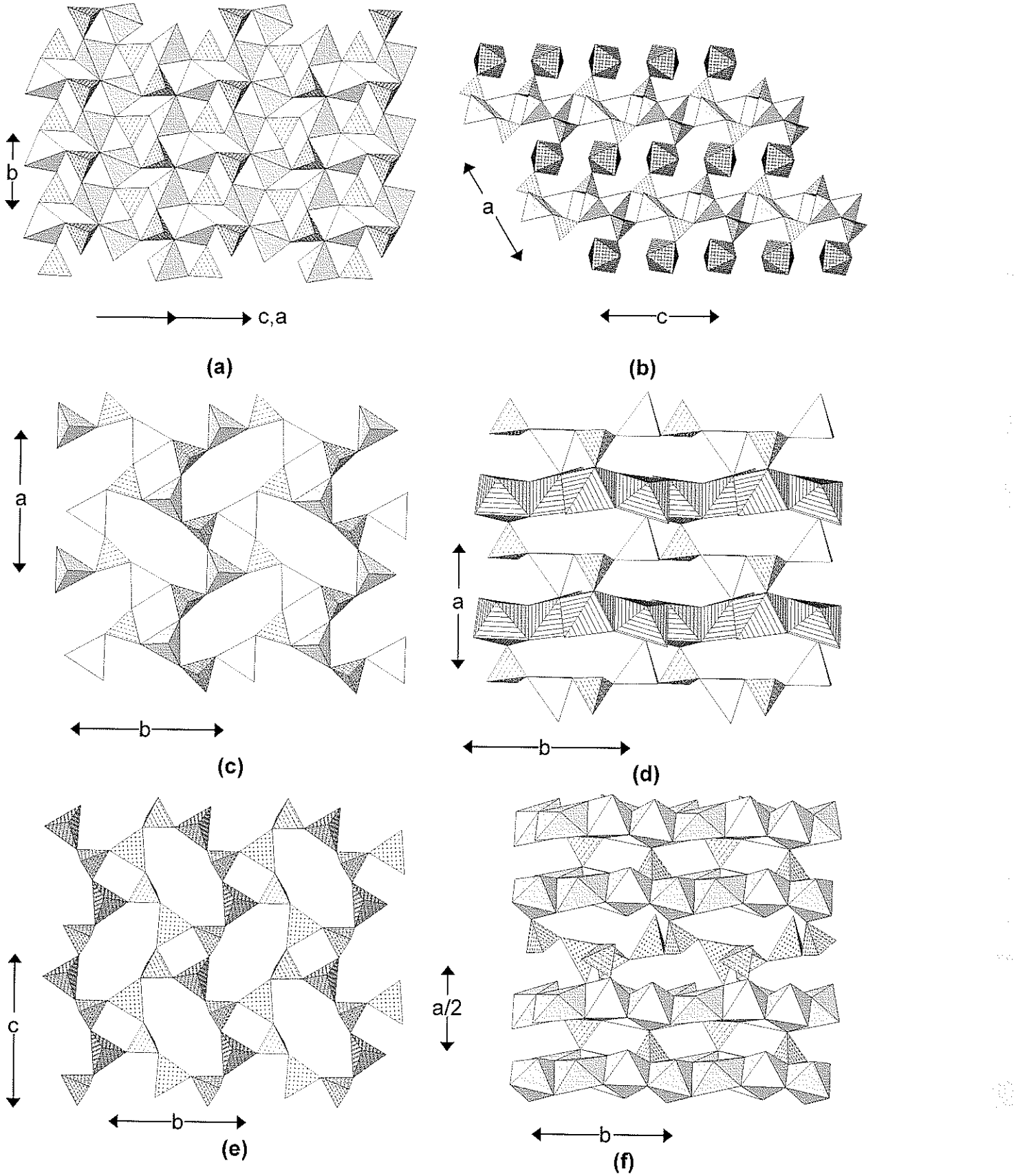

Figure 4.7. (a) phosphophyllite showing (PO_4) and ($Zn\varphi_4$) tetrahedral sheet; (b) phosphophyllite projected onto (010); (c) veszelyite projected onto (001); (d) veszelyite projected onto (100); (e) sheet of (PO_4) and (ZnO_4) tetrahedra in kipushite projected onto (100); (f) the structure of kipushite projected onto (001). ($Zn\varphi_4$): shadow shaded, ($Zn\varphi_6$): 4^4-net-shaded, ($Cu^{2+}\varphi_6$): line-shaded.

phosphophyllite, the O-atoms of the ($Fe^{2+}O_2\{H_2O\}_4$) octahedron are in a *trans* configuration (Fig. 4.7b), whereas in hopeite, the O-atoms of the ($ZnO_2\{H_2O\}_4$) octahedron are in a *cis* configuration (Fig. 4.6b).

In **veszeylite**, $Cu^{2+}_2(OH)_2(H_2O)_2[Zn(PO_4)(OH)]$, ($PO_4$) and ($Zn\varphi_4$) tetrahedra occur at the vertices of a 4.8^2 net (Fig. 4.7c) in which each type of tetrahedron points both up and down relative to the plane of the sheet. Both (PO_4) and ($Zn\varphi_4$) tetrahedra are three-connected within the sheet, and (PO_4) tetrahedra and ($Zn\varphi_4$) tetrahedra always alternate in any path through the 4.8^2 net. In the four-membered ring, the tetrahedra point *uudd*, and in the eight-membered ring, the tetrahedra point *uuuudddd*. The ($Cu^{2+}\varphi_6$) octahedra form an interrupted [$M\varphi_2$] sheet (Hawthorne and Schindler 2000, Hawthorne and Sokolova 2002) in which the vacant octahedra are ordered as dimers. The sheets of tetrahedra and octahedra stack in the *c*-direction (Fig. 4.7d) with hydrogen bonds (not shown) providing additional linkage between octahedra and tetrahedra.

Kipushite, $[Cu^{2+}_5Zn(PO_4)_2(OH)_6(H_2O)]$, contains ($PO_4$) and ($ZnO_4$) tetrahedra that are arranged at the vertices of a 4.8^2 net (as occurs in veszelyite) and link by corner-sharing (Fig. 4.7e, c.f. Fig. 4.7c). ($Cu^{2+}\varphi_6$) octahedra share edges to form a sheet with ordered vacancies. It is actually a sheet of the form $[M_6\varphi_{12}] \equiv [M\varphi_2]_6$ with $M_6 = Cu^{2+}_5\,\square$, where $\square$ is a vacant octahedron; these 'vacant octahedra' share a face with a (PO_4) tetrahedron on one side of the sheet of octahedra. Two of these sheets then link by sharing the apical vertices of their (PO_4) tetrahedra with octahedron vertices of the adjacent sheet to form a thick

slab (Fig. 4.7f). These slabs stack in the *a*-direction and are linked by the (PO_4)–(ZnO_4) sheet through sharing of vertices between tetrahedra and octahedra.

In **scholzite**, $Ca(H_2O)_2[Zn(PO_4)]_2$, (ZnO_4) tetrahedra share pairs of vertices to form simple linear chains parallel to the *c*-direction. Adjacent (ZnO_4) tetrahedra are further linked by sharing vertices with a (PO_4) tetrahedron, and the (PO_4) tetrahedra are in a staggered arrangement along the length of the chain. Chains adjacent in the *b*-direction link through (PO_4) tetrahedra to form a sheet parallel to (100) (Fig. 4.8a). In this sheet, the (ZnO_4) tetrahedra are four-connected and the (PO_4) tetrahedra are three-connected. The bridging anions of the chain of (ZnO_4) tetrahedra are three-connected; all other anions of the sheet are two-connected except for the one-connected anion of the (PO_4) tetrahedron. The resulting sheet (Fig. 4.8a) forms quite a thick slab that is linked by two crystallographically distinct octahedrally coordinated Ca atoms (Fig. 4.8b). In **parascholzite**, $Ca(H_2O)_2[Zn(PO_4)]_2$, the sheet of (PO_4) and (ZnO_4) tetrahedra (Fig. 4.8c) is topologically identical to the analogous sheet in scholzite (Fig. 4.8a). Scholzite and parascholzite are dimorphs, and the difference between these two structures involves linkage of the sheets in the *a*-direction (Figs. 4.8b, 4.8d). The details of the coordination of the interstitial Ca atoms differ in the two structures, leading to a different arrangement of adjacent sheets that produces an orthorhombic arrangement in scholzite and a monoclinic arrangement in parascholzite.

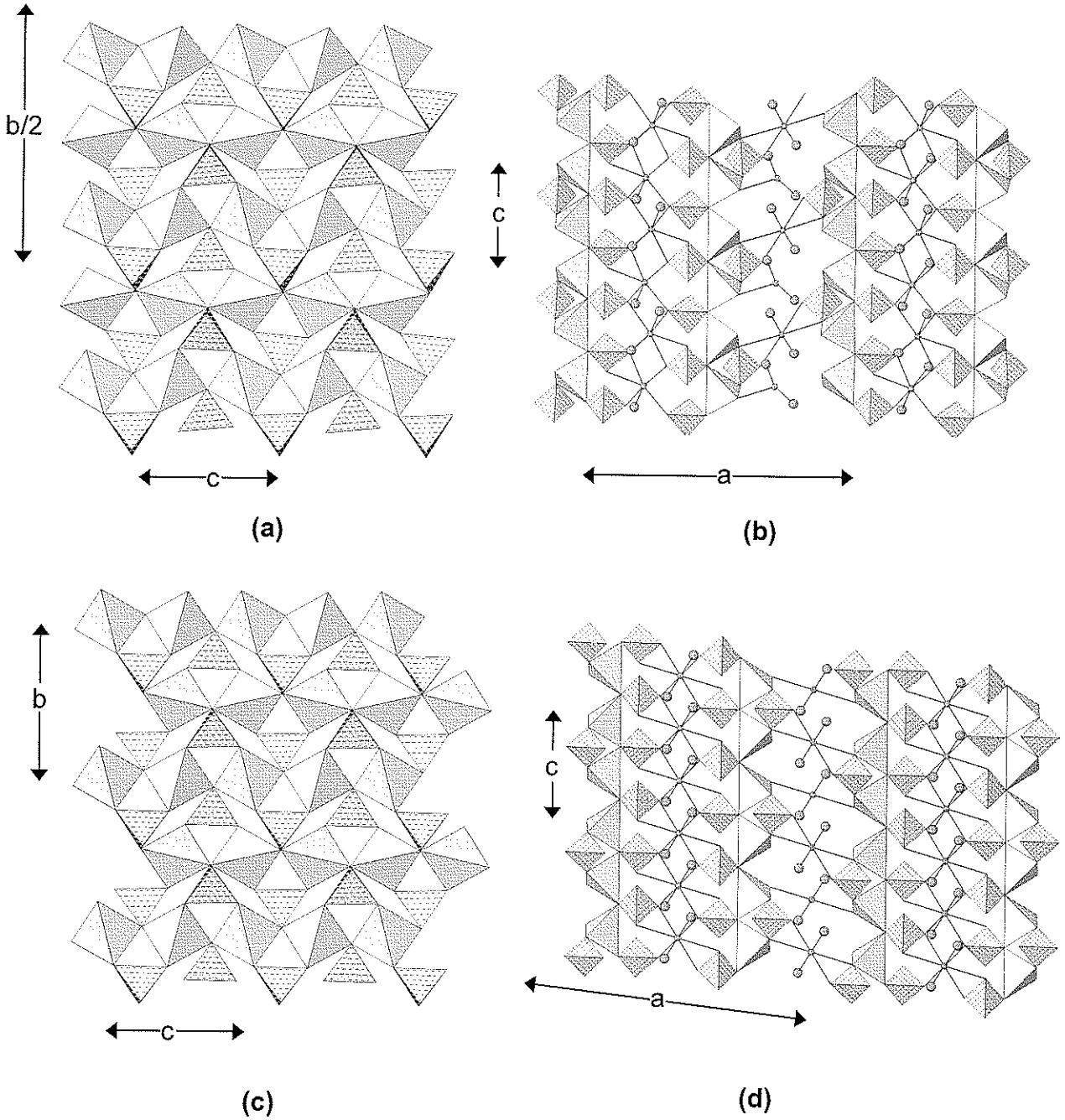

Figure 4.8. (a) scholzite projected onto (100), showing three-connected (PO_4) tetrahedra and four-connected (ZnO_4) tetrahedra; (b) scholzite projected onto (010); (c) parascholzite projected onto (100); (d) parascholzite projected onto (010). (PO_4): line-shaded, (ZnO_4): shadow-shaded, Ca atoms: small grey circles, (H_2O) groups: large grey circles.

4.3.4 Infinite frameworks of (PO_4) and ($T\varphi_4$) tetrahedra

The minerals of this class (Table 4.4) are again dominated by PO_4-BeO_4 linkages. Only berlinite is different from this, but is the only structure with polymerized (PO_4) and AlO_4 groups.

Berlinite, [$AlPO_4$], is a framework structure, topologically identical to the structure of α-quartz. Both structures have the same space group, *P*321, but the *c* dimension in berlinite is twice that of α-quartz in order to incorporate two distinct types of tetrahedra, AlO_4 and PO_4.

Beryllonite, Na[Be(PO_4)], consists of a well-ordered framework of alternating four-connected (PO_4) and (BeO_4) tetrahedra arranged at the vertices of a 6^3 net, with (PO_4) and (BeO_4) tetrahedra pointing in opposing directions along the *b*-axis (Fig. 4.9a). This arrangement is topologically identical to the tridymite framework. These sheets stack along the *b*-direction and share tetrahedron corners to form four-membered and eight-membered rings (Fig. 4.9b). The resultant framework has large channels containing [6]- and [9]-coordinated interstitial Na.

Hurlbutite, Ca[$Be_2(PO_4)_2$], consists of an ordered array of (PO_4) and (BeO_4) tetrahedra in which all tetrahedra are four-connected and there is alternation of (PO_4) and (BeO_4) tetrahedra in the structure. Viewed down [001] (Fig. 4.9c), the tetrahedra are arranged at the vertices of a 4.8^2 net with [7]-coordinated Ca occupying the interstices; these sheets link along the [001] direction by vertex-sharing (Fig. 4.9d).

Babefphite, Ba[Be(PO_4)F], is a rather unusual mineral; it is an ordered framework of (PO_4) and (BeO_3F) tetrahedra. Projected down the *c*-direction,

TABLE 4.4. Phosphate minerals based on infinite frameworks of (PO_4) and ($T\Phi_4$) tetrahedra

Mineral	Framework	Space group	Figure
Berlinite	$[AlPO_4]$	$P3_12$	–
Beryllonite	$[BePO_4]$	$P2_1/n$	4.9a,b
Hurlbutite	$[Be_2(PO_4)_2]$	$P2_1/a$	4.9c,d
Babefphite	$[Be(PO_4)F]$	$F1$	4.9e,f
Tiptopite	$[Be_6(PO_4)_6]$	$P6_3$	4.10a,b
Weinebeneite	$[Be_3(PO_4)_2(OH)_2]$	Cc	4.10c,d
Pahasapaite	$[Be_{24}P_{24}O_{96}]$	$I23$	4.10e

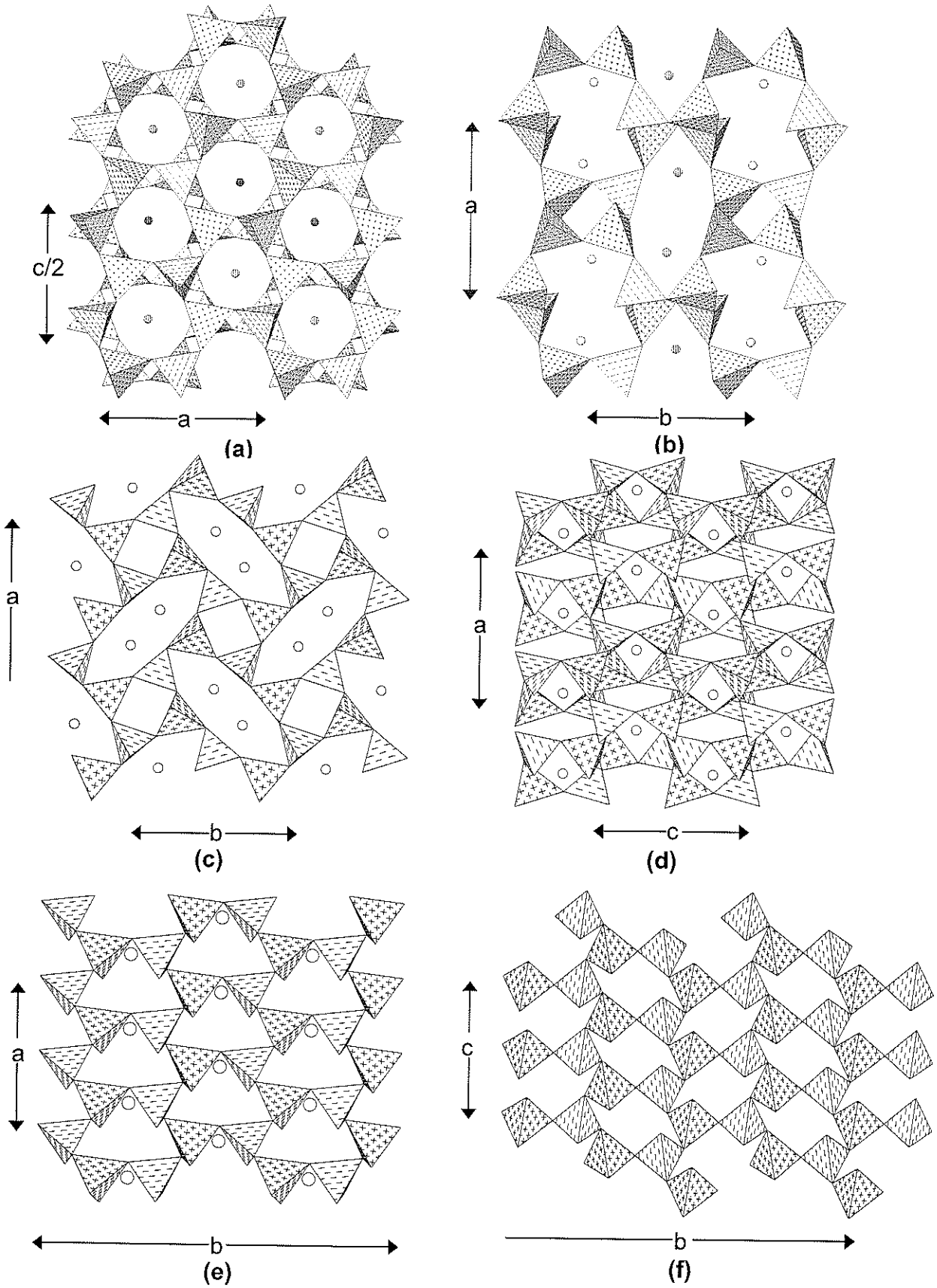

Figure 4.9. (a) beryllonite projected onto (010); (b) beryllonite projected onto (001); (c) hurlbutite projected onto (001); Ca atoms: circles; (d) hurlbutite projected down the *c* axis; (e) babefphite projected onto (001); Ba atoms: circles; (f) babefphite projected down the *a*-axis.

tetrahedra are arranged at the vertices of a 6^3 net (Fig. 4.9e) with the tetrahedra pointing (*uuuddd*). Projected down the *a*-direction, again the tetrahedra occur at the vertices of a 6^3 net (Fig. 4.9f) but the tetrahedra point (*uuuuuu*). Both the (PO_4) and the ($Be\varphi_4$) tetrahedra are three-connected, and the F anions are the non-*T*-bridging species in the ($Be\varphi_4$) tetrahedra. The interstices of the framework are occupied by [9]-coordinated Ba.

Tiptopite, $K_2(Li_{2.9}Na_{1.7}Ca_{0.7}\square_{0.7})[Be_6(PO_4)_6](OH)_2(H_2O)_4$, is isotypic with the minerals of the cancrinite group: $Ca_2Na_6[Al_6(SiO_4)_6(CO_3)_2](H_2O)_2$ for the silicate species. The (PO_4) and (BeO_4) tetrahedra are arranged at the vertices of a two-dimensional net (Fig. 4.10a) such that all tetrahedra are three-connected when viewed down [001]. Prominent twelve-membered rings are arranged at the vertices of a 3^6 net such that they two-connect four-membered rings and three-connect through six-membered rings. These sheets link in the *c*-direction such that all tetrahedra are four-connected and, projected down the *b*-direction, form a two-dimensional net of four- and six-membered rings (Fig. 4.10b). The latter can be considered as a 6^3 net in which every third row of hexagons have a linear defect corresponding to an *a*-glide operation along *c*, *i.e.* double chains of hexagons extending in the *c*-direction and interleaved by single ladders of edge-sharing squares. Details of the rather complex relations between the interstitial species are discussed by Peacor et al. (1987).

Weinebeneite, $Ca[Be_3(PO_4)_2(OH)_2](H_2O)_4$, contains an ordered framework of (PO_4) and (BeO_4) tetrahedra; the (PO_4) tetrahedra connect only to (BeO_4) tetrahedra, but the (BeO_4) tetrahedra connect to both (PO_4) and (BeO_4) tetrahedra, the Be–Be linkages occurring through the (OH) groups of the

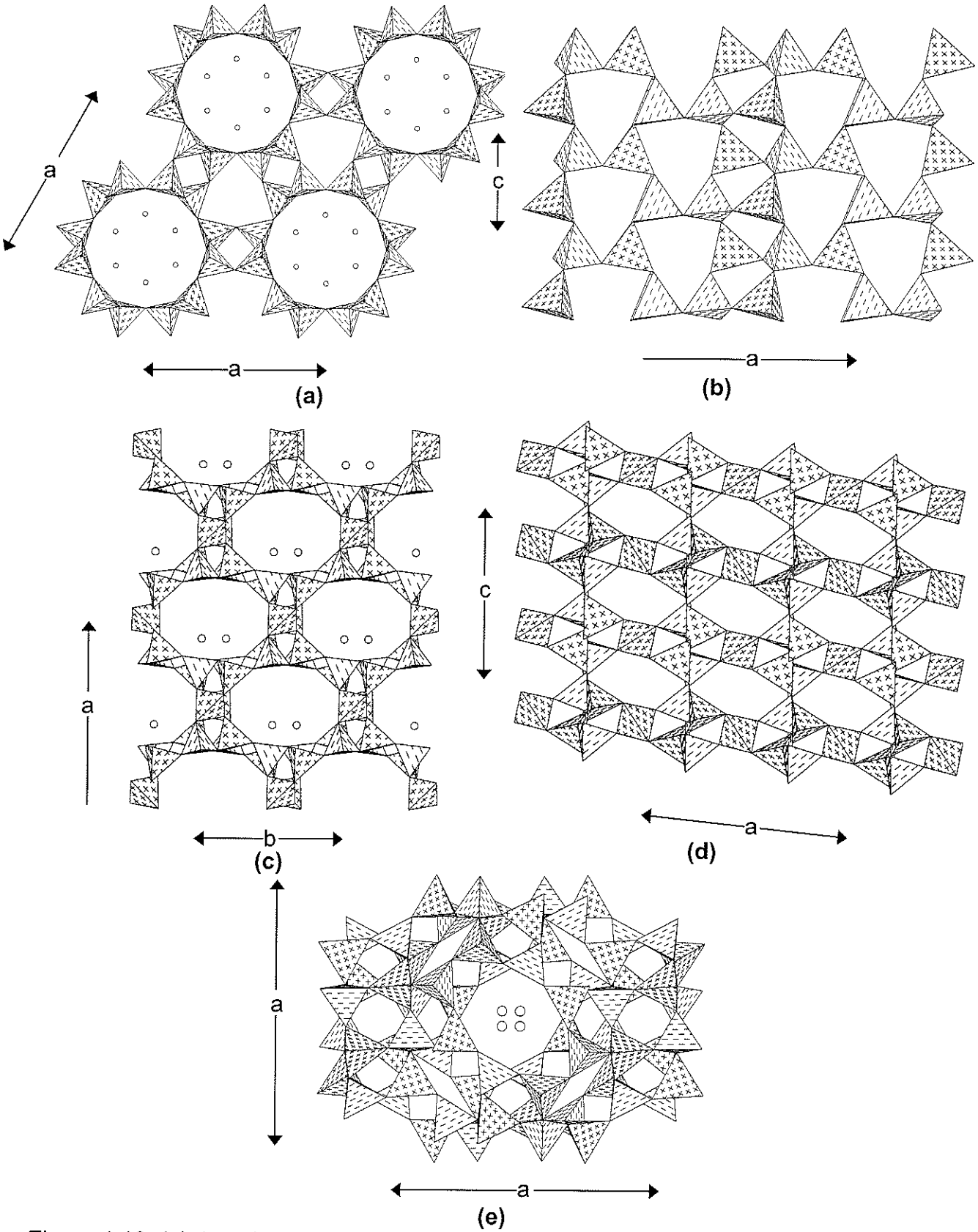

Figure 4.10. (a) tiptopite projected onto (001); alkali cations: circles; (b) tiptopite projected onto (010); (c) weinebeneite projected down the *c*-axis; (d) weinebeneite projected onto (010); in both (c) and (d), 4.8^2 nets of tetrahedra link in the *a*-direction through a (BeO_4) group; (e) pahasapite projected onto (001); Ca atoms: circles; Li and (H_2O) are omitted.

framework. Viewed down [100], the structure consists of alternating (PO_4) and (BeO_4) tetrahedra at the vertices of a 4.8^2 net (view not shown). Projected onto (001) (Fig. 4.10c) and viewed down [010] (Fig. 4.10d), the 4.8^2 sheets stack in the [100] direction and link together through additional (non-sheet) (BeO_4) tetrahedra. Interstitial [7]-coordinated Ca is situated to one side of the large channels thus formed, with channel (H_2O) also bonded to the Ca.

Pahasapaite, $Ca_8Li_8[Be_{24}P_{24}O_{96}](H_2O)_{38}$, has an ordered array of (PO_4) and (BeO_4) tetrahedra arranged in a zeolite-rho framework, topologically similar to the minerals of the faujasite group and related to the synthetic aluminophosphate zeolite-like frameworks. Viewed along any crystallographic axis, the structure consists of prominent eight-membered rings of alternating (PO_4) and (BeO_4) tetrahedra (Fig. 4.10e) in an I-centered (F-centered in projection) array; they are connected along the axial directions by linear triplets of four-membered rings, and to nearest-neighbor eight-membered rings through six-membered rings. All tetrahedra are four-connected; (PO_4) tetrahedra link only to (BeO_4) tetrahedra, and vice versa. The structure has large cages (Rouse et al. 1989) and prominent intersecting channels (Fig. 4.10e) that contain interstitial Li, [7]-coordinated Ca and strongly disordered (H_2O) groups.

4.4 Structures with ($T\varphi_4$) and ($M\varphi_6$) groups

As noted above, the structures within each sub-group are classified in terms of the connectivity of the constituent polyhedra of the structural unit. The nomenclature of Hawthorne (1983a) is used to denote the linkage: – denotes

corner-sharing (*e.g.*, *M*–*M*), = denotes edge-sharing (*e.g.*, *M*=*M*), and ≡ denotes (triangular) face-sharing (*e.g.*, *M*≡*M*).

4.4.1 Structures with unconnected (PO_4) tetrahedra and ($M\varphi_6$) octahedra

Phosphate minerals of this class are listed in Table 4.5. In these minerals, the (PO_4) groups and ($M\varphi_6$) octahedra are linked together by hydrogen bonding.

In **struvite**, $[Mg(H_2O)_6][PO_4]$, the (PO_4) tetrahedra and ($Mg\{H_2O\}_6$) octahedra are linked solely by hydrogen bonding from the (H_2O) groups bonded to Mg directly to the anions of the (PO_4) groups, or by hydrogen bonding from the interstitial (NH_4) group (Fig. 4.11a). In **phosphorrösslerite**, $[Mg(H_2O)_6][PO_3(OH)](H_2O)$, the phosphate group is an acid phosphate, one of the phosphate anions being an (OH) group. The ($Mg\{H_2O\}_6$) octahedron hydrogen bonds to the ($P\varphi_4$) group, but there is also an interstitial (H_2O) group that is held in the structure solely by hydrogen bonding (Fig. 4.11b), acting both as a hydrogen-bond donor and as a hydrogen-bond acceptor.

4.4.2 Structures with finite clusters of (PO_4) tetrahedra and ($M\varphi_6$) octahedra

Phosphate minerals of this class are listed in Table 4.5.

M–T linkage. In **anapaite**, $Ca_2[Fe^{2+}(PO_4)_2(H_2O)_4]$, two ($PO_4$) groups link to *trans* vertices of an ($Fe^{2+}\varphi_6$) octahedron to form an $[M(TO_4)_2\varphi_4]$ cluster, where $M = Fe^{2+}$, $T = P$, and $\varphi = (H_2O)$ (Fig. 4.12a). These clusters are arranged in open layers parallel to (001) (Fig. 4.12b), and these layers are linked by Ca atoms and by hydrogen bonding. The atomic arrangement in **schertelite**, $(NH_4)_2[Mg\{PO_3(OH)\}_2(H_2O)_4]$, is similar to that in anapaite (and also the sulfate

TABLE 4.5. Phosphate minerals based on unconnected (PO_4) tetrahedra and ($M\Phi_6$) octahedra and finite clusters of (PO_4) tetrahedra and ($M\Phi_6$) octahedra

Mineral	Structural unit	Space group	Figure
	Isolated polyhedra		
Strüvite	$[Mg(H_2O)_6][PO_4]$	$Pmn2_1$	4.11a
Phosphorrösslerite	$[Mg(H_2O)_6][PO_3(OH)]$	$C2/c$	4.11b
	Clusters		
Anapaite	$[Fe^{2+}(PO_4)_2(H_2O)_4]$	$P\bar{1}$	4.12a,b
Schertelite	$[Mg(PO_3\{OH\}_2(H_2O)_4]$	$Pbca$	4.12c,d
Morinite	$[Al_2(PO_4)_2F_4(OH)(H_2O)_2]$	$P2_1/m$	4.12e,f

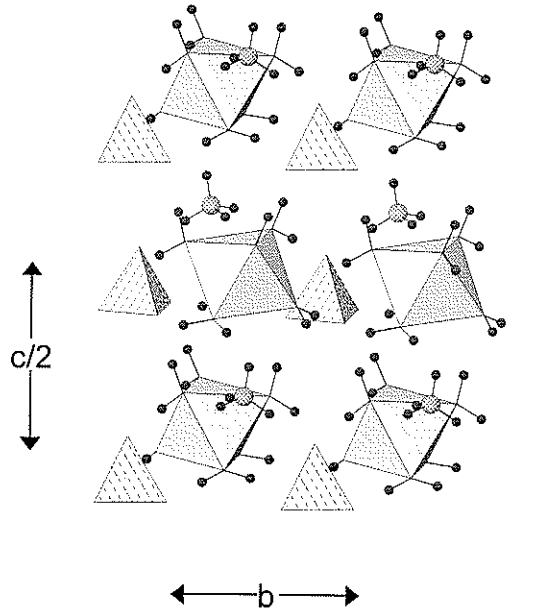

Figure 4.11. (a) struvite projected onto (100); (b) phosphorrösslerite projected onto (100); ($Mg\{H_2O\}_6$): shadow-shaded, hydrogen atoms: small grey circles, N (as part of the (NH_4) group): cross-shaded circles, O-atoms of interstitial (H_2O) groups: large grey circles.

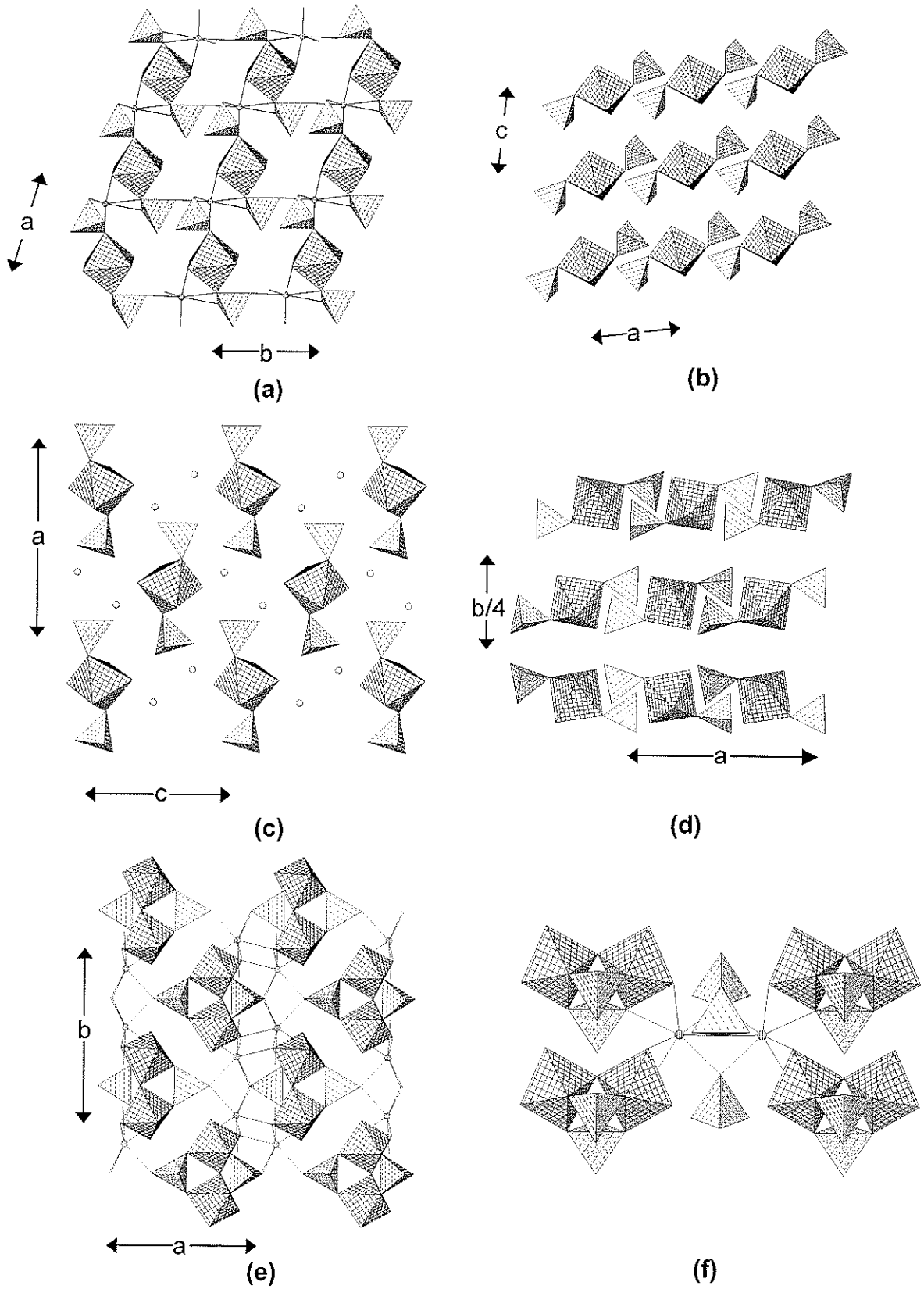

Figure 4.12. (a) anapaite projected onto (001); (b) anapaite projected onto (010); (c) schertelite projected onto (010); N: small circles; (d) schertelite projected onto (001); (e) morinite projected onto (001), Ca atoms: line-shaded circles, Na and hydrogen bonds are not shown; (f) morinite, showing the linkage of adjacent clusters by interstitial Ca atoms.

minerals bloedite, $Na_2[Mg(SO_4)_2(H_2O)_4]$, and leonite, $K_2[Mn^{2+}(SO_4)_2(H_2O)_4]$, Hawthorne 1985b). The $[Mg(PO_3\{OH\})_2(H_2O)_4]$ clusters are arranged in a centered rectangular array (Fig. 4.12c), with the projection of the long axis of the cluster parallel to the *a*-direction. The clusters are arranged in layers parallel to (010) (Fig. 4.12d), and the clusters are linked by hydrogen bonding involving (H_2O) groups of the cluster and interstitial (NH_4) groups.

M–M, M–T linkage. In **morinite**, $NaCa_2[Al_2(PO_4)_2F_4(OH)(H_2O)_2]$, two ($Al\varphi_6$) octahedra link through one vertex to form a dimer, and (two pairs of) vertices from each octahedron, *cis* to their common vertex, are linked by (PO_4) groups to form a cluster of the general form $[M_2(TO_4)_2\varphi_7]$. These clusters are arranged in a centered array when viewed down [001] (Fig. 4.12e). Adjacent clusters are linked by $^{[8]}Ca$ (Fig. 4.12f), $^{[5]}Na$ in triangular-bipyramidal coordination, and by hydrogen bonds. As shown by Hawthorne (1979a), this $[M_2(TO_4)_2\varphi_7]$ cluster is the basis of a short hierarchy of phosphate minerals of higher connectivity: minyulite, olmsteadite, hureaulite, phosphoferrite, kryzhanovskite, melonjosephite and whitmoreite.

4.4.3 Structures with infinite chains of (PO_4) tetrahedra and ($M\varphi_6$) octahedra

The minerals of this class are listed in Table 4.6. The topologically distinct chains and their corresponding graphs are shown in Fig. 4.13.

M–T linkage. **Bøggildite**, $Na_2Sr_2[Al_2(PO_4)F_9]$, is a rare phosphate-aluminofluoride mineral. The structural unit consists of a chain of alternating

TABLE 4.6. Phosphate minerals based on infinite chains of (PO_4) tetrahedra and ($M\Phi_6$) octahedra

Mineral	Structural unit	Space group	Figure
Bøggildite	$[Al_2(PO_4)F_9]$	$P2_1/c$	4.14a,b
Cassidyite	$[Ni(PO_4)_2(H_2O)_2]$	$P\bar{1}$	4.14c
Collinsite*	$[Mg(PO_4)_2(H_2O)_2]$	$P\bar{1}$	4.14c
Fairfieldite*	$[Mn^{2+}(PO_4)_2(H_2O)_2]$	$P\bar{1}$	4.14d
Messelite	$[Fe^{2+}(PO_4)_2(H_2O)_2]$	$P\bar{1}$	4.14d
Childrenite*	$[Al(PO_4)(OH)_2(H_2O)]$	*Bbam*	4.15a,b
Eosphorite	$[Al(PO_4)(OH)_2(H_2O)]$	*Bbam*	4.15a,b
Jahnsite*	$[Fe^{3+}(PO_4)_2(OH)]_2$	*P2/a*	4.15c,d
Rittmanite	$[Al(PO_4)_2(OH)]_2$	*P2/a*	4.15c,d
Whiteite	$[Al(PO_4)_2(OH)]_2$	*P2/a*	4.15c,d
Whiteite-(CaMnMg)	$[Al(PO_4)_2(OH)]_2$	*P2/a*	4.15c,d
Lun'okite	$[Al(PO_4)_2(OH)]_2$	*Pbca*	4.16a,b
Overite*	$[Al(PO_4)_2(OH)]_2$	*Pbca*	4.16a,b
Segelerite	$[Fe^{3+}(PO_4)_2(OH)]_2$	*Pbca*	4.16a,b
Wilhelmvierlingite	$[Fe^{3+}(PO_4)_2(OH)]_2$	*Pbca*	4.16a,b
Tancoite	$[Al(PO_4)_2(OH)]$	*Pbcb*	4.16c,d
Sinkankasite	$[Al(PO_3\{OH\})_2(OH)]$	$P\bar{1}$	4.16e,f
Bearthite	$[Al(PO_4)_2(OH)]$	$P2_1/m$	4.17a,b
Brackebuschite *	$[Mn^{3+}(VO_4)_2(OH)]$	$P2_1/m$	4.17a,b
Goedkenite	$[Al(PO_4)_2(OH)]$	$P2_1/m$	4.17a,b
Tsumebite	$[Cu^{2+}(PO_4)(SO_4)(OH)]$	$P2_1/m$	4.17a,b
Vauquelinite	$[Cu^{2+}(PO_4)(CrO_4)(OH)]$	$P2_1/n$	4.17c,d

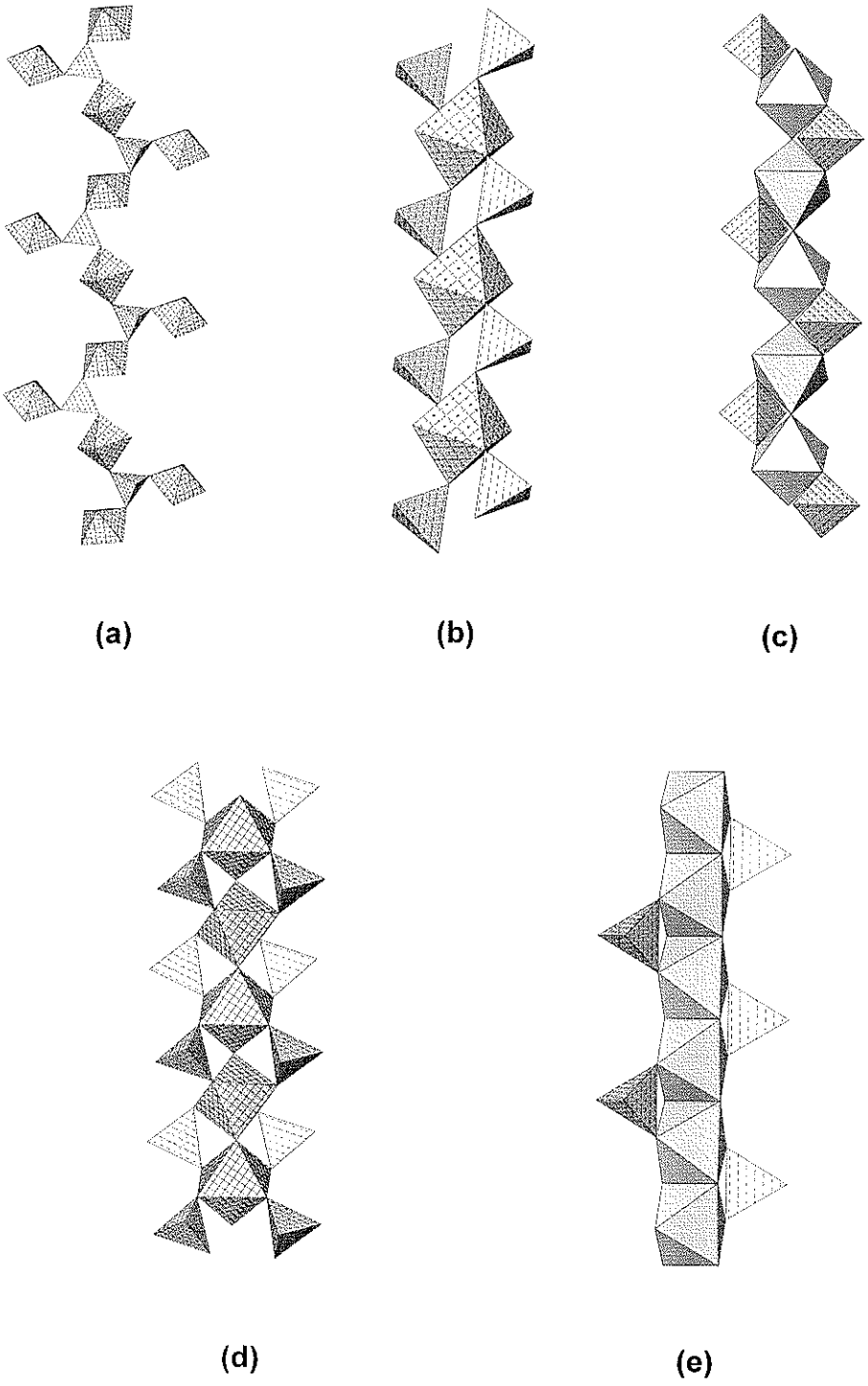

Figure 4.13. The topologically distinct chains of structures with infinite chains of (PO_4) tetrahedra and ($M\varphi_6$) octahedra. (a) the [$M(TO_4)\varphi_9$] chain in bøggildite; (b) the [$M(TO_4)_2\varphi_2$] chain in the minerals of the collinsite and fairfieldite groups; (c) the [$M(TO_4)\varphi_3$] chain in the minerals of the childrenite group; (d) the [$M(TO_4)_2\varphi$] chain in the minerals of the jahnsite group; (e) the [$M(TO_4)_2\varphi$] chain in bearthite (and the minerals of the brackebuschite group).

(PO_4) tetrahedra and (AlO_2F_4) octahedra that is decorated by flanking ($AlOF_5$) octahedra attached to the (PO_4) groups (Figs. 4.13a, 4.14a). The (PO_4) groups are three-connected and alternately point up and down along the length of the chain. The chains extends along the *b*-direction (Fig. 4.14b) and are linked by [8]- and [9]-coordinated Sr, and [7]- and [9]-coordinated Na. Bøggildite is the only phosphate-aluminofluoride mineral currently known.

The minerals of the **collinsite**, $Ca_2[Mg(PO_4)(H_2O)_2]$, and **fairfieldite**, $Ca_2[Mn^{2+}(PO_4)_2(H_2O)_2]$, groups are both based on a general $[M(TO_4)_2\varphi_2]$ chain that also occurs in the (non-phosphate) minerals of the kröhnkite, $Na_2[Cu^{2+}(SO_4)(H_2O)_2]$, group. This chain is formed of alternating ($M^{2+}O_4\{H_2O\}_2$) octahedra and pairs of (PO_4) tetrahedra (Figs 4.14c,d), with the (H_2O) groups in a *trans* arrangement about the divalent cation (Fig. 4.13b). The repeat distance along the length of the chain is ~5.45 Å, and this is reflected in the *c*-dimensions of these minerals. The minerals of the collinsite and fairfieldite groups are often incorrectly grouped together as the fairfieldite group because they all have triclinic symmetry. However, the interaxial angles in the two groups are significantly different (see Appendix). Adjacent chains in both structures are linked by [7]-coordinated Ca atoms and by hydrogen bonding. The two structures differ in the details of their hydrogen bonding (Figs. 4.14c,d).

M–M, M–T linkage. **Childrenite**, $Mn^{2+}(H_2O)[Al(PO_4)(OH)_2]$, consists of $[Al\varphi_5]$ chains in which ($Al\varphi_6$) octahedra link through pairs of *trans* vertices. The chains are decorated by (PO_4) groups that link adjacent octahedra and are arranged in a staggered fashion along the length of the chain (Fig. 4.13c) to give

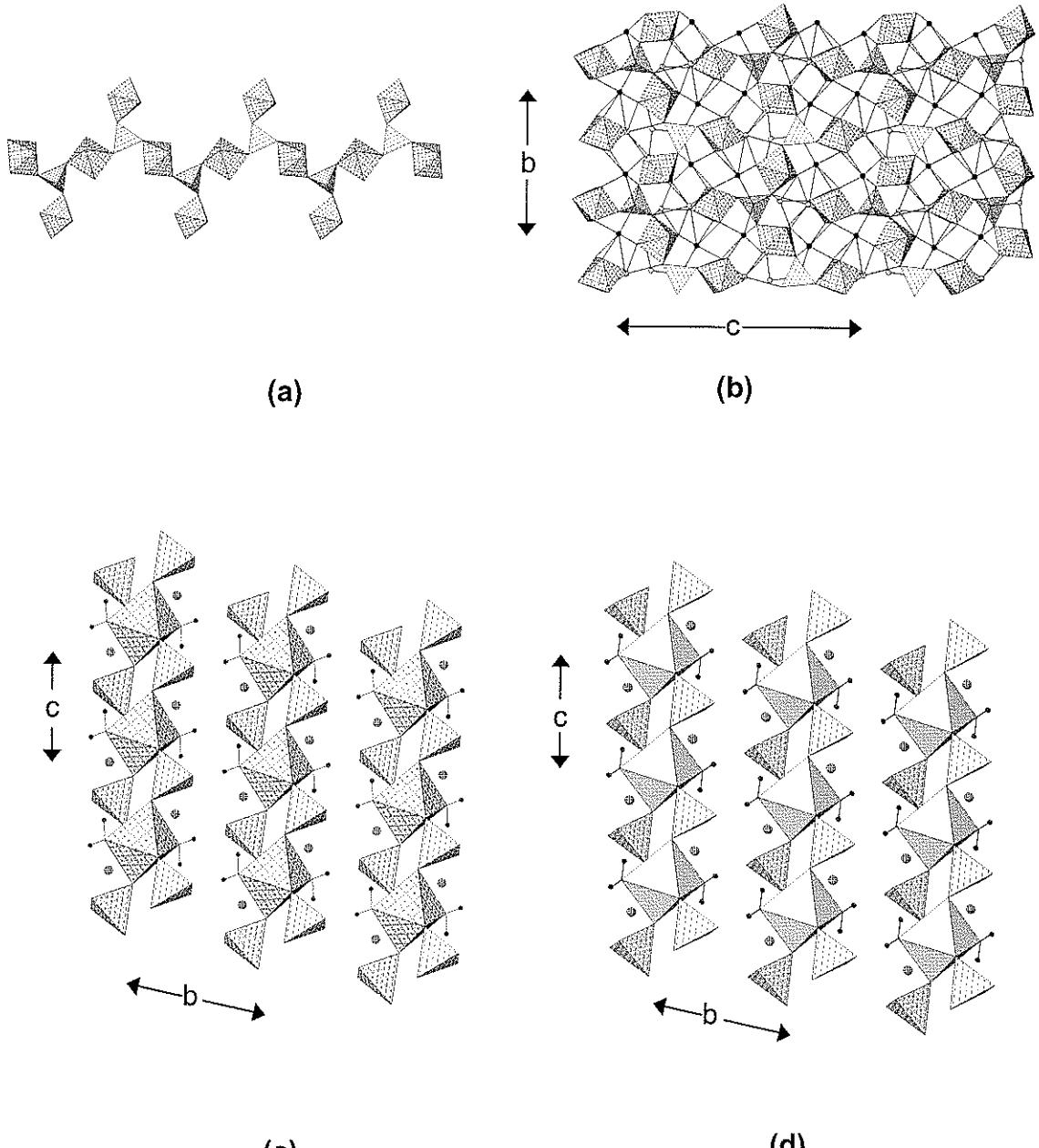

Figure 4.14. (a) the $[Al_2(PO_4)F_9]$ chain in bøggildite; (b) bøggildite projected onto (100), Ca atoms: black spheres, Na atoms: dotted spheres; (c) collinsite projected onto (100); (d) fairfieldite projected onto (100); Ca atoms: cross-shaded spheres, hydrogen atoms: small dark circles.

the general form $[M(TO_4)\varphi_3]$. The chains extend in the *c*-direction in childrenite (Fig. 4.15a) and are cross-linked by [6]-coordinated Mn^{2+}, the coordination octahedra of which form an edge-sharing chain in the *c*-direction. Viewed down [001], the chains are arranged at the vertices of a primitive orthorhombic net, and four adjacent chains are linked through one ($Mn^{2+}\varphi_6$) octahedra (Fig. 4.15b).

Jahnsite, $CaMn^{2+}Mg_2[Fe^{3+}(PO_4)_2(OH)](H_2O)_8$, consists of $[Fe^{3+}\varphi_5]$ chains of *trans*-corner-sharing octahedra that are decorated by bridging (PO_4) groups to give the general form $[M^{3+}(TO_4)_2\varphi]$ (Fig. 18d). These chains extend in the *b*-direction and have a repeat distance of ~7.1 Å, leading Moore (1970) to designate these, and related, chains, as the 7 Å chains. These chains are linked in the *a*-direction by [6]-coordinated Ca (Fig. 4.15c) that form chains of edge-sharing polyhedra in the *b*-direction, forming slabs (Fig. 4.15d) parallel to (100) that are linked by octahedrally coordinated divalent-metal cations and by hydrogen bonding. In addition to the minerals of this group listed in Table 4.6, Matsubara (2000) reports the Fe^{2+} equivalent of jahnsite, ideally $CaFe^{2+}Fe^{2+}{}_2[Fe^{3+}(PO_4)_2(OH)]_2(H_2O)_8$, but this has not been approved as a valid species by the IMA.

Overite, $Ca_2Mg_2[Al(PO_4)_2(OH)]_2(H_2O)_8$, and **tancoite**, $Na_2LiH[Al(PO_4)_2(OH)]$, are both based on the $[Al(PO_4)_2(OH)]$ chain that is shown in Figure 4.13d, and in both structures, this chain defines the *c*-dimension, 7.11 Å in overite and 7.03 x 2 = 14.06 Å in tancoite. ($Al\varphi_6$) octahedra link through one set of *trans* vertices, corresponding to the (OH) groups, to form an $[Al\varphi_5]$ chain. Adjacent octahedra are linked by pairs of (PO_4) tetrahedra that point alternately

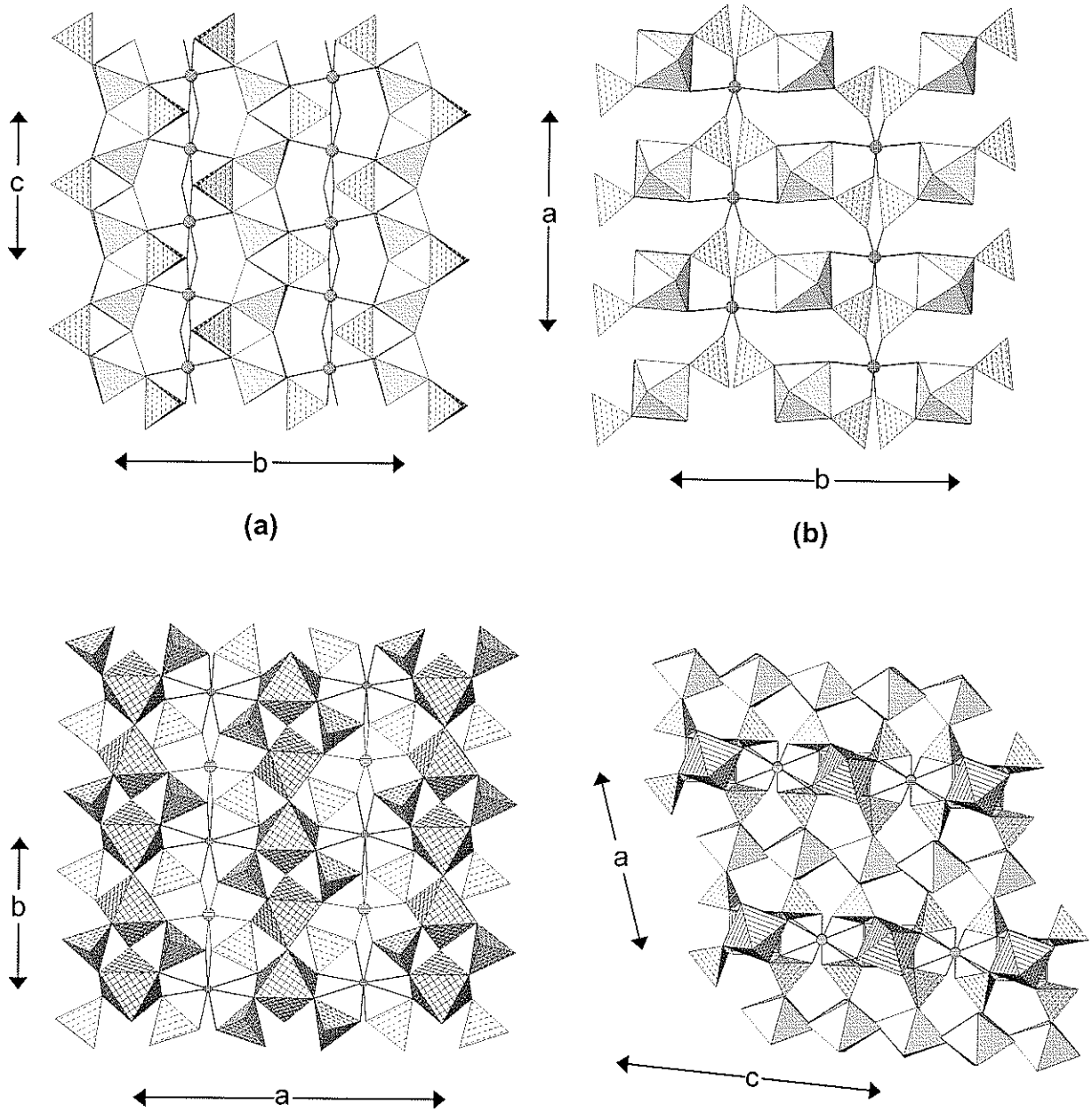

Figure 4.15. The crystal structures of childrenite and jahnsite; (a) childrenite projected onto (100); (b) childrenite projected onto (001), ($Al\Phi_6$): shadow-shaded, Mn^{2+} cations: cross-hatched circles; (c) jahnsite projected onto (001); (d) jahnsite projected onto (010); ($Fe^{3+}\Phi_6$): cross-hatched, Ca atoms: line-shaded circles, ($Mn^{2+}\Phi_6$) and ($Mg\Phi_6$): shadow-shaded.

up and down the *b*-direction in overite (Fig. 4.16a) and the *a*-direction in tancoite (Fig. 4.16c). In overite, the chains are linked in the *a*-direction by [8]-coordinated Ca to form slabs parallel to (010), the Ca linking to both tetrahedra and octahedra. These slabs are linked in the *b*-direction by ($MgO_2\{H_2O\}_4$) octahedra (Fig. 4.16b), and the resulting structure is strengthened by hydrogen bonds from the (H_2O) groups, all of which are bonded to the interstitial Mg cations. In tancoite, the chains are linked in the *b*-direction by [8]-coordinated Na and [5]-coordinated Li, forming slabs parallel to (100) (Fig. 4.16c). These slabs are linked in the *a*-direction by [8]-coordinated Na (Fig. 4.16d). In addition, there is a symmetrical hydrogen-bond between two anions of adjacent (PO_4) groups.

Sinkankasite, $Mn^{2+}(H_2O)_4[Al(PO_3\{OH\})_2(OH)](H_2O)_2$, is also based on the $[M(T\varphi_4)_2\varphi]$ chain of Figure 4.13d, extending in the *c*-direction to give a repeat of ~7 Å. However, it is topochemically different from the analogous chain in overite and tancoite as one of the tetrahedron vertices is occupied by (OH), forming an acid-phosphate group. The chains are linked in the *b*-direction (Fig. 4.16e) by ($Mn^{2+}O_2\{H_2O\}_4$) octahedra to form a thick slab parallel to (100). These slabs stack in the *a*-direction (Fig. 4.16f) and are linked solely by hydrogen bonds involving the H atom of the acid-phosphate group, the (H_2O) groups of the interstitial ($Mn^{2+}O_2\{H_2O\}_4$) octahedron, and interstitial (H_2O) groups not bonded directly to any cations.

M=M, M–T linkage. **Bearthite**, $Ca_2[Al(PO_4)_2(OH)]$, contains ($Al\varphi_6$) octahedra which share one set of *trans* edges with adjacent octahedra to form an $[Al\varphi_4]$ chain. Adjacent octahedra are linked (bridged) by (PO_4) tetrahedra in a staggered arrangement on either side of the chain to form a decorated chain of

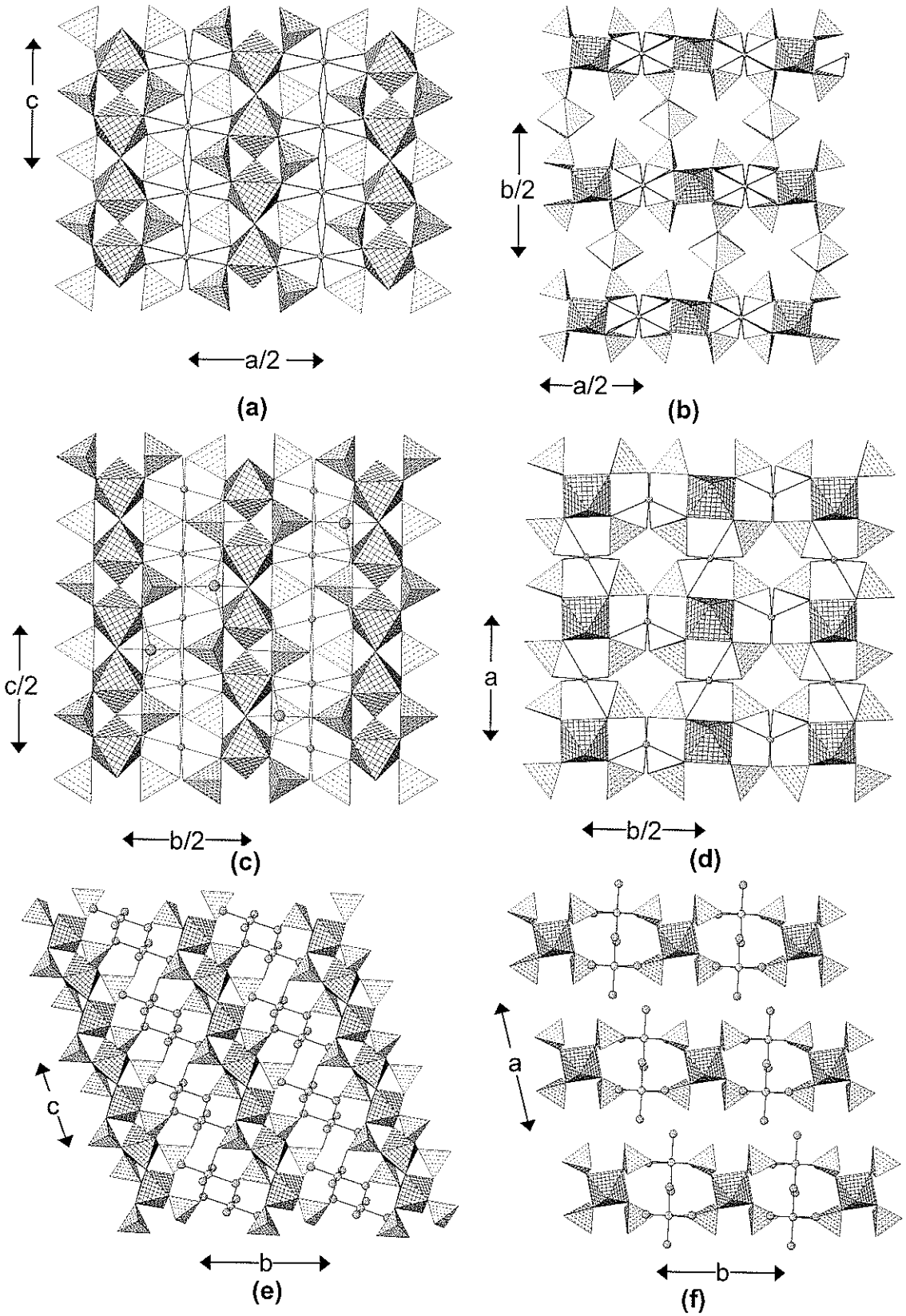

Figure 4.16. (a) overite projected onto (010); (b) overite projected onto (001); (c) tancoite projected onto (100), Ca atoms: small 4^4-shaded circles; (d) tancoite projected onto (001), Na atoms: small 4^4-shaded circles; (e) sinkankasite projected onto (100); (f) sinkankasite projected onto (001), Li atoms: large black circles. Hydrogen atoms and bonds are omitted, ($Al\varphi_6$): line-shaded.

the general form $[M(TO_4)_2\varphi]$ (Fig. 4.13e). These chains are linked in the *a*-direction by [10]-coordinated Ca (Fig. 4.17a). Viewed along [010] (Fig. 4.17b), the chains resemble four-membered pinwheels; linkage in the *c*-direction is also provided by interstitial Ca cations. A topologically identical chain, $[M(TO_4)_2\varphi]$, occurs in **vauquelinite**, $Pb^{2+}{}_2[Cu^{2+}(PO_4)(CrO_4)(OH)]$; however, there are two symmetrically (and chemically) distinct tetrahedra in vauquelinite, (PO_4) and (CrO_4) (Fig. 4.17c). In vauquelinite, $(Cu^{2+}\varphi_6)$ octahedra form the $[M\varphi_4]$-type chain, (PO_4) tetrahedra bridge vertices of adjacent octahedra in the chain, and (CrO_4) tetrahedra link to one vertex of the edge shared between adjacent octahedra (Fig. 4.17c). The resulting $[Cu^{2+}(PO_4)(CrO_4)(OH)]$ chains extend in the *b*-direction, and are linked in the *a*-direction and *c*-direction by [9]-coordinated Pb^{2+}. When viewed end-on (Fig. 4.17d), the chains resemble four-membered pinwheels.

4.4.4 Structures with infinite sheets of (PO_4) tetrahedra and $(M\varphi_6)$ octahedra

The minerals of this class are listed in Table 4.7.

M–T linkage. The minerals of the **olmsteadite**, $K_2Fe^{2+}{}_4(H_2O)_4[Nb_2(PO_4)_4O_4]$, group consist of (PO_4) tetrahedra and (NbO_6) octahedra at the vertices of a 4^4 plane net, linked by sharing corners to form a sheet parallel to (100) (Fig. 4.18a). In the *c*-direction, the (PO_4) groups link to *trans* vertices of the (NbO_6) octahedra, but in the *b*-direction, the (PO_4) groups link to *cis* vertices of the (NbO_6) octahedra, and these *cis* vertices alternate above and below the plane of the sheet in the *b*-direction. The sheets link in pairs

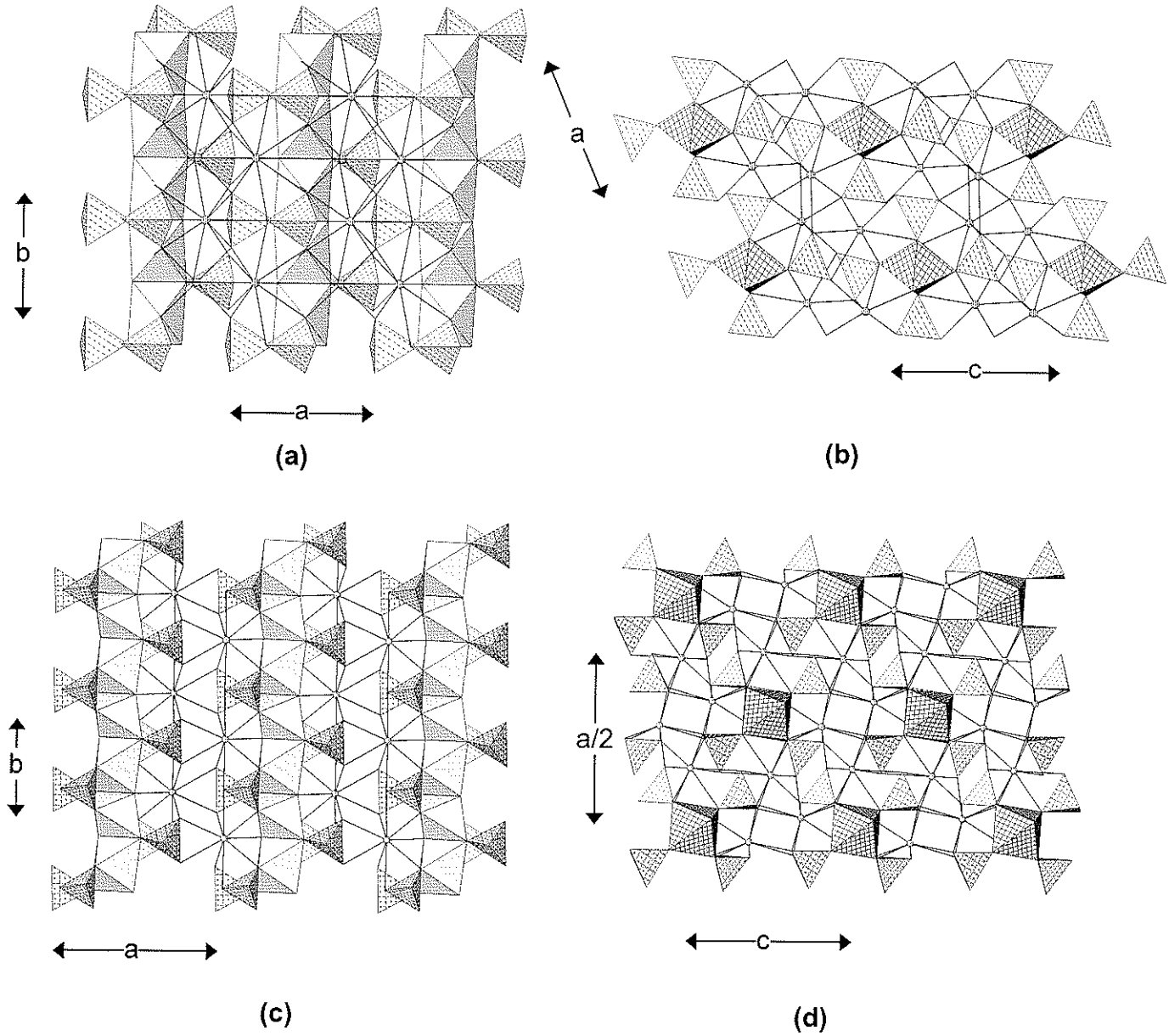

Figure 4.17. (a) bearthite projected onto (001); (b) bearthite projected onto (010), ($Al\varphi_6$): shadow-shaded in (a) and 4^4-net-shaded in (b), Ca atoms: vertical-line-shaded circles; (c) vauquelinite projected onto (100); (d) vauquelinite projected onto (010). (CrO_4): square-pattern-shaded, ($Cu\Phi_6$): shadow-shaded (c) and 4^4-net shaded (d), interstitial Pb^{2+} atoms: diagonal-line-shaded circles.

TABLE 4.7. Phosphate minerals based on infinite sheets of (PO_4) tetrahedra and ($M\Phi_6$) octahedra

Mineral	Structural unit	Space group	Figure
Johnwalkite	$[Nb(PO_4)_2O_2]$	$Pb2_1m$	4.18a,b
Olmsteadite*	$[Nb(PO_4)_2O_2]$	$Pb2_1m$	4.18a,b
Brianite	$[Mg(PO_4)_2]$	$P2_1/c$	4.18c,d
Merwinite*	$[Mg(SiO_4)_2]$	$P2_1/c$	4.18c,d
Newberyite	$[Mg(PO_3OH)(H_2O)_3]$	$Pbca$	4.19a,b
Hannayite	$[Mg_3(PO_3\{OH\})_4]$	$P\bar{1}$	4.19c,d
Minyulite	$[Al_2(PO_4)_2F(H_2O)_4]$	$Pba2$	4.20a,b
Benauite	$[Fe^{3+}{}_3(PO_4)(PO_3\{OH\})(OH)_6]$	$R\bar{3}m$	4.20c,d
Crandallite	$[Al_3(PO_4)(PO_3\{OH\})(OH)_6]$	$R\bar{3}m$	4.20c,d
Eylettersite	$[Al_3(PO_4)(PO_3\{OH\})(OH)_6]$	$R\bar{3}m$	4.20c,d
Florencite-(Ce)	$[Al_3(PO_4)(PO_3\{OH\})(OH)_6]$	$R\bar{3}m$	4.20c,d
Florencite-(La)	$[Al_3(PO_4)(PO_3\{OH\})(OH)_6]$	$R\bar{3}m$	4.20c,d
Florencite-(Nd)	$[Al_3(PO_4)(PO_3\{OH\})(OH)_6]$	$R\bar{3}m$	4.20c,d
Gorceixite	$[Al_3(PO_4)(PO_3\{OH\})(OH)_6]$	$R\bar{3}m$	4.20c,d
Plumbogummite	$[Al_3(PO_4)(PO_3\{OH\})(OH)_6]$	$R\bar{3}m$	4.20c,d
Waylandite	$[Al_3(PO_4)(PO_3\{OH\})(OH)_6]$	$R\bar{3}m$	4.20c,d
Zairite	$[Fe^{3+}{}_3(PO_4)_2(OH)_6]$	$R\bar{3}m$	4.20c,d
Gordonite	$[Al_2(PO_4)_2(OH)_2(H_2O)_2]$	$P\bar{1}$	4.21a,b
Laueite*	$[Fe^{3+}_2(PO_4)_2(OH)_2(H_2O)_2]$	$P\bar{1}$	4.21a,b
Mangangordonite	$[Al_2(PO_4)_2(OH)_2(H_2O)_2]$	$P\bar{1}$	4.21a,b
Paravauxite	$[Al_2(PO_4)_2(OH)_2(H_2O)_2]$	$P\bar{1}$	4.21a,b
Sigloite	$[Al_2(PO_4)_2(OH)_2(H_2O)_2]$	$P\bar{1}$	4.21a,b
Ushkovite	$[Fe^{3+}_2(PO_4)_2(OH)_2(H_2O)_2]$	$P\bar{1}$	4.21a,b
Curetonite	$[Al(PO_4)(OH)]$	$P2_1/n$	4.21c,d
Kastningite	$[Al_2(PO_4)_2(OH)_2(H_2O)_2]$	$P\bar{1}$	4.22a,b
Stewartite*	$[Fe^{3+}_2(PO_4)_2(OH)_2(H_2O)_2]$	$P\bar{1}$	4.22a,b
Pseudolaueite	$[Fe^{3+}(PO_4)(OH)(H_2O)]_2$	$P2_1/a$	4.22c,d
Strunzite*	$[Fe^{3+}(PO_4)(OH)(H_2O)]_2$	$P\bar{1}$	4.23a,b
Ferrostrunzite	$[Fe^{3+}(PO_4)(OH)(H_2O)]_2$	$P\bar{1}$	4.23a,b
Metavauxite	$[Al(PO_4)(OH)(H_2O)]_2$	$P2_1/c$	4.23c,d
Montgomeryite	$[MgAl_4(PO_4)_6(OH)_4(H_2O)]$	$C2/c$	4.24a,b
Mitryaevaite	$[Al_5(PO_4)_2(PO_3\{OH\})_2F_2(OH)_2(H_2O)_8]$	$P\bar{1}$	4.24c,d

TABLE 4.7. continued

Mineral	Structural unit	Space group	Figure
Bonshtedite	$[Fe^{2+}(PO_4)(CO_3)]$	$P2_1/m$	4.24e,f
Bradleyite*	$[Mg(PO_4)(CO_3)]$	$P2_1/m$	4.24e,f
Sidorenkoite	$[Mn^{2+}(PO_4)(CO_3)]$	$P2_1/m$	4.24e,f
Bermanite*	$[Mn^{3+}(PO_4)(OH)]_2$	$P2_1$	4.25a,b
Ercitite	$[Mn^{3+}(PO_4)(OH)]_2$	$P2_1/n$	4.25a,b
Schoonerite	$[Mn^{2+}Fe^{2+}{}_2ZnFe^{3+}(PO_4)_3(OH)_2(H_2O)_7]$	$Pmab$	4.25c,d
Nissonite	$[Cu^{2+}Mg(PO_4)(OH)(H_2O)_2]$	$C2/c$	4.26a,b,c
Foggite	$[Al(PO_4)(OH)_2]$	$A2_122$	4.27a,b,c
Earlshannonite	$[Fe^{3+}(PO_4)(OH)]_2$	$P2_1/c$	4.27d,e
Whitmoreite*	$[Fe^{3+}(PO_4)(OH)]_2$	$P2_1/c$	4.27d,e
Mitridatite*	$[Fe^{3+}_3(PO_4)_3O_2]$	Aa	4.28a
Robertsite	$[Mn^{3+}_3(PO_4)_3O_2]$	Aa	4.28a
Arupite	$[Ni_3(PO_4)_2(H_2O)_8]$	$C2/m$	4.29a,b
Vivianite *	$[Fe^{2+}{}_3(PO_4)_2(H_2O)_8]$	$C2/m$	4.29a,b
Bobierrite	$[Mg_3(PO_4)_2(H_2O)_8]$	$C2/c$	4.29c,d

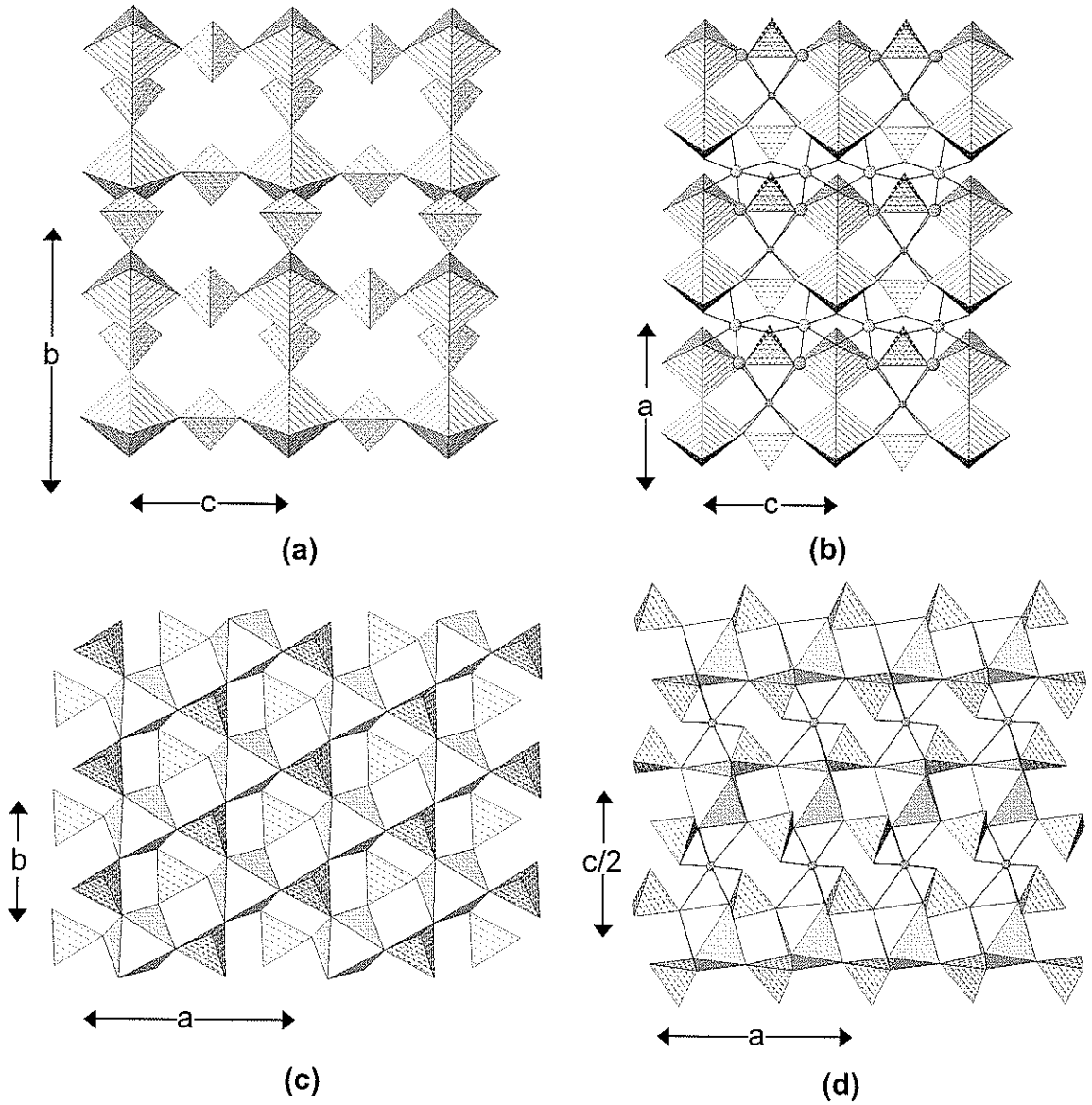

Figure 4.18. (a) olmsteadite projected onto (100); (b) olmsteadite projected onto (010), (NbO_6): line-shaded, Fe^{2+} atoms: line-shaded circles, (H_2O) groups: dot-shaded circles; (c) brianite projected onto (001); (d) brianite projected onto (010), (MgO_6): shadow-shaded, interstitial cations: circles.

by sharing octahedron corners to form slabs that incorporate the interstitial [8]-coordinated K (Fig. 4.18b). These slabs are linked in the *a*-direction by [$M\varphi_4$] chains of ($Fe^{2+}\varphi_6$) octahedra that extend in the *c*-direction.

Brianite, $Na_2Ca[Mg(PO_4)_2]$ is a member of the merwinite group (Table 4.7) and consists of (PO_4) tetrahedra and (MgO_6) octahedral. The (PO_4) groups link to both the upper and lower corners of the octahedra (Fig. 4.18c) to form pinwheels (Moore 1973b) and the resulting sheet has a layer of octahedra inserted in between two layers of tetrahedra (Fig. 4.18d). These sheets are linked in the *c*-direction by interstitial Na and Ca.

Newberyite, $[Mg(PO_3\{OH\})(H_2O)_3]$, consists of ($P\varphi_4$) tetrahedra and ($Mg\varphi_6$) octahedra and the two different types of polyhedra alternate on any path through the resultant network (Fig. 4.19a). The (PO_4) tetrahedra point both up and down relative to the plane of the sheet. Both tetrahedra and octahedra are three-connected, and all one-connected vertices in the net are 'tied-off' by H atoms. Thus the ($P\varphi_4$) group is actually an acid-phosphate group, ($PO_3\{OH\}$), and the three one-coordinated anions of the ($Mg\varphi_6$) octahedron are (H_2O) groups. Hawthorne (1992) used newberyite as an example of the role of H atoms in controlling the dimensional character of a structural unit. The sheets in newberyite stack in the *b*-direction (Fig. 4.19b) and are linked solely by hydrogen bonds. Newberyite undergoes a low-temperature crystal-to-amorphous transition (Sales et al., 1993). When heated above 150°C, newberyite becomes amorphous. With continued heating above 150°C, the amorphous phase develops chains of polymerized (PO_4) tetrahedra (up to 13 tetrahedra long), until

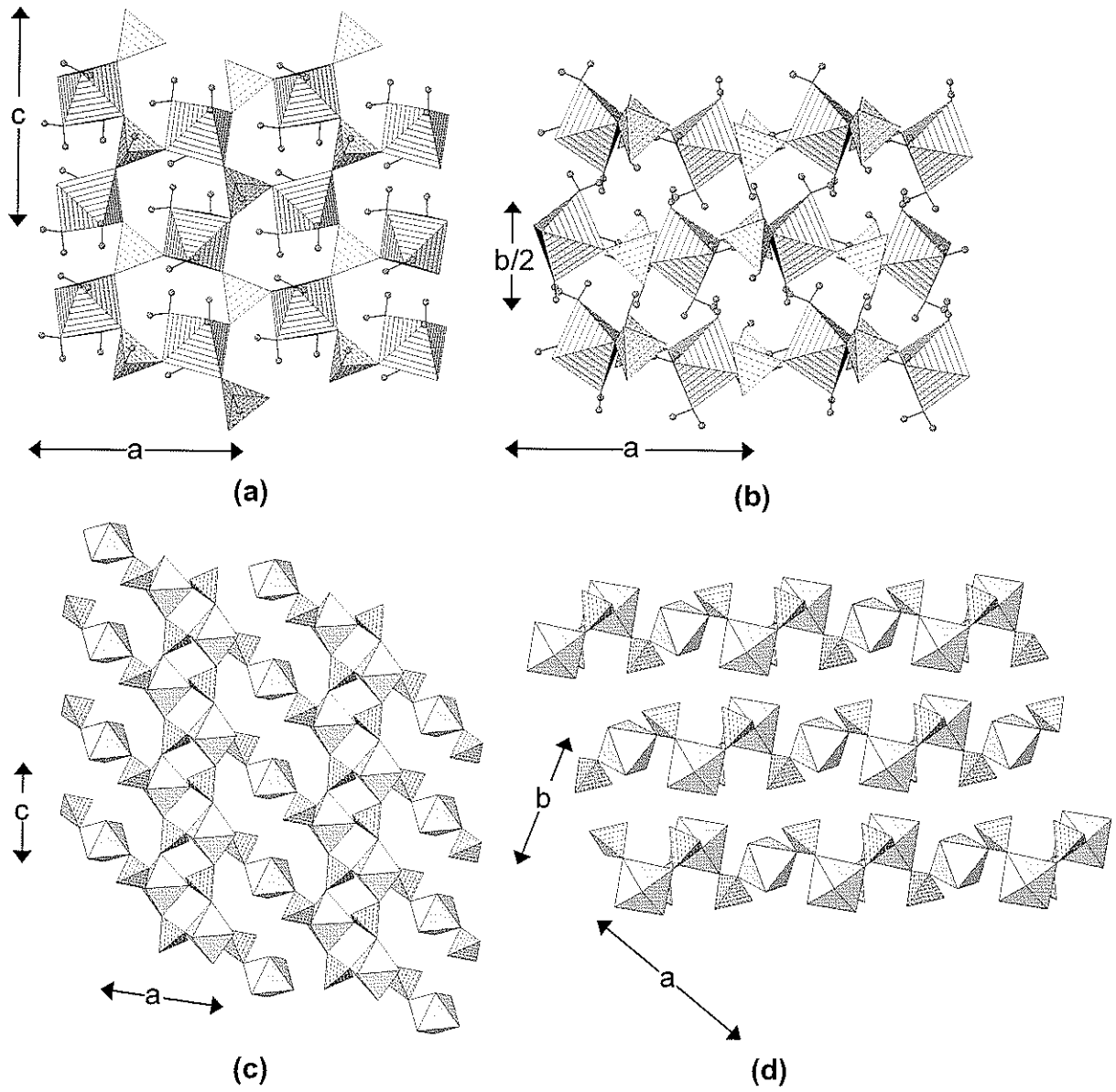

Figure 4.19. (a) newberyite projected onto (010); (b) newberyite projected onto (001), ($Mg\varphi_6$): line-shaded, H atoms: small dark-shaded circles; (c) hannayite projected onto (010); (d) hannayite projected onto (001), ($Mg\varphi_6$): shadow-shaded.

at 600 °C, crystalline $Mg_2P_2O_7$ forms. Heating under (unspecified) pressure results in a phase of the form $Mg_3(PO_3\{OH\})[P_2O_7](H_2O)_{4.5}$, the only known crystalline phosphate containing two different phosphate anions (Sales et al., 1993).

Hannayite, $(NH_4)_2[Mg_3(PO_3\{OH\})_4(H_2O)_{xx}](H_2O)_{yy}$, consists of a sheet of alternating $(PO_3\{OH\})$ tetrahedra and $(Mg\varphi_6)$ octahedral. Alternating tetrahedra and octahedra connect to form an $[M(TO_4)\varphi_4]$ chain. Pairs of these chains attach together by sharing corners between tetrahedra and octahedra to form ribbons of the type $[M(TO_4)\varphi_3]$ that extend in the *c*-direction. These ribbons are linked in the *a*-direction by $[Mg(PO_4)_2\varphi_4]$ clusters to form a sheet parallel to (010) (Fig. 4.19c). These sheets stack in the *b*-direction (Fig. 4.19d) and are linked by hydrogen bonds directly from sheet to sheet, and by hydrogen bonds involving the interstitial (NH_4) groups.

M–M, M–T linkage. **Minyulite**, $K[Al_2(PO_4)_2F(H_2O)_4]$, contains a sheet that is made up of $[Al_2(PO_4)_2F(H_2O)_4O_2]$ clusters that are topologically identical to the $[Al_2(PO_4)_2F_4(OH)(H_2O)_2]$ clusters in morinite (Fig. 4.12e). These clusters (Fig. 4.20a) link by sharing vertices between tetrahedra and octahedra. This arrangement leads to large interstices within the sheet, and these are occupied by [10]-coordinated K atoms (Fig. 4.20a); the sheet is parallel to (001). When viewed in the *b*-direction; it can be seen (Fig. 20b) that each sheet consists of a layer of tetrahedra and a layer of octahedra. The interstitial K atoms actually lie completely *within* each sheet and hence do not participate in intersheet linkage. All (H_2O) groups of the structural unit occur on the one side of each sheet (Fig.

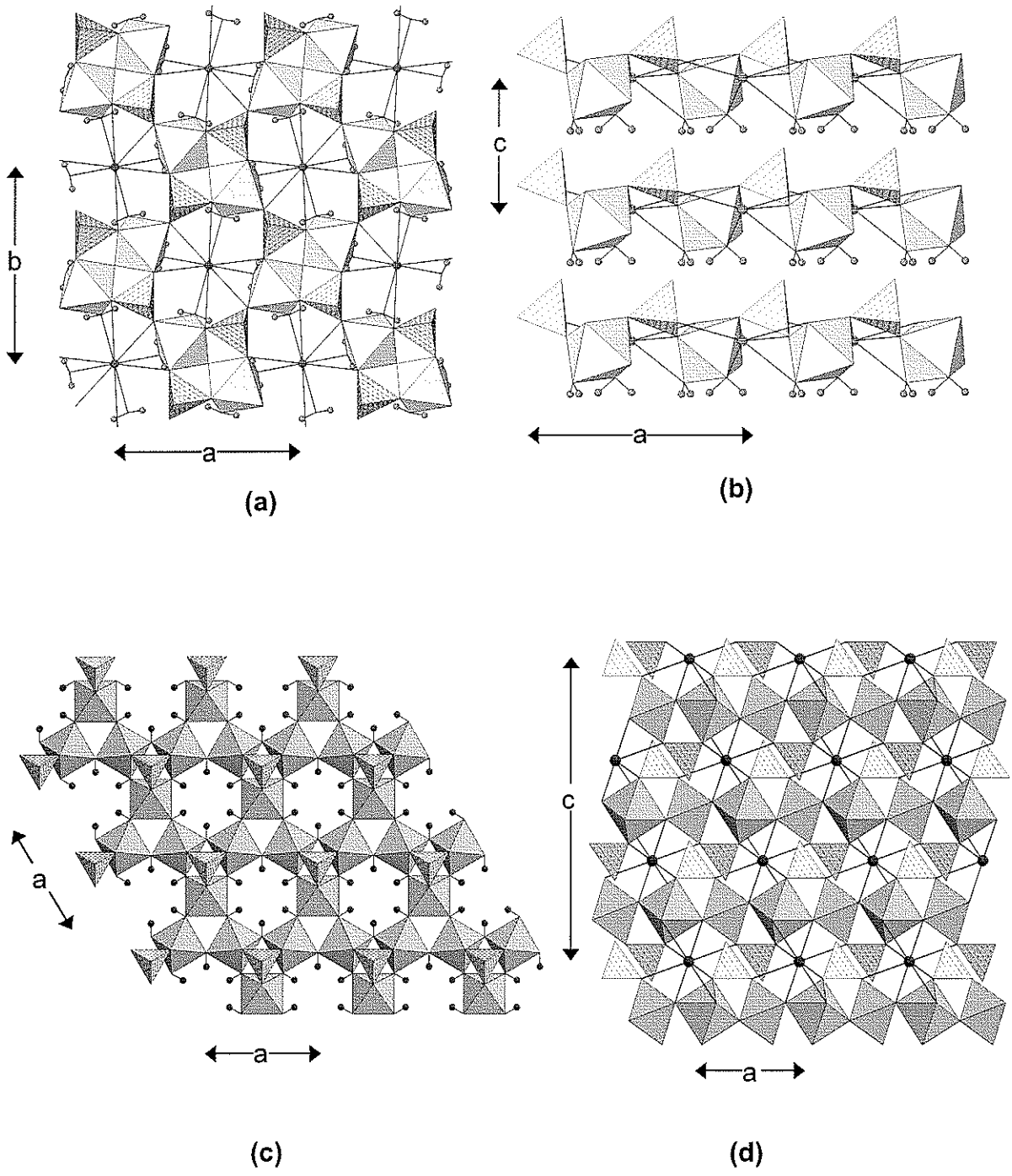

Figure 4.20. (a) minyulite projected onto (001); (b) minyulite projected onto (010), ($Al\varphi_6$): shadow-shaded, H atoms: small dark-shaded circles, K atoms: larger wavy-line-shaded circles; (c) crandallite projected onto (001); (d) crandallite projected onto (010), ($Al\varphi_6$): shadow-shaded, H atoms: small dark-shaded circles, interstital Ca atoms: larger dark-shaded circles.

20b) and adjacent sheets are linked solely by hydrogen bonds.

A prominent feature in **laueite**, $Mn^{2+}(H_2O)_4[Fe^{3+}{}_2(PO_4)_2(OH)_2(H_2O)_2](H_2O)_2$, and the minerals of the laueite group (Table 4.7) is the 7 Å chain shown in Fig. 4.13c. ($Fe^{3+}\varphi_6$) octahedra link by sharing vertices to form an $[M\varphi_5]$ chain that is decorated by flanking (PO_4) groups, and the resulting chains extend in the *c*-direction, giving a *c*-repeat of ~7.1 Å (see Appendix A). These chains link in the *a*-direction by sharing one quarter of the flanking (PO_4) vertices with octahedra of adjacent chains to form an $[Fe^{3+}{}_2(PO_4)_2(OH)_2(H_2O)_2]$ sheet (Fig. 4.21a); note that the sheet is written with two octahedrally coordinated cations, rather than as $[M(TO_4)\varphi_2]_2$ because the two octahedra are topologically distinct. In the resulting sheet, the (PO_4) tetrahedra are three-connected. Note that there are two distinct octahedra in these sheets, one of which is six-connected within the sheet, and the other of which is only four-connected and has (H_2O) at two vertices. Another prominent feature of this sheet is the $[M(TO_4)_2\varphi_2]$ chain (Fig. 4.13b) that extends from SE to NW in Fig. 4.21a. Thus the laueite sheet can also be though of being composed of $[Fe^{3+}(PO_4)_2O_2]$ chains that are linked by ($Fe^{3+}O_6$) octahedra. This occurrence of two different types of chain in a more highly connected structural unit is a common feature in minerals. These sheets stack in the *b*-direction and are linked by ($Mn^{2+}O_2\{H_2O\}_4$) octahedra (Fig. 4.21b), and by hydrogen bonds involving the interstitial (H_2O) groups bonded to Mn^{2+} *and* interstitial (H_2O) groups held in the structure solely by hydrogen bonds.

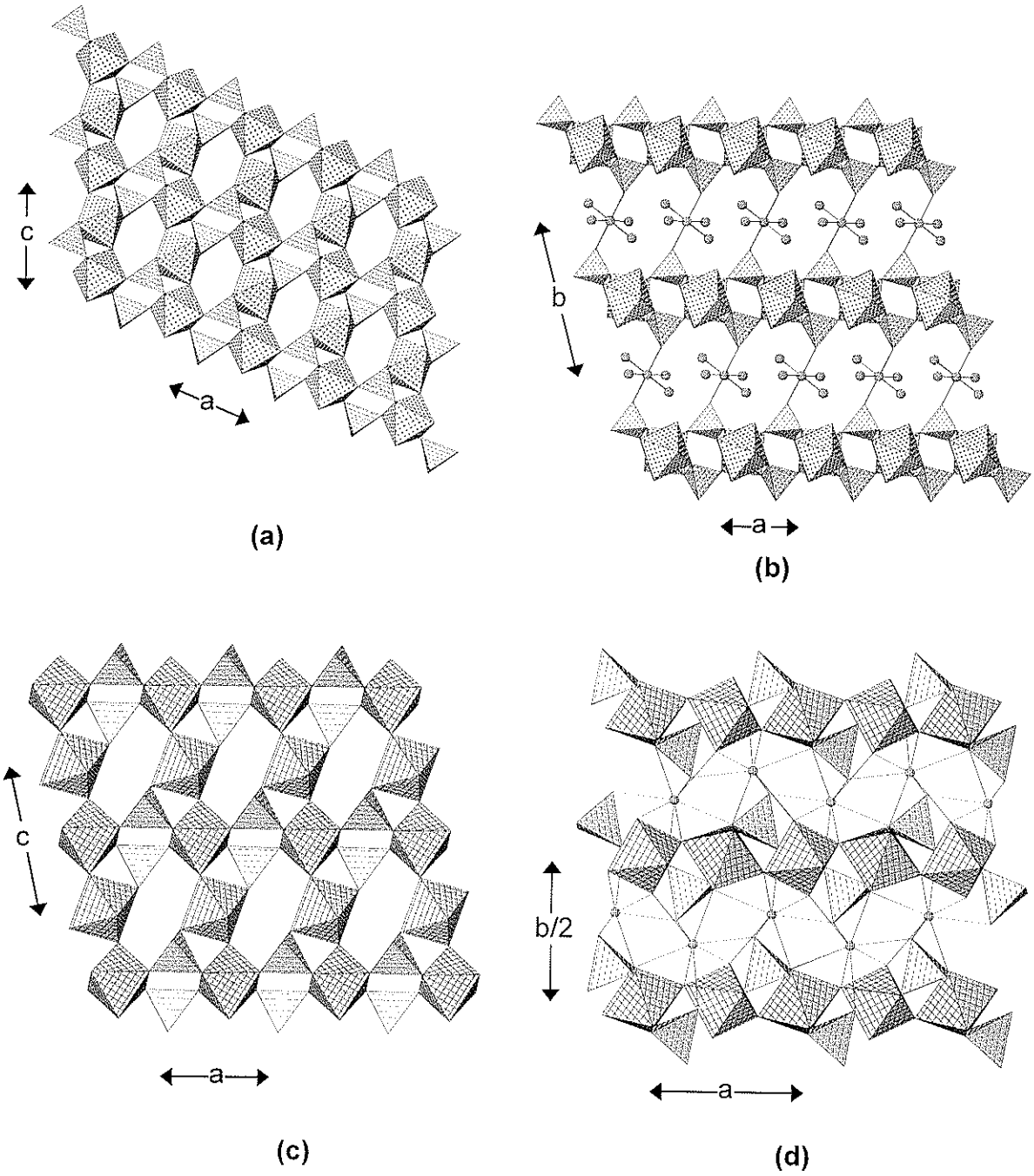

Figure 4.21. (a) laueite projected onto (010); (b) laueite projected onto (001); (c) curetonite projected onto (010); (d) curetonite projected onto (001), ($Fe\varphi_6$) and ($Al\varphi_6$): cross-shaded (a,d) and 4^4 –net-shaded (c,d), Mn^{2+} and Ba atoms: diagonal-line circles (a,b) and 4^4-net shaded circles (c,d), selected (H_2O) groups: grey circles.

Curetonite, $Ba_2[Al_2(PO_4)_2(OH)_2F_2]$, contains an $[Al_2(PO_4)_2(OH)_2F_2]$ sheet (Fig. 4.21c) topologically identical to the analogous sheet in laueite (Figs. 4.21a). Note that the formula of curetonite has previously been written as half the formula unit given above, but that formulation ignored the fact that there are two topologically distinct ($Al\varphi_6$) octahedra in the structural unit. There is also replacement of Al by Ti and (OH) by O^{2-}, which can give local areas of titanite-like arrangement within the sheet. The sheets stack in the *b*-direction (Fig. 4.21d) and are linked by interstitial [10]-coordinated Ba.

Stewartite, $Mn^{2+}(H_2O)_4[Fe^{3+}{}_2(PO_4)_2(OH)_2(H_2O)_2](H_2O)_2$, and **pseudolaueite**, $Mn^{2+}(H_2O)_4[Fe^{3+}{}_2(PO_4)_2(OH)_2(H_2O)_2](H_2O)_2$, are polymorphs of laueite. Both contain $[Fe^{3+}{}_2(PO_4)_2(OH)_2(H_2O)O^P{}_2]$ chains (*cf.* Fig. 4.13c), but the way in which these chains cross-link to form a sheet is different from the analogous linkage in laueite. In stewartite, there are three symmetrically distinct ($Fe\varphi_6$) octahedra in the 7 Å chain, with coordinations ($\{OH\}_2O_2\{H_2O\}_2$), ($\{OH\}_2O_2\{H_2O\}_2$) and ($\{OH\}_2O_4$) with multiplicities of 1, 1 and 2, respectively, whereas in laueite, there are two symmetrically distinct ($Fe\varphi_6$) octahedra in the 7 Å chain, with coordinations ($\{OH\}_2O_2\{H_2O\}_2$) and ($\{OH\}_2O_4$) with multiplicities of 2 and 2, respectively. However, the cross-linkage of chains is different from in laueite, as is apparent from the presence of $[Fe^{3+}(PO_4)_2\varphi_2]$ chains in laueite (Fig. 4.21a) and only fragments of this chain in stewartite (Fig. 4.22a). These sheets stack in the *c*-direction, linked by ($Mn^{2+}O_2\{H_2O\}_4$) octahedra (Fig. 4.22b) and hydrogen bonds involving (H_2O) bonded to interstitial cations and (H_2O) held in the structure solely by hydrogen bonding. In pseudolaueite, the

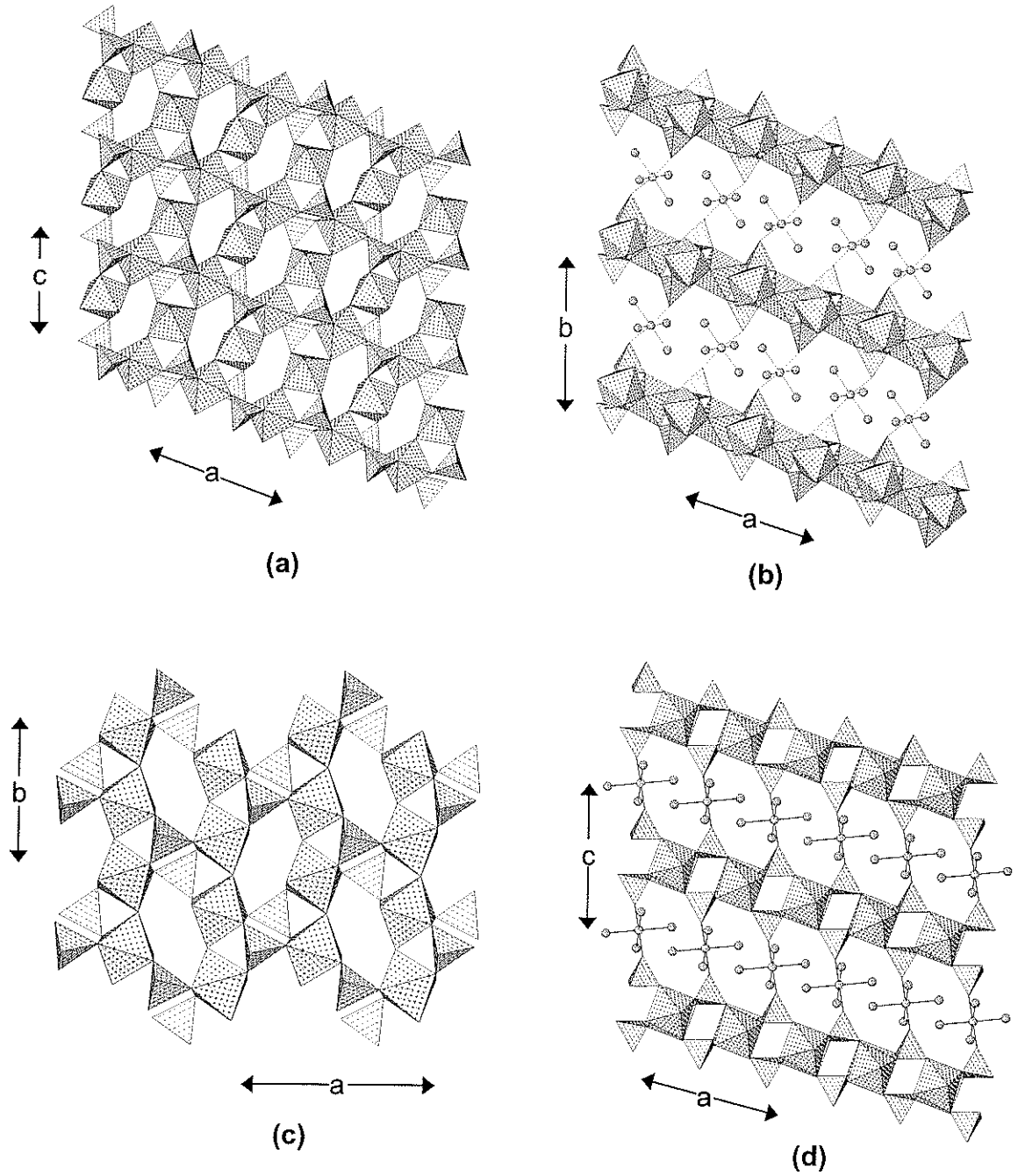

Figure 4.22. (a) stewartite projected onto (010); (b) stewartite projected onto (001); (c) pseudolaueite projected onto (001); (d) pseudolaueite projected onto (010), ($Fe^{3+}\varphi_6$): cross-shaded, interstitial Mn^{2+} atoms: diagonal-line-shaded circles, (H_2O) groups: 4^4-net shaded circles.

$[Fe^{2+}{}_2(PO_4)_2(OH)_2(H_2O)O^P{}_2]$ chains condense to form a sheet (Fig. 4.22c) topologically distinct from those in laueite and stewartite; Moore (1975b) discusses in detail the isomeric variation in these (and related) sheets. These sheets stack along the *c*-direction (Fig. 4.22d) and are linked by $(Mn^{2+}O_2\{H_2O\}_4)$ octahedra and by hydrogen bonds.

The sheets in **strunzite**, $Mn^{2+}(H_2O)_4[Fe^{3+}(PO_4)_2(OH)(H_2O)]_2$, and **metavauxite**, $Fe^{2+}(H_2O)_6[Al(PO_4)(OH)(H_2O)]_2$, are built from topologically identical $[M(TO_4)\varphi_3]$ chains. In strunzite, the 7 Å chains extend in the *c*-direction and cross-link to form an $[Fe^{3+}(PO_4)(OH)(H_2O)]$ sheet (Fig. 4.23a) that is a graphical isomer of the $[Fe^{3+}{}_2(PO_4)_2(OH)_2(H_2O)_2]$ sheet in stewartite (Fig. 4.22a). These sheets stack in the *a*-direction (Fig. 4.23b) and are linked by $(Mn^{2+}O_2\{H_2O\}_4)$ octahedra and hydrogen bonds. In metavauxite, the 7 Å chains also extend in the *c*-direction, and cross-link to form an $[Al(PO_4)(OH)(H_2O)]$ sheet (Fig. 4.23c). These sheets stack in the *a*-direction (Fig. 4.23d) and are linked by hydrogen bonds emanating from the interstitial $(Fe^{2+}\{H_2O\}_6)$ groups.

Montgomeryite, $Ca_4Mg(H_2O)_{12}[Al_2(PO_4)_3(OH)_2]_2$, contains 7 Å chains of the form $[M(T\varphi_4)\varphi_2]$ (Fig. 4.13c) in which alternate octahedra are decorated by two tetrahedra that attach to *trans* vertices (Fig. 4.24a) to give a chain of the form $[M_2(TO_4)_4\varphi_4]$ that extends in the [101] direction. These chains meld in the $[10\bar{1}]$ direction by sharing flanking (PO_4) groups to form an $[Al_2(PO_4)_3(OH)_2]$ sheet that is parallel to (010) (Fig. 4.24a). These sheets stack in the [010] direction (Fig. 4.24b). The decorating tetrahedra of the 7 Å chains project above and below the plane of the sheet, and one Ca cation occurs in the interstices created by these tetrahedra, being coordinated by four O-atoms of the sheet and four interstitial

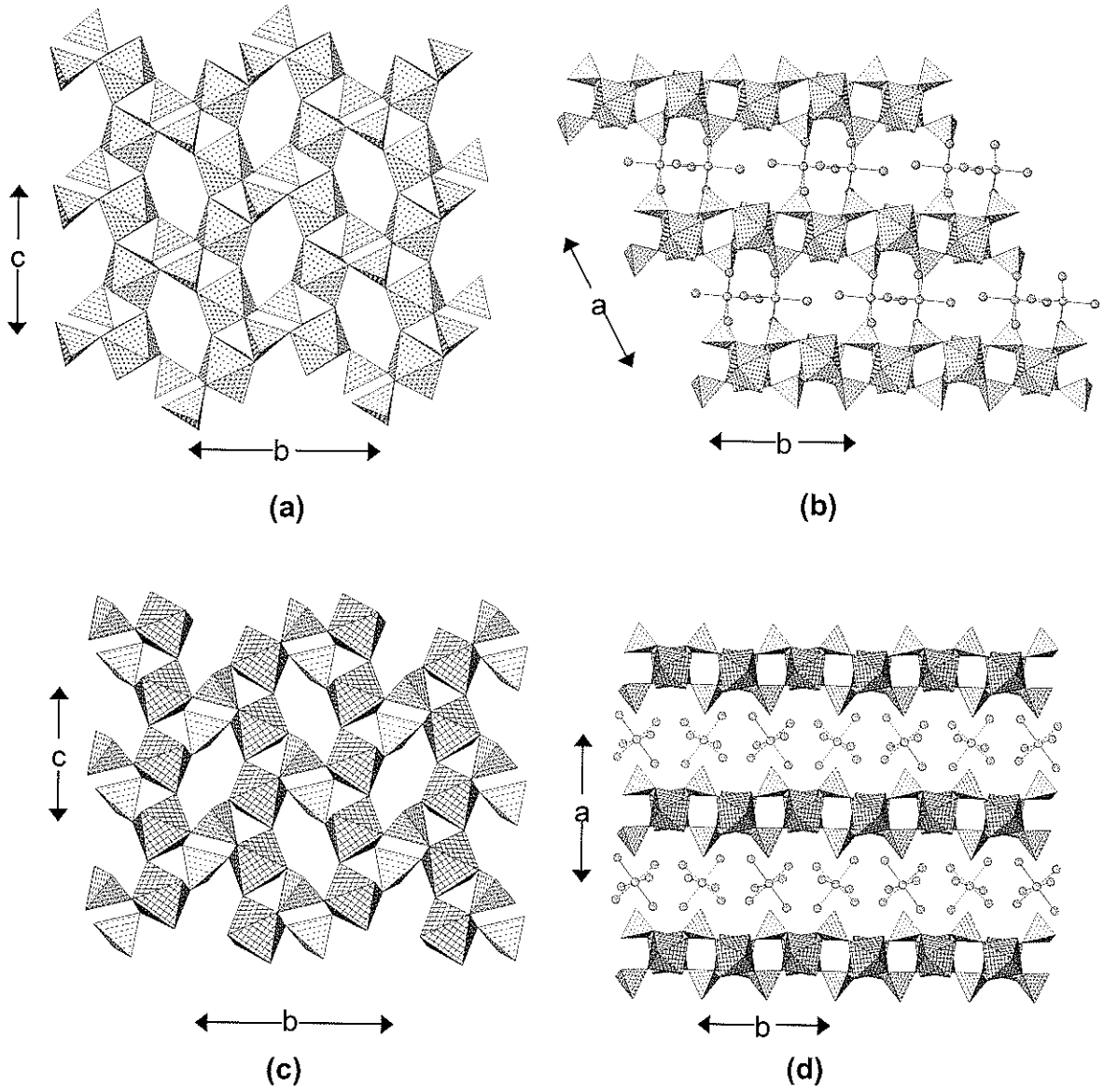

Figure 4.23. (a) strunzite projected onto (100); (b) strunzite projected onto (001), ($Fe^{3+}\varphi_6$): cross-shaded; (c) metavauxite projected onto (100); (d) metavauxite projected onto (001), ($Al\varphi_6$): 4^4-net-shaded, interstitial Mn^{2+} atoms: diagonal-line-shaded circles, (H_2O) groups: 4^4-net shaded circles.

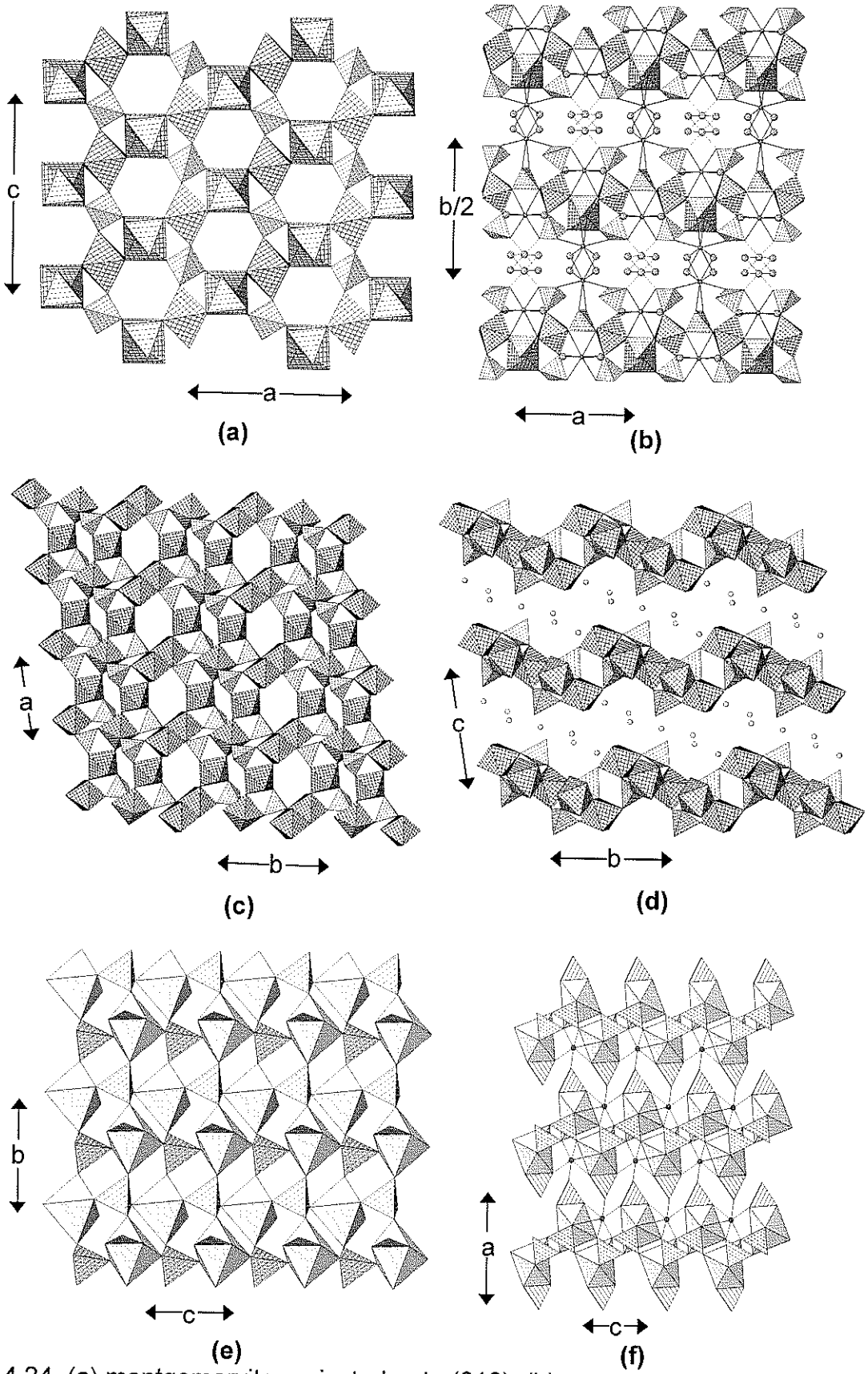

Figure 4.24. (a) montgomeryite projected onto (010); (b) montgomeryite projected onto (001); (c) mitryaevaite projected onto (001), $[Al_5(P\varphi_4)_4\varphi_{12}]$ sheet made of $[M_5(TO_4)_4\varphi_{17}]$ fragments of the 7 Å $[M(TO_4)\varphi]$ chain; (d) mitryaevaite projected onto (100), $(Al\varphi_6)$: 4^4-net-shaded; (e) sidorenkoite projected onto (100); (f) sidorenkoite projected onto (010), $(Mn^{2+}\varphi_6)$: shadow-shaded, (CO_3): triangles.

(H_2O) groups. The second Ca cation links to four anions of the sheet, and shares four interstitial (H_2O) groups with an adjacent Ca that, in turn, links to the adjacent sheet. Further intersheet linkage is provided by octahedrally coordinated interstitial Mg that bonds to four interstitial (H_2O) groups.

Mitryaevaite, $[Al_5(PO_4)_2(PO_3\{OH\})_2F_2(OH)_2(H_2O)_8](H_2O)_{6.5}$, has quite a complex sheet that, nevertheless, can be related to other sheets in this group. An important motif in this sheet is an $[M_5(TO_4)_4\varphi_{17}]$ fragment (see blackened fragment in Fig. 4.24c) of the $[M(TO_4)\varphi]$ chain (Fig. 4.13c) that extends along ~ [120]. These fragments melds in the ~ $[1\bar{1}0]$ direction through tetrahedron-octahedron linkages to form a sheet (Fig. 4.24c) parallel to (110). The chain fragments are inclined to the plane of the sheet, giving it a very corrugated appearance in cross-section (Fig. 4.24d). These sheets stack in the *c*-direction and are linked by hydrogen bonds *via* inclined sheets of interstitial (H_2O) groups that do not bond to any cation.

Sidorenkoite, $Na_3[Mn^{2+}(PO_4)(CO_3)]$, and the other minerals of the **bradleyite** group consist of (PO_4) groups and ($M^{2+}O_6$) octahedra at the vertices of a 4^4 plane net and link by sharing corners to form a sheet parallel to (100) (Fig. 4.24e). This leaves two octahedron vertices that do not link to (PO_4) groups; these link to (CO_3) groups that decorate the sheet above and below the plane of the sheet (Fig. 4.24f). These sheets are linked in the *a*-direction by [6]- and [7]-coordinated interstitial Na cations.

M=M, M–T linkage. **Bermanite**, $Mn^{2+}(H_2O)_4[Mn^{3+}(PO_4)(OH)]_2$, and **ercitite**, $Na_2(H_2O)_4[Mn^{3+}(PO_4)(OH)]_2$, are not formally isostructural as they have

different space-group symmetries, but they contain topologically and chemically identical structural units. ($M\varphi_6$) octahedra share pairs of *trans* edges to form an [$M\varphi_4$] chain decorated with flanking tetrahedra that link vertices of adjacent octahedra (Fig. 4.13e). These chains extend parallel to [101] and link together by sharing octahedral vertices to form an [$M(TO_4)\varphi$] sheet that is parallel to (010) in bermanite and ercitite (Fig. 4.25a). These sheets stack in the *b*-direction and are linked by ($Mn^{2+}O_2\{H_2O\}_4$) octahedra and by hydrogen bonds (Fig. 4.25b). The interstitial linkage is somewhat different in ercitite. One Mn^{2+} atom plus one vacancy (space group $P2_1$) is replaced by two Na atoms (space group $P2_1/m$), the Mn^{2+} and □ being ordered in bermanite and giving rise to the non-centrosymmetric space group.

M=M, M–M, M–T linkage. **Schoonerite**, $[Mn^{2+}Fe^{2+}{}_2ZnFe^{3+}(PO_4)_3(OH)_2(H_2O)_7](H_2O)_2$, is a very complicated structure, and its assignment to a specific structural class is somewhat ambiguous. Figures 4.25c,d show the polyhedra and their connectivity. Inspection of Figure 4.25c indicates the sheet-like nature of the structure. However, this involves both divalent *and* trivalent cations, and is further complicated by the fact that Zn is [5]-coordinated. There are two prominent motifs within the sheet, an [$Fe^{2+}\varphi_4$] chain of edge-sharing octahedra extending in the *c*-direction, and an [Fe^{3+} $^{[5]}Zn(PO_4)_2\varphi_6$] cluster. These link in the *a*-direction to form a continuous sheet (Fig. 4.25d) that is further strengthened by ($Mn^{2+}O_2\{H_2O\}_4$) octahedra occupying dimples in the sheet. These sheets stack in the *b*-direction and are linked by hydrogen bonds. Assigning the divalent cations as interstitial species results in a

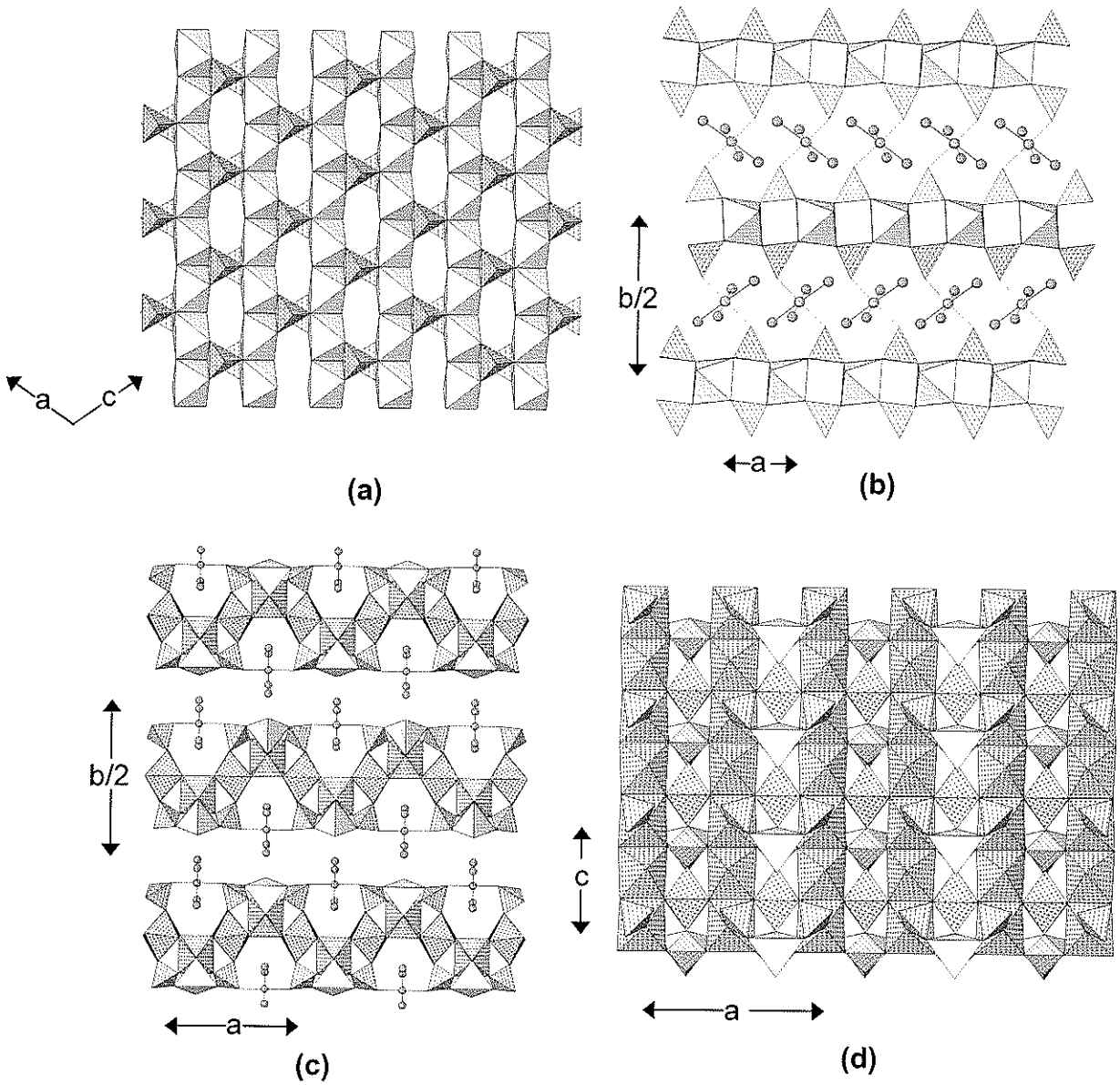

Figure 4.25. (a) bermanite projected onto (010); bermanite projected onto (001), ($Mn^{3+}\varphi_6$): shadow-shaded; (c) schoonerite projected onto (001); (d) schoonerite projected onto (010), ($Zn\varphi_5$): [5]-coordinated, shadow-shaded, ($\{Mn^{2+},Fe^{2+},Fe^{3+}\}\varphi_6$): cross-shaded, Mn^{2+} atoms: diagonal-line-shaded, (H_2O) groups: 4^4-net-shaded.

finite-cluster structure, and this does not accord with the dense distribution of polyhedra in the sheet arrangement of Figure 4.25d. However, this is a somewhat arbitrary aspect of the assignment here. Another aspect that suggests a sheet structure is the 7 Å chain that extends in the *a*-direction; this chain involves both Fe^{3+} and Fe^{2+}.

Nissonite, $[Cu^{2+}Mg(PO_4)(OH)(H_2O)_2]_2(H_2O)$, consists of a thick slab of polyhedra linked solely by hydrogen bonds. ($Mg\varphi_6$) octahedra and (PO_4) tetrahedra lie at the vertices of a 6^3 plane net (Fig. 4.26a); this layer, $[Mb(PO_4)(OH)(H_2O)_2]$, is topologically identical with the $[Mg(PO_3\{OH\})(H_2O)_3]$ sheet in newberyite (Fig. 4.19a). However, the tetrahedra in newberyite point alternately up and down relative to the plane of the sheet, whereas the tetrahedra in nissonite all point in the same direction; hence these sheets are topologically identical but graphically distinct, and are geometrical isomers (Hawthorne 1983a, 1985a). Edge-sharing $[Cu^{2+}{}_2O_8(OH)_2]$ dimers link by sharing corners to form the sheet shown in Figure 4.26b. The $[Mg(PO_4)(OH)(H_2O)_2]$ sheets sandwich the $[Cu^{2+}{}_2O_8(OH)_2]$ sheet to form a thick slab parallel to (100). These slabs link through hydrogen bonds both directly and involving interstitial (H_2O) groups not bonded to any cation (Fig. 4.26c).

Foggite, $Ca[Al(PO_4)(OH)_2](H_2O)$, contains $[Al\varphi_4]$ chains of edge-sharing ($Al\varphi_6$) octahedra that extend in the *c*-direction and are cross-linked into a sheet by (PO_4) tetrahedra (Fig. 4.27a). These sheets are parallel to (010), and are linked by [8]- and [10]-coordinated interstitial Ca (Fig. 4.27b) and by hydrogen bonds involving interstitial (H_2O) groups. The structure of foggite is closely related to the pyroxene structure.

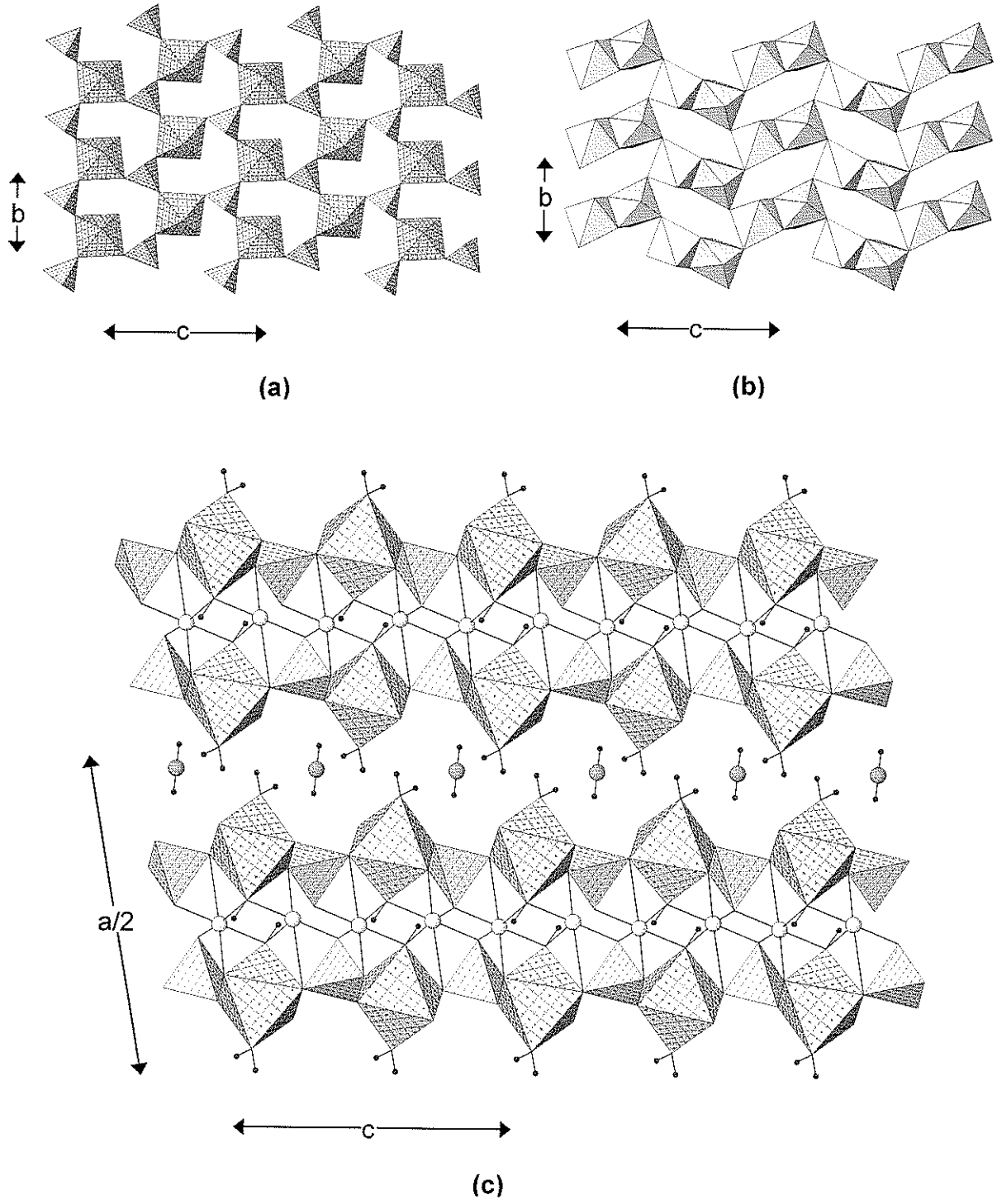

Figure 4.26. The crystal structure of nissonite; (a) the $[Mg(PO_4)(OH)(H_2O)_2]$ layer parallel to (100); (b) the $[Cu^{2+}{}_2O_8(OH)_2]$ layer parallel to (100); (c) a view of the $[Cu^{2+}Mg(PO_4)(OH)(H_2O)_2]$ sheet in the *b*-direction, showing the $[Cu^{2+}{}_2O_8(OH)_2]$ layer sandwiched by two $[Mg(PO_4)(OH)(H_2O)_2]$ layers. ($Mg\varphi_6$): cross-hatched, ($Cu^{2+}\varphi_6$): shadow-shaded, Cu^{2+} cations: highlighted circles, H atoms: small black circles, and O atoms of interstitial (H_2O) groups: 4^4-net-shaded circles.

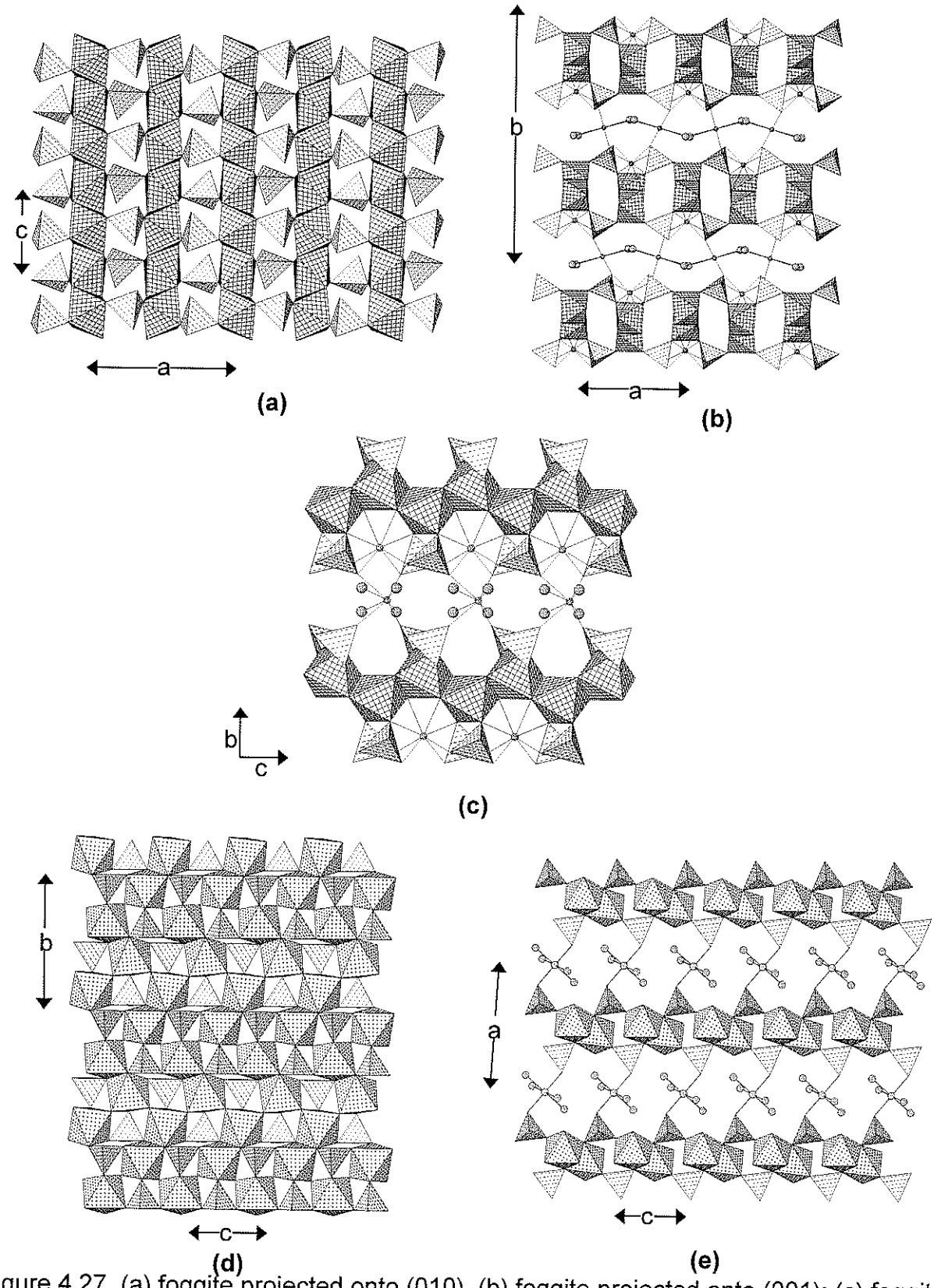

Figure 4.27. (a) foggite projected onto (010), (b) foggite projected onto (001); (c) foggite projected onto (100), (d) whitmoreite projected onto (100); (e) whitmoreite projected onto (010), (Alφ_6): 4^4-net shaded, ($Fe^{3+}\varphi_6$): cross-shaded, Ca atoms: small 4^4-net-shaded circles, (H_2O) groups: larger 4^4-net-shaded circles, Fe^{2+} atoms: large diagonal-line-shaded circles.

Fig. 4.27c depicts the structure of foggite projected onto (100), showing the *M*(1)-like chains and their associated tetrahedra. Moore et al. (1975b) expressed the relation as follows:

Foggite $[CaAl_2P_2O_8(OH)_4]$–$Ca(H_2O)_2$

Px $[CaAl_2{}^{[6]}T_2O_{12}]$–$Ca^{[4]}T_2$

Whitmoreite, $Fe^{2+}(H_2O)_4[Fe^{3+}(PO_4)(OH)]_2$, consists of a fairly densely packed sheet of (PO_4) tetrahedra and $(Fe^{3+}\varphi_6)$ octahedra parallel to (100) (Fig. 4.27d). Pairs of $Fe^{3+}\varphi_6)$ octahedra condense to form edge-sharing $[Fe^{3+}{}_2\varphi_{10}]$ dimers that occupy the vertices of a 4^4 plane net and link by sharing corners. This results in an interrupted sheet of octahedra, the interstices of which are occupied by (PO_4) tetrahedra (Fig. 4.27d). These sheets stack in the *a*-direction, and are linked by interstitial $(Fe^{2+}O_2\{H_2O\}_4)$ octahedra and by hydrogen bonds (Fig. 4.27e).

Mitridatite, $Ca_6(H_2O)_6[Fe^{3+}{}_9O_6(PO_4)_9](H_2O)_3$, has a sheet structural unit of unusual complexity. $(Fe^{3+}\varphi_6)$ octahedra share edges to form triangular rings that are held together by a central (PO_4) group that shares corners with six octahedra (Fig. 4.28a). These clusters link by their corners linking to the mid-points of the edges of adjacent clusters. The resulting interstices are occupied by (PO_4) tetrahedra that point in the opposite direction to the tetrahedra occupying the centres of the clusters. These sheets are linked by [7]-coordinated interstitial Ca and by hydrogen bonds involving interstitial (H_2O) bonded to Ca and interstitial (H_2O) groups not bonded to any cation.

Vivianite, $[Fe^{2+}{}_3(PO_4)_2(H_2O)_8]$, contains two crystallographically distinct Fe^{3+} cations octahedrally coordinated by $(O_2\{H_2O\}_4)$ and $(O_4\{H_2O\}_2)$, respectively.

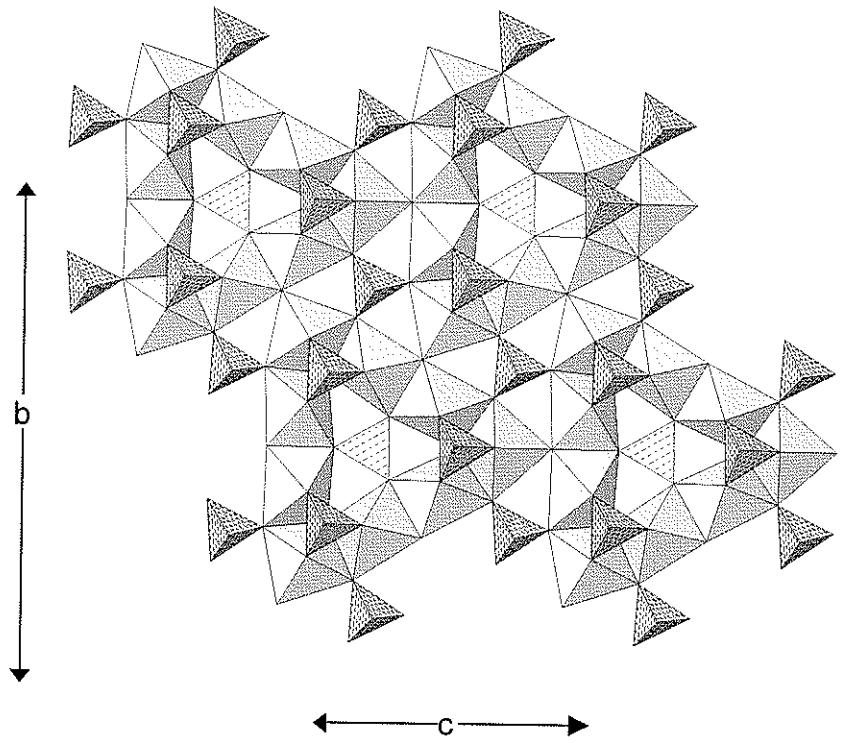

(a)

Figure 4.28. (a) The crystal structure of mitridatite projected onto (100); ($Fe^{3+}\varphi_6$): shadow-shaded.

Pairs of ($Fe^{2+}O_4\{H_2O\}_2$) octahedra share edges to form a dimer that is decorated by two (PO_4) groups that each link to corners of each octahedron, forming an $[Fe^{2+}{}_2(PO_4)_2\varphi_6]$ cluster. These clusters are linked in the *c*-direction by ($Fe^{2+}O_2\{H_2O\}_4$) octahedra (Fig. 4.29a). These chains link in the *a*-direction (Fig. 4.29b) by corner-sharing between tetrahedra and octahedra to form sheets parallel to (010). The sheets are linked solely by hydrogen bonds in the *b*-direction (Fig. 4.29a).

Bobierrite, $[Mg_3(PO_4)(H_2O)_8]$, has a structure very similar to that of vivianite. The sheets of octahedra and tetrahedra are topologically identical (Figs. 4.29c,d), but the position of adjacent sheets in the *b*-direction is sufficiently different that the hydrogen-bond linkage between the sheets differs from that in vivianite. In vivianite, the hydrogen-bond linkages are at an angle to the plane of the sheet (Fig. 4.29a), whereas in bobierrite, the hydrogen-bond linkages are orthogonal to the plane of the sheet (Fig. 4.29c). These difference in the position of adjacent sheets is reflected in the symmetries of the two structures: *C*2/*m* versus *C*2/*c*.

4.4.5 Structures with infinite frameworks of (PO_4) tetrahedra and ($M\varphi_6$) octahedra

The minerals of this class are listed in Table 4.8. These are by far the largest class of phosphate minerals.

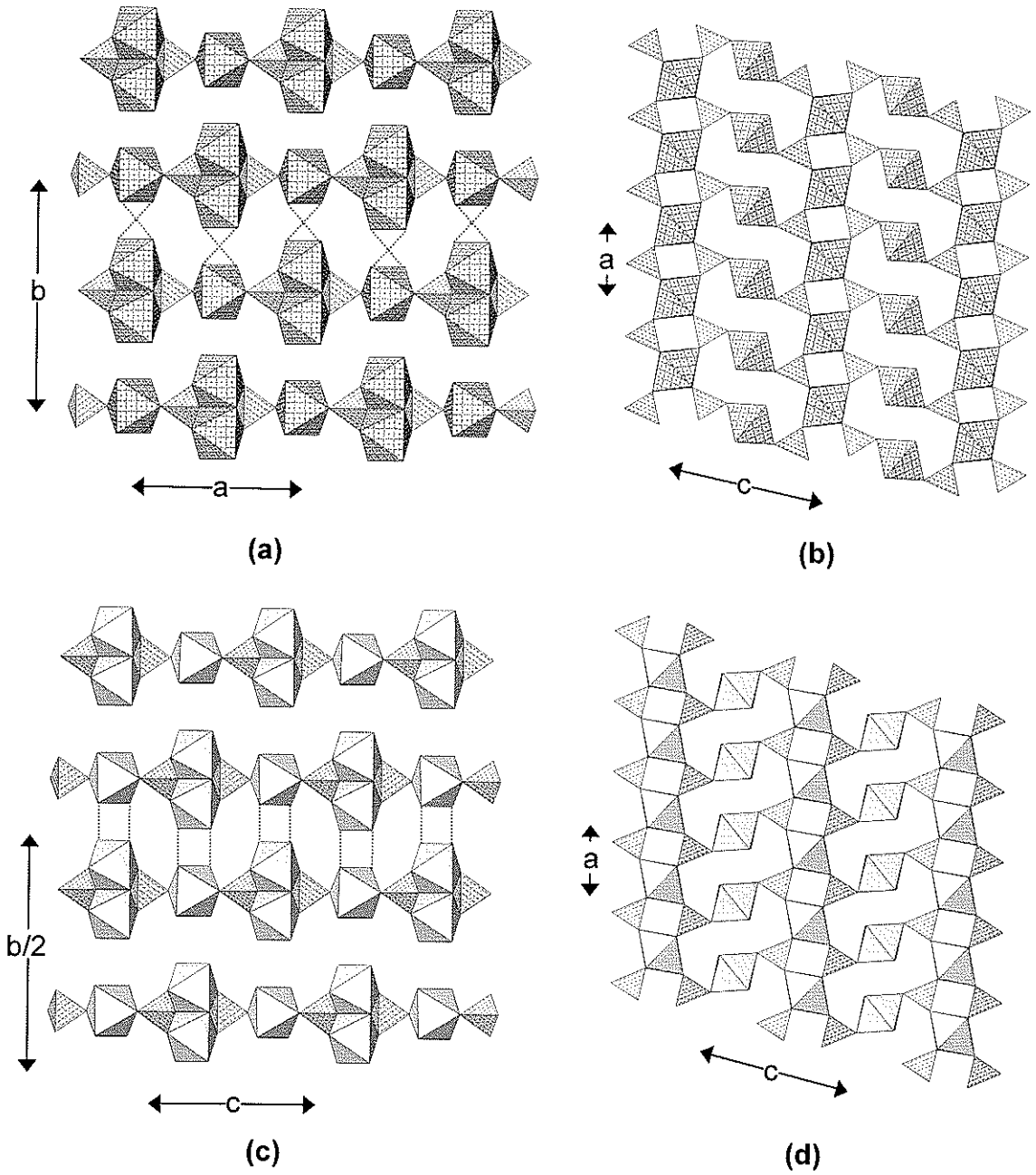

Figure 4.29. (a) vivianite projected onto (001); (b) vivianite projected onto (010); (c) bobierrite projected onto (100); (d) bobierrite projected onto (010); ($Fe^{2+}\varphi_6$): cross-hatched, ($Mg\varphi_6$): shadow-shaded, donor-acceptor pairs for hydrogen bonds are shown by dotted lines.

TABLE 4.8. Phosphate minerals based on infinite chains of ($P\Phi_4$) tetrahedra and ($M\Phi_6$) octahedra

Mineral	Structural unit	Space group	Figure
Kolbeckite	$[Sc(PO_4)(H_2O)_2]$	$P2_1/n$	4.30a,b
Metavariscite*	$[Al(PO_4)(H_2O)_2]$	$P2_1/n$	4.30a,b
Phosphosiderite	$[Fe^{3+}(PO_4)(H_2O)_2]$	$P2_1/n$	4.30a,b
Strengite	$[Fe^{3+}(PO_4)(H_2O)_2]$	$Pbca$	4.30c,d
Variscite*	$[Al(PO_4)(H_2O)_2]$	$Pbca$	4.30c,d
Kosnarite	$[Zr_2(PO_4)_3]$	$R\bar{3}c$	4.30e,f
Isokite	$[Mg(PO_4)F]$	$C2/c$	4.31a,b
Lacroixite	$[Al(PO_4)F]$	$C2/c$	4.31a,b
Panasqueraite	$[Mg(PO_4)(OH)]$	$C2/c$	4.31a,b
Titanite *	$[Ti(SiO_4)O]$	$C2/c$	4.31a,b
Amblygonite *	$[Al(PO_4)F]$	$C\bar{1}$	4.31c,d
Montebrasite	$[Al(PO_4)(OH)]$	$C\bar{1}$	4.31c,d
Natromontebrasite	$[Al(PO_4)(OH)]$	–	4.31c,d
Tavorite	$[Fe^{3+}(PO_4)(OH)]$	–	4.31c,d
Cyrilovite	$[Fe^{3+}{}_3(PO_4)_2(OH)\_]$	$P4_12_12$	4.32a,b
Wardite*	$[Al_3(PO_4)_2(OH)\_]$	$P4_12_12$	4.32a,b
Fluellite	$[Al_2(PO_4)F_2(OH)]$	$Fddd$	4.32c,d
Wavellite	$[Al_3(PO_4)_2(OH)_3(H_2O)_2]$	$Pcmn$	4.32e,f
Augelite	$[Al_2(PO_4)(OH)_3]$	$C2/m$	4.33a,b
Jagowerite *	$[Al(PO_4)(OH)]_2$	$P\bar{1}$	4.33c,d
Maricite	$[Fe^{2+}(PO_4)]$	$Pmnb$	4.33e,f
Kovdorskite	$[Mg_2(PO_4)(OH)(H_2O)–]$	$P2_1/a$	4.34a,b
Libethenite	$[Cu^{2+}{}_2(PO_4)(OH)]$	$Pnnm$	4.34c,d
Adamite*	$[Cu^{2+}{}_2(AsO_4)(OH)]$	$Pnnm$	4.34c,d
Tarbuttite	$[Zn_2(PO_4)(OH)]$	$P\bar{1}$	4.34e,f
Paradamite*	$[Zn_2(AsO_4)(OH)]$	$P\bar{1}$	4.34e,f
Mixite*	$[Cu^{2+}{}_6(AsO_4)_3(OH)_6]$	$P6_3/m$	4.35a,b
Petersite-(Y)	$[Cu^{2+}{}_6(PO_4)_3(OH)_6]$	$P6_3/m$	4.35a,b
Brazilianite	$[Al_3(PO_4)_2(OH)_4]$	$P2_1/n$	4.35c,d
Pseudomalachite	$[Cu^{2+}{}_5(PO_4)_2(OH)_2(H_2O)]$	$P2_1/c$	4.36a,b
Reichenbachite	$[Cu^{2+}{}_5(PO_4)_2(OH)_4(H_2O)]$	$P2_1/a$	4.36c,d
Ludjibaite	$[Cu^{2+}{}_5(PO_4)_2(OH)_4(H_2O)]$	$P\bar{1}$	4.36e,f

TABLE 4.8. continued

Mineral	Structural unit	Space group	Figure
Magniotriplite	$[Mg_2(PO_4)F]$	*I*2/*a*	4.37a,b
Triplite *	$[Mn^{2+}{}_2(PO_4)F]$	*I*2/*c* (?)	4.37a,b
Zweiselite	$[Fe^{2+}{}_2(PO_4)F]$	*I*2/*a* (?)	4.37a,b
Triploidite *	$[Mn^{2+}{}_2(PO_4)(OH)]$	$P2_1/a$	4.37c,d
Wagnerite	$[Mg_2(PO_4)F]$	$P2_1/a$	4.37c,d
Wolfeite	$[Fe^{2+}{}_2(PO_4)(OH)]$	$P2_1/a$	4.37c,d
Alluaudite *	$[Fe^{2+}(Mn,Fe^{2+},Fe^{3+},Mg)_2(PO_4)_3]$	*I*2/*a*	4.38a,b
Hagendorfite	$[Mn^{2+}(Fe^{2+},Mg,Fe^{3+})_2(PO_4)_3]$	*I*2/*a*	4.38a,b
Maghagendorfite	$[Mn^{2+}(Mg,Fe^{2+},Fe^{3+})_2(PO_4)_3]$	–	4.38a,b
Quingheite			4.38a,b
Varulite	$[Mn^{2+}(Mn,Fe^{2+},Fe^{3+})_2(PO_4)_3]$	–	4.38a,b
Rosemaryite	$[Mn^{2+}Fe^{3+}Al(PO_4)_3]$	*C*2/*c* (?)	4.38c,d
Wyllieite *	$[\quad Al(PO_4)_3]$	$P2_1/n$	4.38c,d
Bobfergusonite	$[Mn^{2+}Fe^{3+}Al(PO_4)_6]$	$P2_1/n$	4.38e,f
Ludlamite	$[Fe^{2+}{}_3(PO_4)_2(H_2O)_4]$	$P2_1/a$	4.40a,b
Melonjosephite	$[(Fe^{2+},Fe^{3+})(PO_4)(OH)]$	*Pnam*	4.40c,d
Bertossaite *	$[Al(PO_4)(OH)]_4$	*I*aa*	4.40e,f
Palermoite	$[Al(PO_4)(OH)]_4$	*Imcb*	4.40e,f
Arrojadite*	$[Fe^{2+}{}_{14}Al(PO_4)_{12}(OH)_2]$	*C*2/*c*	–
Dickinsonite	$[Mn^{2+}{}_{14}Al(PO_4)_{12}(OH)_2]$	*C*2/*c*	–
Farringtonite	$[Mg_3(PO_4)_2]$	$P2_1/n$	4.41a,b
Beusite	$[Mn^{2+}{}_3(PO_4)_2]$	$P2_1/c$	4.41c,d
Graftonite*	$[Fe^{2+}{}_3(PO_4)_2]$	$P2_1/c$	4.41c,d
Bederite	$[Mn^{2+}{}_2Fe^{3+}{}_2Mn^{3+}{}_2(PO_4)_6]$	*Pcab*	4.42a,b,c
Wicksite	$[Fe^{2+}{}_4MgFe^{3+}(PO_4)_6]$	*Pcab*	4.42a,b,c
Aheylite	$[Al_6(PO_4)_4(OH)_8]$	$P\bar{1}$	4.42d,e
Chalcosiderite	$[Fe^{3+}{}_6(PO_4)_4(OH)_8]$	$P\bar{1}$	4.42d,e
Coeruleolactite	$[Al_6(PO_4)_4(OH)_8]$	$P\bar{1}$	4.42d,e
Faustite	$[Al_6(PO_4)_4(OH)_8]$	$P\bar{1}$	4.42d,e
Planerite	$[Al_6(PO_4)_2(PO_3\{OH\})_2(OH)_8]$	$P\bar{1}$	4.42d,e
Turquoise *	$[Al_6(PO_4)_4(OH)_8]$	$P\bar{1}$	4.42d,e
Leucophosphite*	$[Fe^{3+}{}_2(PO_4)_2(OH)(H_2O)]$	$P2_1/n$	4.43a,b,c
Tinsleyite	$[Al_2(PO_4)_2(OH)(H_2O)]$	$P2_1/n$	4.43a,b,c

TABLE 4.8. continued

Mineral	Structural unit	Space group	Figure
Cacoxenite	$[Fe^{3+}_{25}(PO_4)_{17}O_6(OH)_{12}]$	$P6_3/m$	4.44a,b,c,d
Althausite	$[Mg_4(PO_4)_2(OH)F]$	$Pnma$	4.45a,b
Hureaulite	$[Mn^{2+}_5(PO_3\{OH\})_2(PO_4)_2(H_2O)_4]$	$C2/c$	4.45c,d
Thadeuite	$[CaMg_3(PO_4)_2(OH)_2]$	$C222_1$	4.45e,f
Bakhchisaraitsevite	$[Mg_5(PO_4)_4(H_2O)_5]$	$P2_1/c$	4.46a,b
Kryzhanovskite	$[Mn^{2+}Fe^{3+}_2(PO_4)_2(OH)_2(H_2O)]$	$Pbna$	4.46c,d
Phosphoferrite*	$[Fe^{2+}_3(PO_4)_2(H_2O)_3]$	$Pbna$	4.46c,d
Griphite	$[A_{24}Fe^{2+}_4Al_8(PO_4)_{24}]$	$Pa\bar{3}$	4.47a,b,c,d
Cornetite	$[Cu^{2+}_3(PO_4)(OH)_3]$	$Pbca$	4.47e,f
Chladniite	$[Mg_7(PO_4)_6]$	$R\bar{3}$	–
Fillowite*	$[Mn^{2+}_7(PO_4)_6]$	$R\bar{3}$	–
Galileiite	$[Fe^{2+}_7(PO_4)_6]$	$R\bar{3}$	–
Johnsomervilleite	$[Mg_7(PO_4)_6]$	$R\bar{3}$	–
Gladiusite	$[Fe^{2+}_4Fe^{3+}_2(PO_4)(OH)_{11}(H_2O)$	$P2_1/n$	4.48a,b,c
Lipscombite	$[Fe^{2+}Fe^{3+}_2(PO_4)_2(OH)_2]$	$P4_32_12$	4.48d,e
Burangaite	$[Fe^{2+}Al_5(PO_4)_4(OH)_6(H_2O)_2]$	$C2/c$	4.49a
Dufrénite	$[Fe^{2+}Fe^{3+}_5(PO_4)_4(OH)_6(H_2O)_2]$	$C2/c$	4.49a
Natrodufrénite	$[Fe^{2+}Fe^{3+}_5(PO_4)_4(OH)_6(H_2O)_2]$	$C2/c$	4.49a
Frondellite	$[Fe^{2+}Fe^{3+}_4(PO_4)_3(OH)_5]$	$Bbmm$	4.49b,c
Rockbridgeite*	$[Fe^{2+}Fe^{3+}_4(PO_4)_3(OH)_5]$	$Bbmm$	4.49b,c
Barbosalite	$[Fe^{3+}(PO_4)(OH)]_2$	$P2_1/c$	4.49d,e
Hentschelite	$[Fe^{3+}(PO_4)(OH)]_2$	$P2_1/c$	4.49d,e
Lazulite*	$[Al(PO_4)(OH)]_2$	$P2_1/c$	4.49d,e
Scorzalite	$[Al(PO_4)(OH)]_2$	$P2_1/c$	4.49d,e
Trolleite	$[Al_4(PO_4)_3(OH)_3]$	$I2/c$	4.50a,b
Seamanite	$[Mn^{2+}_3(PO_4)(B\{OH\}_4)(OH)_2]$	$Pbnm$	4.50c,d
Holtedahlite	$[Mg_{12}(PO_3\{OH\})(PO_4)_5(OH)_6]$	$P31m$	4.50e,f
Satterlyite	$[Fe^{2+}_4(PO_4)_2(OH)_2]$	$P\bar{3}1m$	4.50e,f
Triphylite*	$[Fe^{2+}(PO_4)]$	$Pbnm$	4.51a,b
Lithiophylite	$[Mn^{2+}(PO_4)]$	$Pbnm$	4.51a,b
Natrophilite	$[Mn^{2+}(PO_4)]$	$Pbnm$	4.51a,b
Ferrisicklerite	$[Mn^{2+},Fe^{3+}(PO_4)]$	$Pbnm$	4.51c,d
Sicklerite*	$[Fe^{2+},Mn^{3+}(PO_4)]$	$Pbnm$	4.51c,d
Heterosite*	$[Fe^{3+}(PO_4)]$	$Pmnb$	4.51e,f

TABLE 4.8. continued

Mineral	Structural unit	Space group	Figure
Purpurite	$[Mn^{3+}(PO_4)]$	*Pmnb*	4.51e,f
Senegalite	$[Al_2(PO_4)(OH)_3(H_2O)]$	$P2_1nb$	4.52a,b,c
Sarcopside	$[Fe^{2+}{}_3(PO_4)_2]$	$P2_1/a$	4.53a,b
Bjarebyite*	$[Al_2(PO_4)_3(OH)_3]$	$P2_1/m$	4.53c,d
Kulanite	$[Al_2(PO_4)_3(OH)_3]$	$P2_1/m$	4.53c,d
Penikisite	$[Al_2(PO_4)_3(OH)_3]$	$P2_1/m$	4.53c,d
Perloffite	$[Fe^{3+}{}_2(PO_4)_3(OH)_3]$	$P2_1/m$	4.53c,d

M–T linkage. The minerals of the **metavariscite**, $[Al(PO_4)(H_2O)_2]$, and **variscite**, $[Al(PO_4)(H_2O)_2]$, groups consist of simple frameworks of alternating (PO_4) tetrahedra and $(Al\varphi_6)$ octahedra. As there are equal numbers of tetrahedra and octahedra, both polyhedra are four-connected, and hence two vertices of the $(Al\varphi_6)$ octahedron must be one-connected. The local bond-valence requirements of the anions at these one-connected vertices require that the anions be (H_2O) groups. When viewed down the *c*-direction, octahedra and tetrahedra occupy the vertices of a 6^3 net, and Figures 4.30a, c show two layers of such nets. When metavariscite viewed in the *a*-direction (Fig. 4.30b), the tetrahedra and octahedra occupy the vertices of a 4.8^2 net. It can be noted that the one-connected vertices of the octahedra project into the large eight-membered ring, which allows room for the H atoms of the (H_2O) groups at these vertices. When viewed down [100] (Fig. 4.30d), variscite shows alternating tetrahedra and octahedral. As with metavariscite, the one-connected vertices of the octahedra project into the large cavities.

Kosnarite, $X[Zr_2(PO_4)_3]$, contains octahedrally coordinated Zr. In projection down [001] (Fig. 4.30e), (ZrO_6) octahedra occupy the vertices of a 6^3 net, and all octahedron vertices link to (PO_4) tetrahedra, forming a block with prominent interstices. These blocks stack in the *c*-direction and link by sharing of octahedron-tetrahedron vertices (Fig. 4.30f), with [6]-coordinated X cations in the interstices of the framework.

M–M, M–T linkage. The minerals of the **amblygonite**, $Li[Al(PO_4)F]$, group and the phosphate members of the titanite group, such as **lacroixite**,

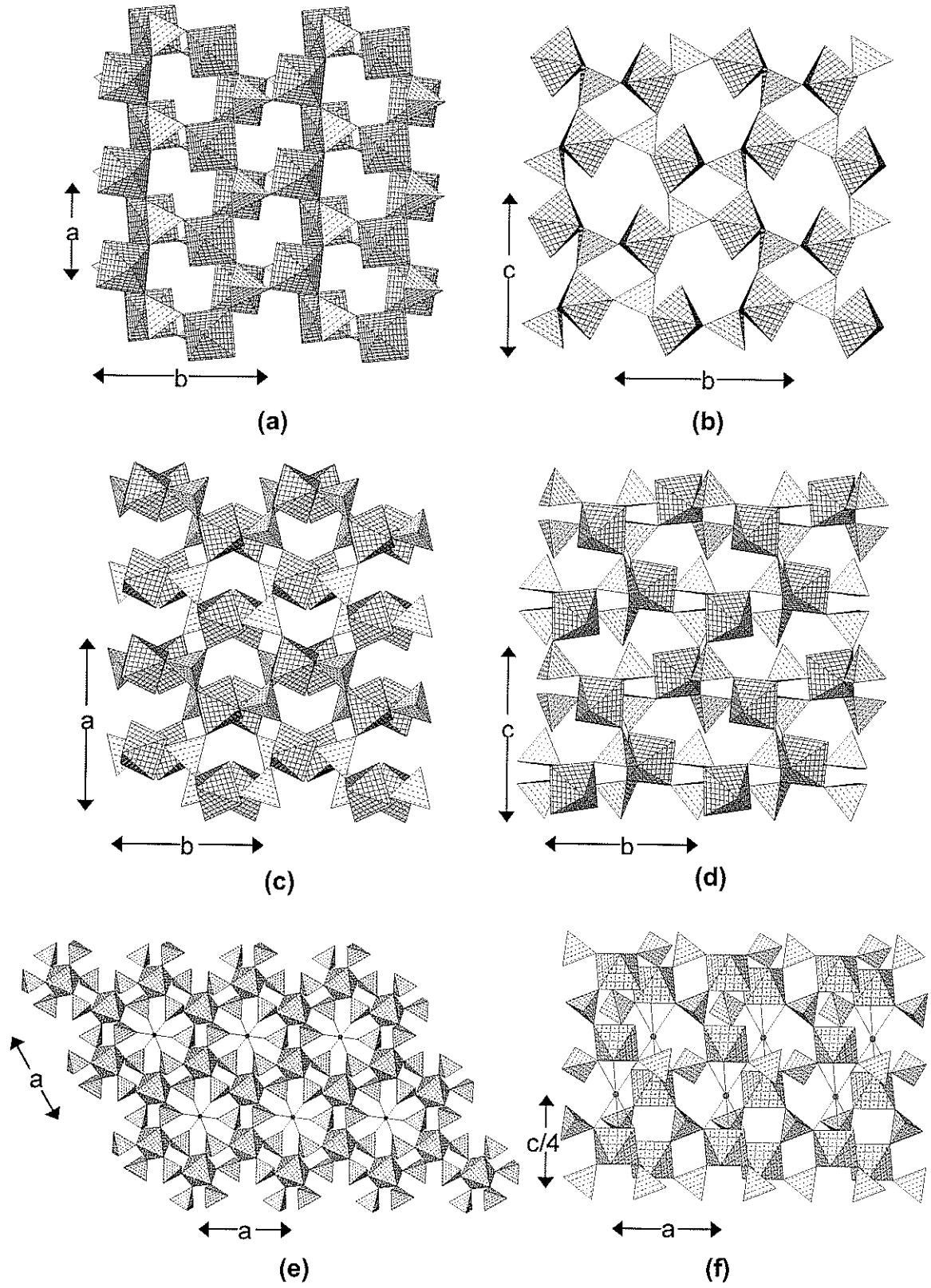

Figure 4.30. (a) metavariscite projected onto (001); (b) metavariscite projected onto (100); (c) variscite projected onto (001); (d) variscite projected onto (100); (e) kosnarite projected onto (001): (f) kosnarite projected onto (010). ($Al\varphi_6$): 4^4-net-shaded, ($Zr\varphi_6$): cross-hatched.

$Na[Al(PO_4)F]$, have topologically identical structural units. However, lacroixite is monoclinic, whereas the amblygonite-group minerals are triclinic; because of their topological identity, we use the unconventional space group C-1 to emphasize the congruity of these two structures (Table 4.8). A key feature of both structures is the 7 Å $[M\varphi_5]$ chain of corner-sharing octahedra that extends in the *c*-direction (Figs. 4.31a,c). This chain is decorated by staggered flanking (PO_4) groups that link the chains in both the *a*- and *b*-directions, a feature that is very apparent in an end-on view of the chains (Figs. 4.31b,d). The frameworks are strengthened by interstitial alkali cations Na and Li in the minerals of the amblygonite group and both Ca and Na in the minerals of the titanite group.

Cyrilovite, $Na[Fe^{3+}_3(PO_4)_2(OH)_4(H_2O)_2]$ is a member of the wardite group (Table 4.8). The principal motif in cyrilovite is the $[Fe^{3+}\varphi_5]$ chain that is decorated by (PO_4) tetrahedra arranged in a staggered fashion at the periphery of the chain (the $[M(TO_4)\varphi_3]$ chain shown in Fig. 4.13c). These chains extend parallel to the *a*- and *b*-directions (note the tetragonal symmetry) to form a slab of corner-sharing octahedra and tetrahedra (Fig. 4.32a), tetrahedra on opposite sides of each chain pointing in opposing directions along *c*. The tetrahedral vertices that project out of the plane of the slab link to octahedra of adjacent slabs (Fig. 4.32a) to form a framework that consists of successive layers of octahedra and tetrahedra along the *c*-direction. [8]-coordinated Na occupies the large interstices in this framework (Fig. 4.32b), and hydrogen bonds strengthen the framework.

Fluellite, $[Al_2(PO_4)F_2(OH)(H_2O)_3](H_2O)_4$, is an open framework of corner-sharing (PO_4) tetrahedra and $(Al\varphi_6)$ octahedra. The principal motif of the framework is a 7 Å chain of the form $[M(TO_4)\varphi_3]$ (Fig. 4.13c) consisting of

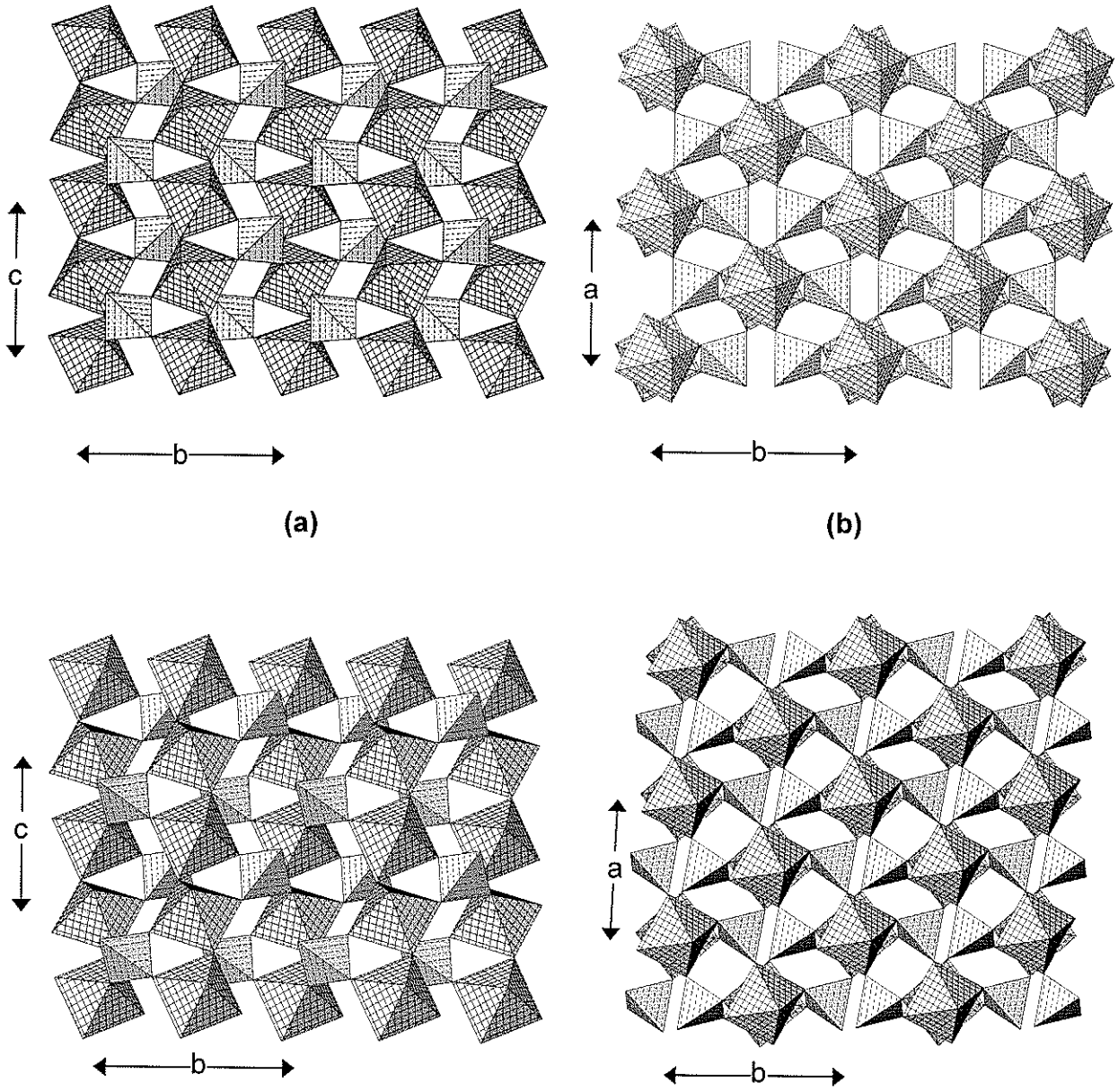

Figure 4.31. (a) lacroixite projected onto (100); (b) lacroixite projected onto (001); (c) amblygonite projected onto (100), note the similarity with (a); (d) amblygonite projected onto (001), note the similarity with (b), ($Al\varphi_6$): 4^4-net-shaded.

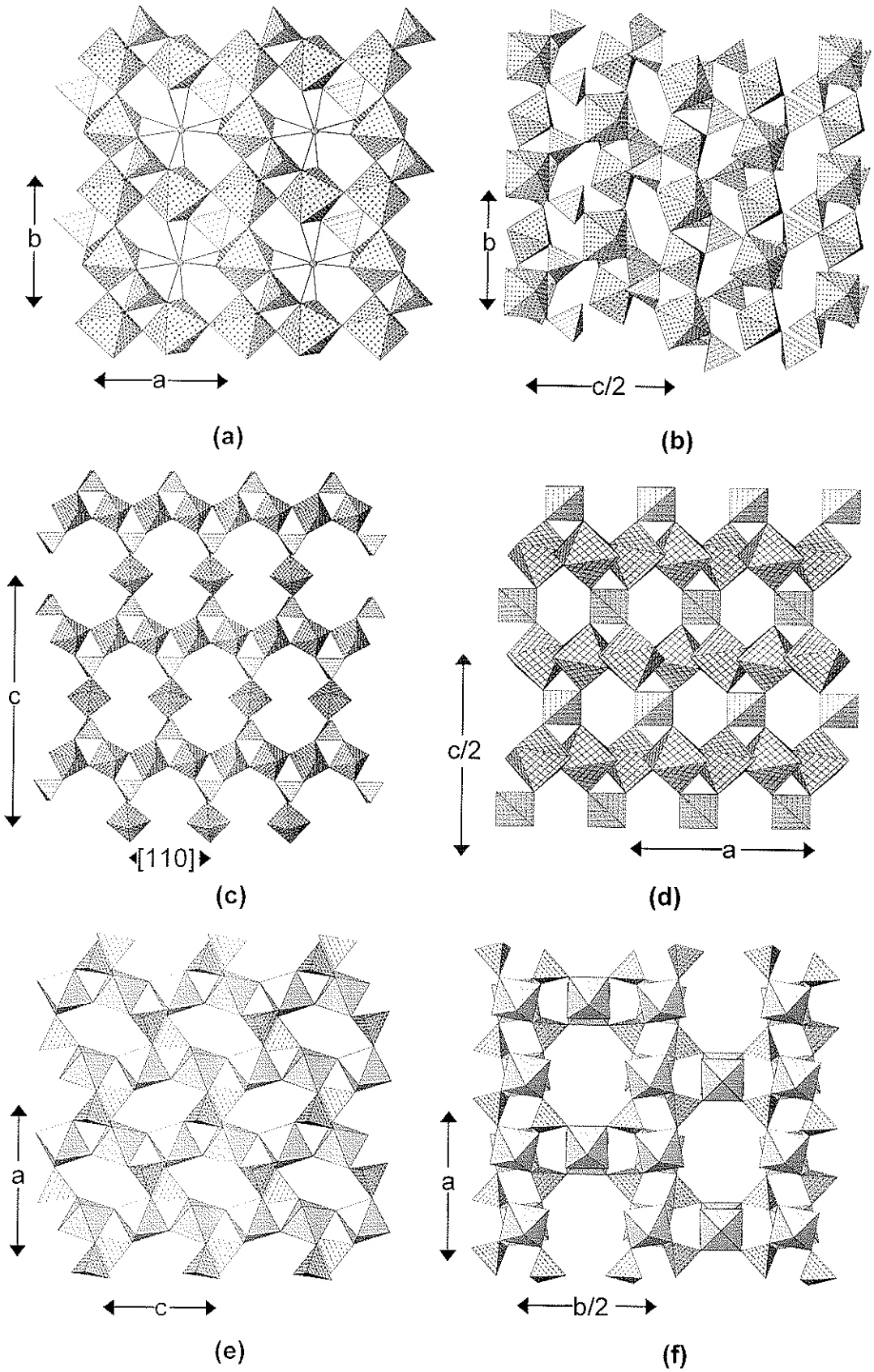

Figure 4.32. (a) cyrilovite projected onto (001); (b) cyrilovite projected onto (100); (c) fluellite projected down [110]; (d) fluellite projected onto (010); (e) wavellite projected onto (010); (f) wavellite projected onto (001). ($Fe^{3+}\varphi_6$): cross shaded, ($Al\varphi_6$): 4^4-net shaded (c,d) and shadow-shaded (e,f).

$(AlF_2\{OH\}(H_2O)_3)$ octahedra linked through pairs of *trans* vertices (= F) and decorated by (PO_4) tetrahedra that link adjacent octahedra along the chain. These chains extend in both the *a*- and *b*-directions (Fig. 4.32c) by sharing (PO_4) groups between chains extending in orthogonal directions (Fig. 4.32d). There are large interstices within the framework that accommodate (H_2O) groups held in the structure solely by hydrogen bonds emanating from the (H_2O) groups bonded directly to the Al of the structural unit.

Wavellite, $[Al_3(PO_4)_2(OH)_3(H_2O)_4](H_2O)$, is an open framework of corner-sharing octahedra and tetrahedra (Fig. 4.32e) with interstitial non-transformer (H_2O) groups held in the interstices by hydrogen bonds. $(Al\varphi_6)$ octahedra share one set of *trans* corners with each other to form $[M\varphi_5]$ chains that are decorated by (PO_4) tetrahedra bridging adjacent octahedra (Fig. 4.32e) to give chains of the form $[M(TO_4)\varphi]$ extending in the *c*-direction (Fig. 4.13c). These chains cross-link in the *a*-direction by sharing octahedron-tetrahedron corners (Fig. 4.32f) with undecorated $[Al\varphi_5]$ chains (*i.e.*, the tetrahedra linked to these chains do not bridge octahedra within the chain). The resulting framework (Figs. 4.32e,f) has large cavities that contain the interstitial (H_2O) groups held in the structure solely by hydrogen bonds.

M=M, M–T linkage. **Augelite**, $[Al_2(PO_4)(OH)_3]$, contains Al in both octahedral and trigonal-bipyramidal coordinations. Pairs of $(Al\varphi_6)$ octahedra share an edge to form $[Al_2\varphi_{10}]$ dimers that are oriented with their long axis in the *b*-direction. The dimers are arranged at the vertices of a centered orthorhombic plane net (Fig. 4.33a), and dimers adjacent in the *b*-direction are linked through

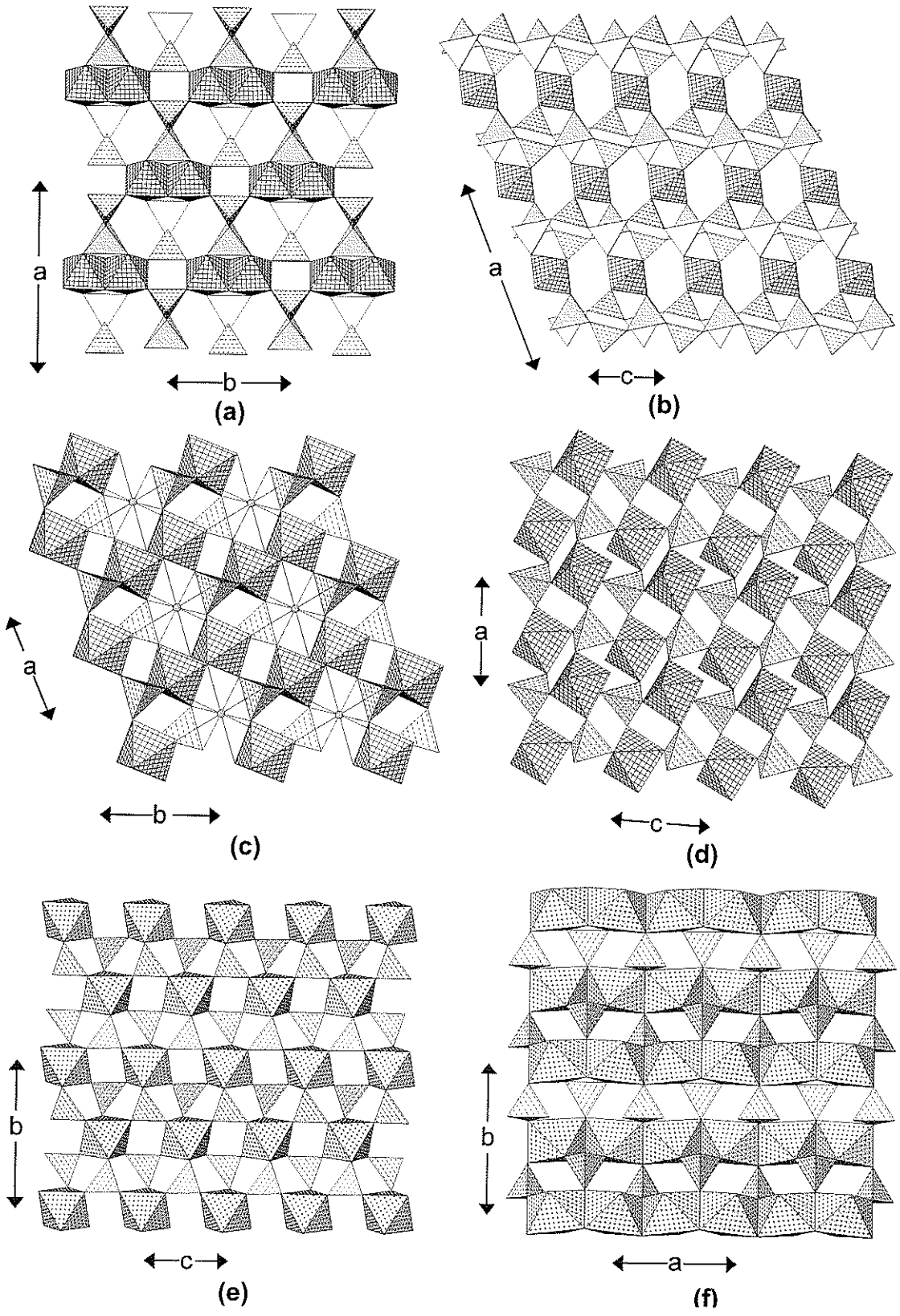

Figure 4.33. (a) augelite projected onto (001); (b) augelite projected onto (010); (c) jagowerite projected onto (001); (d) jagowerite projected a few degrees away from onto (010); (e) maricite projected onto (100); (e) maricite projected a few degrees away from onto (001). Legend as in Fig. 4.32.

pairs of (PO_4) tetrahedra to form [$Al_2(PO_4)_2\varphi_6$] chains. The dimers are decorated by ($Al\varphi_5$) trigonal bipyramids that bridge pairs of vertices from each octahedron. These ($Al\varphi_5$) groups link to (PO_4) groups of adjacent chains to link them in the *a*-direction. Viewed in the *b*-direction (Fig. 4.33b), the structure appears as layers of dimers linked by chains of (PO_4) and ($Al\varphi_5$) groups.

Jagowerite, $Ba[Al(PO_4)(OH)]_2$, contains ($Al\varphi_6$) octahedra that have condensed to form [$Al_2\varphi_{10}$] dimers that link by corner-sharing with pairs of (PO_4) tetrahedra to form [$Al_2(PO_4)_2\varphi_6$] chains that extend along [110], and cross-link by shared octahedron-tetrahedron corners to form a sheet in the (110) plane (Fig. 4.33c). Viewed down [010] (Fig. 4.33d), the structure consists of ($Al\varphi_6$) octahedra and (PO_4) tetrahedra at the vertices of a 4^4 net, linked by sharing polyhedron corners. The interstitial Ba ia [12]-coordinated, and occupies interstices between the chains shown in Figure 4.33c.

Marićite, $Na[Fe^{2+}(PO_4)]$, is a dense-packed framework of ($Fe^{2+}O_6$) octahedra and (PO_4) tetrahedra. Each ($Fe^{2+}O_6$) octahedron links to six (PO_4) groups to form what Moore (1973b) calls a "pinwheel". The octahedra occupy the vertices of a 3^6 net, and the resulting sheet (Fig. 4.33e) is topologically identical to the [$Mg(PO_4)_2$] sheet in brianite (Fig. 4.18c). These sheets stack along the *a*-direction with octahedra from adjacent sheets sharing edges to form [MO_4]-type chains extending in the *a*-direction when viewed down [001] (Fig. 4.33f). [10]-coordinated Na occupies interstices in the framework.

Kovdorskite, [$Mg_2(PO_4)(OH)(H_2O)_3$], consists of two distinct ($Mg\varphi_6$) octahedra that condense to form tetramers via edge-sharing, and these tetramers are decorated by pairs of (PO_4) tetrahedra to form [$Mg_4(PO_4)_2\varphi_8$]

clusters. These clusters occur at the vertices of a 4^4 plane net and link together by sharing octahedron-tetrahedron vertices to form open sheets parallel to (001) (Fig. 4.34a). These sheets stack in the *c*-direction by sharing octahedron-tetrahedron vertices (Fig. 4.34b) to form a very open framework that is strengthened by extensive hydrogen bonding involving the (OH) and (H_2O) groups of the structural unit.

Libethenite, $[Cu^{2+}_2(PO_4)(OH)]$, is a member if the **adamite** group (Table 4.8) (Hawthorne 1976) in which Cu^{2+} is both [5]- and [6]-coordinated, triangular bipyramidal and octahedral, respectively. Chains of *trans* edge-sharing ($Cu^{2+}\varphi_6$) octahedra extend in the *c*-direction and are decorated by (PO_4) tetrahedra to give chains of the general form $[M_2(TO_4)_2\varphi_4]$ (Fig. 4.34c). These chains link in the *a*- and *b*-directions by sharing octahedron-tetrahedron corners (Fig. 4.34d) to form an open framework with channels extending in the *c*-direction. These channels are packed with dimers of edge-sharing ($Cu\varphi_5$) triangular bipyramids. Note that this is also the structure of andalusite, $[Al_2(SiO_4)O]$.

Tarbuttite, $[Zn_2(PO_4)(OH)]$, is a member of the paradamite group (Table 4.8) (Hawthorne 1979b). ($Zn\varphi_5$) bipyramids share edges to form a chain extending in the *b*-direction: $[Zn\varphi_4]$. (PO_4) groups and ($Zn\varphi_3$) bipyramids alternate along a chain of corner-sharing polyhedra that also extends in the *b*-direction. These chains link in the *a*-direction by sharing polyhedron vertices (Fig. 4.34e) to form a rather thick slab parallel to (001). These slabs stack in the *c*-direction (Fig. 4.34f) by sharing polyhedron edges and corners. Apart from the

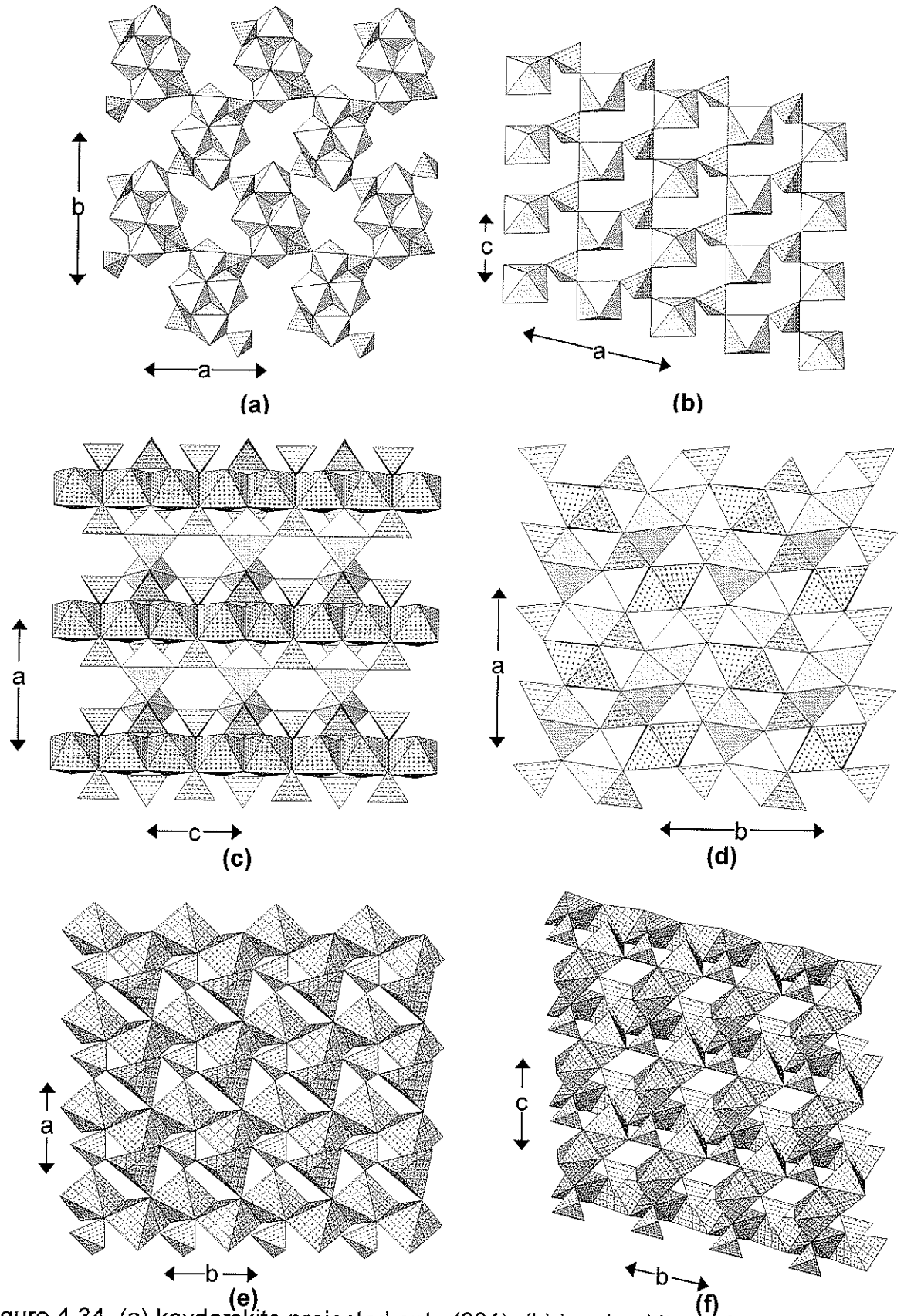

Figure 4.34. (a) kovdorskite projected onto (001); (b) kovdorskite projected onto (010), ($Mg\varphi_6$): shadow-shaded; (c) libethenite projected onto (010); (d) libethenite projected onto (001), ($Cu^{2+}\varphi_6$): cross-shaded, ($Cu^{2+}\varphi_5$): shadow-shaded; (e) tarbuttite projected onto (001); (f) tarbuttite projected onto (100), ($Zn\varphi_6$) and ($Zn\varphi_5$): cross-hatched.

presence of both [5]-coordinated divalent cations, there is no structural relation with the stoichiometrically similar libethnite, $Cu^{2+}_2(PO_4)(OH)$.

Petersite-(Y), $Y[Cu^{2+}_6(PO_4)_3(OH)_6](H_2O)_3$, is the only phosphate member of the mixite group (Table 4.8). Cu^{2+} is [5]-coordinated with a long sixth distance to (H_2O). Six-member rings of corner-sharing alternating (PO_4) tetrahedra and $(Cu^{2+}\varphi_5)$ square-pyramids occur parallel to (001) and link by corner-sharing to form four-membered and twelve-membered rings of polyhedra (Fig. 4.35a). An alternative description is as six-member rings occupying the vertices of a 6^3 net. The layers of Figure 4.35a stack along the *c*-direction (Fig. 4.35b), and link by edge-sharing between the $(Cu^{2+}\varphi_5)$ square pyramids. In the cross-linkage of the rings in the (001) plane, note how the (PO_4) groups bridge apical vertices of square pyramids adjacent along the *c*-direction (Fig. 4.35b). The interstitial (H_2O) groups occupy the channels of the twelve-membered rings, and interstitial Y occupies the channels generated by the six-membered rings (Fig. 4.35a).

Brazilianite, $Na[Al_3(PO_4)_2(OH)_4]$, contains chains of edge-sharing $(Al\varphi_6)$ octahedra that extend in the $[10\bar{1}]$ direction (Fig. 4.35c). These chains are fairly contorted as the shared edges are not in a *trans* configuration and hence a slight helical character results. The chains are decorated by (PO_4) tetrahedra which link next-nearest-neighbour octahedra, a rather unusual linkage that is promoted by the helical nature of the chains (Fig. 4.35c). Adjacent chains link by sharing octahedron vertices with the decorating tetrahedra (Fig. 4.35c,d). Interchain linkage is also promoted by [7]-coordinated interstitial Na.

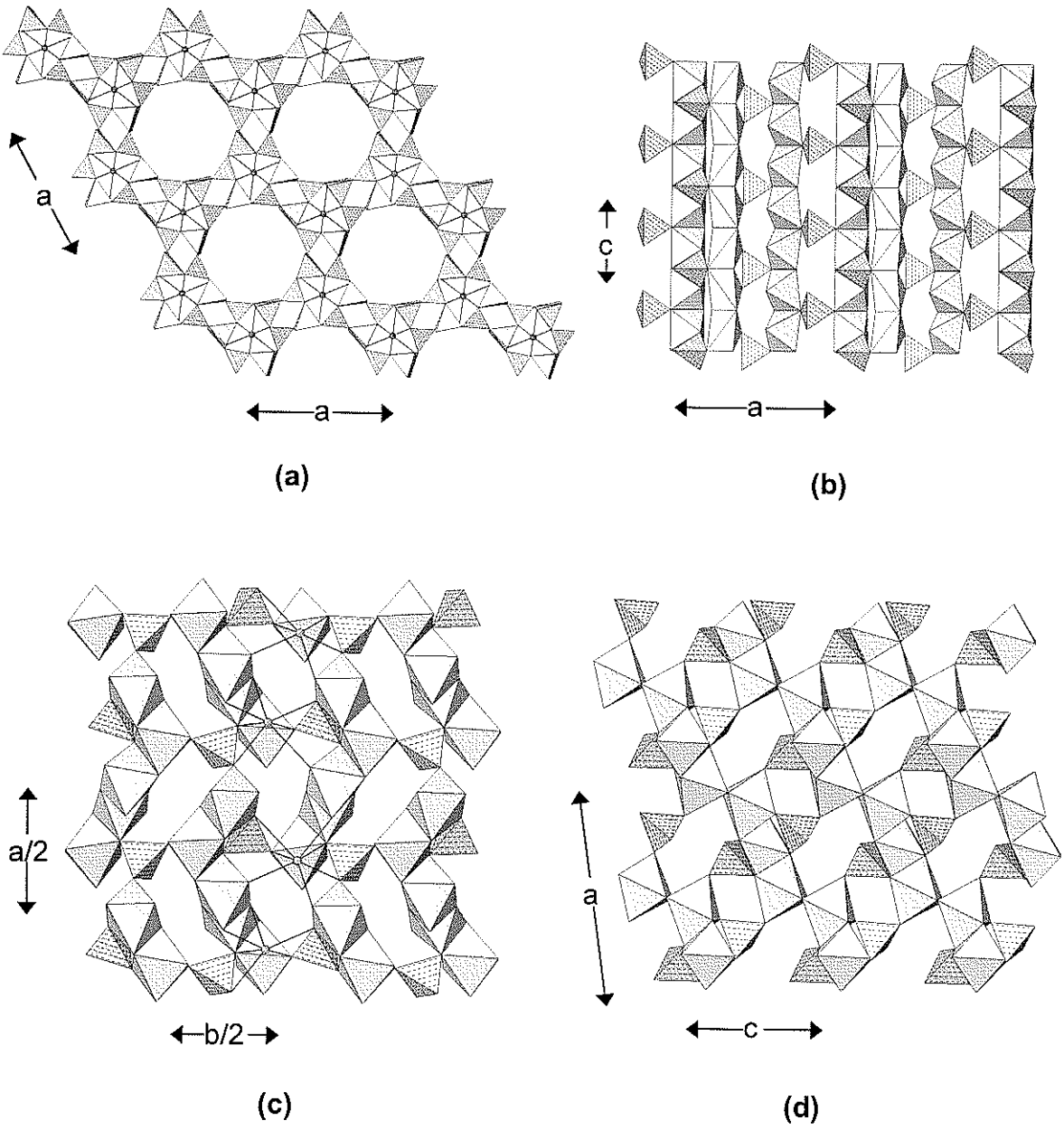

Figure 4.35. (a) petersite-(Y) projected onto (001); (b) petersite-(Y) projected onto (010), Y atoms: shaded circles, ($Cu^{2+}\varphi_6$) octahedra are shadow-shaded; (c) brazilianite projected onto (001); (d) brazilianite projected onto (010), ($Al\varphi_6$): shadow-shaded; Na atoms: shaded circles.

M=M, M–M, M–T linkage. There are three polymorphs of $[Cu^{2+}_5(PO_4)_2(OH)_4(H_2O)]$, pseudomalachite, reichenbachite and ludjibaite, and their structures are all based on sheets of octahedra that are linked by (PO_4) tetrahedra. The sheets of octahedra are somewhat unusual in that they are not close-packed octahedra interspersed with vacancies (as is common in this type of structure). In pseudomalachite (Fig. 4.36a), linear $[M\varphi_4]$ chains of octahedra extend in the *b*-direction at $z \approx \frac{1}{4}$ and $\frac{3}{4}$, and are linked by trimers of edge-sharing octahedra packed such that there are square interstices in the sheet. The sheets stack in the *a*-direction and are linked by (PO_4) groups that share two vertices with each sheet (Fig. 4.36b). In reichenbachite (Fig. 4.36c), the arrangement of octahedra within the sheet is fairly irregular. It can be envisioned as edge-sharing trimers of octahedra at (0 ½ *z*) and (½ 0 *z*) linked by edge-sharing with dimers of edge-sharing octahedra at (0 ⅛ *z*) and at (⅝ ⅜ *z*) (Fig. 4.36c). These sheets stack in the *c*-direction (Fig. 4.36d) and are linked by (PO_4) groups that each share two vertices with adjacent sheets. In ludjibaite (Fig. 4.36e), linear $[M\varphi_4]$ chains extend in both the *b* and *c*-directions, and link together by sharing edges with an $[M\varphi_5]$ chain of corner-sharing octahedra that extends in the *c*-direction. These sheets stack in the *a*-direction (Fig. 4.36f) and, as with the other two structures, are linked by (PO_4) groups that share pairs of vertices with adjacent sheets.

In the minerals of the **triplite**, $[Mn^{2+}_2(PO_4)F]$, group (Table 4.8), $(M^{2+}\varphi_6)$ octahedra share edges to form $[M^{2+}_2\varphi_{10}]$ dimers (Fig. 4.37a) that share corners with (PO_4) tetrahedra to form slightly corrugated layers that are parallel to (010)

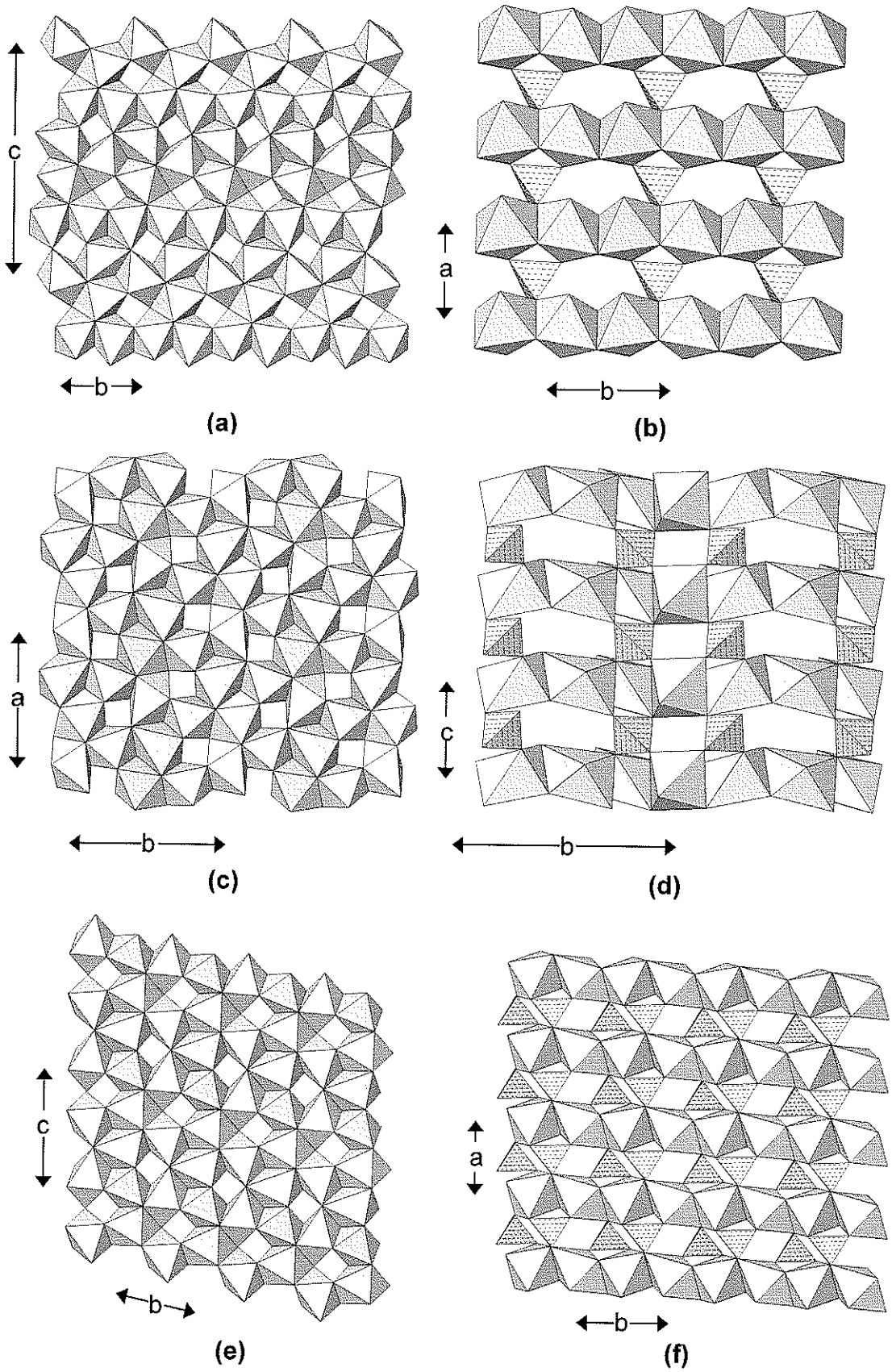

Figure 4.36. (a) pseudomalachite projected onto (100); (b) pseudomalachite projected onto (001); (c) reichenbachite projected onto (001); (d) reichenbachite projected onto (100); (e) ludjibaite projected onto (100); (f) ludjibaite projected onto (001), ($Cu^{2+}\varphi_6$): shadow-shaded.

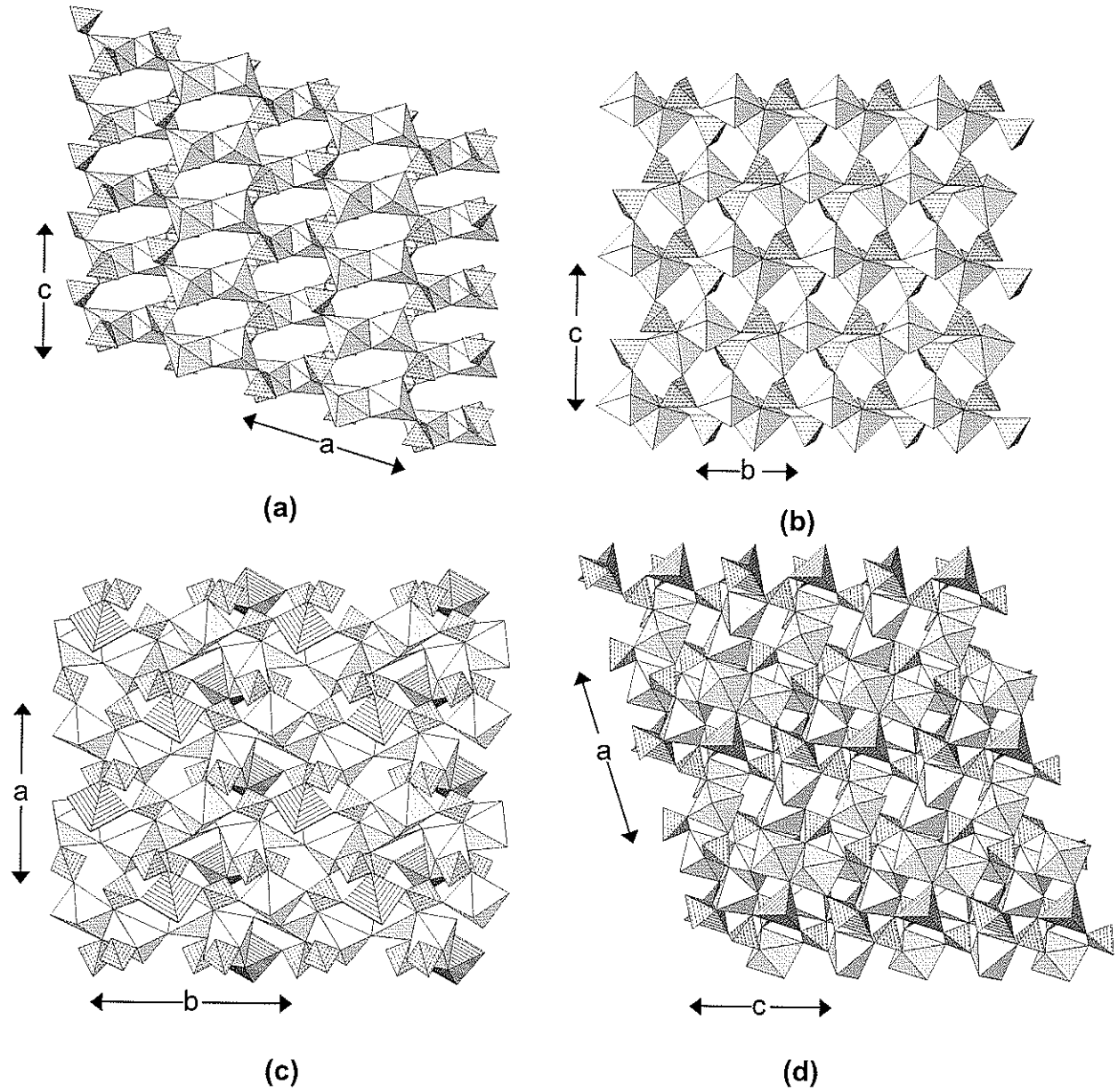

Figure 4.37. (a) triplite projected onto (010); (b) triplite projected onto (100); (c) triploidite projected onto (001); (d) triploidite projected onto (001), ($Mn\varphi_5$): line-shaded, ($Mn\varphi_6$): shadow-shaded.

(Fig. 4.37a). These layers link in the *b*-direction by sharing corners between tetrahedra and octahedra (Fig. 4.37b).

The minerals of the **triploidite**, $[Mn^{2+}_2(PO_4)(OH)]$, group have divalent cations in both octahedral and triangular bipyramidal coordinations. Pairs of octahedra share an edge to form $[M^{2+}_2\varphi_{10}]$ dimers, and these dimers are linked by sharing corners with both triangular bipyramids and (PO_4) groups, and by sharing one octahedron edge with a tetrahedron (Fig. 4.37c). Triangular bipyramids also form edge-sharing dimers, $[M^{2+}_2\varphi_8]$, and chains of corner-sharing octahedra, triangular bipyramids and tetrahedra extend in the *b*-direction (Fig. 4.37d). It should be noted that this is an extremely complicated structure, and is not easily related to any other structure.

The minerals of the **alluaudite**, **wyllieite** and **bobfergusonite** groups are topologically identical but are distinguished by different cation-ordering schemes over the octahedrally coordinated cation sites in the basic structure. The principal feature of each structure is a linear trimer of edge-sharing octahedra (Figs. 4.38a,c,e). These trimers link together by sharing edges to form chains of octahedra in the (010) plane that are linked by sharing octahedron corners with (PO_4) groups to form thick sheets parallel to (010). These sheets link in the *b*-direction by sharing corners between tetrahedra and octahedra (Figs. 4.38b,d,f). The minerals of these three groups differ primarily in (1) their Al content, and (2) the pattern of cation order over the trimer of edge-sharing octahedra. The minerals of the alluaudite group contain negligible Al (Al_2O_3 < 0.10 wt.%), the minerals of the wyllieite group contain moderate Al (Al_2O_3 ~ 3 wt.%), and bobfergusonite contains far more Al than wyllieite (Al_2O_3 ~ 7.5 wt.%). In addition,

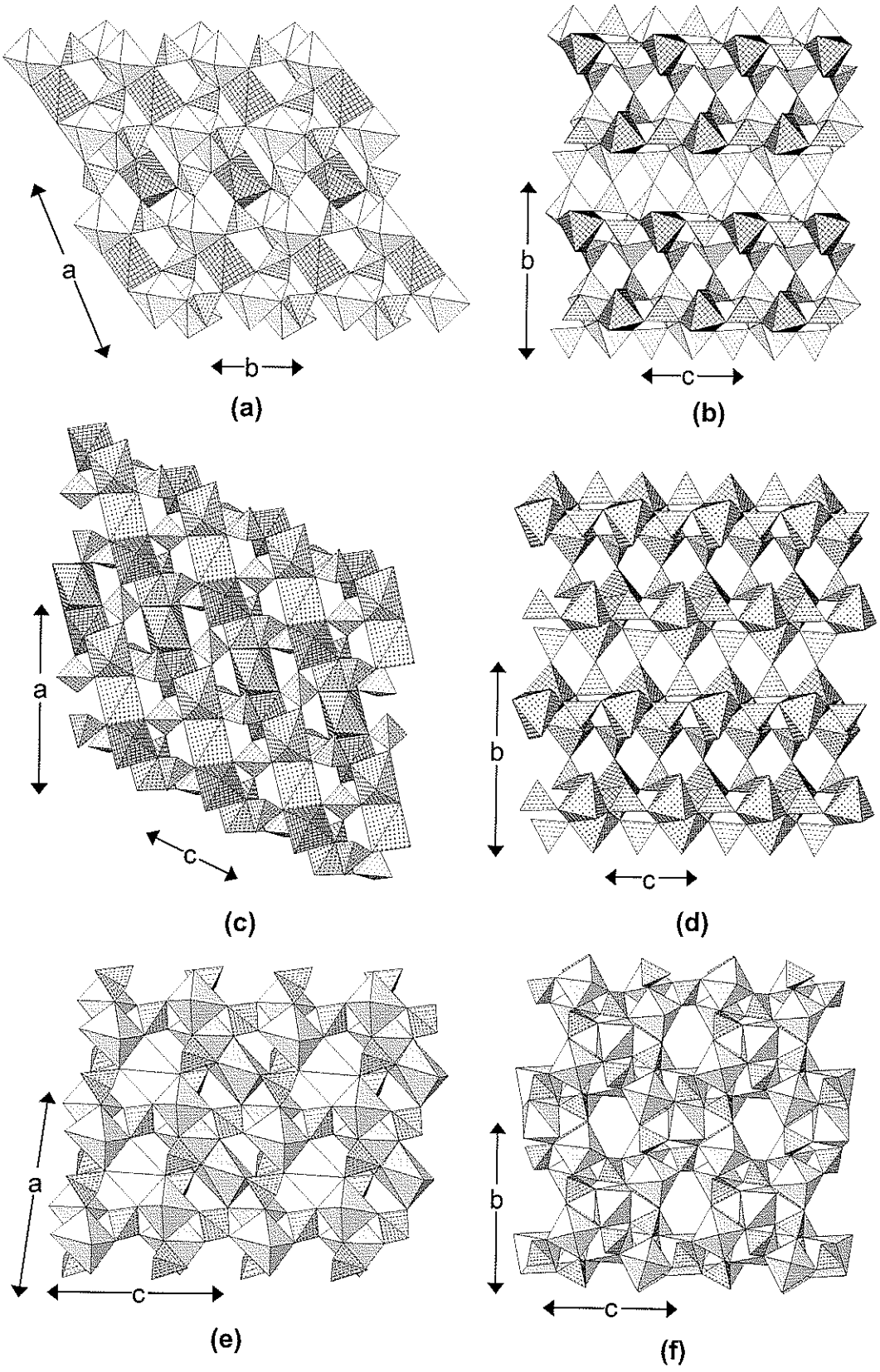

Figure 4.38. (a) alluaudite projected onto (001); (b) alluaudite projected onto (100), ($Mn^{2+}\varphi_6$): shadow-shaded, ($Fe^{3+}\varphi_6$): 4^4-net-shaded; (c) wyllieite projected onto (010); (d) wyllieite projected onto (100), ($Fe^{2+}\varphi_6$): cross-shaded, ($Al\varphi_6$): 4^4-net-shaded; (e) bobfergusonite projected onto (010); bobfergusonite projected onto (100), ({Mn^{2+}, Fe^{3+},Al}φ_6): shadow-shaded.

there is a fourth (as yet undescribed) structure type with ~ 15 wt.% Al_2O_3 (unpublished data). The differences in cation order in these three structure types are summarized in Figure 4.39. In alluaudite, there is no Al, and hence Al is not involved in the ordering scheme. There are only two distinct sites in the trimer in alluaudite, and the pattern of cation order can vary from complete M^{2+}-cation disorder to complete Fe^{3+}–M^{2+} order (Fig. 4.39a). In wyllieite, there are three distinct sites in the trimer; Al is completely ordered at one site, and the other two sites can vary from complete M^{2+}-cation disorder to complete Fe^{3+}–M^{2+} order (Fig. 4.39b). In bobfergusonite, there are two crystallographically distinct trimers (Fig. 4.39c); Al is ordered in one trimer, Fe^{3+} is ordered in the other trimer, and M^{2+} is disordered over the other sites. This picture is somewhat idealized, and each structure-type may show minor ordering characteristic of one or more of the other structure types. Moore and Ito (1979) discuss the nomenclature of the alluaudite and wyllieite groups in detail and propose a nomenclature based on suffixes, but this has not been used very extensively.

Ludlamite, $[Fe^{3+}{}_3(PO_4)_2(H_2O)_4]$ consists of $(Fe^{3+}\varphi_6)$ octahedra that share edges to form $[Fe^{3+}{}_3\varphi_{14}]$ linear trimers with (PO_4) tetrahedra bridging between adjacent octahedra in a staggered fashion on each site of the trimer: $[Fe^{3+}{}_3(PO_4)_2\varphi_{10}]$. These trimers extend in the *c*-direction and link by sharing octahedron corners (Fig. 4.40a). The crankshaft chains link in the *b*-direction by sharing octahedron corners and by sharing corners between tetrahedra and octahedra (Fig. 4.40a) to form a sheet parallel to (100). These sheets link in the *a*-direction by sharing corners between (PO_4) tetrahedra and octahedra (Fig. 4.40b). Note that the chains of octahedra shown in this figure are not completely

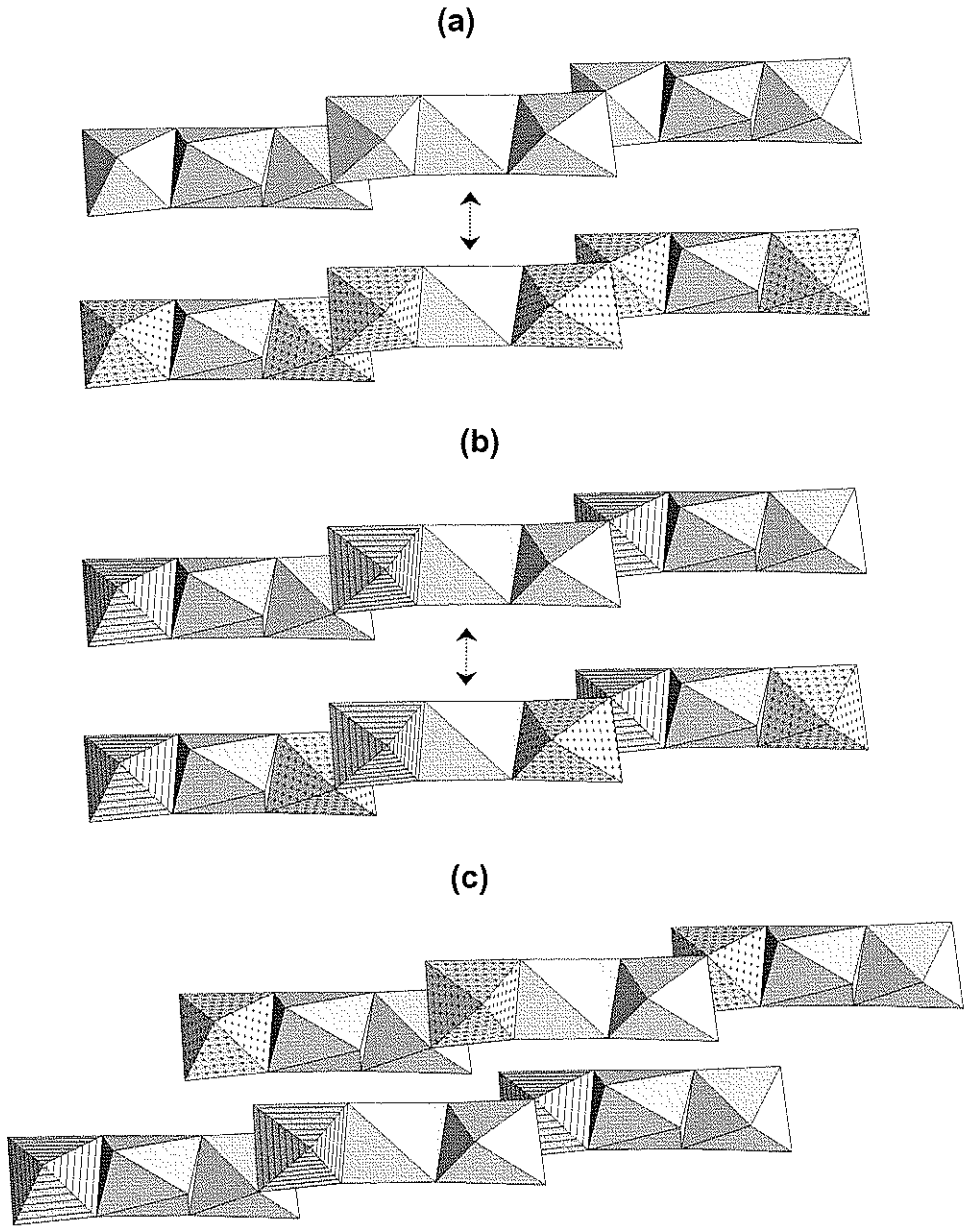

Figure 4.39. Octahedral-cation-ordering patterns in a) alluaudite; b) wyllieite; c) bobfergusonite; shadow-shaded octahedra are occupied by any divalent M^{2+} cation, cross-shaded octahedra are occupied by Fe^{3+}, line-shaded octahedra are occupied by Al. In a) and b), the arrows indicate the range of possible ordering within a single chain; in bobfergusonite c), there are two distinct chains (shown here) in which the ordering is different (after Ercit et al. 1986b).

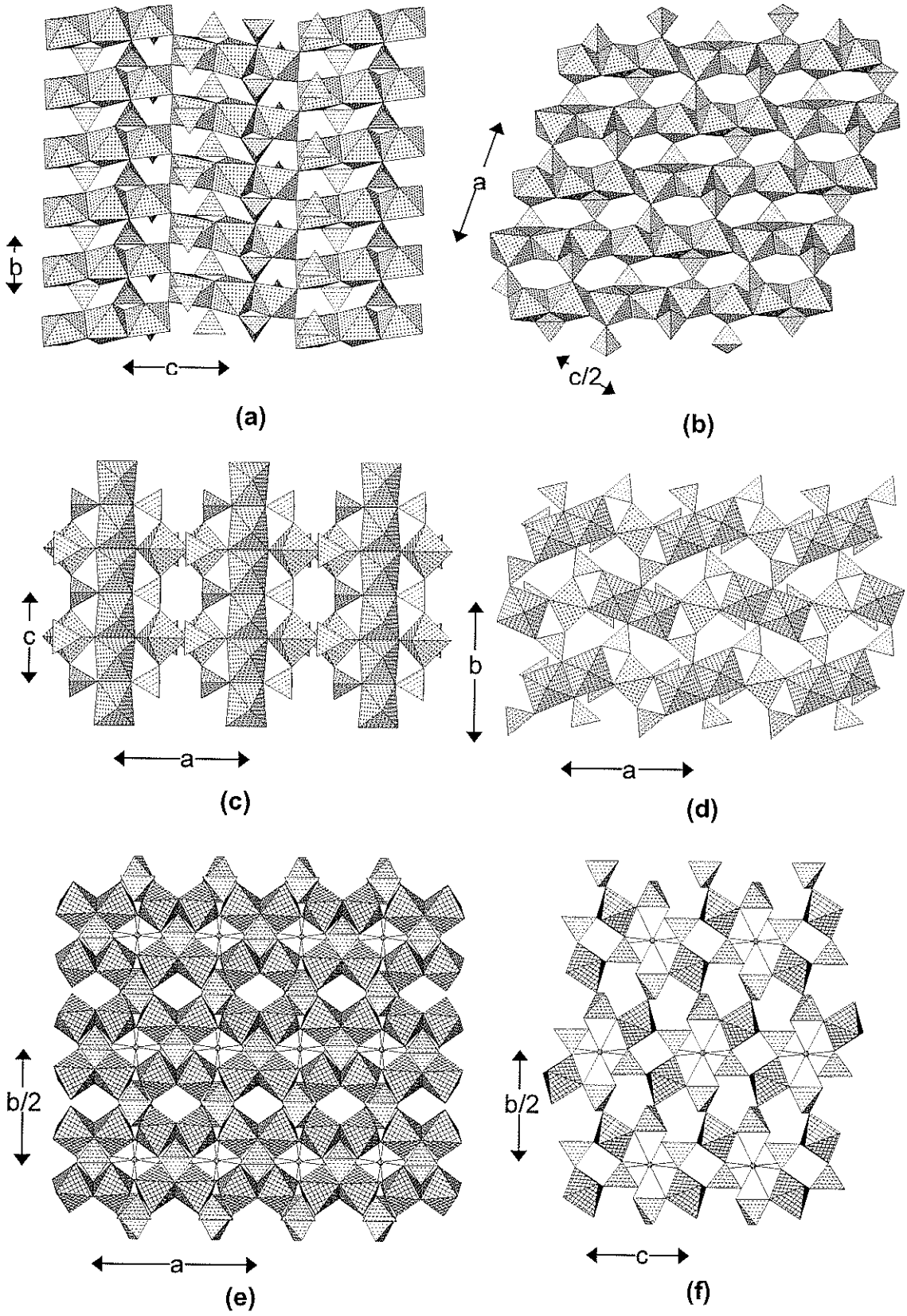

Figure 4.40. (a) ludlamite projected onto (100); (b) ludlamite projected onto (010); (c) melonjosephite projected onto (010); (d) melonjosephite projected onto (001), ($\{Fe^{2+},Fe^{3+}\}\varphi_6$): cross-shaded; (e) palermoite projected onto (001); (f) palermoite projected onto (100), ($Al\varphi_6$): 4^4-net-shaded, Ca atoms: small shaded circles.

edge-sharing; for every third octahedra, the linkage is by corner-sharing, as is apparent by the change in direction of the top triangular faces of the octahedra (Fig. 4.40a).

In **melonjosephite**, $Ca[Fe^{2+}Fe^{3+}(PO_4)_2(OH)]$, there are two crystallographically distinct octahedra, both of which are occupied by equal amounts of Fe^{2+} and Fe^{3+}. One type of octahedron forms linear chains of edge-sharing octahedra ($[M\varphi_4]$ of the rutile-type) extending in the *c*-direction. This chain is decorated by (PO_4) tetrahedra linking free vertices of adjacent octahedra in a staggered arrangement, producing an $[M(T\varphi_4)\varphi_2]$ chain (Fig. 4.13e). The other crystallographically distinct octahedron links to (PO_4) tetrahedra to form $[M(PO_4)\varphi_4]$ chains. These $[M(PO_4)\varphi_4]$ chains link in a pair-wise fashion by the octahedra sharing edges, and the resulting structure consists of the two types of chains, both extending in the *c*-direction and cross-linked by sharing octahedron-tetrahedron and octahedron-octahedron corners (Fig. 4.40c). Viewed down the length of the chains (Fig. 4.40d), the dimers linking the two $[M(PO_4)\varphi_4]$ chains are very prominent, and the key role of the (PO_4) groups in cross-linking the chains is very apparent. The interstices of the framework are occupied by [7]-coordinated Ca.

In **palermoite**, $SrLi_2[Al(PO_4)(OH)]_4$, ($Al\varphi_6$) octahedra condense by sharing edges to form $[Al_2\varphi_{10}]$ dimers, and these dimers share corners to form an $[Al_2\varphi_8]$ chain that extends in the *a*-direction. One pair of octahedron vertices in each dimer is bridged by a (PO_4) tetrahedron to form an $[Al_2(PO_4)\varphi_6]$ chain (Fig. 4.40e); these chains link in the *b*-direction by sharing octahedron-tetrahedron vertices. These chains are seen end-on when viewed in the *a*-direction (Fig.

4.40f), cross-linked by (PO_4) tetrahedra. The framework has large interstices that are occupied by [8]-coordinated Sr and [5]-coordinated Li.

Arrojadite, $KNa_4Ca[Fe^{2+}_{14}Al(PO_4)_{12}(OH)_2]$, and **dickinsonite**, the Mn^{2+} analogue, are tediously complex structures, each with several partly occupied cation sites, and the complete details of their structure exceeds our spatial parameters. Moore et al. (1981) describe the structure as six distinct rods (columns) of cation polyhedra decorated by (PO_4) tetrahedra and occurring at the vertices of a {6·3·6·3} and {6·6·3·3} net. Moore et al. (1981) also compare the structure of arrojadite with wyllieite, but the relation to the general alluaudite-type structures has not been explored.

Farringtonite, $[Mg_3(PO_4)_2]$, contains Mg in both octahedral and square-pyramidal coordinations. As is common with [5]-coordinated polyhedra, $[Mg\varphi_5]$ square pyramids share an edge to form $[Mg_2\varphi_8]$ dimers, and the terminal edges of this dimer are shared with (PO_4) tetrahedra to form a $[Mg_2(PO_4)_2\varphi_4]$ cluster (Fig. 4.41a). These clusters are linked by sharing corners with ($Mg\varphi_6$) octahedra. When projected onto (010), prominent $[Mg(PO_4)_2\varphi_2]$ chains are evident, extending in the *c*-direction (*cf.* Fig. 4.13b). These chains are bridged in the a-direction by $[Mg_2(PO_4)_2\varphi_4]$ clusters (Fig. 4.41b).

Beusite, $[Mn^{2+}_3(PO_4)_2]$, and **graftonite**, $[Fe^{2+}_3(PO_4)_2]$, show unusual coordination numbers for the divalent cations: $^{[7]}M(1)$, $^{[5]}M(2)$, $^{[6]}M(3)$; perhaps as a result, these minerals can accept considerable Ca at the *M*(1) site (Wise et al. 1990), and the latter authors report a composition for Ca-rich beusite close to

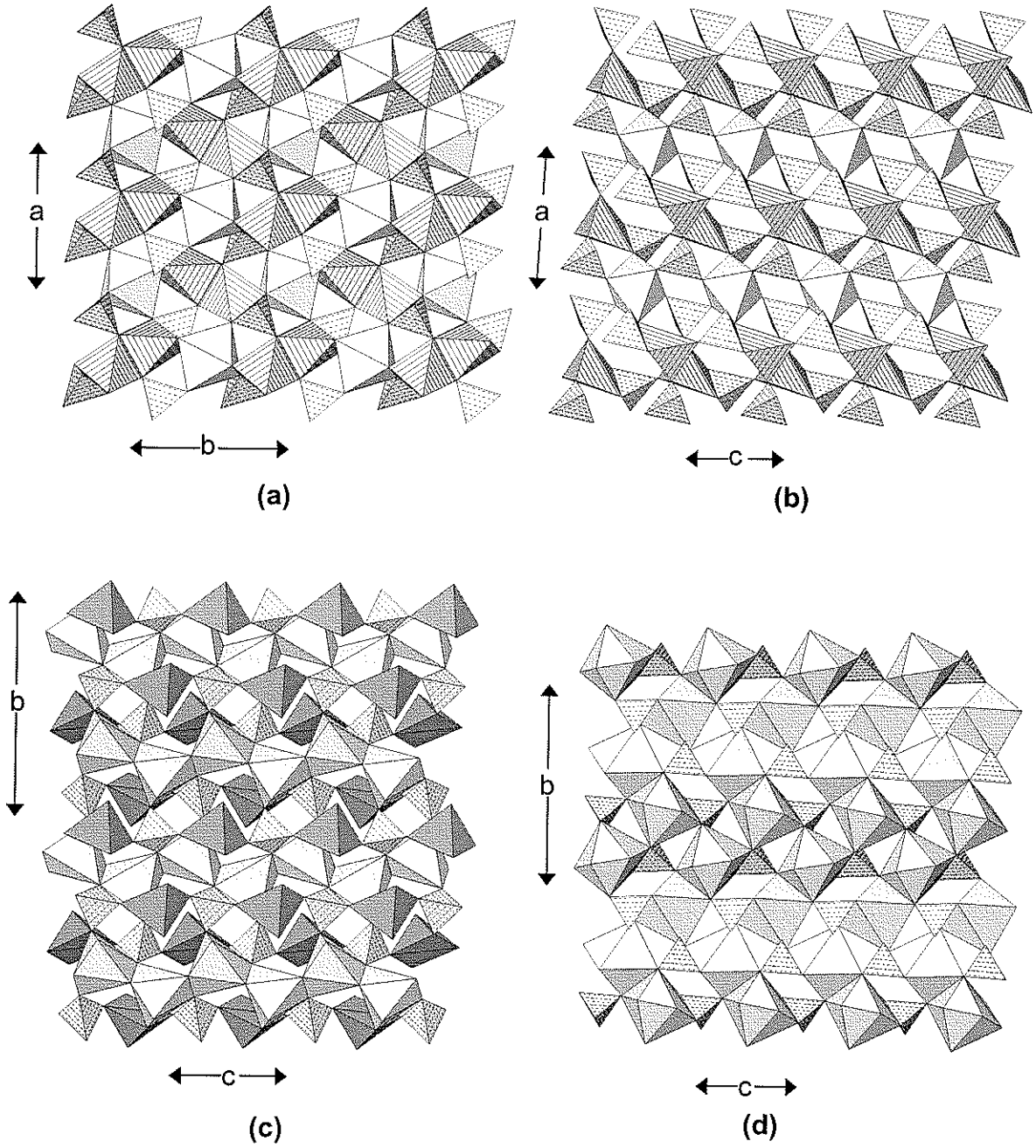

Figure 4.41. (a) farringtonite projected onto (001); (b) farringtonite projected onto (010); (c) a layer of the beusite structure projected onto (100), (MgO_6): shadow-shaded, (MgO_5): line-shaded; (d) another layer of the beusite structure projected onto (100), [7]- and [8]- coordinated polyhedra: shadow-shaded, [5]-coordinated polyhedra: dark-shadow-shaded.

$CaFe^{2+}Mn(PO_4)_2$. $^{[7]}M(1)$ polyhedra share an edge to form a dimer; these dimers occur at the vertices of a 4^4 net and share corners to form a sheet parallel to (100) that is strengthened by (PO_4) groups (Fig. 4.41c). Pyroxene-like edge-sharing chains of $M(3)$ octahedra extend in the *c*-direction and are linked by chains of alternating (PO_4) groups and $M(2)$ square pyramids (Fig. 4.41d), and these two types of sheet alternate in the [100] direction.

Wicksite, $NaCa_2[Fe^{2+}{}_2(Fe^{2+}Fe^{3+})Fe^{2+}{}_2(PO_4)_6(H_2O)_2]$, and the isostructural **bederite**, $\square Ca_2[Mn^{2+}{}_2Fe^{3+}{}_2Mn^{2+}{}_2(PO_4)_6(H_2O)_2]$,, are complex heteropolyhedral framework structures that may be resolved into layers parallel to (001). In wicksite at $z \approx 1/4$, ($Fe^{2+}\varphi_6$) and ($Fe^{3+}\varphi_6$) octahedra share an edge to form $[M_2\varphi_{10}]$ dimers that are canted to both the *a* and *b* axes, and are linked by (PO_4) tetrahedra to form the sheet shown in Figure 4.42a. At $z \approx 0$, two ($Fe^{2+}\varphi_6$) octahedra share edges with an ($Na\varphi_6$) octahedra to form an $[M_3\varphi_{14}]$ trimer that is decorated by (PO_4) tetrahedra linking adjacent free octahedron vertices to form a cluster of the form $[M_3(Po_4)_2\varphi_6]$. These clusters link by sharing of octahedron-tetrahedron vertices to form the layer shown in Figure 4.42b. There are two types of interstice within this layer. In the first type of interstice is the Ca site coordinated by nine anions; in the second type of interstice are four H atoms that belong to the two peripheral (H_2O) groups (Fig. 4.42b). The layers of Figure 4.42a and 4.42b link by edge-sharing between the ($Fe^{2+}\varphi_6$) [= $M(1)$] octahedron of one sheet with the ($Fe^{2+}\varphi_6$) [= $M(3)$ octahedron of the other sheet (Fig. 4.42c). The relation between wicksite and bederite is as follows: the Fe^{2+}=Na=Fe^{2+} triplet in wicksite (*cf.* Fig. 4.42b) is replaced by the [Mn^{2+}=□=Mn^{2+}] triplet in bederite.

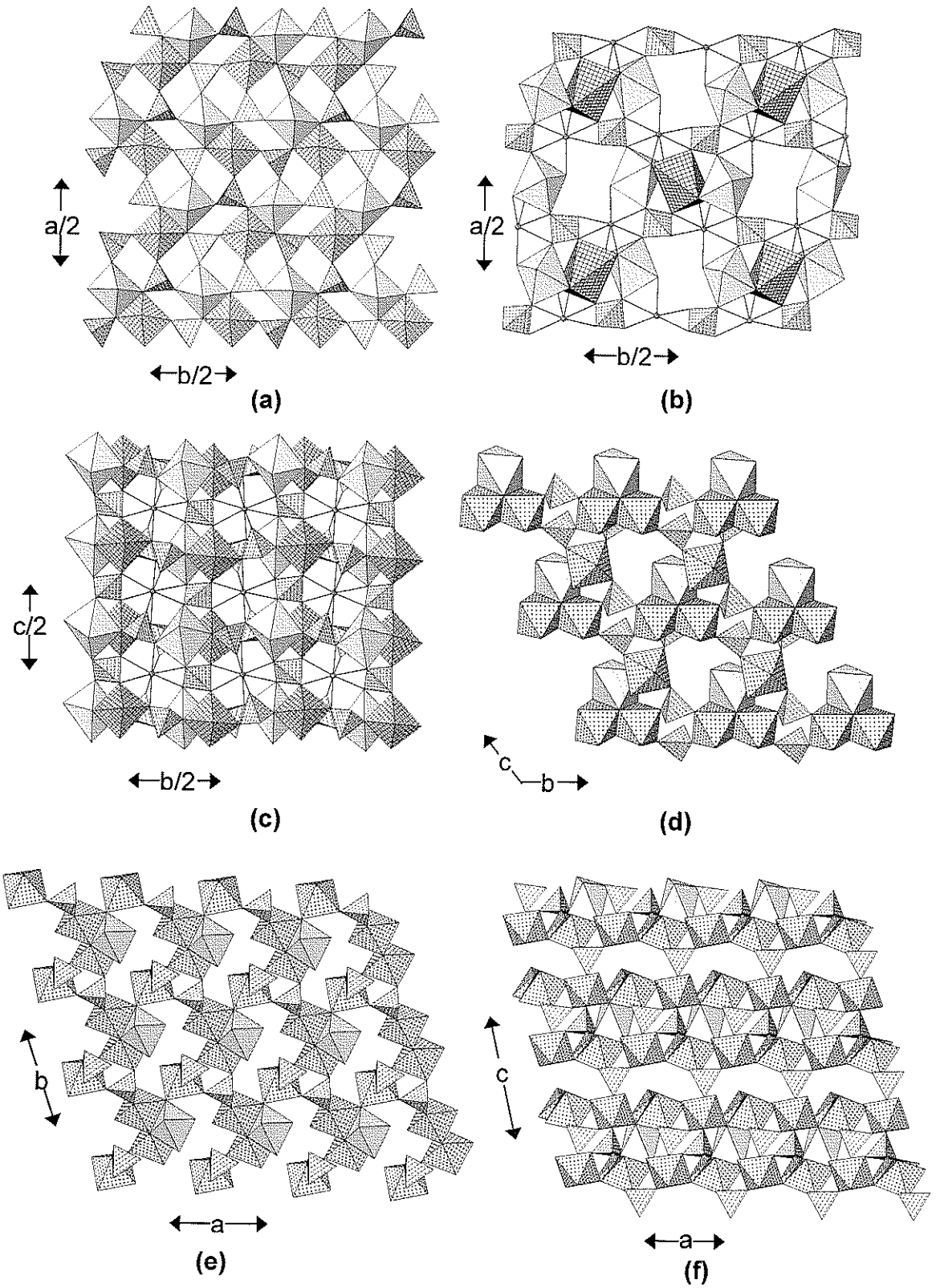

Figure 4.42. (a) layer 1 of bederite projected onto (001); (b) layer 2 of bederite projected onto (001); (c) stacking of layers projected onto (100); ($Fe^{3+}\varphi_6$): cross-shaded (a) and 4^4-net-shaded (b), ($Mn^{2+}\varphi_6$): shadow-shaded, Ca atoms: 4^4-net-shaded circles; (d) chalcosiderite projected onto (100); (e) chalcosiderite projected onto (001); (f) chalcosiderite projected onto (010), ($Fe^{3+}\varphi_6$): cross-shaded, ($Cu^{2+}\varphi_6$): shadow-shaded.

Chalcosiderite, $[Cu^{2+}Fe^{3+}_6(PO_4)_4(OH)_8(H_2O)_4]$, is a member of the turquoise group (Table 4.8). The structure contains trimers of edge-sharing octahedra, two ($Fe^{3+}\varphi_6$) and one ($Cu^{2+}\varphi_6$) octahedra that link by sharing corners with (PO_4) tetrahedra and other ($Fe^{3+}\varphi_6$) octahedra parallel to (100) (Fig. 4.42d). This linkage is also seen in Figure 4.42e, with additional linkage between trimers through corner-sharing with additional ($Fe^{3+}\varphi_6$) octahedra and (PO_4) groups to form a thick slab parallel to (001). These slabs stack along the *c*-direction (Fig. 4.42f) and are linked through bridging (PO_4) tetrahedra. The structure is fairly open to accommodate the extensive hydrogen-bonding associated with the (OH) and (H_2O) groups of the structural unit.

Leucophosphite, $K_2(H_2O)[Fe^{3+}_2(PO_4)_2(OH)(H_2O)]_2(H_2O)$, and **tinsleyite**, $K_2(H_2O)[Al_2(PO_4)_2(OH)(H_2O)]_2(H_2O)$, are based on a prominent tetramer of octahedra in which two ($Fe^{3+}O_6$) octahedra share an edge, and an additional ($Fe^{3+}O_6$) octahedron links to the anions at each end of the shared edge. Moore (1972b) notes that the topologically identical cluster occurs in the sulfate mineral amarantite. This cluster is decorated by four (PO_4) tetrahedra to form an $[Fe^{3+}_4(SO_4)_4\varphi_{12}]$ cluster (Fig. 4.43a). These clusters link by sharing vertices between octahedra and tetrahedra to form a framework (Figs. 4.43b,c) with K in the interstices. Inspection of Figure 4.43a shows that the decorated tetramer can be regarded as a condensation of two $[M_2(TO_4)_2\varphi_7]$ clusters (Fig. 4.12e), a group that Hawthorne (1979a) showed is common as a fragment in several complex phosphate structures. In fact, when the structure is viewed down [100], it can be considered as sheets of corner-shared $[M_2(TO_4)_2\varphi_3]$ clusters, similar to those in the structure of minyulite (Fig. 4.20a).

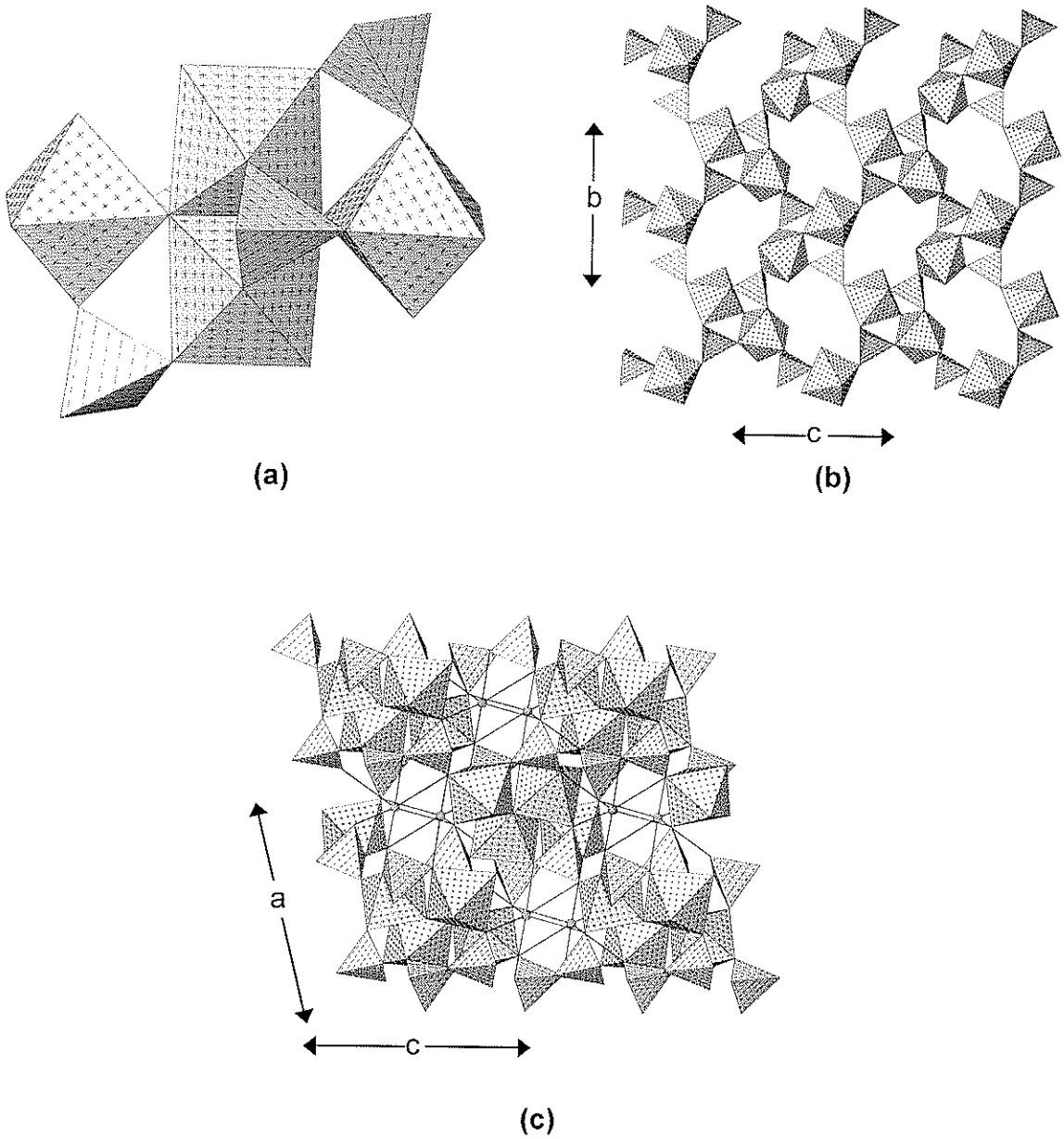

Figure 4.43. The crystal structure of leucophosphite; (a) the $[Fe^{3+}{}_4(PO_4)_4\varphi_{12}]$ cluster; (b) projected onto (100); (c) projected onto (010); $(Fe^{3+}\varphi_6)$: cross-shaded, K atoms: shaded circles.

Cacoxenite, $[Fe^{3+}_{24}Al(PO_4)_{17}O_6(OH)_{12}(H_2O)_{24}](H_2O)_{51}$, surely has to qualify as one of the more complicated of Nature's masterpieces. Moore and Shen (1983a) identified two key *FBB*s in this structure. Pairs of $(Fe^{3+}\varphi_6)$ octahedra share an edge to form dimers, and three dimers share octahedron corners to form a ring that has a (PO_4) group at its core, linking to one end of each of the shared edges in the cluster (Fig. 4.44a). The resulting *FBB* has the form $[Fe^{3+}_6(PO_4)\varphi_{24}]$ and resembles the $[Fe^{3+}_6(PO_4)\varphi_{24}]$ group in mitridatite (Fig. 4.28). The second *FBB* consists of one dimer of edge-sharing octahedra with two additional octahedra linked by sharing corners with each end of the shared edge of the dimer. Four (PO_4) groups each share two corners with octahedra at the periphery of the cluster, and a fifth (PO_4) group shares corners with three of the octahedra (Fig. 4.44b). The resulting *FBB* has the form $[Fe^{3+}_3Al(PO_4)_5\varphi_9]$, and has some similarities with clusters in melonjosephite (Fig. 4.40c) and leucophosphate (Fig. 4.43a). These two *FBB*s polymerize by sharing polyhedron corners to form rings consisting of twelve *FBB*s, each type alternating around the ring. These rings are arranged at the vertices of a 3^6 net (Fig. 4.44c). The layer shown in Figure 4.44c repeats in the *c*-direction (Fig. 4.44d), linking by sharing polyhedron edges and corners, with the addition of some linking octahedra, to form a framework with extremely wide channels that are filled with (H_2O) groups.

Althausite, $[Mg_4(PO_4)_2(OH)F]$, and **satterlyite**, $[Fe^{2+}_4(PO_4)_2(OH)_2]$, have their divalent cations in both [5]- and [6]-coordination, triangular bipyramidal and octahedral. In althausite, $[M\varphi_4]$ chains of *trans* edge-sharing $(Mg\varphi_6)$ octahedra extend in the *b*-direction. These chains link in the *a*-direction by sharing corners

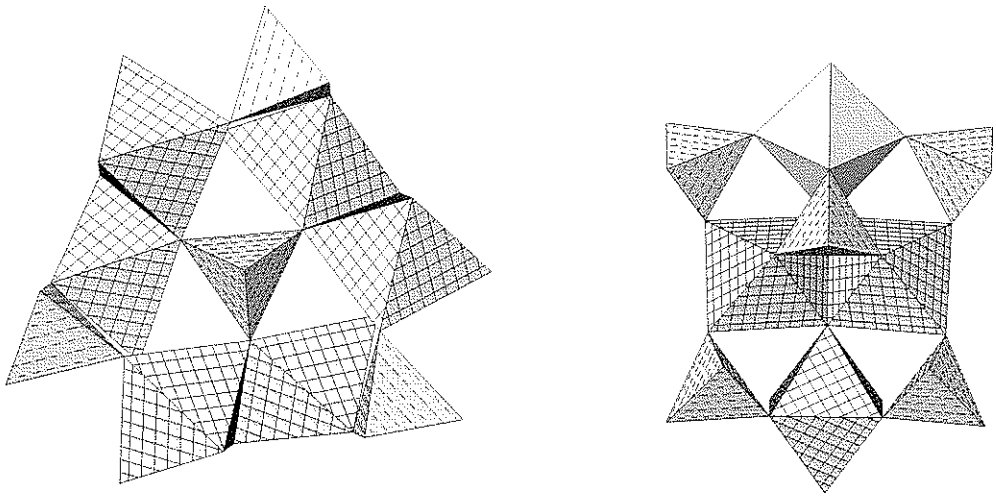

(a) (b)

Figure 4.44. The crystal structure of cacoxenite; (a) the $[Fe^{3+}{}_6(PO_4)\varphi_{24}]$ cluster; (b) the $[Fe^{3+}{}_3Al(PO_4)_5\varphi_9]$ cluster; $(Fe^{3+}\varphi_6)$: 4^4-net shaded, $(Al\varphi_6)$: shadow-shaded.

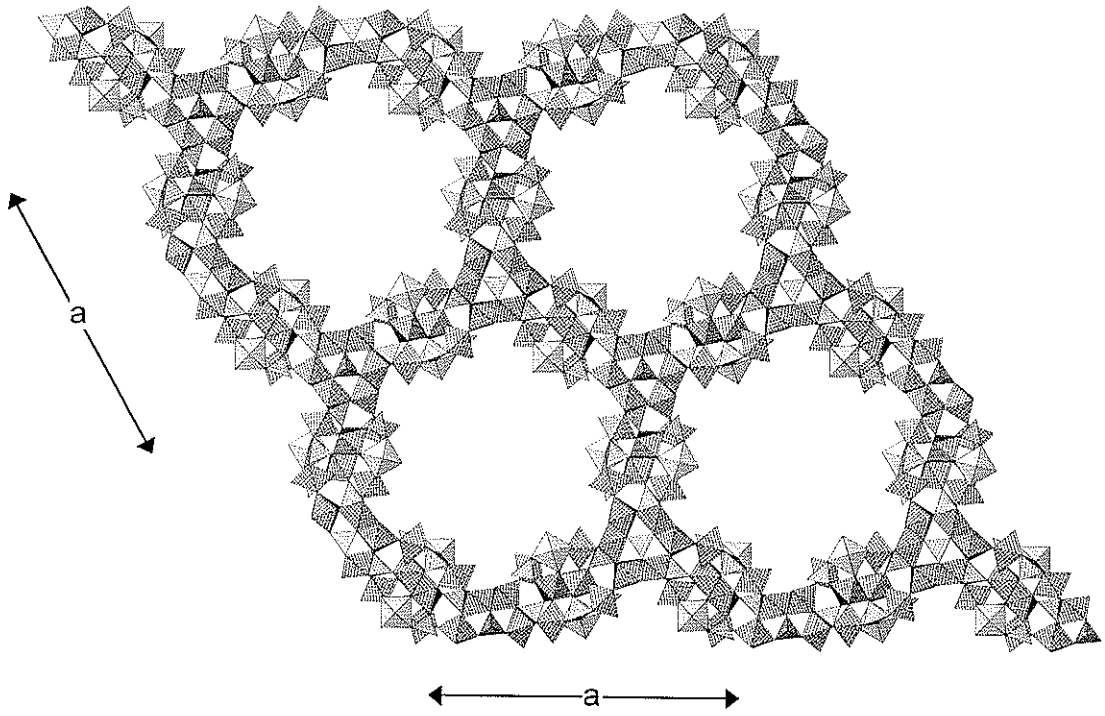

(c)

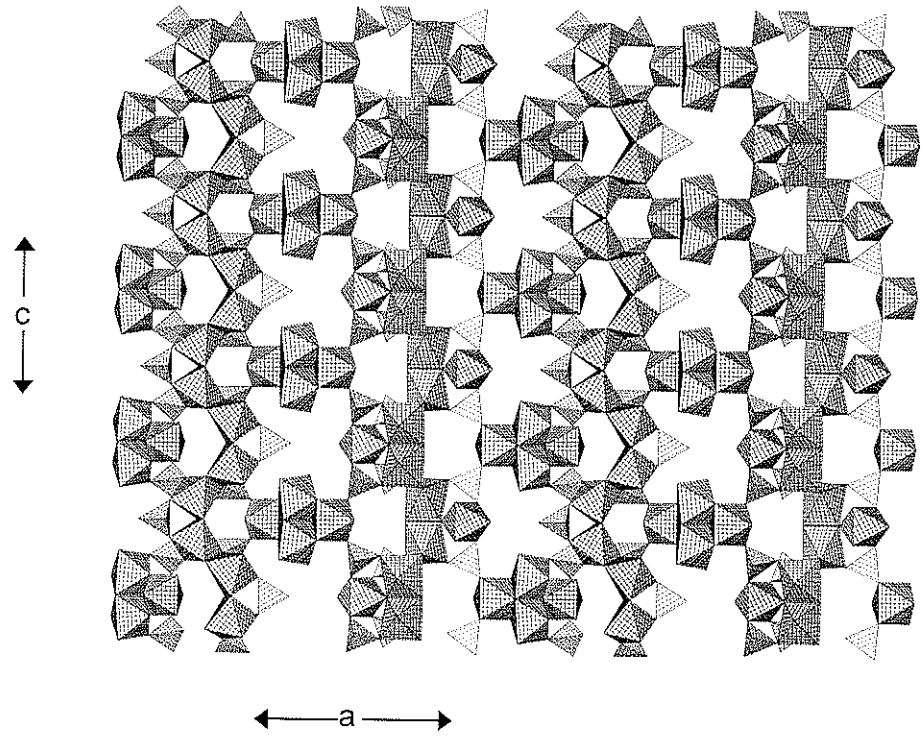

(d)

Figure 4.44. The crystal structure of cacoxenite; (c) the structure projected onto (001); (d) the structure projected onto (010). Legend as in Fig. 4.44a,b.

between tetrahedra and octahedra (Fig. 4.45a) to form a sheet parallel to (001). These sheets are linked in the *c*-direction by sharing octahedron edges with ($Mg\varphi_5$) triangular bipyramids (Fig. 4.45b). In althausite, ~ 20% of the (OH) is replaced by O^{2-} and the excess charge is compensated by omission (*i.e.*, incorporation of vacancies) of F.

In **hureaulite**, $[Mn^{2+}{}_5(PO_3\{OH\})_2(PO_4)_2(H_2O)_4]$, five ($Mn^{2+}\varphi_6$) octahedra share edges to form a kinked linear pentamer that extends in the *a*-direction (Fig. 4.45c). These pentamers occur at the vertices of a plane centered orthorhombic net and link by sharing corners (4 per pentamer) to form a sheet of octahedra parallel to (001). Adjacent pentamers are also linked through (PO_4) groups with which they share corners to form a thick slab parallel to (001). These slabs link in the *c*-direction through corner sharing between octahedra and tetrahedra (Fig. 4.45d). There are fairly large interstices within the resulting framework (Fig. 4.45c), but these are usually unoccupied. However, Moore and Araki (1973) suggest that alkalis or alkaline earths could occupy this cavity with loss of the acid character of the acid-phosphate groups.

Thadeuite, $[CaMg_3(PO_4)_2(OH)_2]$, is a densely packed framework of (PO_4) tetrahedra and both ($Ca\varphi_6$) and ($Mg\varphi_6$) octahedra. ($Mg\varphi_6$) octahedra share edges to form chains that extend in the *c*-direction (Fig. 4.45e). These chains are decorated by (PO_4) tetrahedra that link octahedra along the chain, and also link between chains in the *a*-direction. Interchain linkage also occurs by edge-sharing with ($Ca\varphi_6$) octahedra (shown as ball-and-stick in Figure 4.45e). The resulting layers stack in the *b*-direction (Fig. 4.45f) and are linked by (PO_4) groups. In this view, the more complicated nature of the chains of octahedra is apparent: two

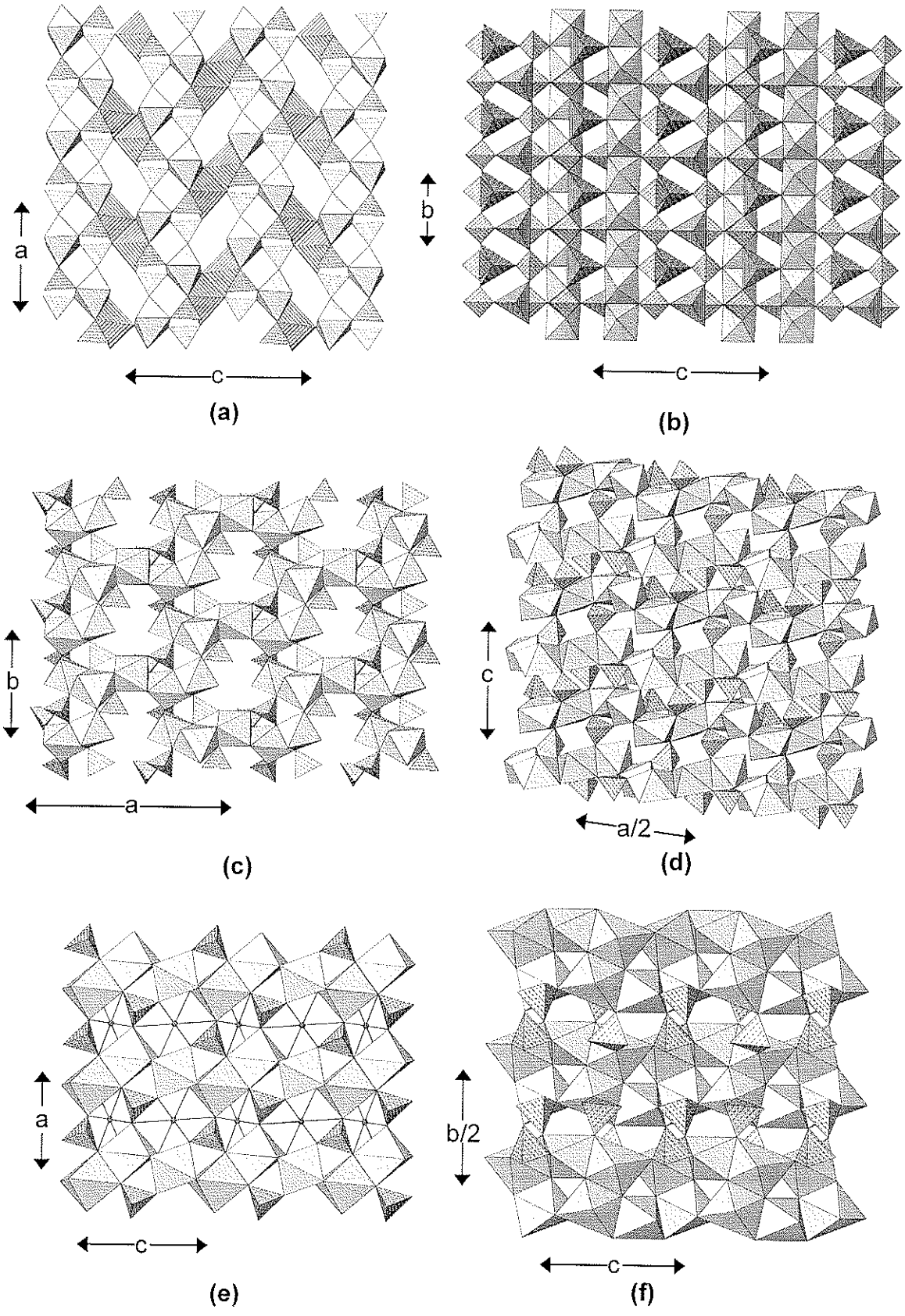

Figure 4.45. (a) althausite projected onto (010); (b) althausite projected onto (100), ($Mg\varphi_5$): line-shaded; (c) hureaulite projected onto (001); (d) hureaulite projected onto (010); (e) thadeuite projected onto (010); (f) thadeuite projected onto (100), ($Mg\varphi_6$): shadow-shaded.

single [$M\varphi_4$] chains are joined by edge-sharing between octahedra, and these two chains twist together in a helical fashion. Despite its common stoichiometry, $M_2(T\varphi_4)\varphi$, thadeuite shows no close structural relation with any other minerals of this stoichiometry.

Bakhchisaraitsevite, $Na_2(H_2O)[Mg_5(PO_4)_4(H_2O)_5](H_2O)$, is one of themost complex minerals found in Nature. Pairs of ($Mg\varphi_6$) octahedra meld to form [$Mg_2\varphi_{10}$] dimers which then link by sharing edges to form zig-zag [$Mg\varphi_4$] chains that extend in the *a*-direction (Fig. 4.46a). The vertices of the shared edge of each dimer link to (PO_4) groups which also link to the corresponding vertices of the neighboring dimer in the chain, and chains adjacent in the *b*-direction link by octahedron-tetrahedron and octahedron-octahedron corner-linkages, forming a complex sheet parallel to (001).These sheets are cross-linked in the *c*-direction by [$Mg_2\varphi_{10}$] dimers, leaving large interstices between the sheets (Fig. 4.46b). Within these interstices are interstitial Na and (H_2O) groups: [5]- and [7]-coordinated Na each bond to one (H_2O) group and four and six O-atoms, respectively, of the structural unit, and there is one interstitial (H_2O) group not bonded to any cations, but held in the structure solely by hydrogen bonds.

The minerals of the **phosphoferrite** group have the general formula $M(1)M(2)_2(PO_4)_2X_3$, where the *M* cations may be divalent or trivalent and *X* = (OH), (H_2O); these minerals are isostructural, despite differences in both cation and anion charges (Moore and Araki 1976, Moore et al. 1980). The currently known species of this group are **phosphoferrite**, $[Fe^{2+}_3(PO_4)_2(H_2O)_3]$, **reddingite**, $[Mn^{2+}_3(PO_4)_2(H_2O)_3]$, **landesite**, $[Fe^{3+}Mn^{2+}_2(PO_4)_2(OH)(H_2O)_2]$, and **kryzhanovskite**, $[Fe^{3+}_3(PO_4)_2(OH)_3]$. A prominent feature of these structures is a

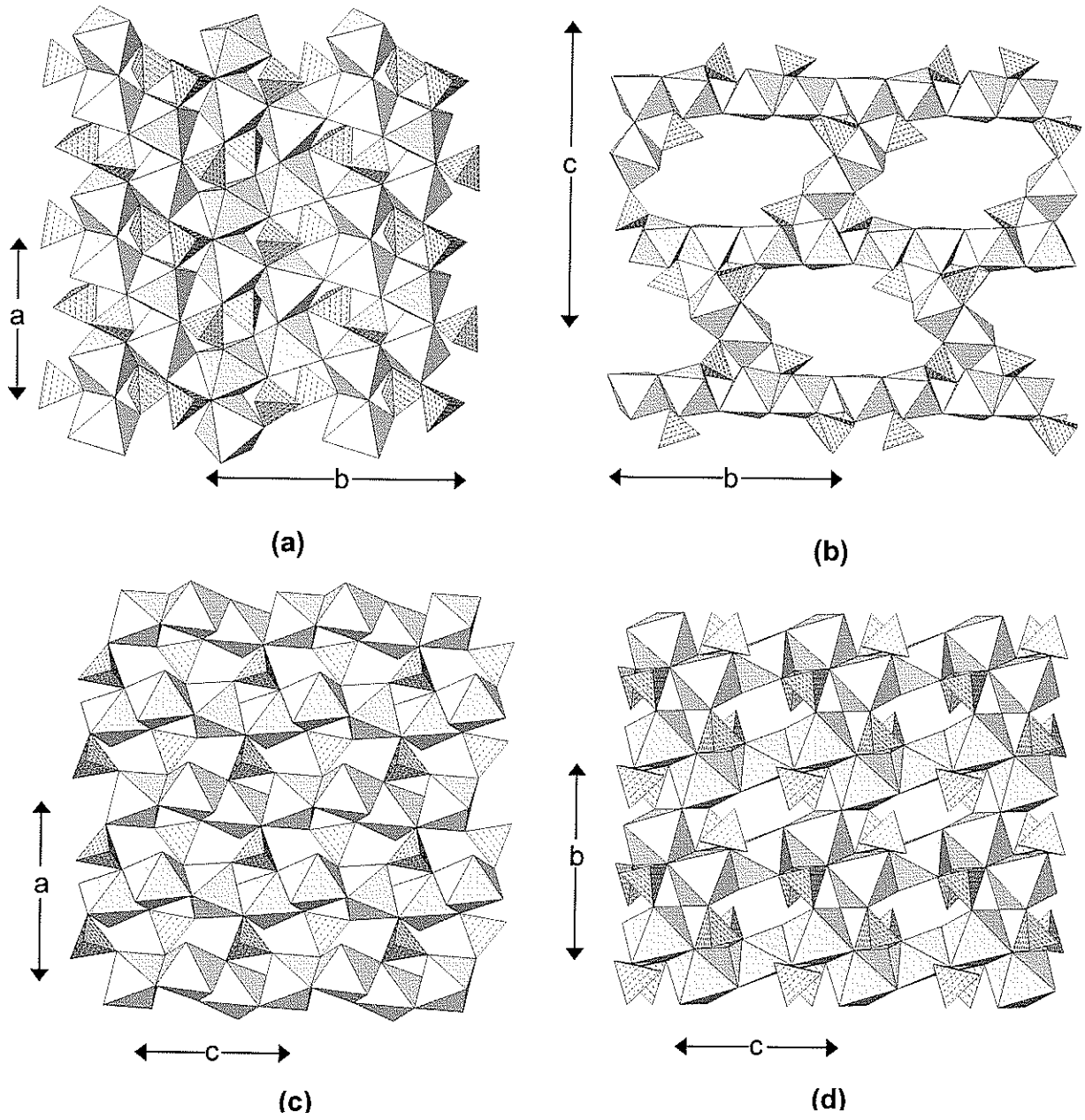

Figure 4.46. (a) bakhchisaraitsevite projected onto (001); (b) bakhchisaraitsevite projected onto (100); (c) kryzhanovskite/phosphoferrite projected onto (010); (d) kryzhanovskite/phosphoferrite projected onto (100); ($Fe\Phi_6$): shadow-shaded.

trimer of edge-sharing octahedra that is canted at about 20° to the *c*-axis (Fig. 4.46c). These trimers link by sharing octahedron edges to form chains of en-echelon trimers that extend in the *c*-direction. These chains link in the *b*-direction by sharing octahedron vertices to form a sheet of octahedra parallel to (100). The upper and lower surfaces of the sheet are decorated by (PO_4) tetrahedra, and a prominent feature of this decorated sheet is the $[M_2(TO_4)_2\varphi_7]$ cluster (Fig. 4.12e) (Hawthorne 1979a). These sheets stack in the *a*-direction, and link by sharing octahedron and tetrahedron vertices (Fig. 4.46d). Moore and Araki (1976) showed that single crystals of phosphoferrite can be transformed by heating (oxidation-dehydroxylation) in air to single crystals of kryzhanovskite.

Griphite, $Ca_4F_8[A_{24}Fe^{2+}_4Al_8(PO_4)_{24}]$, where $A \approx Li_2Na_4Ca_2Fe^{2+}_2Mn^{2+}_{14}$ and has triangular bipyramidal coordination, is rather complicated from both a chemical and a structural perspective, and we could not write a satisfactory end-member chemical formula; even the simplification of the above formula produces a substantial (~ 2^+) charge imbalance. (AlO_6) octahedra share all vertices with (PO_4) tetrahedra, forming –(AlO_6)–(PO_4)–(AlO_6)–(PO_4)– chains that extend in the *a*-, *b*- and *c*-directions to form a very open framework of the form $[Al_8(PO_4)_{24}]$ (Fig. 4.47a). The ($Fe^{2+}O_6$) octahedron links to six (PO_4) groups by sharing corners, and the resultant clusters link to a framework of corner-sharing (PO_4) groups and (CaO_8) cubes (Fig. 4.47b). The triangular bipyramids of the *A* cations share corners to form a very irregular sheet centered on $z \sim 0.62$ (Fig. 4.47c). The three sheets of Figures 4.47a,b,c meld to form a very complicated heteropolyhedral framework (Fig. 4.47d) (in which the *A* cations are shown as circles for simplicity).

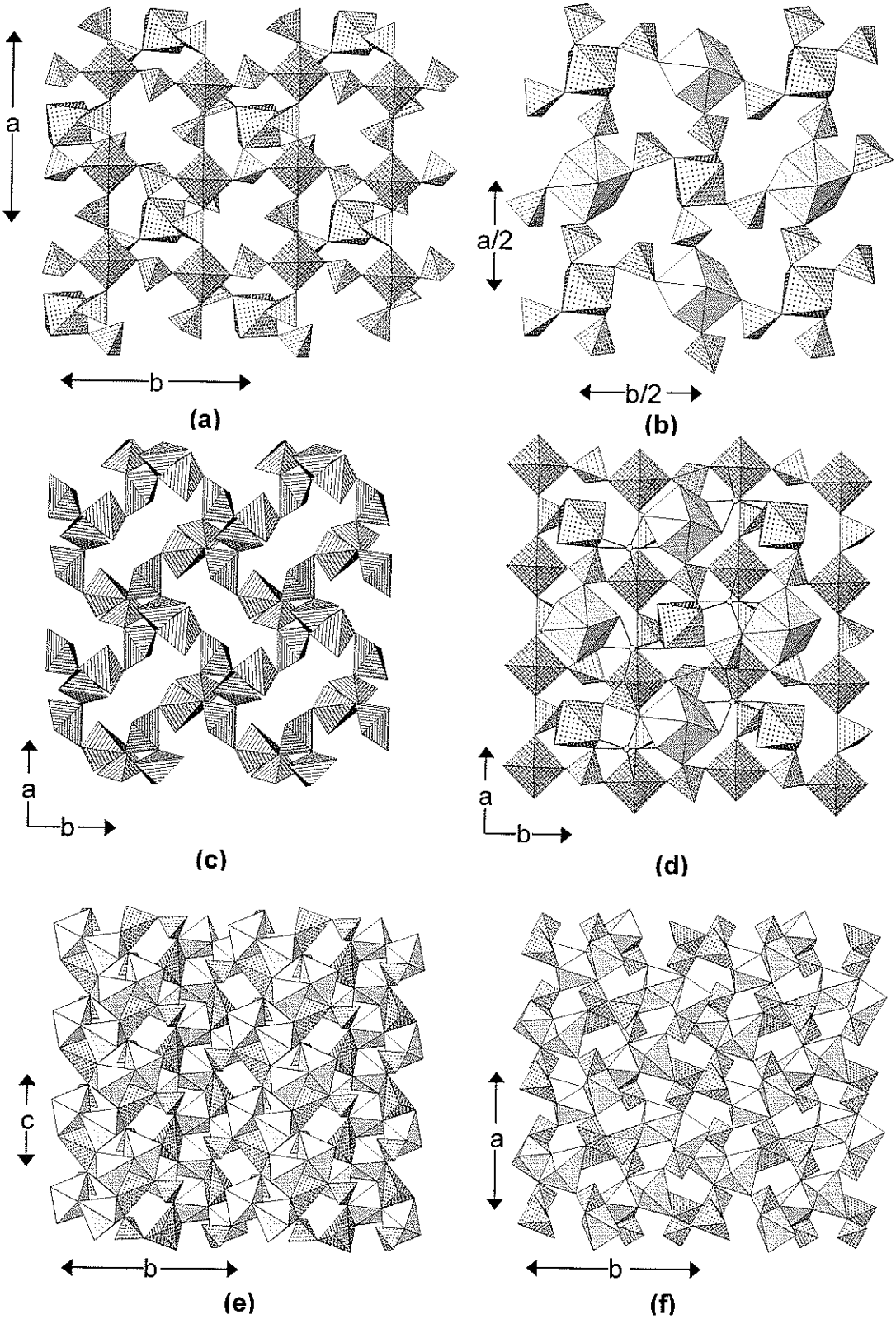

Figure 4.47. (a) griphite layer at $z \sim 1/4$ projected onto (001); (b) griphite layer at $z \sim 1/2$ projected onto (001); (c) griphite layer at $z \sim 0.62$ projected onto (001); (d) griphite structure projected onto (001); ($Al\varphi_6$): 4^4-net shaded, ($Ca\varphi_8$): shadow-shaded, ($Fe^{3+}\varphi_6$): cross-shaded, triangular bipyramids: line-shaded in (c) and circle; (e) cornetite projected onto (100); (f) cornetite projected onto (001); ($Cu^{2+}\varphi_6$): shadow-shaded, ($Cu^{2+}\varphi_5$): cross-shaded.

Cornetite, $[Cu^{2+}_3(PO_4)(OH)_3]$, contains Cu^{2+} in both octahedral and triangular bipyramidal coordinations. Pairs of $(Cu^{2+}\varphi_6)$ octahedra share an edge to form $[Cu^{2+}_2\varphi_{10}]$ dimers that are inclined at ~30° to the *b*-direction (Fig. 4.47e). Dimers adjacent in the *c*-direction show opposite cants and link by an octahedron from one dimer bridging the apical vertices of the adjacent dimer to form serrated ribbons that extend in the *c*-direction. These ribbons are linked by sharing corners with (PO_4) tetrahedra, and edges and corners with$(Cu^{2+}\varphi_5)$ triangular bipyramids (Fig. 4.47f).

Gladiusite, $Fe^{2+}_4Fe^{3+}_2(PO_4)(OH)_{11}(H_2O)$, is an open framework structure with extensive hydrogen bonding. In the structure, $(Fe^{2+}\varphi_6)$ and $(Fe^{3+}\varphi_6)$ octahedra form $[M\varphi_4]$ chains of edge-sharing octahedra that extend in the *c*-direction (Fig. 4.48a). Pairs of these chains meld by sharing edges to form ribbons, and these ribbons link in triplets by sharing corners between octahedra such that the plane of each succeeding ribbon is offset from the first (Fig. 4.48b). The ribbons are further linked through $(P\varphi_4)$ groups that share one vertex with each ribbon (Figs. 4.48a,b). Figure 4.48c illustrates the linkage between these ribbons in three dimensions. The ribbons are inclined at ~ 45° to the *c*-axis and are repeated by the *b*-translation to form a row of parallel ribbons centered on $z \approx 0$. Adjacent rows centered on $z \approx ½$ have the ribbons arranged with the opposite inclination to the *a*-axis, and adjacent ribbons link by sharing octahedron vertices (Fig. 4.48c). The resultant framework is very open, and the interstitial space is criss-crossed by a network of hydrogen bonds.

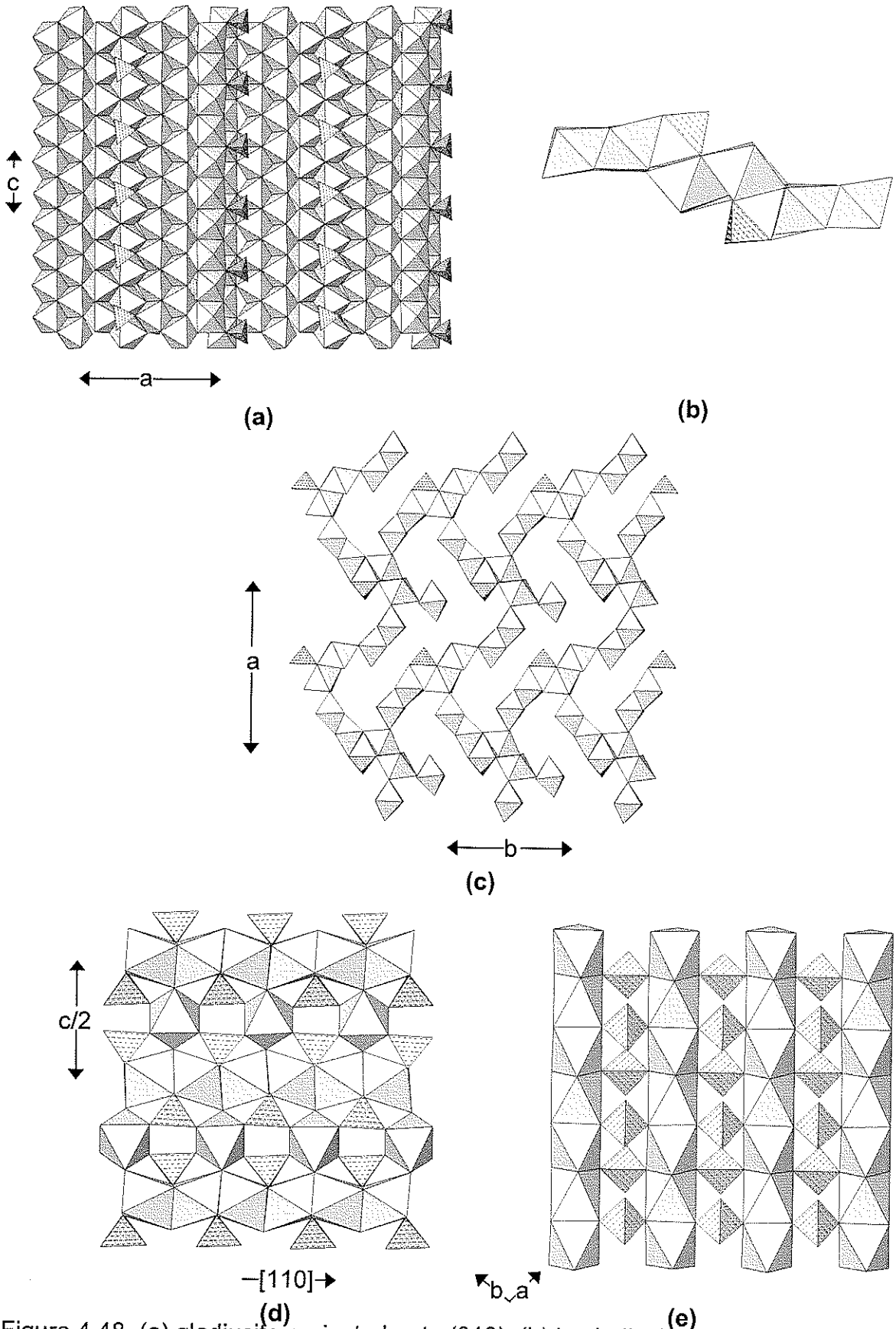

Figure 4.48. (a) gladiusite projected onto (010); (b) in gladiusite, the linking of adjacent pairs of chains to form a triplet of offset chains with linking (PO_4) tetrahedra; (c) gladiusite projected onto (001); (d) lipscombite projected onto (100); (e) lipscombite projected onto (001), ($\{Fe^{2+},Fe^{3+}\}\varphi_6$): shadow-shaded.

M≡M, M–M, M–T linkage. **Lipscombite**, $[Fe^{2+}Fe^{3+}_2(PO_4)_2(OH)_2]$, is somewhat of an enigma. Katz and Lipscomb (1951) applied this name to synthetic $Fe_7(PO_4)_4(OH)_4$ with symmetry $I4_122$ and a = 5.37, c = 12.81 Å. Gheith (1953) used the name for tetragonal synthetic compounds varying between $Fe^{2+}_8(PO_4)_4(OH)_4$ and $Fe^{3+}_{3.5}(PO_4)_4(OH)_4$. More recently, Vochten and DeGrave (1981) and Vochten et al. (1983) gave the cell parameters of synthetic lipscombite as $a = b$ = 5.3020(5), c = 12.8800(5) Å. However, Lindberg (1962) reported natural manganoan lipscombite with symmetry $P4_12_12$ and a = 7.40, c = 12.81 Å. Vencato et al. (1989) presented the structure of synthetic lipscombite with symmetry $P4_32_12$ and a = 7.310(3), c = 13.212(7) Å, in accord with the results of Lindberg (1962), who seems to be the only person who has actually characterized the mineral.

The structure reported by Vencato et al. (1989) consists of face-sharing chains of $(Fe^{2+}\varphi_6)$ and $(Fe^{3+}\varphi_6)$ octahedra that extend in the [110] and $[1\bar{1}0]$ directions (Fig. 4.48d,e). These chains link by corner-sharing between octahedra of adjacent chains, and also by sharing corners with (PO_4) tetrahedra. Because of the 4_3 symmetry, the structure consists of layers in which the face-sharing chains extend only in a single direction, and adjacent layers that are related by 4_3 symmetry have the chains extending in orthogonal directions. A single layer is shown in Figure 4.45e, in which all the chains extend along [110] and are linked within the layer by rows of bridging (PO_4) groups. Note that in the face-sharing chain, two of the three symmetrically distinct octahedra are partly occupied.

The minerals of the **burangaite**, $Na[Fe^{2+}Al_5(PO_4)_4(OH)_6(H_2O)_2]$, group contain a trimer of face-sharing octahedra that is a feature of several basic iron-

phosphate minerals (Moore 1970). An ($Fe^{2+}\varphi_6$) octahedron shares two *trans* faces with ($Al\varphi_6$) octahedron to form a trimer of the form [$M_3\varphi_{12}$] (the *h* cluster of (Moore 1970). This trimer is corner linked to two ($Al\varphi_6$) octahedra and two (PO_4) tetrahedra to produce a cluster of the general form [$M_5(TO_4)_2\varphi_{18}$]. This cluster polymerized in the *c*-direction to form a dense slab by corner-sharing between ($Al\varphi_6$) octahedra and by corner-sharing between octahedra and tetrahedra. This slab is oriented parallel to (100) (Fig. 4.49a) and adjacent slabs are weakly linked in the [100] direction by additional ($Al\varphi_6$) octahedra that share corners with both tetrahedra and octahedra. The resulting framework has large interstices that are occupied by [8]-coordinated Na that is bonded to two (H_2O) groups. Note that Moore (1970) gave the formula of the isostructural dufrénite as $Ca_{0.5}Fe^{2+}Fe^{3+}{}_5(PO_4)_4(OH)_6(H_2O)_2$, which is in accord with the requirements for an end-member composition (Hawthorne 2002). However, both Moore (1984) and Nriagu (1984) incorrectly list the formula of dufrénite as $CaFe^{3+}{}_6(PO_4)_4(OH)_6(H_2O)_2$; this formula has a net charge of 2^+. Van der Westhuizen et al. (1990) reported electron-microprobe analyses for dufrénite, but many of the resultant formulae are incompatible with the dufrénite structure.

The minerals of the **rockbridgeite**, [$Fe^{2+}Fe^{3+}{}_4(PO_4)_3(OH)_5$], group are also based on the *h* cluster, but the mode of linkage of these clusters is very different from that in the minerals of the burangaite group The face-sharing trimers link by sharing octahedron corners to form chains of octahedra that extend in the *b*-direction (Fig. 4.49b). Chains adjacent in the *a*-direction are linked by [$M_2(TO_4)\varphi_8$] clusters and (PO_4) groups that link to two adjacent trimers and two

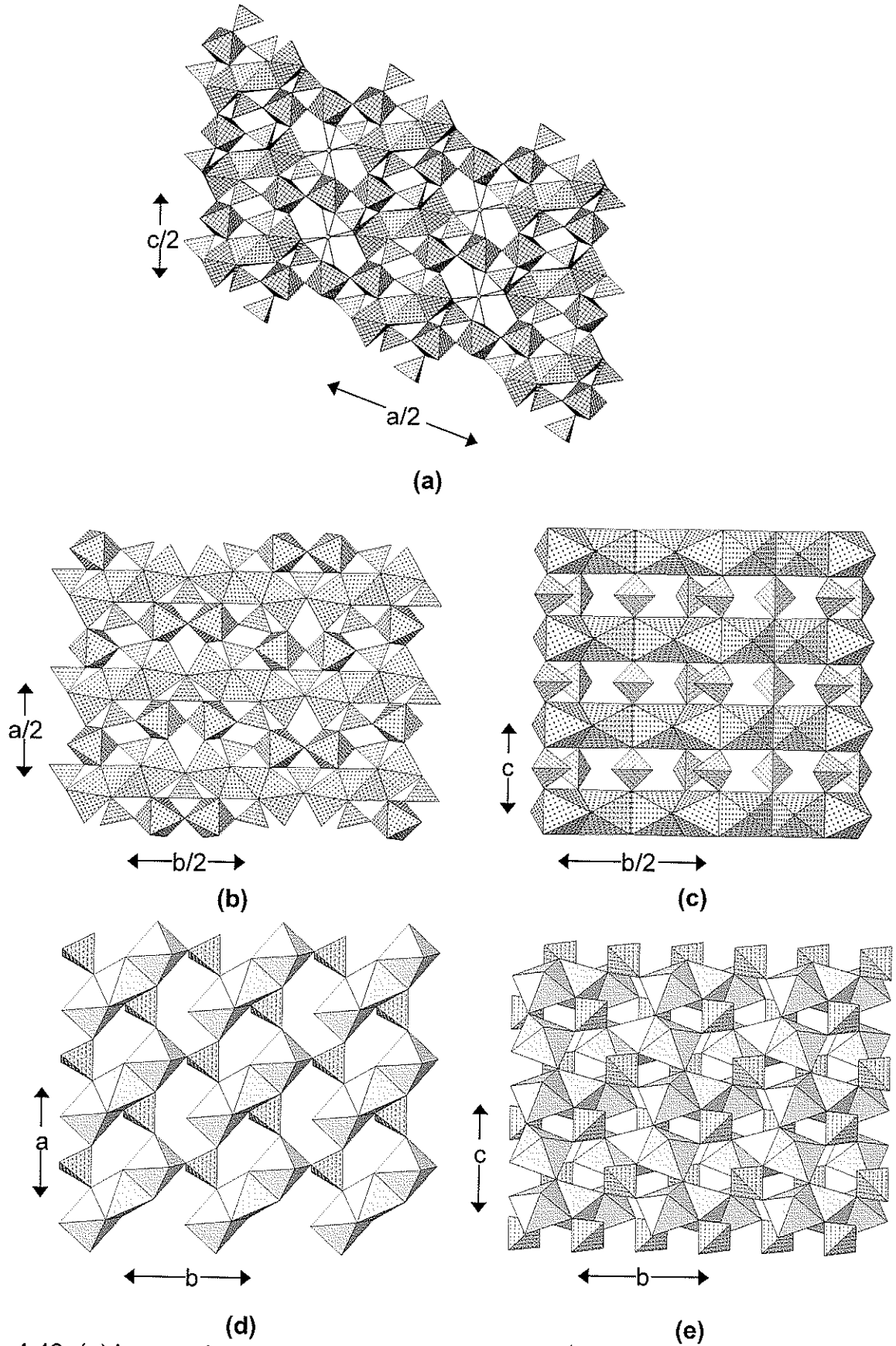

Figure 4.49. (a) burangaite projected onto (010), (Alφ_6): 4^4-net-shaded, ($Fe^{3+}\varphi_6$): cross-shaded, Na atoms: shaded circles; (b) rockbridgeite projected onto (001); (c) rockbridgeite projected onto (100); ({Fe^{2+},Fe^{3+}}φ_6): cross-shaded; (d) barbosalite projected onto (001); (e) barbosalite projected onto (100), ({Mg,Al}φ_6): shadow-shaded .

[$M_2(TO_4)\varphi_8$] clusters, forming complex sheets parallel to (001). When viewed in the *a*-direction (Fig. 4.49c), the very layered aspect of the structure is apparent, layers of octahedra alternating with layers of tetrahedra.

The minerals of the **lazulite**, [$MgAl_2(PO_4)_2(OH)_2$], group contain the *h* cluster, a trimer of face-sharing octahedra, that is characteristic of several basic phosphate minerals. An ($Mg\varphi_6$) octahedron is sandwiched between two ($Al\varphi_6$) octahedra, and the resulting trimers are arranged at the vertices of a 4^4 net and extending in the [110] direction (Fig. 4.49d). Adjacent trimers are linked by sharing corners with (PO_4) groups, and when viewed down [001], the structure consists of layers of octahedra and tetrahedra. When viewed down [100] (Fig. 4.49e), it can be seen that the trimers of adjacent layers are canted in opposing direction, thereby promoting linkage of each (PO_4) tetrahedron to four different trimers. The resulting arrangement is quite densely packed.

Trolleite, [$Al_4(PO_4)_3(OH)_3$], is a very dense structure with some similarities to the structural arrangement of the minerals of the lazulite group (Table 4.8). There are two prominent chain motifs that constitute the building blocks of this structure. There is an [$Al(PO_4)\varphi_3$] 7 Å chain (Fig. 4.13c) that extends in the *c*-direction (Fig. 4.50a), giving the 7.1 Å repeat along the *c*-axis. There is also an [$Al(PO_4)\varphi_4$] chain that assumes a very contorted geometry (Fig. 4.50a) so that it has the same repeat distance along its length as the [$Al(PO_4)\varphi_3$] chain to which it is attached by sharing octahedron faces. These rather complex double-chains link in the *b*-direction by sharing vertices of the tetrahedra of the [$Al(PO_4)\varphi_3$] chain with the octahedra of the [$Al(PO_4)\varphi_4$] chain (Fig. 4.50a). These slabs repeat

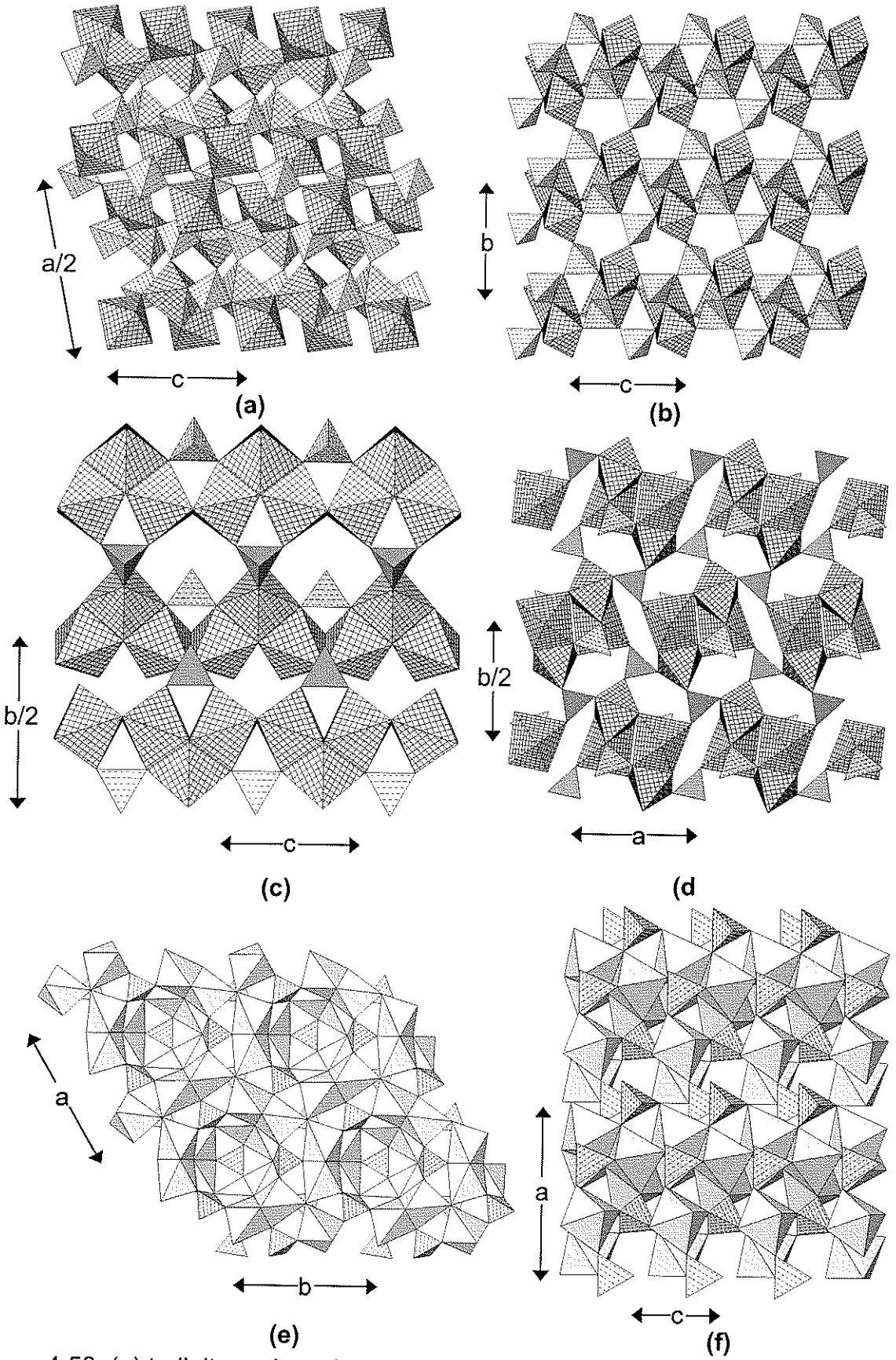

Figure 4.50. (a) trolleite projected onto (010); (b) trolleite projected onto (100), ($Al\varphi_6$): 4^4-net-shaded; (c) seamanite projected onto (100); (d) seamanite projected onto (001), ($Mn^{2+}\varphi_6$): 4^4-net-shaded ; (e) holtedahlite projected onto (001); (f) holtedahlite projected onto (010), ($Mg\varphi_6$): shadow-shaded .

in the *a*-direction in a very complex manner. As shown in Figure 4.50b, these slabs meld by sharing octahedron-tetrahedron vertices between adjacent $[Al(PO_4)\varphi_3]$ chains to form a thick slab: $[Al(PO_4)\varphi_4]$–$[Al(PO_4)\varphi_3]$–$[Al(PO_4)\varphi_3]$–$[Al(PO_4)\varphi_4]$ that constitute one-half the cell in the *a*-direction. The thick slabs link by sharing octahedron vertices between $[Al(PO_4)\varphi_4]$ chains to form a very dense framework.

Seamanite, $[Mn^{2+}{}_3(B\{OH\}_4)(PO_4)]$, is a mixed phosphate-borate mineral based on chains of $(Mn\varphi_6)$ octahedra which consist of free-sharing $[M_3\varphi_{12}]$ trimers that link by sharing octahedron edges to form an $[M_3\varphi_{10}]$ chain that extends in the *c*-direction (Fig. 4.50c). The rather unusual $[M_3\varphi_{12}]$ trimer is apparently stabilized by the $(B\varphi_4)$ group that spans the apical vertices of the edge-sharing octahedra (Moore and Ghose 1971). Additional linkage along the length of the chain is provided by (PO_4) tetrahedra that link apical vertices on neighboring $(M\varphi_6)$ octahedra such that the (PO_4) and $(B\varphi_4)$ tetrahedra adopt a staggered configuration on either side of the $[M(B\varphi_4)(PO_4)\varphi_6]$ chain. These chains condense in pairs by sharing both octahedron-octahedron and octahedron-tetrahedron vertices to form columns, seen end-on in Figure 4.50d. These columns link together in the *a*- and *b*-directions by sharing vertices between tetrahedra and octahedra, with additional linkage involving hydrogen bonds.

M=M, M=T, M–T linkage. **Holtedahlite**, $[Mg_{12}(PO_3\{OH\})(PO_4)_5(OH)_6]$, contains dimers of face-sharing $(Mg\varphi_6)$ (Fig. 4.50e). These dimers link by sharing edges to form ribbons that extend in the *c*-direction and contain $(PO_3\{OH\})$

tetrahedra that link to all three ribbons (Fig. 4.50e). These channels link in the *a*- (and *b*-) direction by sharing octahedron corners and by sharing octahedron corners with bridging (PO_4) tetrahedra (Figs. 4.50e,f).

The minerals of the **triphylite-lithiophyllite**, **sicklerite-ferrisicklerite** and **heterosite-purpurite** groups all have structures that have the olivine arrangement. [MO_4] chains of edge-sharing (LiO_6) or (NaO_6) octahedra extend parallel to the *a*-direction (Fig. 4.51a,c,e) and are decorated by (Fe^{2+},$Mn^{2+}O_6$) or ($\square O_6$) octahedra ($\square$ = vacancy). These decorated chains are linked in the *b*-direction by sharing octahedron corners with (PO_4) groups, although such "linkage" is not effective when the decorating octahedra are vacant (Fig. 4.51e); in this case, the chains link to other chains above and below the plane (Fig. 4.51f).

Let us consider the Fe end-members of each group:

triphylite	Li	Fe^{2+}	(PO_4)
ferrisicklerite	$(Li,\square)$	(Fe^{2+},Fe^{3+})	(PO_4)
heterosite	$\square$	Fe^{3+}	(PO_4)

As all three minerals have the same structure, the ranges in chemical composition for triphylite and heterosite are $LiFe^{2+}(PO_4)$– $(Li_{0.5}\square_{0.5})(Fe^{2+}_{0.5}Fe^{3+}_{0.5})(PO_4)$ and $\square_{0.5}Li_{0.5}(Fe^{3+}_{0.5}Fe^{2+}_{0.5})(PO_4)$– $\square Fe^{3+}(PO_4)$, respectively. Ferrisicklerite is an unnecessary name for intermediate-composition triphylite and heterosite. Similarly, sicklerite is an unnecessary name for intermediate lithiophyllite and purpurite.

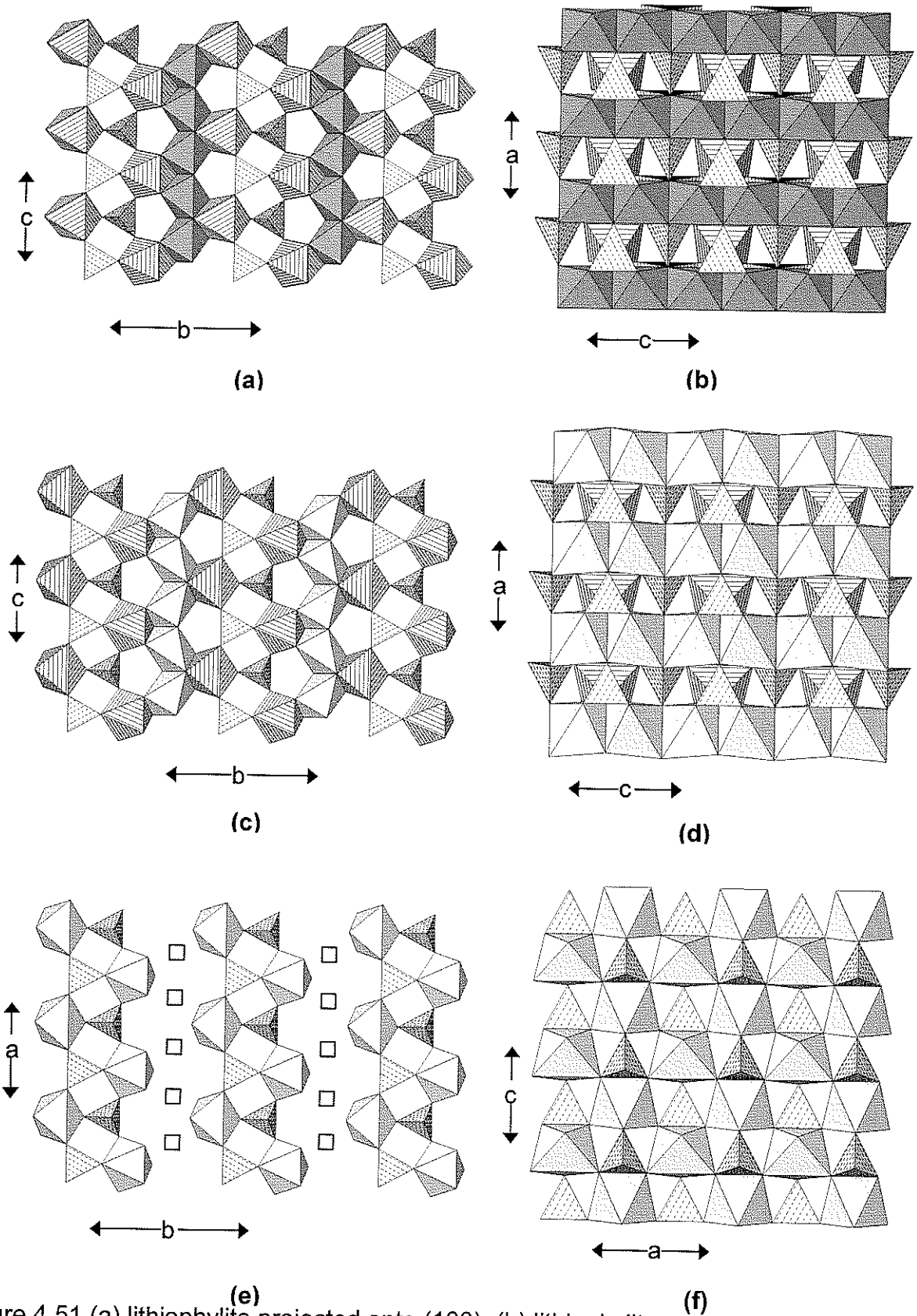

Figure 4.51 (a) lithiophylite projected onto (100); (b) lithiophylite projected onto (010), ($Mn^{2+}\varphi_6$): dark-shadow-shaded, (c) ferrisicklerite projected onto (100); (d) ferricsicklerite projected onto (010); (e) heterosite projected onto (001); (f) heterosite projected onto (010), ($\{Fe^{3+},Fe^{2+}\}\varphi_6$): shadow-shaded, ($Li\varphi_6$): line-shaded, vacancies: squares.

Senegalite, $[Al_2(PO_4)(OH)_3(H_2O)]$, contains Al in both triangular bipyramidal and octahedral coordinations. ($Al\varphi_5$) and ($Al\varphi_6$) polyhedra share an edge to form a dimer, and these dimers link by sharing corners to form a $[^{[5]}Al^{[6]}Al\varphi_8]$ chain that extends in the [101] (and $[\bar{1}01]$) direction (Fig. 4.52a). These chains are decorated by (PO_4) groups that link them to form a slab parallel to (010). These slabs stack in the *b*-direction, and link by sharing tetrahedron-octahedron and tetrahedron-bipyramid corners (Fig. 4.52b). This framework is fairly open, and the interstices are criss-crossed by a network of hydrogen bonds.

M=M, M–M, M=T, M–T linkage. **Sarcopside**, $[Fe^{2+}{}_3(PO_4)_2]$, is chemically similar to the minerals of the graftonite group but is structurally more similar to the structures of triphylite-lithiophyllite and its derivatives (Table 4.8). When viewed down [100] (Fig. 4.53a), the structure consists of a sheet of corner-linked octahedra at the vertices of a 4^4 net, and further linked by edges and corners with (PO_4) tetrahedra. When viewed down [010], the structure consists of trimers of edge-sharing octahedra linked into a sheet by sharing corners with (PO_4) groups (Fig. 4.53b). Sarcopside usually contains significant Mn^{2+}, but assuming complete solid-solution between graftonite and beusite, it seems that sarcopside is a polymorph of graftonite.

In **bjarebyite**, $BaMn^{2+}{}_2[Al_2(PO_4)_3(OH)_3]$, and the minerals of the bjarebyite group (Table 4.8), pairs of ($Al\varphi_6$) octahedra link by sharing edges to form dimers, and these dimers link together by sharing corners to form a chain of the form $[Al_2\varphi_9]$, intermediate between the corner-sharing $[Al\varphi_5]$ chain and the edge-sharing $[Al\varphi_4]$ chain (*i.e.*, $[Al_2\varphi_9] \equiv 2\ [Al\varphi_{4.5}]$). Octahedra that share corners are

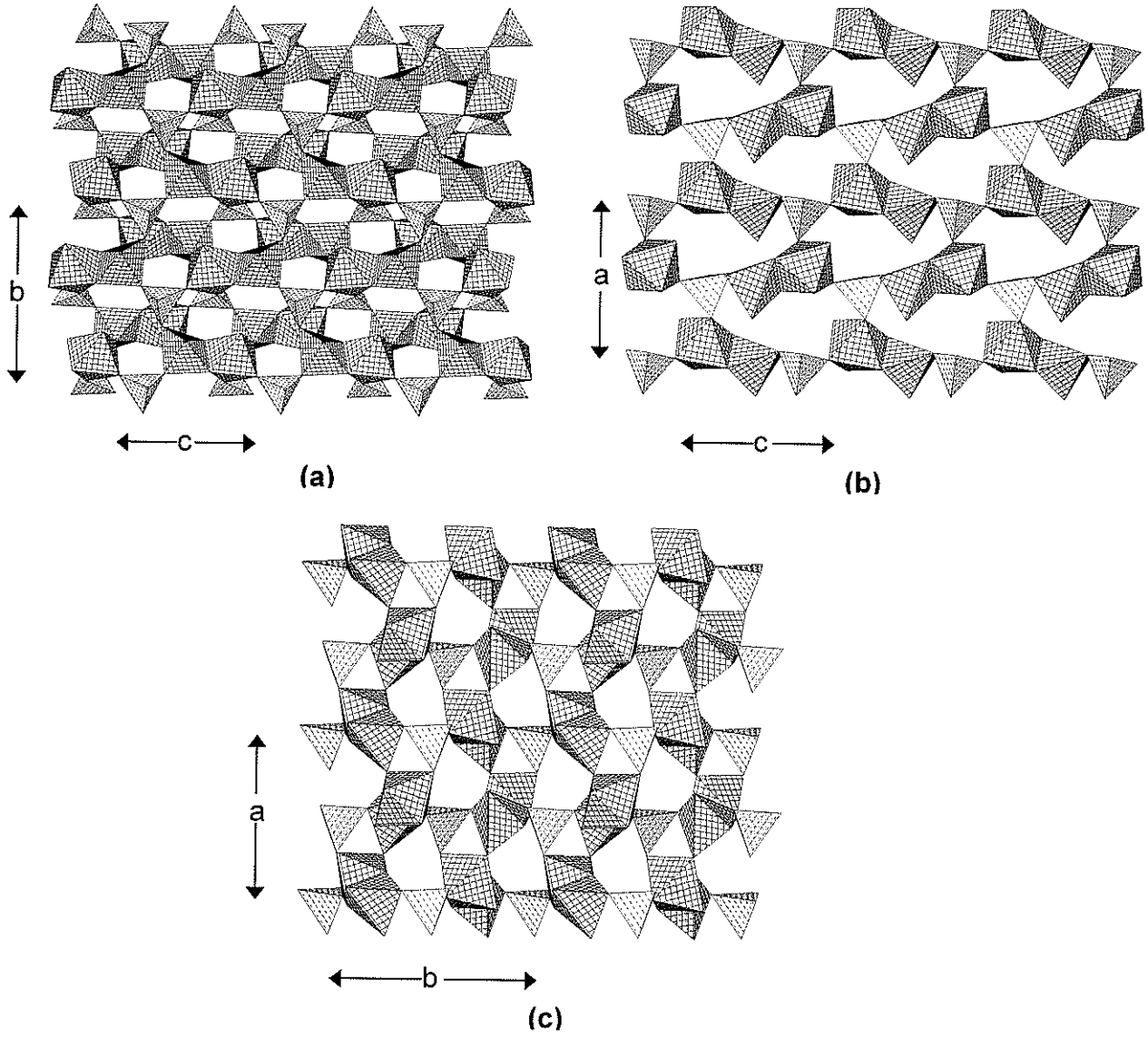

Figure 4.52. (a) senegalite projected onto (100); (b) senegalite projected onto (010); (c) senegalite projected onto (001), ($Al\varphi_6$): 4^4-net-shaded.

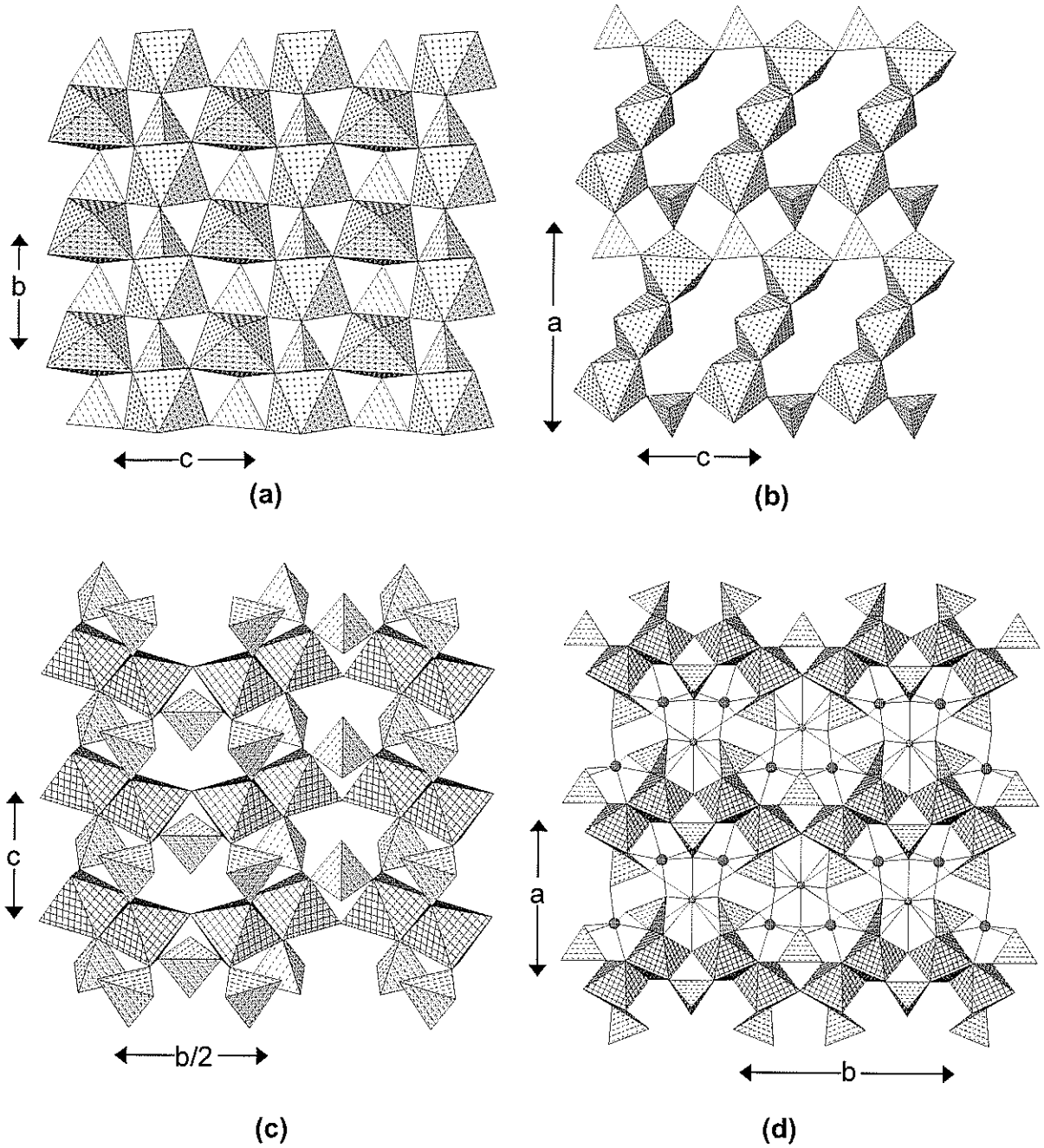

Figure 4.53. (a) sarcopside projected onto (100); (b) sarcopside projected onto (010), ($Fe^{2+}\varphi_6$): cross-shaded; (c) bjarebyite projected onto (100); (d) bjarebyite projected onto (001), ($Al\varphi_6$): 4^4-net-shaded, Mn^{2+} atoms: larger shaded circles, Ba atoms: smaller circles.

also linked by a flanking (PO_4) tetrahedron, similar to the linkage in the chain of Fig. 4.13c. The *cis* vertex of each octahedron also links to a (PO_4) tetrahedron to give a chain of the form $[Al_2(PO_4)_3(OH)_3]$. These chains extend in the *b*-direction (Fig. 4.53c) and are linked in the *a*-direction by [6]-coordinated Mn^{2+} and by [11]-coordinated Ba (Fig. 4.53d). Kulanite and penikisite were originally reported as triclinic (Mandarino and Sturman 1976, Mandarino et al. 1977). However, Cooper and Hawthorne (1994a) showed that kulanite is monoclinic (and is isostructural with bjarebyite). It is probable that penikisite is also monoclinic.

4.5 Structures with large-cations and ($P\varphi_4$) groups

These structures are considered separately since they can be considered as having either a [(PO_4)] structural unit or a neutral [$M^{n+}(PO_4)$] structural unit (Table 4.9) . In the case where the structural unit is defined based on a bond-valence of greater than 0.33 *vu* then the large cations such as Ce^{3+} in [8]-coordination would have to be considered as part of the structural unit because the bond-valence is 0.375 *vu*. However, since 0.33 *vu* is a rather arbitrary cut off value, in order to be able to consider a binary structural representation, the large cations can also be considered as the interstitial part of the structure.

Xenotime-(REE), (REE)(PO_4), and **pretulite**, Sc(PO_4), belong to the zircon, Zr(SiO_4), group. The larger trivalent cation is coordinated by eight O-atoms in an arrangement that is known as a Siamese dodecahedron (Hawthorne and Ferguson 1975). These dodecahedra link by sharing edges to form chains that extend in the *b*-direction (Fig. 4.54a). These chains are linked in the *c*-direction by (PO_4) tetrahedra that share an edge with a dodecahedron of one

TABLE 4.9. LARGE-CATION PHOSPHATE MINERALS

Mineral	Formula	Space Group	Figure
	Xenotime group		
Pretulite	$Sc(PO_4)$	$I4/amd$	4.54a,b
Xenotime-(Y)	$Y(PO_4)$	$I4/amd$	4.54a,b
Xenotime-(Yb)	$Yb(PO_4)$	$I4/amd$	4.54a,b
	Monazite group		
Brabantite	$CaTh(PO_4)_2$	$P2_1$	4.54c,d
Cheralite-(Ce)	$Ce(PO_4)$	$P2_1/n$	4.54c,d
Monazite-(Ce)	$Ce(PO_4)$	$P2_1/n$	4.54c,d
	Rhabdophane group		
Brockite		Aa	4.55a,b
Grayite	$Th(PO_4)(H_2O)$	$P6_222$	4.55a,b
Ningyoite	$U_2(PO_4)_2(H_2O)_{1-2}$	$P222$	4.55a,b
Rhabdophane	$Ce(PO_4)$	$P6_222$	4.55a,b
	General		
Archerite	$K(PO_3\{OH\}_2)$	$I\bar{4}2d$	4.55c,d
Biphosphammite	$(NH_4)(PO_2\{OH\}_2)$	$I\bar{4}2d$	4.55c,d
Brushite	$Ca(PO_3\{OH\})(H_2O)_2$	Ia	4.56a,b
Churchite-(Y)	$Y(PO_4)(H_2O)_2$	$I2/a$	4.56a,b
Ardealite	$Ca_2(PO_3\{OH\})(SO_4)(H_2O)_4$	Cc	4.56c,d,e
Dorfmanite	$Na_2(PO_3\{OH\})(H_2O)_2$	$Pbca$	4.57a,b,c
Monetite	$Ca(PO_3\{OH\})$	$Pmna$	4.57d
Nacaphite	$Na_2Ca(PO_4)F$	$P\bar{1}$	4.58a,b
Arctite	$(Na_5Ca)Ca_6Ba(PO_4)_6F_3$	$R\bar{3}m$	4.58c,d
Nabaphite	$NaBa(PO_4)(H_2O)_9$	$P2_13$	–
Nastrophite	$NaSr(PO_4)(H_2O)_9$	$P2_13$	–
Lithiophosphate	$[Li_3(PO_4)]$	$Pcmn$	4.59a,b
Nalipoite	$NaLi_2(PO_4)$	$Pmnb$	4.59c,d
Nefedovite	$Na_5Ca_4(PO_4)_4F$	$I\bar{4}$	4.60a,b
Olgite	$NaSr(PO_4)$	$P3$	4.60c,d,e
Phosphammite	$(NH_4)_2(PO_3\{OH\})$	$P2_1/c$	4.61a,b
Vitusite-(Ce)	$Na_3Ce(PO_4)_2$	$Pca2_1$	4.61c
Stercorite	$Na(NH_4)(PO_3\{OH\})(H_2O)_4$	$P\bar{1}$	4.62a,b
Natrophosphate	$Na_7(PO_4)_2F(H_2O)_{19}$	$Fd\bar{3}c2$	4.62c
Buchwaldite	$NaCa(PO_4)$	$Pn2_1a$	4.63a,b
Olympite	$LiNa_5(PO_4)_2$	$Pcmn$	–

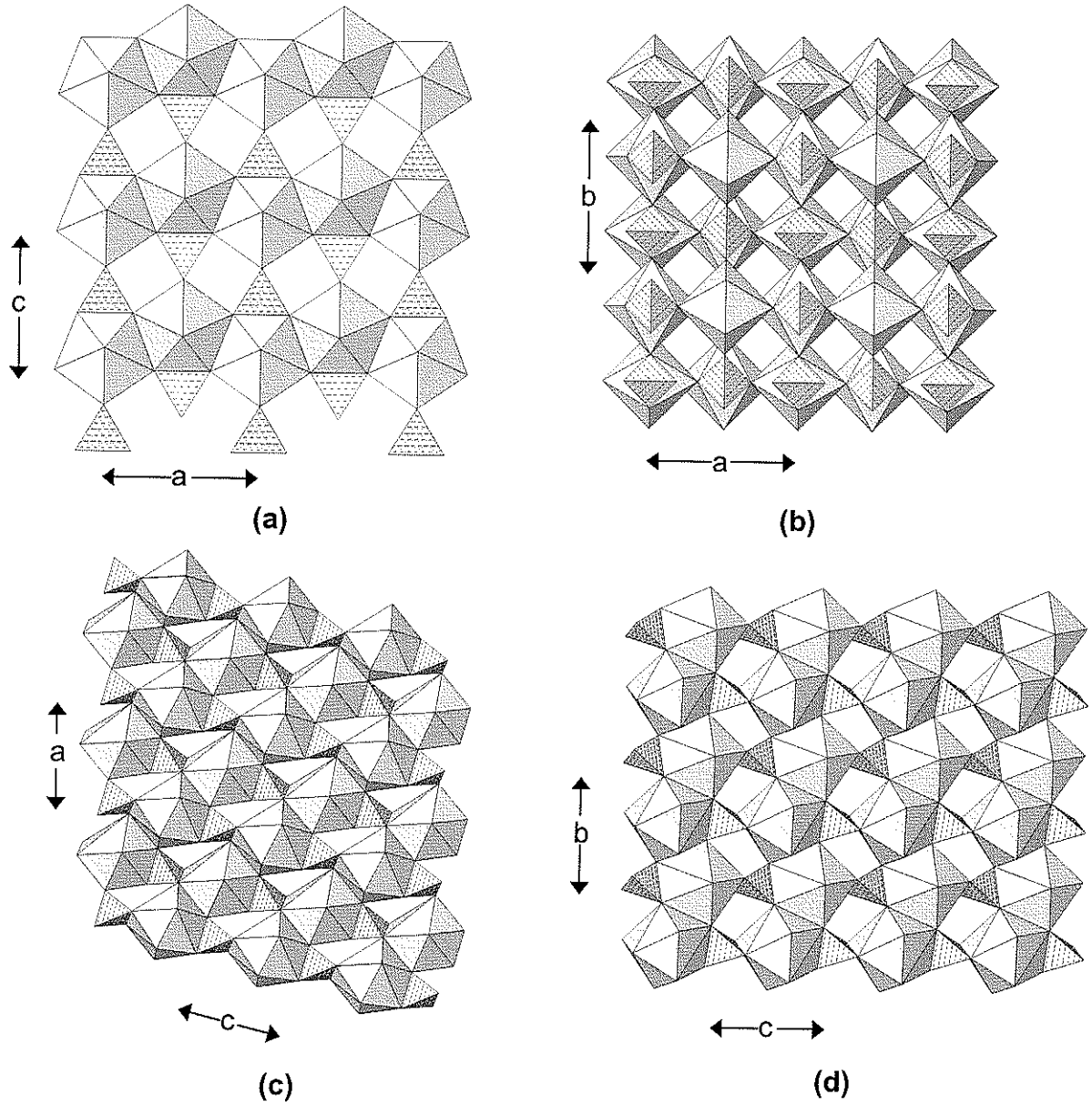

Figure 4.54. (a) xenotime-(Y) projected onto (010); (b) xenotime-(Y) projected onto (001); (c) monazite-(Ce) projected onto (010); (d) monazite-(Ce) projected onto (100). (REEφ_7): shadow-shaded.

chain and a vertex with a dodecahedron of the adjacent chain, forming a layer in the (100) plane (Fig. 4.54a). These layers stack in the *a*-direction by edge-sharing between dodecahedra of adjacent layers to form dodecahedral chains orthogonal to the layers. Hence the zircon structure is tetragonal (Fig. 4.54b).

Monazite-(REE), (REE)(PO_4), is a dimorph of xenotime-(REE). In this structure, the larger trivalent cation is coordinated by nine O-atoms in a rather irregular arrangement. These polyhedra link by sharing edges to form chains that extend in the *b*-direction (Fig. 4.54c). The chains are linked in the *c*-direction by (PO_4) tetrahedra that share edges with polyhedra of adjacent chain to form a layer parallel to (100) (Fig. 4.54c). These layers stack in the *a*-direction by sharing edges between the ({REE}O_9) polyhedra to form rather staggered chains that extend in the [101] direction (Fig. 4.54d). The monazite structure preferentially incorporates the larger light REEs whereas the xenotime structure preferentially incorporates the smaller heavy REEs (Ni et al. 1995); this is in accord with the difference in trivalent-cation coordination numbers in these two structure-types, and is also in accord with Sc(PO_4) crystallizing in the xenotime (zircon) structure (as pretulite) rather than in the monazite-type structure.

Rhabdophane, Ca(PO_4), contains Ce coordinated by eight O-atoms in a dodecahedral arrangement. These dodecahedra polymerize by sharing edges to form chains that extend in the *a*- and *b*-directions (Fig. 4.55a). These chains link in the *c*-direction by sharing edges with (PO_4) tetrahedra to form sheets parallel to (100) and (010) (Fig. 4.55a). These sheets interpenetrate in the *a*- and *b*-

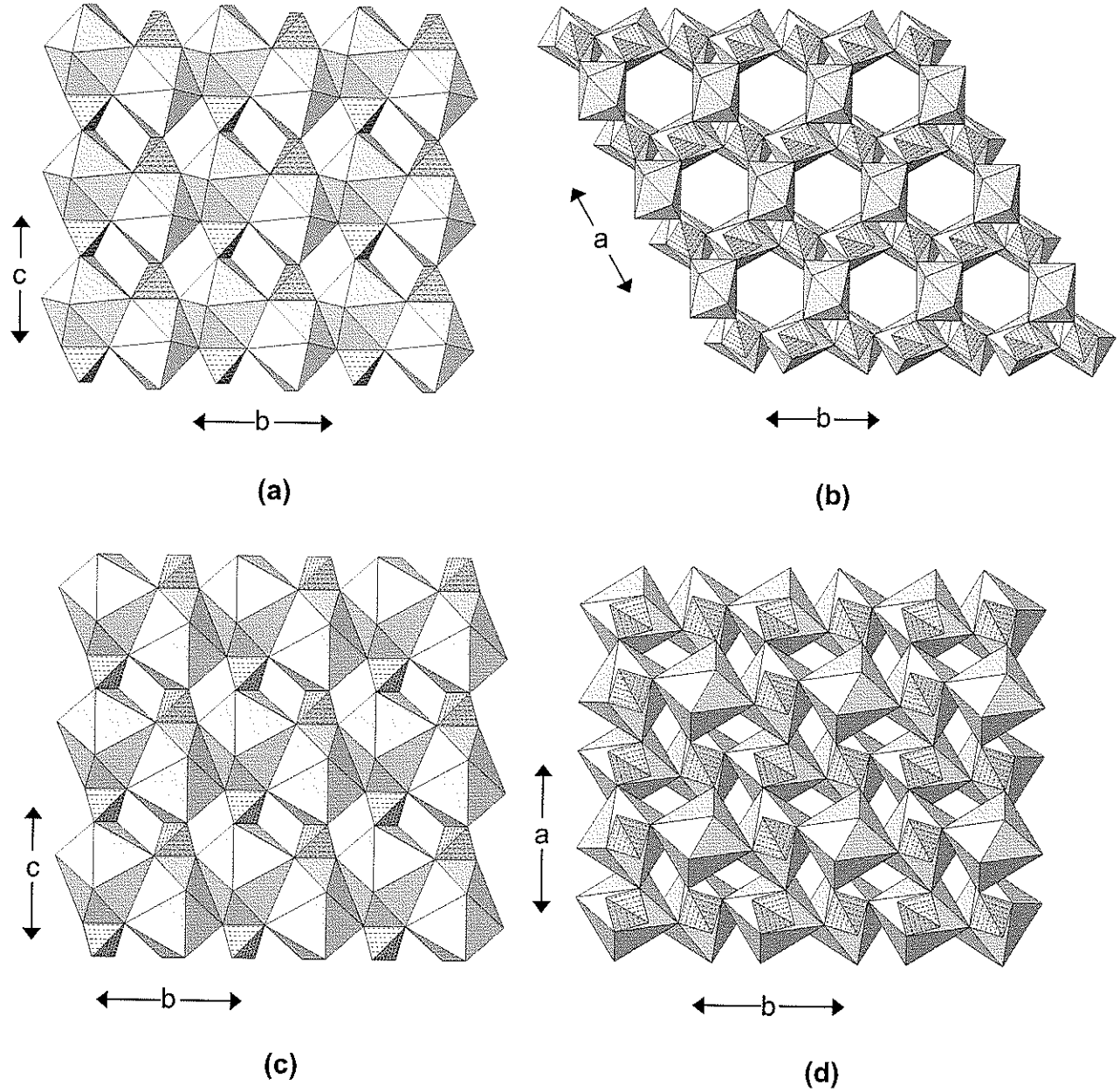

Figure 4.55. (a) rhabdophane projected onto (010); (b) rhabdophane projected onto (001); (REEφ_7): shadow-shaded; (c) archerite projected onto (100); (d) archerite projected onto (001); (Kφ_8): shadow-shaded.

directions (Fig. 4.55b) to form a framework with large hexagonal channels extending parallel to the *c*-axis.

Archerite, $K(PO_2\{OH\}_2)$, and **biphosphammite**, $(NH_4)(PO_2\{OH\}_2)$, are isostructural. In archerite, K is [8]-coordinated by O-atoms that are arranged at the vertices of a siamese dodecahedron. These dodecahedra share edges to form a chain in the *b*- (and *a*-) directions, and adjacent chains link by sharing edges with (PO_4) tetrahedra (Fig. 4.55c) to form layers parallel to (011) and (101). These layers meld by sharing edges (*i.e.*, mutually intersecting) to form a framework (Fig. 4.55d) that is topologically identical to the framework in xenotime (Figs. 4.54a,b), although geometrical distortions result in a lower symmetry arrangement in archerite (*I*42*d*) as compared with xenotime ($I4_1/amd$).

Brushite, $Ca(H_2O)_2(PO_3\{OH\})$, and **churchite**, $Y(H_2O)_2(PO_4)$, are essentially isostructural, although Curry and Jones (1971) report the space group *Ia* for brushite and Kohlmann et al. (1994) report *I*2/*a* for churchite. The large cation is [8]-coordinated with the bonded anions in a dodecahedral arrangement. The dodecahedra share edges with the ($P\varphi_4$) tetrahedra to form chains that extend in the [101] direction (Fig. 4.56a); these chains are a common feature of large-cation structures, and occur in gypsum and other Ca-sulfate minerals. These chains link in the [101] direction by sharing edges between ($Ca\varphi_8$) polyhedra of adjacent chains, and by sharing of vertices between ($P\varphi_4$) tetrahedra and ($Ca\varphi_8$) dodecahedra, forming a dense sheet parallel to (101) (Fig. 4.56a). These sheets stack in the *b*-direction linked solely by hydrogen bonds (not shown in Fig. 4.56b).

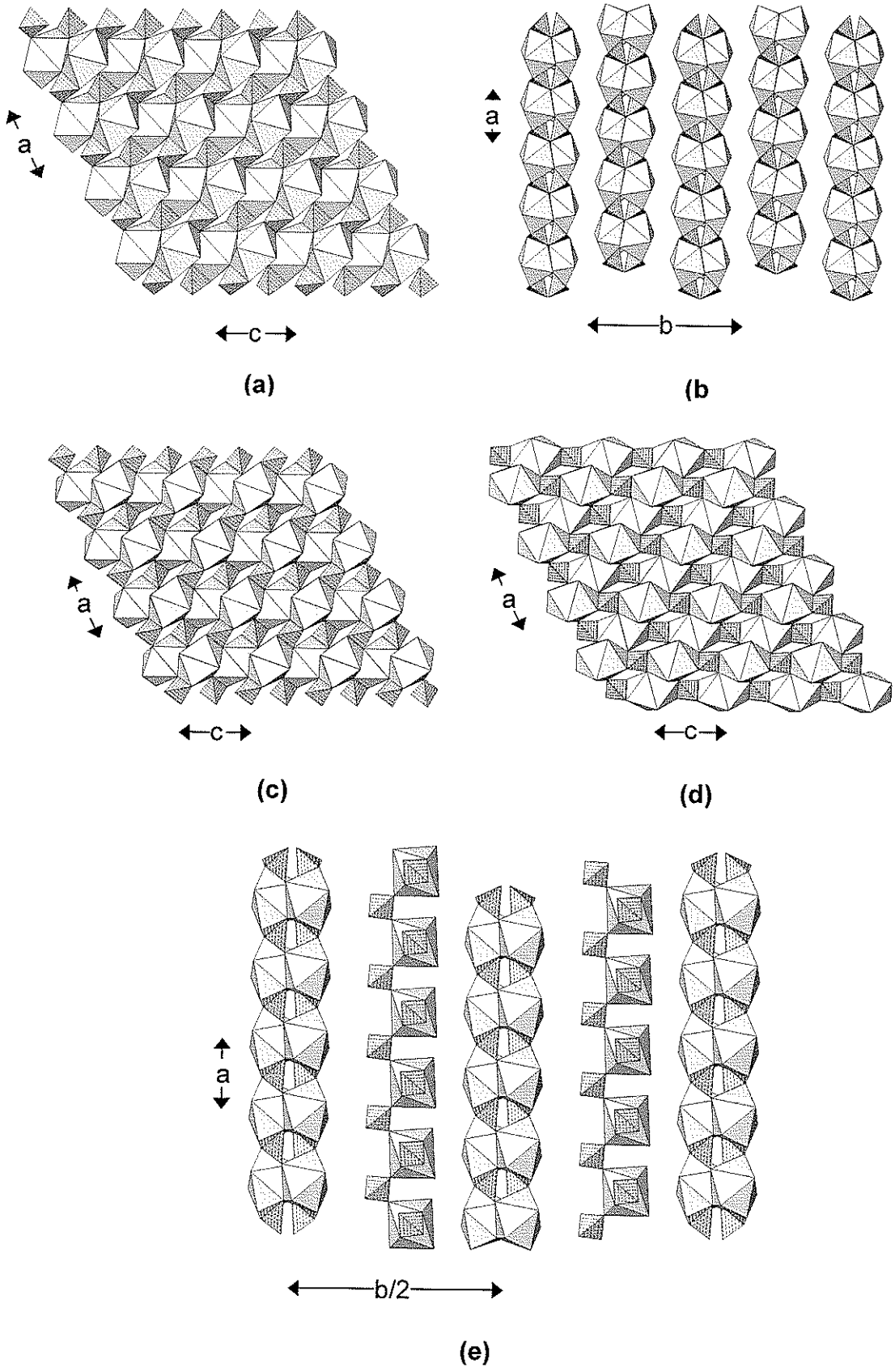

Figure 4.56. (a) brushite projected onto (010); (b) brushite projected onto (001); (c) ardealite: one layer projected onto (010); (d) ardealite: the next layer projected onto (010); (e) ardealite projected onto (001), ($Ca\varphi_8$): shadow-shaded.

Ardealite, $Ca_2(H_2O)_4(PO_3\{OH\})(SO_4)$, is an intriguing structure in that P and S seem to be disordered over the two symmetrically distinct tetrahedrally coordinated sites (Sakae et al. 1978); presumably, the acid H atom is locally associated with the ($P\varphi_4$) tetrahedra and hence shows analogous disorder. In the synthetic analogue, each of the two Ca atoms is coordinated by six O-atoms and two (H_2O) groups in a dodecahedral arrangement (as is the case in brushite). Chains of ($Ca\varphi_8$) and ($\{P,S\}\varphi_4$) polyhedra are formed by edge-sharing between the two types of polyhedra, chains that are topologically identical to the corresponding chains in brushite (Fig. 4.56a). These chains extend along [110] (Fig. 4.56c) and [001] (Fig. 4.56d), forming thick slabs that resemble the slabs in brushite (*cf.* Figs. 4.56b,e). Intercalated between these slabs are sheets of [8]-coordinated Ca and tetrahedra (Fig. 4.56e), and the structure is held together by a network of hydrogen bonds, the details of which are not known.

Dorfmanite, $Na_2(PO_3\{OH\})(H_2O)_2$, contains Na in both [5]- and [6]-coordination. ($Na\varphi_5$) polyhedra occur at the vertices of a 6^3 plane net and link by sharing corners (Fig. 4.57a) to form a sheet that is decorated by ($P\varphi_4$) tetrahedra. ($Na\varphi_6$) octahedra share edges to form chains that extend in the *c*-direction and are linked in the *b*-direction by the ($P\varphi_4$) groups (Fig. 4.57b) that decorate the underlying sheet of Fig. 62a. These two sheets stack in the *a*-direction (Fig. 4.57c) and link through the ($P\varphi_4$) groups.

Monetite, $CaH(PO_4)$, contains Ca in both [7]- and [8]-coordination, and the polyhedra share edges to form chains that extend in the *a*-direction. These chains are linked in the *b*-direction by sharing edges and vertices of the (CaO_n) polyhedra with ($P\varphi_4$) groups (Fig. 4.57d). These sheets link in the *c*-direction via

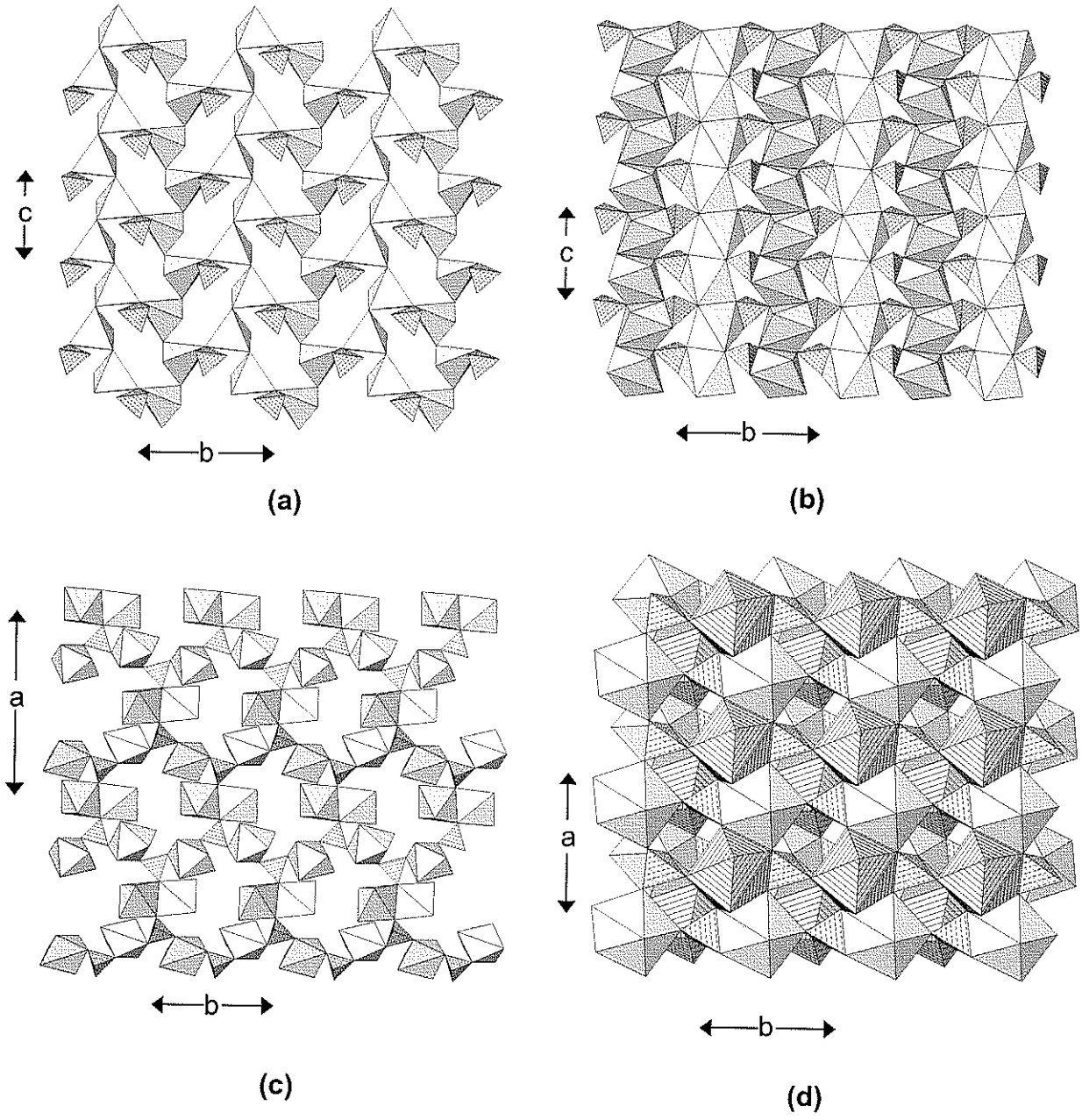

Figure 4.57. (a), (b) dorfmanite sheets projected onto (100); (c) dorfmanite projected onto (001); (Naφ_5) and (Naφ_6): shadow-shaded; (d) monetite projected onto (001); (Caφ_7): shadow-shaded, (Caφ_8): line-shaded.

corner-sharing between (CaO_n) polyhedra and ($P\varphi_4$) groups. Catti et al. (1977a) have carefully examined the evidence for a symmetrical hydrogen-bond in monetite. In space group *P*1, one of the three symmetrically distinct H-atom sites lies on, or disordered off, a centre of symmetry, and another H-atom is statistically distributed between two centrosymmetric positions. In space group *P*1, the first H-atom is displaced slightly off the pseudo-centre of symmetry, and another H-atom is either ordered or disordered. Catti et al. (1977a) propose that the crystal they examined is a mixture of domains of both *P*1 and *P*1 structure.

Nacaphite, $Na_2Ca(PO_4)F$, contains six octahedrally coordinated sites, four of which are each half-occupied by Ca and Na, and two of which are occupied solely by Na. Two {($Ca_{½}Na_{½}$)O_6] and one (NaO_6) octahedra link to form an [$M_3\varphi_{11}$] trimer, and there are two such symmetrically distinct trimers in this structure. The trimers link in the (100) plane by sharing corners (Fig. 4.58a), and the resultant sheet is braced by (PO_4) tetrahedra that link three adjacent trimers. The sheets stack in the *a*-direction (Fig. 4.58b), and are linked by edge-and face-sharing between trimers and by corner-sharing between (PO_4) groups and trimers of adjacent layers. This nacaphite structure is related to the structures of arctite, quadruphite (Table 4.13) and several alkali-sulfate minerals (Sokolova & Hawthorne 2001).

Arctite, $(Na_5Ca)Ca_6Ba(PO_4)_6F$, contains one [12]-coordinated Ba, one [7]-coordinated Ca, and one [7]-coordinated site occupied by both Na and Ca. The (CaO_7) and ({Na,Ca}O_7) polyhedra link to form trimers (Fig. 4.58c), and these trimers link in the (001) plane to form a sheet. These sheets stack in the *c*-direction, the trimers linking to form truncated columns parallel to the *c*-direction;

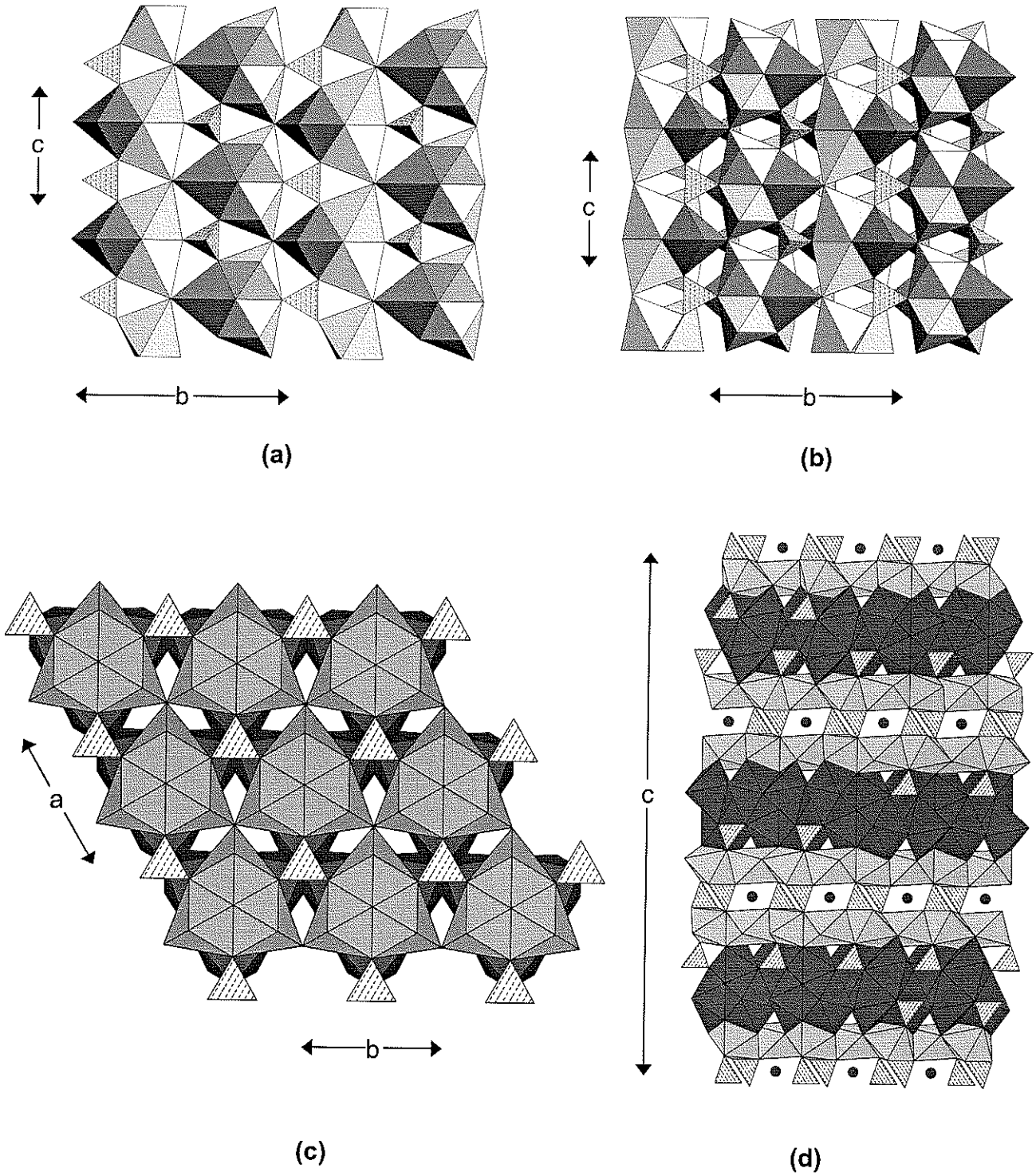

Figure 4.58. (a) one layer of nacaphite projected onto (100); (b) two layers of nacaphite projected onto (100); (c) two layers of arctite projected onto (001); (d) the stacking of layers along [001] in arctite, ({Na,Ca}φ_n): shadow-shaded, Ba atoms: dark circles.

the result is a thick slab parallel to (001). The (BaO_{12}) icosahedra form a hexagonal array parallel to (001) and are linked by corner-sharing with (PO_4) groups in an arrangement that is also found in the glaserite (and related) structures. This layer is intercalated with the thick slabs to form the rather densely packed arctite arrangement (Fig. 4.58d).

Nabaphite, $NaBa(PO_4)(H_2O)_9$, and **nastrophite**, $NaSr(PO_4)(H_2O)_9$, are isostructural. Their cation positions have been located but the (PO_4) groups show extensive orientational disorder. There is one Na site and one Ba(Sr) site; the former is octahedrally coordinated and the latter is [9]-coordinated with the anions in a triaugmented triangular-prismatic arrangement. Baturin et al. (1981) note that nastrophite dehydrates easily 'in air', and the (PO_4)-group disorder may be associated with incipient dehydration.

Lithiophosphate, Li_3PO_4, consists of a framework of (LiO_4) and (PO_4) tetrahedra. From a geometrical perspective, it could also be classified as a member of the class of structures with polymerized (TO_4) groups (*i.e.*, a framework structure of the types listed in Table 4.4). However, because of the low bond-valence (~0.25 *vu*) of the (LiO_4) groups, we have chosen to classify it as a 'large-cation' phosphate. (LiO_4) and (PO_4) tetrahedra are arranged at the vertices of a 3^6 plane net (Fig. 4.59a) and link by sharing corners; each (PO_4) group is surrounded by six (LiO_4) groups, and each (LiO_4) group is surrounded by two (PO_4) groups and four (LiO_4) groups. Both types of tetrahedra point both up and down the *c*-axis and link between adjacent sheets that stack in the *c*-direction (Fig. 4.59b).

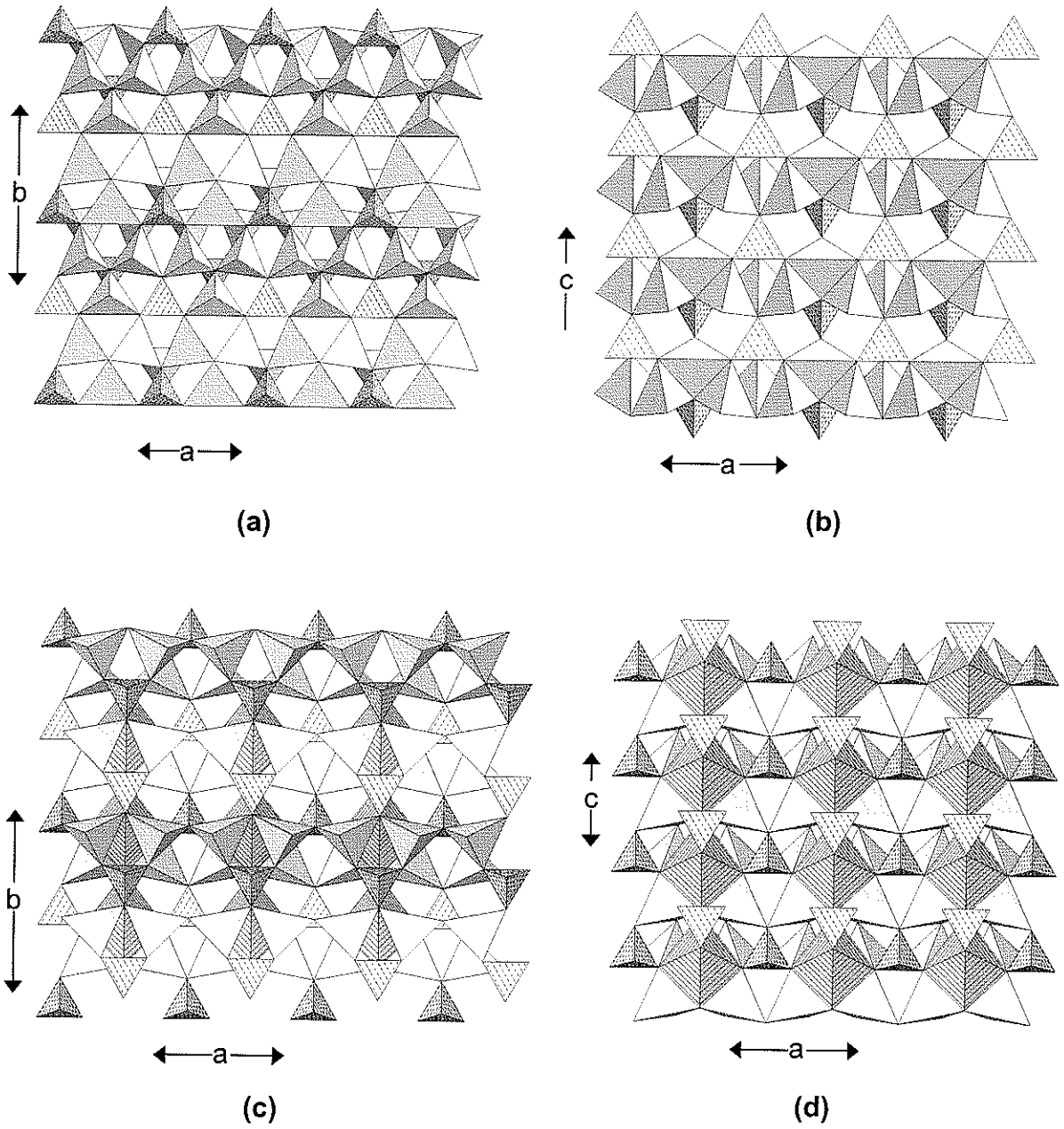

Figure 4.59. (a) lithiophosphate projected onto (001); (b) lithiophosphate projected onto (010); (c) nalipoite projected onto (001); (d) nalipoite projected onto (010). (LiO_4): shadow-shaded, (NaO_6): line-shaded.

Nalipoite, $NaLi_2(PO_4)$, contains octahedrally coordinated Na and tetrahedrally coordinated Li. From a geometrical perspective, nalipoite could be classified as a structure involving polymerization of tetrahedra. Conversely, it can be classified as a large-cation structure from a bond-valence perspective, as the bond valence of $^{[4]}$Li–O is only 0.25 *vu*. We adopt the latter approach here. The (PO_4) and (LiO_4) tetrahedra occur at the vertices of a (6.3.6.3)(3.6.6.3) net; all 3-rings consist of two (LiO_4) tetrahedra and one (PO_4) tetrahedron, and the 6-rings show the sequence (Li–Li–P–Li–Li–P). The result is a layer of tetrahedra parallel to (100) (Fig. 4.59c,d) in which chains of corner-sharing (LiO_8) tetrahedra extend in the *a*-direction, and are linked in the *b*-direction by (PO_4) tetrahedra. Tetrahedra point along ± *c*, and layers of tetrahedra meld in this direction to form a framework. Octahedrally coordinated Na occupies the interstices within this framework.

Nefedovite, $Na_5Ca_4(PO_4)_4F$, consists of [8]-coordinated Ca and both [7]- and [10]-coordinated Na. The $(Na\varphi_{10})$ polyhedra share apical corners to form chains that extend in the *c*-direction (Fig. 4.60a) with (PO_4) tetrahedra linked to half of the meridional vertices. The (NaO_7) polyhedra share apical corners to form chains extending in the *c*-direction, and the individual polyhedra share corners with the $(Na\varphi_{10})$ polyhedra, each bridging adjacent polyhedra along each chain (Fig. 4.60a). These chains are linked in the (001) plane by $(Ca\varphi_8)$ polyhedra. The decorated $(Na\varphi_{10})$-polyhedron chains have a square pinwheel appearance when viewed down [001] (Fig. 4.60b), and they are surrounded by a dense edge-sharing array of (NaO_7) and $(Ca\varphi_8)$ polyhedra.

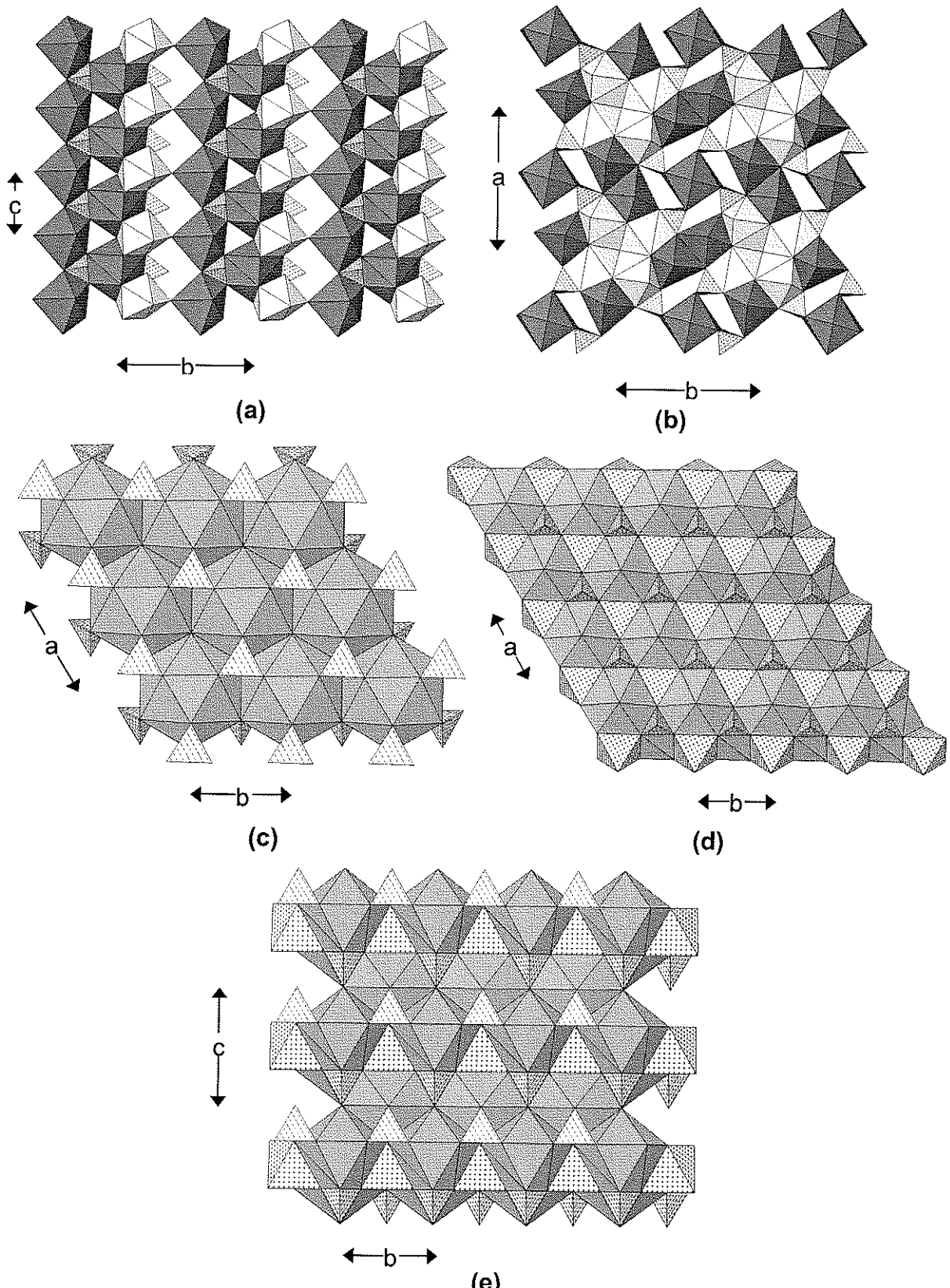

Figure 4.60. (a) nefedovite projected onto (100); (b) nefedovite projected onto (001); ($Na\varphi_n$): dark-shadow-shaded, ($Ca\varphi_8$): light-shadow-shaded; (c) (SrO_{12})-icosahedron layer in olgite projected onto (001); (d) the (Sr,NaO_{10})$B(NaO_7)$-polyhedron layer in olgite projected onto (001); (e) the stacking of layers along [001] in olgite; (SrO_{12}) icosahedra: dark-shadow-shaded, (NaO_{10}): dark-shaded, (NaO_6): cross-shaded.

Olgite, $NaSr(PO_4)$, contains one [12]-coordinated site occupied by Sr (+ Ba), one [6]-coordinated site occupied by Na, and two [10]-coordinated sites occupied by both Sr and Na. The Sr site is situated at the vertices of a 3^6 plane net and is icosahedrally coordinated; adjacent icosahedra share edges to form a continuous sheet parallel to (001) (Fig. 4.60c) that is decorated by (PO_4) tetrahedra that share edges with the icosahedra. The [10]-coordinated Sr, Na sites share corners to form a sheet parallel to (001) (Fig. 4.60d). The [10]-coordinated polyhedra each have six peripheral anions, one apical anion along $+c$ and three apical anions along $-c$ (obscured in Fig. 4.60d). (NaO_6) octahedra are embedded on the underside of this sheet, sharing faces with the (Sr,NaO_{10}) polyhedra, and only one octahedron face is visible in Fig. 4.60d (except at the edges of the sheet). This sheet is also decorated with (PO_4) tetrahedra. These two types of sheets stack alternately in the *c*-direction (Fig. 4.60e).

Phosphammite, $(NH_4)_2(PO_3\{OH\})$, consists of isolated $(P\varphi_4)$ groups linked by hydrogen bonds involving (NH_4) groups. Khan et al. (1972) show that there are five oxygen atoms closer than 3.4 □, but give a persuasive argument (based on stereochemistry) that there are only four hydrogen bonds from the (NH_4) group to the coordinating oxygen atoms. Consequently, we have drawn the 'large-cation' polyhedron as an $\{(NH_4)O_4\}$ tetrahedron (Figs. 4.61a,b). The $\{(NH_4)O_4\}$ tetrahedra occur at the vertices of a 6^3 net, linking to adjacent $\{(NH_4)O_4\}$ tetrahedra by sharing corners. The $(PO_3\{OH\})$ tetrahedra link to the $\{(NH_4)O_4\}$ tetrahedra, bridging across the six-membered rings of $\{(NH_4)O_4\}$ tetrahedra (Fig. 4.61a). The resultant layers link in the *c*-direction by corner-

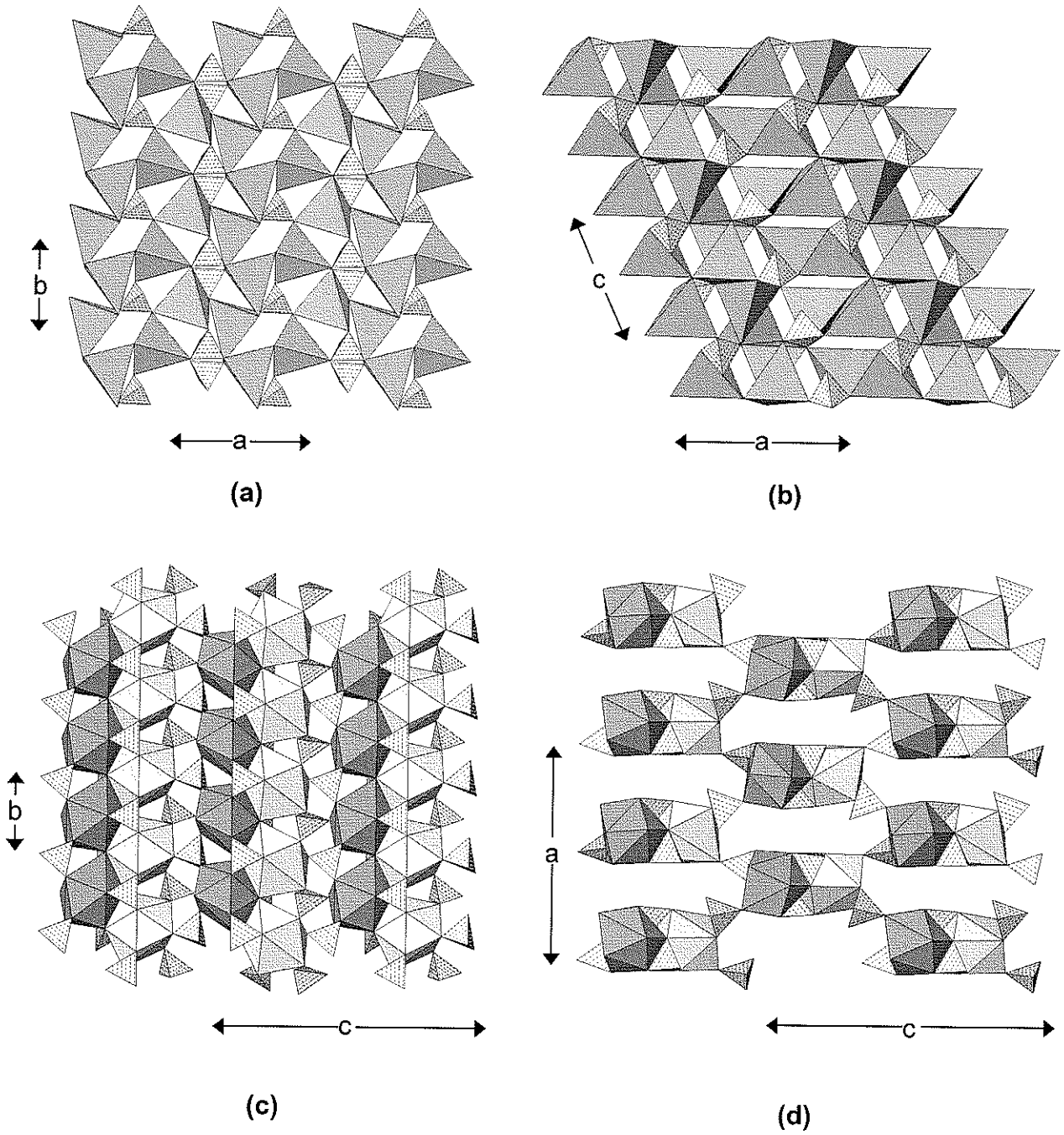

Figure 4.61. (a) phosphammite projected onto (001); (b) phosphammite projected onto (010); ({NH_4}O_4): shadow-shaded; (c) vitusite-(Ce) projected onto (001); (d) vitusite-(Ce) projected onto (100), ($REEO_8$): shadow-shaded.

sharing between both $\{(NH_4)O_4\}$ tetrahedra, and between $\{(NH_4)O_4\}$ and $(PO_3\{OH\})$ tetrahedra (Fig. 4.61b).

Vitusite-(Ce), $Na_3Ce(PO_4)_2$, is a modulated structure, the substructure of which is related to the glaserite structure-type. The substructure contains two [8]-coordinated REE sites and six Na sites, two of which are [6]-coordinated and four of which are [7]-coordinated, together with four distinct (PO_4) groups. The typical unit of the glaserite arrangement is a large-cation polyhedron surrounded by a 'pinwheel' of six tetrahedra. In vitusite-(Ce), this unit is present (Fig. 4.61c), but is perturbed by edge-sharing between the large-cation polyhedra. The layers of Fig. 4.61e stack in the *a*-direction by linkage between (PO_4) groups and the large-cation polyhedra. The structure is modulated in the *a*-direction, producing 5*a*, 8*a* and 11*a* modulations; the 8*a* modulated structure seems to be the most common, and was that characterized by Mazzi and Ungaretti (1994). The modulations involve displacements of some O-atoms of the structure such there are changes in the large-cation coordinations from those observed in the substructure.

Stercorite, $(NH_4)Na(H_2O)_3(PO_3\{OH\})(H_2O)$, consists of octahedrally coordinated Na that polymerizes by sharing *trans* edges to form an $[Na\varphi_4]$ chain that extends in the *b*-direction and is decorated by acid $(P\varphi_4)$ groups that share vertices with the octahedra and are arranged in a staggered fashion on each side of the chain (Figs. 4.62a,b). All ligands not involving $(P\varphi_4)$ groups are (H_2O) groups, *i.e.*, $(NaO\{H_2O\}_5)$. Chains are linked in the *a*- and *c*-directions by a complicated network of hydrogen bonds (Ferraris and Franchini-Angela 1974) involving the interstitial (NH_4) group and an interstitial (H_2O) group that is held in the structure solely by hydrogen bonds.

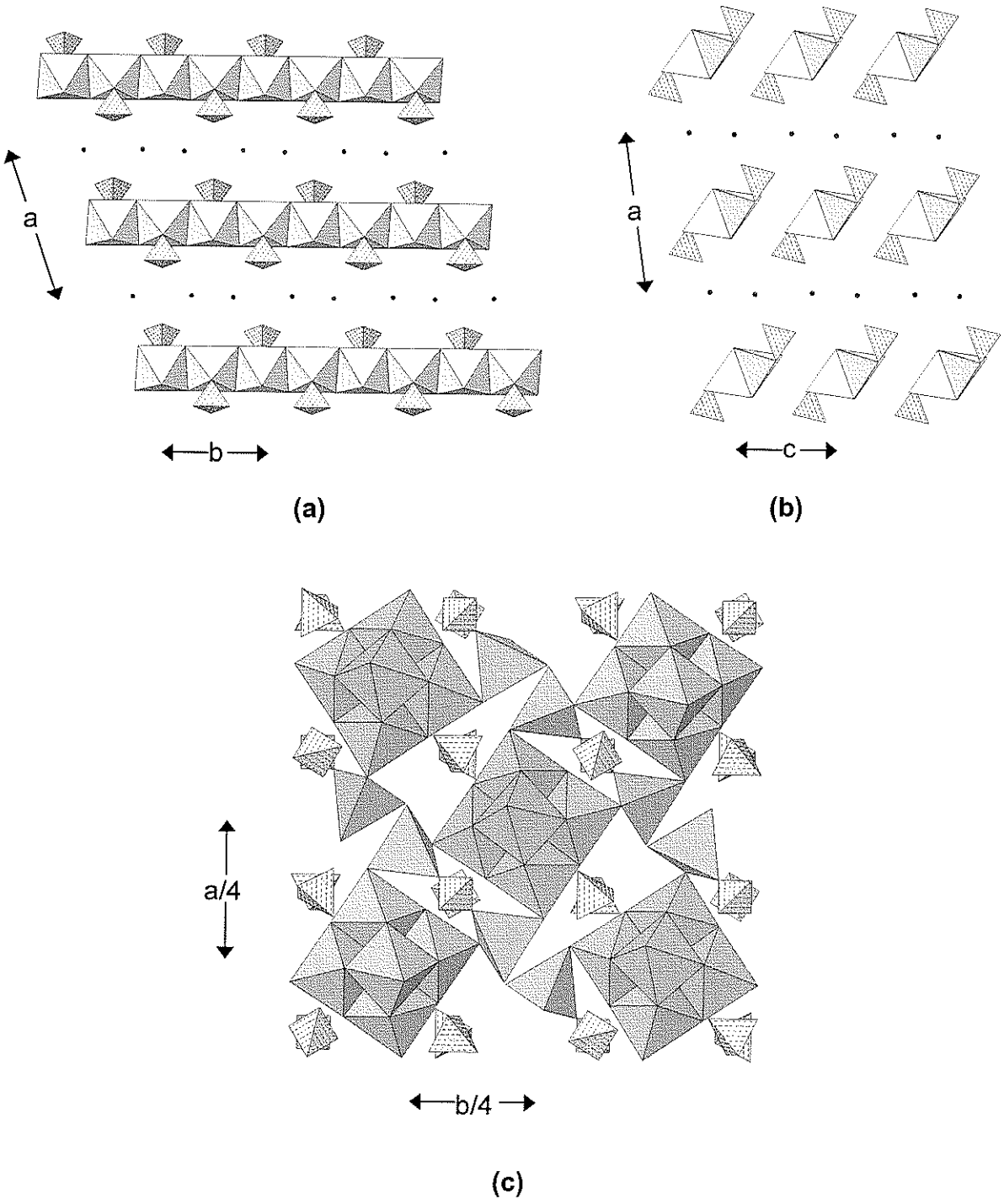

Figure 4.62. (a) stercorite projected onto (001); (b) stercorite projected onto (010); (c) natrophosphate projected onto (001). ($Na\varphi_6$) and ($Na\varphi_5$): shadow-shaded, (NH_4): small black circles.

Natrophosphate, $Na_7(PO_4)_2F(H_2O)_{19}$, contains octahedrally and tetrahedrally coordinated Na. Six ($Na\varphi_6$) octahedra share edges to form a compact cluster of the form $[Na_6\varphi_{18}]$ (Fig. 4.62c). At the centre of this cluster is one F atom that is coordinated by six Na atoms; the remaining anions of the cluster are either [2]- or [1]-coordinated and hence are (H_2O) groups. The (PO_4) groups do not link directly to these clusters, but link to ($Na\varphi_4$) tetrahedra that also bridge adjacent clusters (Fig. 4.62c). The [4]-coordinated site is only half-occupied (as required for electroneutrality) by Na, and is also half-occupied by (H_2O), giving rise to the rather unusual stoichiometry (for such a high-symmetry mineral).

Buchwaldite, $NaCa(PO_4)$, contains three unique Ca atoms, each with a coordination number of [8], and three distinct Na atoms with coordination numbers of [7], [6] and [9], respectively. The (CaO_8) polyhedra share edges to form two distinct chains that extend in the *a*-direction (Fig. 4.63a). These chains link in the *c*-direction through (NaO_n) polyhedra and (PO_4) groups. The (CaO_8) polyhedra share both edges and vertices with (PO_4) groups to link in the *b*-direction (Fig. 4.63b), further linkage being provided by (NaO_n) polyhedra to produce a densely packed structure.

4.6 Apatite-related structures

The minerals with apatite-like structures can be considered similar to the large cation structures and are listed in Table 4.10. The apatite group minerals typically have exstensive chemical variation which has an effect on the apatite structure (Elliot 1994, Hughes et al.1989, Rakovan and Hughes 2000, etc.). The

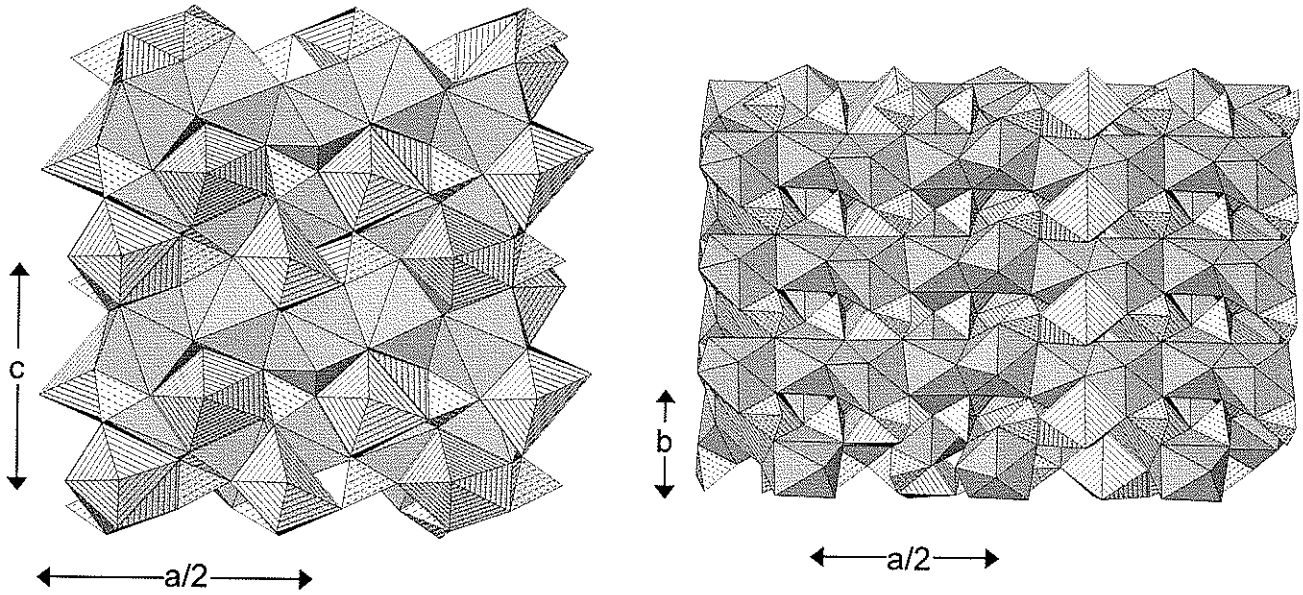

Figure 4.63. The crystal structure of buchwaldite; (a) projected onto (010); (b) projected onto (001). (CaO_8): shadow-shaded, (NaO_n): line-shaded.

TABLE 4.10. MINERALS WITH APATITE-LIKE STRUCTURES.

Mineral	Formula
Alforsite	$Ba_5(PO_4)_3Cl$
Belovite-(Ce)	$Sr_3NaCe(PO_4)_3(OH)$
Belovite-(La)	$Sr_3NaLa(PO_4)_3F$
Carbonate-fluorapatite	$Ca_5(PO_4,CO_3)_3F$
Carbonate-hydroxylapatite	$Ca_5(PO_4,CO_3)_3(OH)$
Chlorapatite	$Ca_5(PO_4)_3(Cl,F)$
Fluorapatite	$Ca_5(PO_4)_3F$
Hydroxylapatite	$Ca_5(PO_4)_3(OH)$
Pyromorphite	$Pb_5(PO_4)_3Cl$
Strontiumapatite	$Sr_6Ca_4(PO_4)_6F_2$

general formula is, $\boldsymbol{A}_5(\boldsymbol{T}O_4)_3\boldsymbol{Z}$, where typically $\boldsymbol{A}$ = Ca, Sr, Pb, Ba; $\boldsymbol{T}$ = P, As, V and also Si, S, and possibly CO_3; $\boldsymbol{Z}$ = OH, F, Cl, and possibly CO_3. Only apatite-like structures containg P are listed in Table 4.10.

4.7 Silicophosphate structures

The silicophosphate (and related phosphate) minerals are a small group of extremely complicated structures are not described here, as their complexity requires extensive illustration. For completeness, these minerals are listed in Table 4.11.

4.8 Hexavalent-uranium phosphate structures

The hexavalent-uranium phosphate minerals are important and widespread uranyl-oxysalt minerals. Their structures and behaviour are dominated by the crystal chemistry of the $(U^{6+}O_2)^{2+}$ uranyl group; they have been described in detail by Burns (1999) in a similar manner to this current classification scheme.

TABLE 4.11. SILICOPHOSPHATE STRUCTURES

Name	Formula	Space group
Attakolite	$CaMn^{2+}Al_4(SiO_3\{OH\})(PO_4)_3(OH)_4$	*C*2/*m*
Clinophosinaite	$Na_3Ca(SiO_3)(PO_4)$	*P*2/*c*
Harrisonite	$CaFe^{2+}(SiO_4)_2(PO_4)_2$	$R\bar{3}m$
Lomonosovite	$Na_5Ti^{4+}{}_2(Si_2O_7)(PO_4)O_2$	$P\bar{1}$
Polyphite	$Na_{17}Ca_3MgTi_4(Si_2O_7)_2(PO_4)_6O_3F_5$	$P\bar{1}$
Quadruphite	$Na_{14}CaMgTi^{4+}{}_4(Si_2O_7)_2(PO_4)_4O_4F_2$	$P\bar{1}$
Sobolevite	$Na_{11}(Na,Ca)_4(Mg,Mn^{2+})Ti^{4+}{}_4(Si_2O_7)_2(PO_4)_4O_3F_3$	$P\bar{1}$
Steenstrupine	$Na_{14}Ce_6Mn^{2+}Mn^{3+}Fe^{2+}{}_2Zr(Si_6O_{18})_2(PO_4)_7(H_2O)_3$	$R\bar{3}m$
Vuonnemite	$Na_{11}Ti^{4+}Nb_2(Si_2O_7)_2(PO_4)_2O_3(OH)$	$P\bar{1}$
Yoshimuraite	$Ba_2Mn_2TiO(Si_2O_7)(PO_4)(OH)$	$P\bar{1}$
Benyacarite	$(H_2O,K)_2TiMn^{2+}{}_2(Fe^{3+},Ti)_2(PO_4)_4(OH)_2(H_2O)_{14}$	*Pbca*

CHAPTER 5

A bond-valence approach to the chemical composition and occurrence of complex minerals

5.1 Binary structural representation of complex minerals

As already discussed, complex minerals can be divided into (1) a *structural unit*, which is defined by strong bonds between atoms, and (2) an *interstitial complex*, which links structural units into a continuous structure by weak bonds. By using this binary representation, a simple quantitative model can then be used to calculate the Lewis acidity and Lewis basicity of the interstitial complex and the structural unit of complex oxysalt minerals (Hawthorne 1985, 1986). The valence-matching principle can then be applied to evaluate mineral stability *via* the weaker bonding between the structural unit and interstitial complex. Definitions are listed in Appendix B.

5.2 Role of (H_2O) and (OH) in complex oxysalt minerals

When dealing with structural aspects of a mineral, the question of why some minerals are hydrated and others are anhydrous and the amount of hydration in a mineral is very important. The nature of H-bonding in (H_2O) and (OH) groups will affect mineral behavior in different ways, depending on where in the mineral structure the (H_2O) and (OH) groups are located as the amount of water it contains and where in the structure the water is located will affect the structural arrangement of a mineral. Hawthorne (1992) initially described the possible roles of (H_2O) and (OH) groups as either part of the structural unit or

interstitial complex. The H^+ cation is typically [2]-coordinated, but can also have higher coordination numbers. As already discussed, there is a spontaneous distortion of the H^+ coordination toward one strongly electronegative (donor) atom (such as O^{2-}) to form a strong bond, and away from another electronegative (acceptor) atom to form a weaker (hydrogen) bond (Fig. 5.1a). The commonly assigned bond-valences are as follows: D–H = 0.80 *vu*, H–A = 0.20 *vu* (Brown 1976).

Hawthorne (1992) shows different bonding schemes for H-bearing groups (Fig. 5.1). Both (OH) and (H_2O) groups are polar and the Lewis-base part of each of these groups have high bond-valence requirements (1.2 *vu* and 0.4 *vu* for (OH) and (H_2O), respectively) (Fig. 5.1.a,b) in order to satisfy bond-valence requirements of the donor oxygen (valence sum at the donor should be 2.0 *vu*). The opposite is the case with the Lewis-acid parts of the groups, where the required bond-valence is relatively weak (less than 0.33 *vu*). Therefore, the Lewis-base part of the group can belong to the structural unit, whereas the Lewis-acid part of the group is too weakly bonded to be considered as part of the structural unit. The very asymmetric nature of the D–H and H–A interactions in (OH) and (H_2O) plays a major role in dictating the dimensional polymerization of the structural unit and will prevent the polymerization of the structural unit in specific directions.

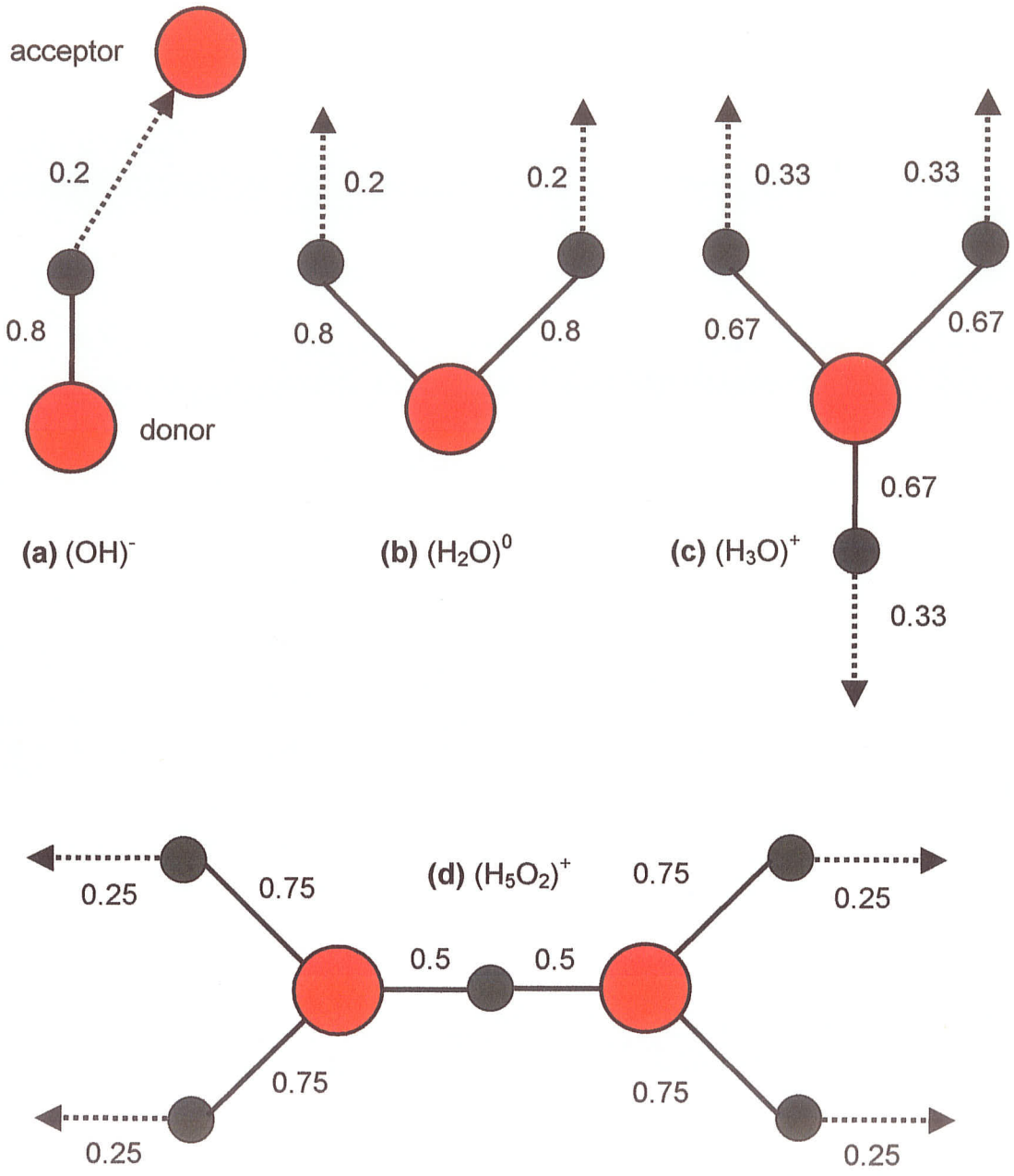

Figure 5.1. Bond-valence (*vu*) distributions for the H-bearing groups in minerals: (a) $(OH)^-$ (b) $(H_2O)^0$ (c) $(H_3O)^+$ (d) $(H_5O_2)^+$ (after Hawthorne 1992).

5.3 (H_2O) as an interstitial species

Hawthorne (1992) described the different roles of (H_2O) groups in crystal structures, and drew a strong distinction between (H_2O) as part of the structural unit and (H_2O) as an interstitial species. In particular, Hawthorne (1985, 1992) described the role of (H_2O) as a bond-valence transformer in minerals, and Schindler and Hawthorne (2001a) developed these ideas further.

5.3.1 Interstitial (H_2O) not bonded to interstitial cations

When (H_2O) is not bonded to a cation of the interstitial complex, it typically behaves as part of a weakly hydrogen-bonding network [rarely it will occur as occluded (H_2O)]. The O atom of the (H_2O) group is usually [4]-coordinated, two (D–H) bonds from two hydrogen atoms and two hydrogen (H–A) bonds from two other hydrogen atoms (Fig. 5.2a). Let the two hydrogen bonds to the O atom of the (H_2O) group have an incident bond-valence of v *vu* each. The incident bond-valence requirements (2 *vu*) for the O atom are satisfied by the two O-H bonds of the (H_2O) group that each have a bond-valence of 1-v *vu*, together with the two hydrogen bonds: 2(1-v) + 2v = 2 *vu*. The hydrogen atoms of the (H_2O) group therefore each require an additional bond-valence of v *vu* by forming a bond to an anion of the structural unit or another (H_2O) group to satisfy the bond-valence requirements of 1 *vu* per H atom; v + (1-v) = 1 *vu*. The strength of the bonds are not changed in this arrangement, the bond-valence is merely propagated through space by the (H_2O) group. These (H_2O) groups are called *non-transformer* (H_2O).

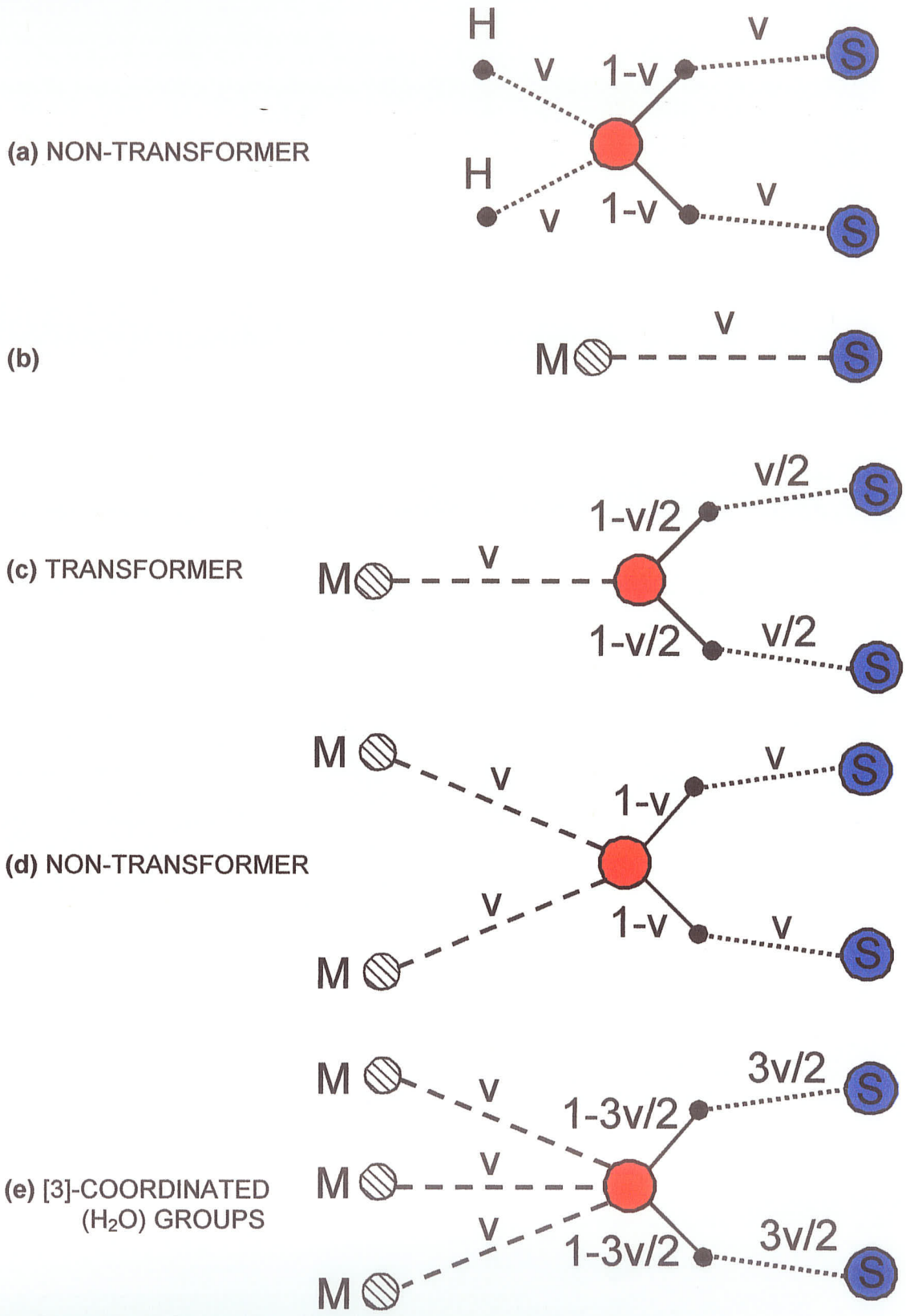

Figure 5.2. The role of water in complex oxysalt minerals (after Schindler & Hawthorne 2001a).

5.3.2 Interstitial (H_2O) bonded to one interstitial cation

If a cation *M* bonds to an anion, *S*, of the structural unit, the *S* anion will receive v *vu* from that cation (Fig. 5.2b). If a cation *M* bonds to an (H_2O) group that bonds to an *S* anion, the O atom of the (H_2O) group receives a bond-valence of v *vu* from the *M* cation and requires two O-H bonds with a bond-valence of (1-v/2) *vu* each; v + 2(1 – v/2) = 2. To satisfy the bond-valence requirements at the H atoms, each H atom forms one or more hydrogen bonds with surrounding anions. If the H atom bonds to one *S* anion, then the bond valence to *S* will be half of the bond valence from the *M* cation to the O atom of the (H_2O) group, effectively transforming the strength of the initial bond; hence this type of (H_2O) is called a *transformer* (H_2O) group. This type of (H_2O) group acts as a *bond-valence transformer*, causing one bond (bond valence = v *vu*) to be split into two weaker bonds (bond valence = v/2 *vu*). These types of (H_2O) groups will strongly affect the Lewis acidity of the interstitial complex.

Example: For $^{[6]}Fe^{2+}$ in the interstitial complex, the Lewis acidity would be the charge divided by the coordination; 2/6 = 0.33 *vu*. However, if $^{[6]}Fe^{2+}$ is coordinated by six transformer (H_2O) groups, then the Lewis acidity becomes 2/(6 x 2) = 0.17 *vu* (Fig. 5.3).

5.3.3 Interstitial (H_2O) bonded to two interstitial cations

If two *M* cations bond to an (H_2O) group in which each H atom H-bonds to an *S* anion, then the O atom of the (H_2O) group receives 2v *vu* from the two *M* cations (Fig. 5.2d). Therefore, the O atom requires (1-v) *vu* from each of the O-H

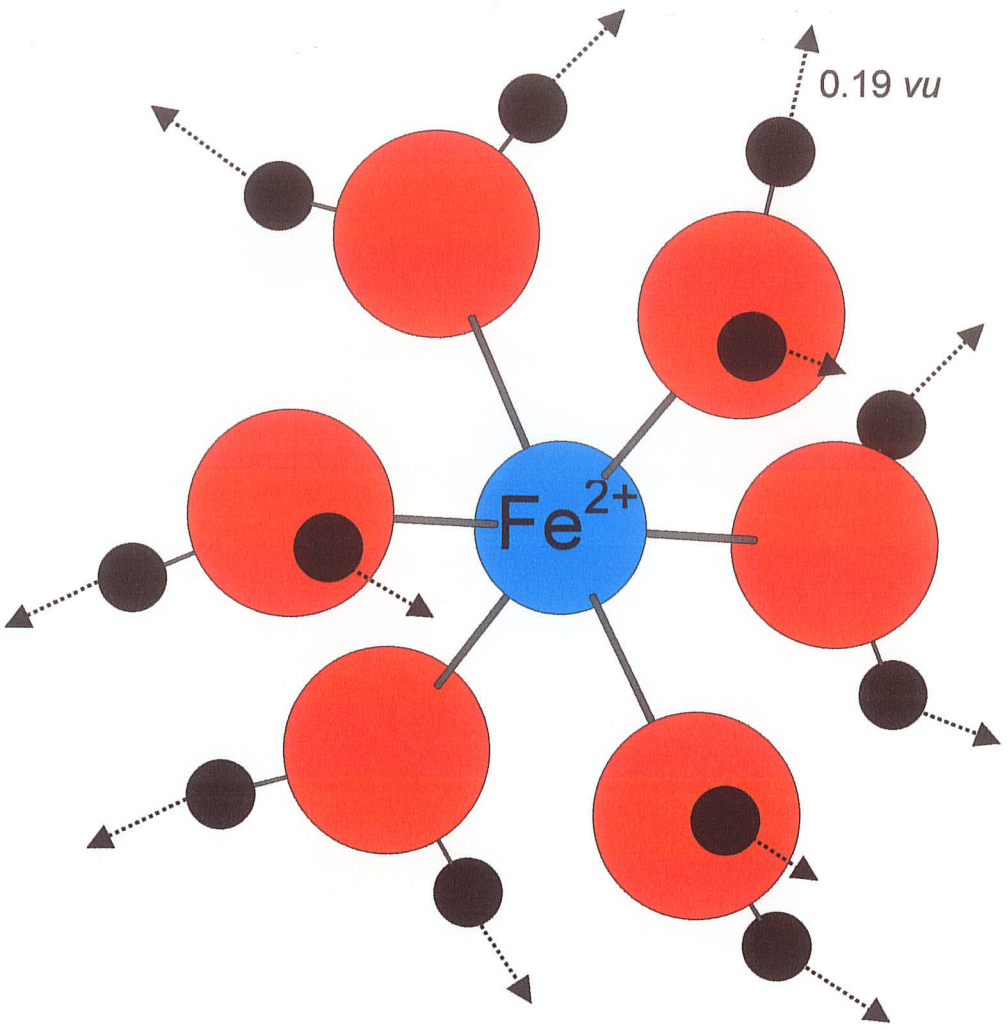

Lewis-acidity
= effective charge / no. of bonds
= 3.2^{+} / (6 x 2) = 0.19 *vu*

Figure 5.3. Schematic diagram showing the effect of transformer (H_2O) groups on Lewis-acidity.

bonds of the (H_2O) group; 2v + 2(1-v) = 2 *vu*. The bond-valence requirements of each of the H atoms of the (H_2O) group are satisfied by each H forming one or more hydrogen bonds with neighbouring anions. If a H atom forms one bond to an *S* anion, then the bond-valence would be v *vu*. In this case, the incident bond-valence is the same as the inititial bond-valence, and therefore the bond-valence is not transformed. This type of (H_2O) group bonds to two interstitial cations and does *not* act as a bond-valence transformer; it is a *non-transformer* (H_2O) group.

5.3.4 Interstitial (H_2O) bonded to three interstitial cations

If there are three *M* cations bonded to an O atom of an (H_2O) group, then the incident bond-valence is 3v *vu* at the O atom (Fig. 5.2e). The O atom will require (1-3v/2) from each of the O-H bonds; 3v + 2(1-3v/2) = 2. Each H atom will require 3v/2 *vu* from a neighbouring anion. In this case, the transformed bond-valence will actually increase from the cation bonds of the interstitial complex to the *S* anions of the structural unit; this is called a *reverse-transformer* (H_2O) group.

5.3.5 (OH) and monovalent anions as interstitial species

When an interstitial species, the (OH) group generally bonds to two trivalent interstitial cations (Schindler and Hawthorne, 2001a). Thus it accepts two bonds from the interstitial cations and forms only one bond from the interstitial complex to the structural unit (or less commonly to another anion of the structural unit). Essentially, (OH) groups act as bond-valence absorbers; they

decrease the net charge of the interstitial complex and also affect the number of bonds from the interstitial complex, which, in turn, affects the Lewis acidity of the interstitial complex.

5.4 Hydrogen bonding from the structural unit

Schindler and Hawthorne (2001a) considered the different possible hydrogen-bonding scenarios from the structural unit to an interstitial complex of chemical composition $M^{k+}(H_2O)_2$ (Fig. 5.4). In the first situation (Fig 5.4a), there are four bonds from the interstitial complex to the structural unit and there are two transformer (H_2O) groups, so the interstitial complex shown in Fig. 5.4a can be denoted as $\{^{[2]}M^{k+}(H_2O)_2(H_2O)_0\}^{k+}$. Following the method of determining the number of bonds from the interstitial complex to a structural unit for a general interstitial complex (above), the number of bonds from the interstitial complex reduces to 2 x 1 (contributed by the *M* cation) + 2 (contributed by the transformer $(H_2O)_d$ group) = 4 bonds.

In the next scenario, a hydrogen of the structural unit hydrogen bonds to an interstitial (H_2O) group bonded to an interstitial cation (Fig. 5.4b). One interstitial (H_2O) group is not a transformer (H_2O) as it bonds to the *M* cation *and* is a hydrogen-bond acceptor. The chemical composition for this interstitial complex can be written as $\{^{[2]}M^{k+}(H_2O)_1(H_2O)_1\}^{k+}$ and will have 2 x 1 (contributed by the *M* cation) + 1 (contributed by the transformer $(H_2O)_d$ group) = 3 bonds from the interstitial complex to the structural unit. Inspection of Fig. 5.4b shows that this is not the number of bonds actually seen if this initial calculation is used.

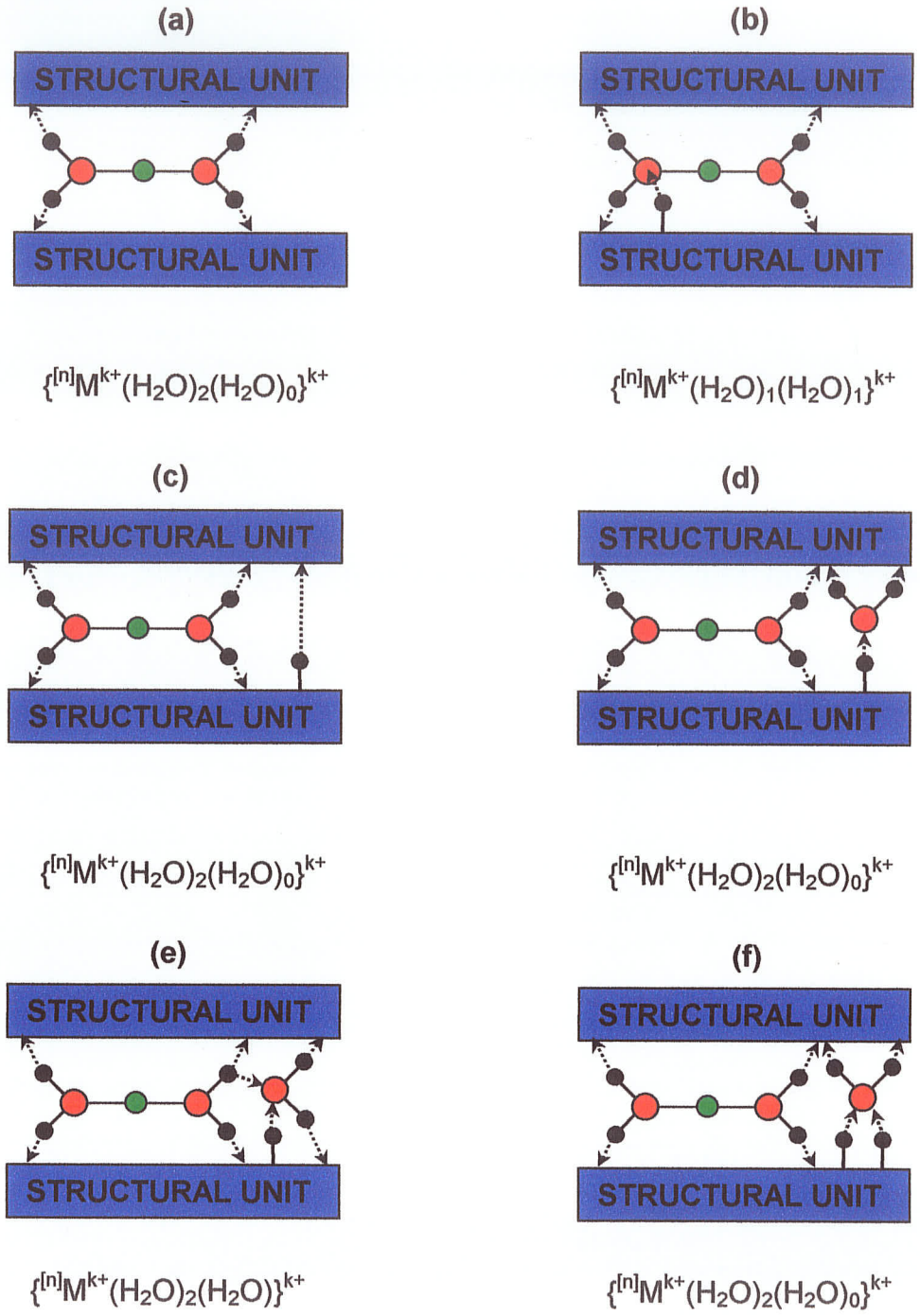

Figure 5.4. Different possible configurations of hydrogen bonds emanating from the structural unit (after Schindler and Hawthorne 2001a): (a) no hydrogen bonds from structural unit; (b) one hydrogen from structural unit bonds to a non-transformer $(H_2O)_g$ of the interstitial complex; (c) one hydrogen bond from one structural unit to another; (d) one hydrogen bonds from the structural unit to an (H_2O) that does not bond to the interstitial complex; (e) one hydrogen bond from the structural unit to a non-transformer (H_2O) group not bonded to an interstitial cation; (f) two hydrogen bonds from the structural unit to and (H_2O) group not bonded to an interstitial cation (Schindler and Hawthorne 2001a). *M* cations are shown as green circles, O atoms and H atoms of (OH) and (H_2O) groups are shown as red and black circles respectively, hydrogen bonds are shown as dotted lines.

Schindler and Hawthorne (2001a) showed that a term, *s*, where *s* is the number of bonds from the structural unit, must be added to the original calculation for the number of bonds from an interstitial complex [$(a \times m + b \times n + c \times l) + d - (q - 1) \times f + s$].

In the situation where there is a hydrogen from one structural unit to another structural unit, the number of bonds from the interstitial complex is four but the number of bonds to the structural unit is now five, the bonds from the interstitial complex to the structural unit plus the hydrogen bond from the adjacent structural unit (Fig. 5.4c). This means that the number of bonds from the interstitial complex to the structural unit may be different than the number of bonds incident at the structural unit.

In the next situation (Fig. 5.4d), there is a hydrogen that hydrogen-bonds to an (H_2O) group that links only by hydrogen bonding to the next structural unit. This (H_2O) group can be considered to transform the hydrogen bond from one structural unit to the next, splitting one hydrogen bond into two hydrogen bonds with half the bond-valence (Fig. 5.4d). A structural unit will receive six bonds in this situation.

If there is a hydrogen atom of the structural unit that hydrogen bonds to an (H_2O) group that already accepts a hydrogen bond from a transformer (H_2O) group (Fig. 5.4e), then it becomes a non-transformer (H_2O) group and the number of bonds to the structural unit is five (Fig. 5.4e). However, if this (H_2O) group doesn't receive another hydrogen bond, it will be a transformer (H_2O) group.

In the last scenario (Fig. 5.4f), there are two hydrogen bonds from two hydrogen atoms of the structural unit that bond to an (H_2O) group that would otherwise be occluded (not bonded to anything) (Fig. 5.4f). However, this (H_2O) group is a non-transformer group as the hydrogen bonds are propagated through the (H_2O) group to the next structural unit without any change in the bond valence (or number of bonds) and the number of bonds to the structural unit is six.

5.5 A generalized interstitial complex

Schindler and Hawthorne (2001a) wrote a general interstitial complex as

$$\{^{[m]}M^{+}_{a}\ ^{[n]}M^{2+}_{b}\ ^{[l]}M^{3+}_{c}\ (H_2O)_d\ (H_2O)_e\ ^{[q]}(OH)_f\ (H_2O)_g\}^{(a+2b+3c-f)+}$$

where M is any type of interstitial monovalent, divalent and trivalent cation, d denotes the number of transformer (H_2O) groups, e denotes the number of non-transformer (H_2O) groups bonded to two interstitial cations or bonded to one interstitial cation and receiving one hydrogen bond from another interstitial (H_2O) group, f denotes the number of interstitial (OH) groups of coordination number [q], and g denotes the number of (H_2O) groups bonded to no interstitial cations. The number of bonds from the interstitial complex to the structural unit can be written as follows:

$$\text{Number of bonds} = (a \times m + b \times n + c \times l) + d - (q - 1) \times f$$

5.6 Structural unit and effective Lewis basicity

If the structural unit is considered as a very complex anion, then a Lewis-base strength can be calculated for the structural unit. The effective Lewis-base

strength (Lewis basicity) of the structural unit is the *effective charge* of the structural unit divided by the number of bonds from the structural unit (Schindler and Hawthorne 2001a). The *effective charge* of the structural unit is the formal charge of the structural unit as modified by the hydrogen bonds emanating from it, taking the average bond-valence of a hydrogen bond as h vu. Thus a structural unit with a net formal charge of Z^- and with t hydrogen bonds from the structural unit to acceptor anions in the interstitial complex has an effective charge of Z^-, modified by 'loss' of $(h \times t)^+$ (from the hydrogen bonds) to become $(Z + h \times t)^-$. Likewise, the effective charge of the interstitial complex (or the anionic side of a polar structural unit) is supplemented by this influx of bond valence: $(Z + h \times t)^+$. The Lewis basicity is the *effective* charge divided by the overall number of interstitial bonds (i.e., bonds from the interstitial complex plus the hydrogen bonds from the structural unit).

5.7 Interstitial complex and effective Lewis acidity

The interstitial complex is characterized by its Lewis-acid strength (Lewis acidity). The *effective* Lewis acidity of an interstitial complex is the *effective charge* of the interstitial complex, as modified by the hydrogen bonding, divided by the number of bonds emanating from the interstitial complex (Schindler and Hawthorne 2001a). Thus for the general interstitial complex given above, the Lewis acidity can be written as

$$(a + 2b + 3c - f + h \times t) / [m \times a + n \times b + l \times c + d - f / (q - 1) + t]$$

where *t* is the number of hydrogen bonds emanating from the structural unit.

5.7.1 Graphical representation of the Lewis acidity of a general interstitial complex

The variation in Lewis acidity of an interstitial complex can be represented graphically as a function of its variable constituents (Fig. 5.5). The Lewis acidity of the interstitial complex decreases as the number of transformer (H_2O) groups increases, as the cation-coordination numbers increase, and as the interstitial-cation charge decreases.

5.8 Average basicity of a structural unit

Hawthorne (1985) calculated the Lewis basicity of the structural unit; however, the mean coordination number for the anions of the structural unit needs to be specified using this method. An average oxygen coordination of [3] or [4] is not appropriate for all mineral groups. There is a variation of O-coordination in different minerals. If all aspects of the interstitial complex are to be predicted, then it is not useful to use the observed mean O-coordination. Schindler and Hawthorne (2000a) developed a method to predict the average O-coordination number in borate minerals. Schindler et al. (2000) defined the *average basicity* of a structural unit as the average bond-valence sum per O-atom contributed by the interstitial species and other structural units. This is the *modified charge* of the structural unit divided by the number of oxygen atoms in the structural unit, where the *modified charge* is the formal charge of the

Lewis Acidity as a Function of the Composition of the Interstitial Complex

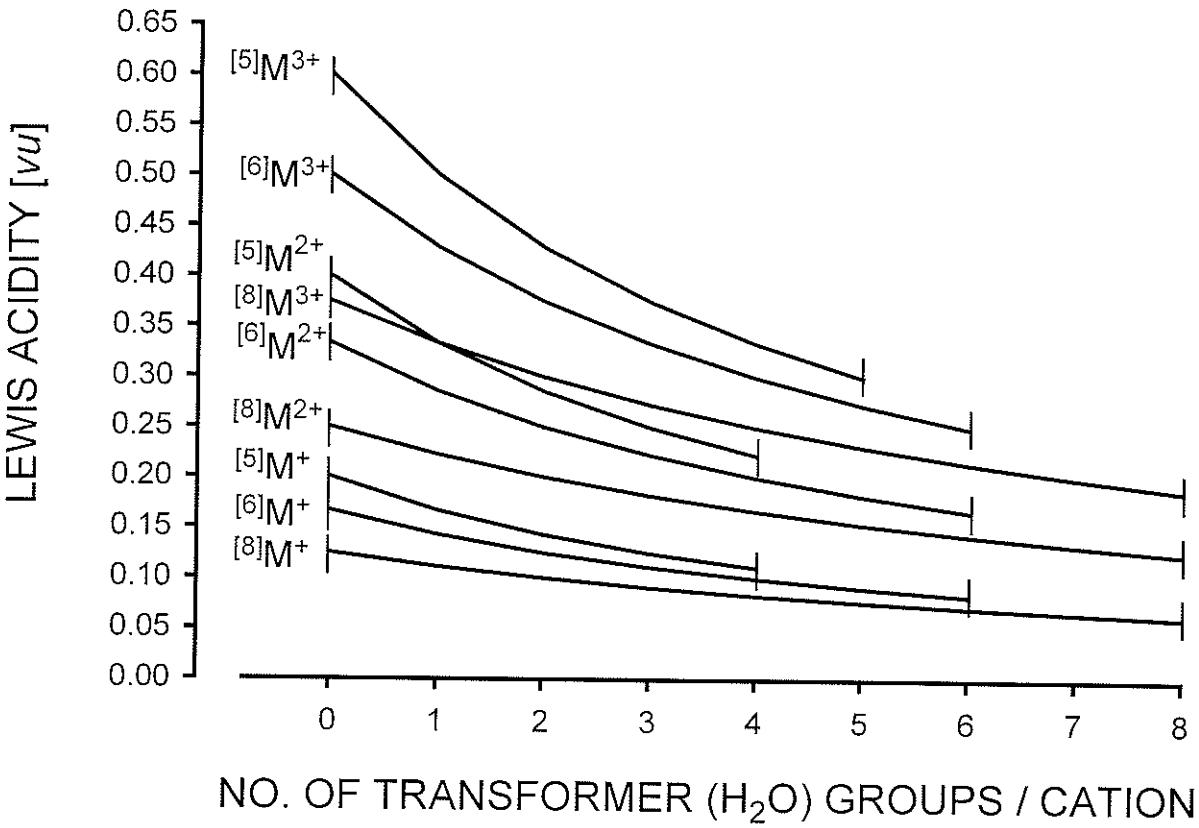

Figure 5.5. The Lewis acidity of a general interstitial complex as a function of the number of transformer (H_2O) groups per cation. The lines indicate the formal charges and possible coordination numbers for the components of an interstitial complex.

structural unit as modified by transfer of charge involved in the hydrogen bonds emanating from the structural unit (i.e., 0.20 *vu* per average hydrogen-bond). *Example:* the structural unit of anapaite is $[Fe^{2+}(PO_4)_2(H_2O)_4]^{4-}$. The modified charge is $(4^- + 0.2 \times 8)^- = 5.6^-$ and the number of O atoms in the structural unit is 12; the resulting average basicity = 5.6/12 = 0.467 *vu*. The average basicity is a measure of the bond valence required for the stability of the structure; Schindler and Hawthorne (2001a) showed that it correlates with the average coordination number of oxygen for borate minerals.

5.9 Derivation of the coordination number of oxygen for structural units

Average basicity has been defined by Schindler and Hawthorne (2001a) as a measure of the average bond-valence required by each O atom of the structural unit (from the interstitial complex and adjacent structural units). Schindler and Hawthorne (2001a) showed that there is a positive correlation between the average basicity and the mean coordination number of oxygen in borate minerals (Fig. 5.6). The data defines a band rather than a single line, in accord with the observation that a specific structural unit usually exhibits a range of mean coordination numbers for its constituent O atoms in different (but structurally related) minerals. As well as predicting a specific average coordination number for O atoms in a given structural unit, Figure 5.6 also predicts the *range of possible average coordination numbers of O atoms* in a structural unit. Where a specific structural unit occurs in a series of minerals, the O atoms of the structural unit show a range of mean coordination numbers. As

Average Basicity *vs.* Average Coordination Number of Oxygen Atoms in the Structural Units of Borate Minerals

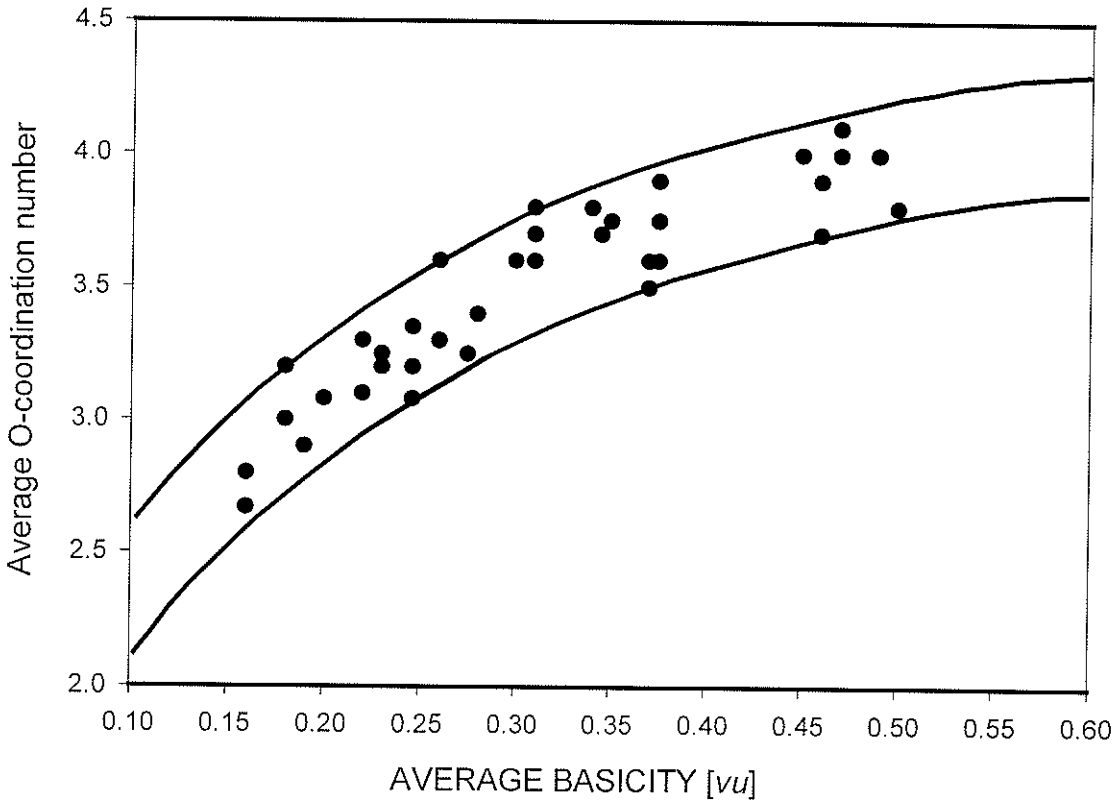

Figure 5.6. The correlation between the average coordination number of oxygen in the structural unit and the average basicity for different borate structural units (Schindler and Hawthorne 2001a).

discussed by Schindler and Hawthorne (2001b), this range of average coordination numbers reflects the range in pH (and other parameters) over which the mineral is stable. Change in O coordination number is the way in which a specific structural unit maintains its stability as the pH of its environment changes. Moreover, Figure 5.6 allows the calculation of the range of possible Lewis basicities for a specific borate structural unit.

5.10 Importance of *a priori* prediction

This *a priori* method of determining average oxygen-coordination number is an important step in the development of a predictive model for mineral structure. In order to be able to completely predict a mineral composition that is possible for specific structural unit, *a priori* determination of the average O coordination number is required. Figure 5.6 allows this prediction for a specific structural unit using the correlation of average basicity with the average O coordination. The following examples will consider borate minerals and the development of this method for phosphate minerals will be discussed in Chapter 6.

5.11 Binary structural representation and the application of the valence-matching principle

According to the valence-matching principle, if the Lewis basicity of a structural unit closely matches the Lewis acidity of an interstitial complex, then

the mineral may be stable (Fig. 5.7). Using this premise, it is then possible to be able to predict:

(1) the possible interstitial chemical composition of an interstitial complex

(2) the coordination numbers of the interstitial cations

(3) the number of transformer (H_2O) groups

For a structure to be stable, the Lewis acidity of an interstitial complex must overlap the **range** of Lewis basicity of a structural unit. The range of Lewis basicity of a specific structural unit may be ploted on a graph of the variation in Lewis acidity of generalized interstitial complex (Fig. 5.8). Where the properties of the structural unit and the interstitial complex intersect, the valence-matching principle is satisfied and structures of those specific compositions are stable. Where the properties of the structural unit and interstitial complexes do not overlap, the valence-matching principle is not satisfied and structures of those compositions are not stable.

Example: Consider the borate structural unit, $[B_4O_5(OH)_4]^{2-}$ (Schindler and Hawthorne 2001b). The steps to determine the possible interstitial chemical composition are as follows: (1) calculate its average basicity, (2) determine the range in coordination of O atoms in the structural unit, (3) calculate the corresponding range in Lewis basicity. The modified charge of the structural unit is $(2 + 0.2 \times 4)^- = 2.8^-$ thus the average basicity is 2.8/9 = 0.31 *vu*. From Fig. 5.6, the range of average O coordination number is 3.4-3.8. The range in Lewis-basicity is 2.8/[(3.4 x 9) – (2 x 4 + 2 x 3 + 4)] to 2.8/[(3.8 x 9) – (2 x 4 +2 x 3 + 4)]

OVERVIEW

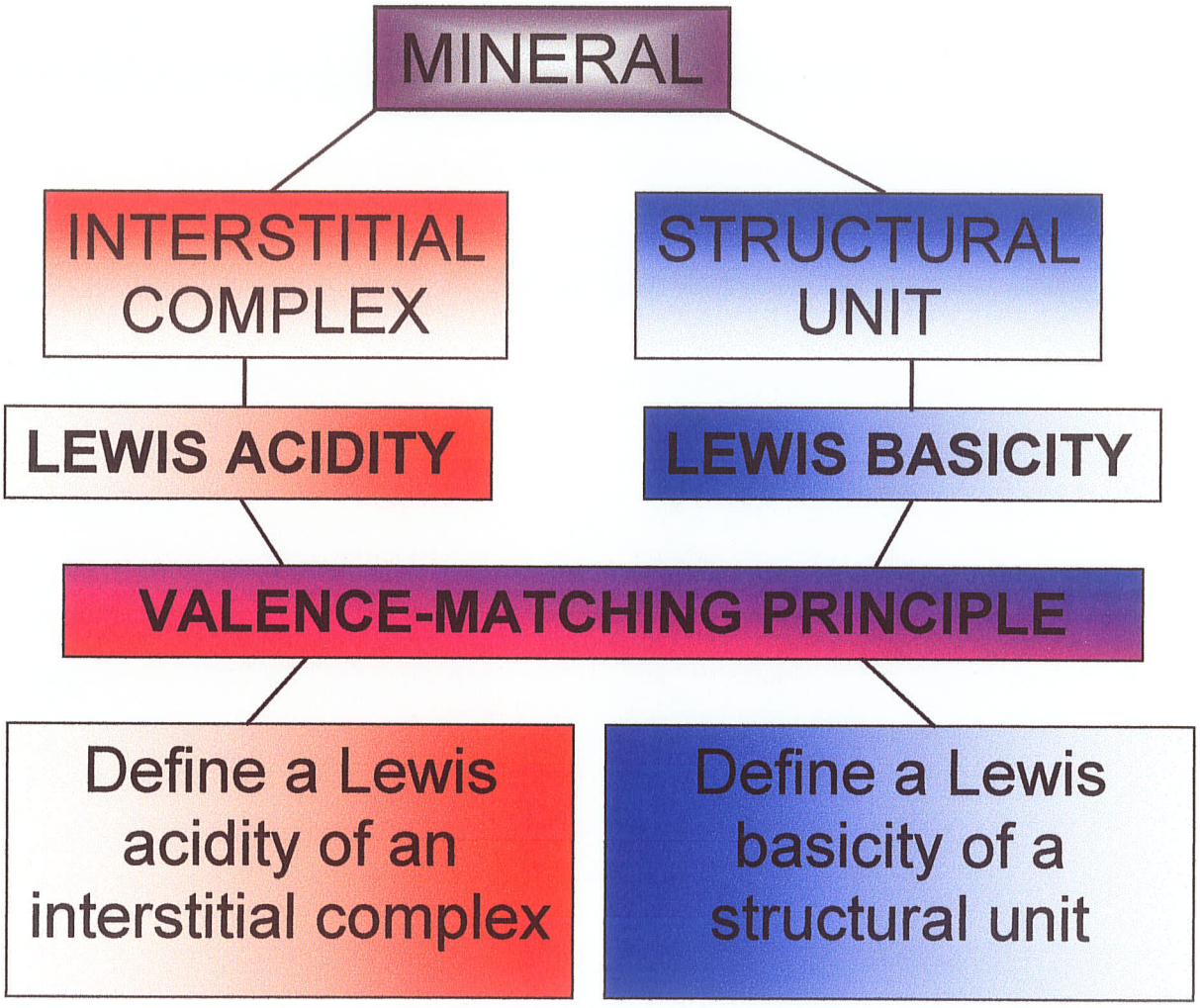

Figure 5.7. Overview of mineral stability based on the valence-matching principle.

Lewis Basicity Range for the Borate Structural Unit $[B_4O_5(OH)_4]^{2-}$

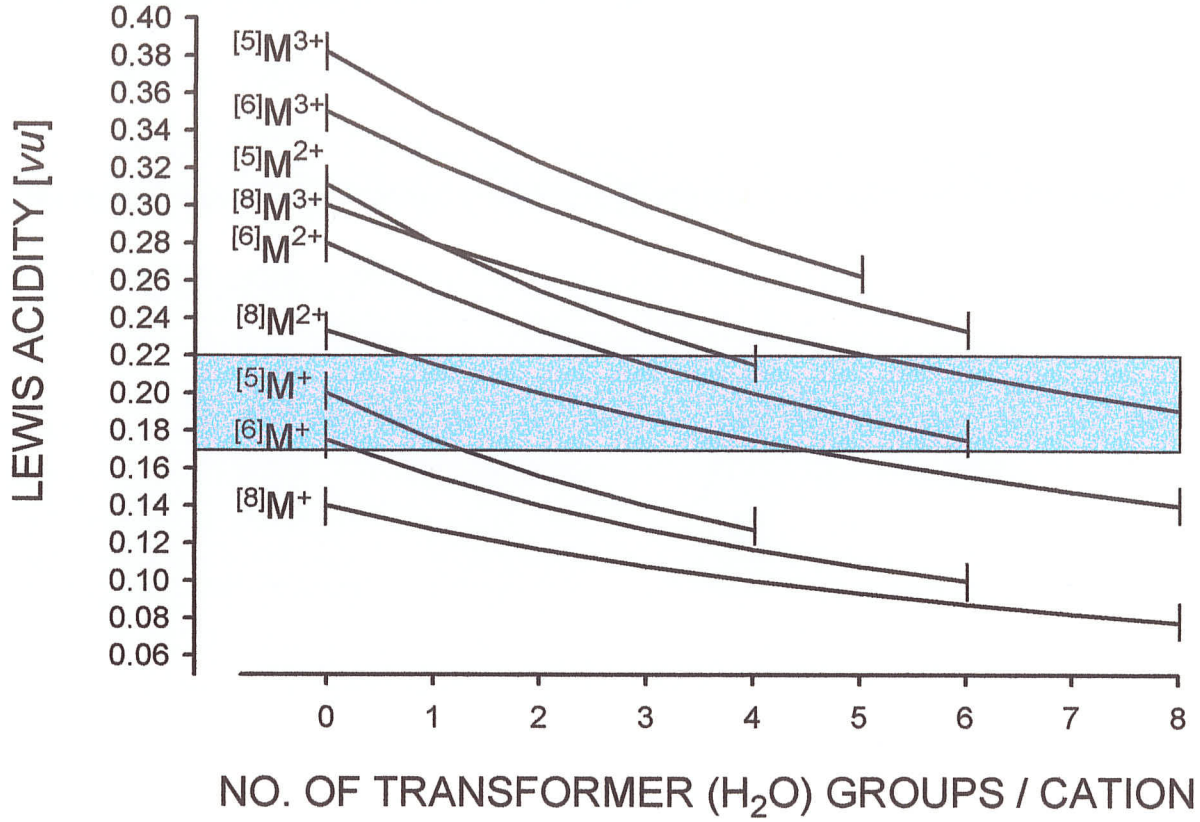

Figure 5.8. Variation in Lewis acidity of a general interstitial complex as a function of the number of transformer (H_2O) groups for mono-, di- and trivalent cations in [5]-, [6]- and [8]-coordination, with the range in Lewis basicity 0.17-0.22 *vu* (Schindler and Hawthorne 2001a).

or 0.17-0.22 *vu* (Table 5.1). From Fig. 5.8, the composition for possible interstitial complexes will fall within this range (Table 5.2).

5.11.1 Prediction of interstitial (H_2O) groups

Figure 5.8 indicates that the range in Lewis basicity determines the type of interstitial cation and the number of transformer (H_2O) groups. Consider a structural unit with a formal charge of 2^-, four (OH) groups and a range in Lewis basicity from 0.17 to 0.22 vu (Schindler et al. 2002). The Lewis acidities of all possible stable interstitial complexes must match this range. Thus the following restrictions may be applied for interstitial complexes with monovalent interstitial cations:

$$\{^{[m]}M^{+}{}_2\,(H_2O)_d\,(H_2O)_e\}^{2+} \qquad 0.17 < 2(1 + 2h) / (2m + d + 4) < 0.22$$

For monovalent cations in different coordinations (m), the possible ranges in number of transformer (H_2O) groups and the possible coordination numbers for the interstitial cations can be predicted. For cation coordination numbers m > [6], the above expression does not hold, and hence there can be no minerals of this type with interstitial monovalent cations of coordination number > [6]. When m = [6], the expression holds only for d = 0, and hence there can be no transformer (H_2O) groups for [6]-coordinated monovalent cations. When m = [5], the expression holds for d = 0–2, and hence there can be 0–2 transformer (H_2O) groups for [5]-coordinated monovalent cations.

TABLE 5.1. DETAILS OF THE $[B_4O_5(OH)_4]^{2-}$ STRUCTURAL UNIT*

Structural Unit	Average Basicity [*vu*]	Structure Type	$^{[4]}B = \square$ $^{[3]}B = \Delta$	Average Oxygen CN Range	Lewis-basicity Range [*vu*]
$[B_4O_5(OH)_4]^{2-}$	0.31	cluster	$2\square 2\Delta$	3.4-3.8	0.17-0.22

TABLE 5.2. THE $[B_4O_5(OH)_4]^{2-}$ STRUCTURAL UNIT: PREDICTED AND OBSERVED INTERSTITIAL COMPLEXES**

Structural Unit	Lewis-basicity Range [*vu*]	Predicted Interstitial Complexes	Observed Interstitial Complexes	Mineral
$[B_4O_5(OH)_4]^{2-}$	0.17-0.22	$\{^{[3]}M^{+}(H_2O)_{1\text{-}3}(H_2O)_{0\text{-}2}\}^{-}{}_2$		
		$\{^{[4]}M^{+}(H_2O)_{0\text{-}2}(H_2O)_{0\text{-}4}\}^{-}{}_2$	$\{^{[6]}Na_{1.33}Na_{0.67}(H_2O)_0(H_2O)_4\}^{3+}$	Tinacalconite
		$\{^{[5]}M^{+}(H_2O)_{0\text{-}1}(H_2O)_{0\text{-}5}\}^{-}{}_2$	$\{^{[6]}Na_2(H_2O)_0(H_2O)_8\}^{2+}$	Borax
		$\{^{[6]}M^{+}(H_2O)_0(H_2O)_{0\text{-}6}\}^{-}{}_2$		
		$\{^{[7],[8]}M^{+}\}^{-}{}_2$: not possible	$\{^{[6]}Mg(H_2O)_4(H_2O)_1(H_2O)_2\}^{2+}$	Hungchaoite
		$\{^{[6]}M^{2+}(H_2O)_{2\text{-}6}(H_2O)_{0\text{-}3}\}^{2+}$		
		$\{^{[7]}M^{2+}(H_2O)_{1\text{-}5}(H_2O)_{0\text{-}5}\}^{2+}$		
		$\{^{[8]}M^{2+}(H_2O)_{0\text{-}4}(H_2O)_{0\text{-}5}\}^{2+}$		
		$\{^{[6]}M^{3+}(H_2O)_6(H_2O)_0(OH)_1\}^{2+}$		
		$\{^{[7]}M^{3+}(H_2O)_{5\text{-}7}(H_2O)_{0\text{-}1}\}^{3+}$		
		$\{^{[8]}M^{3+}(H_2O)_{4\text{-}8}(H_2O)_{0\text{-}3}\}^{3+}$		

*Schindler and Hawthorne (2001a)
**Schindler and Hawthorne (2001b)

CHAPTER 6

Predicting mineral stability based on bond-valence relationships: Application to phosphate minerals

6.1 Characterization of structural units in phosphate minerals

Schindler et al. (2000) and Hawthorne et al. (1996) considered structural units in vanadate and borate minerals as consisting of polymerized ($V^{5+}\varphi_n$), ($V^{4+}\varphi_n$) and ($B\varphi_3$), ($B\varphi_4$) polyhedra, respectively. The corresponding average bond-valences in those polyhedra are between 0.66 and 1.25 *vu*, and are higher than the maximum bond-valence for interstitial cations (*i.e.*, a trivalent octahedrally coordinated cation, 0.50 *vu*). In the case of the phosphate minerals, bonds with the highest bond-valence are $^{[4]}P^{5+}$–O bonds at 1.25 *vu*. The next highest bond-valences are 0.50 and 0.33 *vu* for $^{[6]}M^{3+}$ and $^{[6]}M^{2+}$ cations, respectively. Schinindler et al. (2002) considered structural units as anionic polymerized complexes of (SO_4) and ($M\varphi_n$) polyhedra, with the minimum *average* bond-valence between a linking O-atom of a sulfate tetrahedron and an ($M\varphi_n$) polyhedron $\geq$ 0.30 *vu*. Phosphate minerals have similar structural characterstics as sulfate minerals and can be considered in a similar manner. The identification of the structural unit for the minerals of the first major group involving polymerization of (PO_4) groups and other ($T\varphi_4$) groups is straightforward. The tetrahedra that polymerize with (PO_4) are considered as part of the structural unit. The minerals of the second major group with structural units consisting of (PO_4) groups and other ($M\varphi_6$) octahedra, a more flexible approach is used to distinguish which cations are considered as part of the structural unit. The *M*

cations in octahedral coordination with higher bond-valences (≥ 0.33 *vu*) that polymerize with (PO_4) are considered as part of the structural unit. If both $^{[6]}M^{2+}$ and $^{[6]}M^{3+}$ cations polymerize with (PO_4), only the M^{3+} cation is considered as part of the structural unit. However, if *only* M^{2+} cations polymerize with (PO_4), then they are considered as part of the structural unit. Similar to the sulfates, the structural unit of a complex phosphate may be written as $[M^{3+}(PO_4)_k\varphi_n]$ or $[M^{2+}{}_n(PO_4)_k\varphi_n]$. In the case of the third major group of large-cations, the (PO_4) groups are considered as the structural unit. Below, various examples are considered.

(1) **Spencerite**, $Zn_2[Zn(OH)(H_2O)(PO_4)]_2(H_2O)$, contains Zn^{2+} in both tetrahedral and octahedral coordination. There are simple linear chains of alternating ($Zn\varphi_4$) [$\varphi_4 = O_2(OH)(H_2O)$] and ($PO_4$) tetrahedra, with average bond-valences of about 0.50 and 1.25 *vu*, respectively. These tetrahedral chains are cross-linked into sheets by ($Zn\varphi_6$) octahedral that involve a bond-valences of approximately 0.33 *vu* (Fig 4.4e, f). The ($Zn\varphi_6$) octahedra share all vertices with ($Zn\varphi_4$) and (PO_4) tetrahedra. The sheets link solely *via* hydrogen bonding that involves one (H_2O) group held in the structure only by hydrogen bonds.

(2) **Laueite**, $Mn^{2+}(H_2O)_4[Fe^{3+}{}_2(PO_4)_2(OH)_2(H_2O)_2](H_2O)_2$, and the minerals of the laueite group (Table 4.7) have the 7 Å chain shown in Fig. 4.13c. ($Fe^{3+}\varphi_6$) octahedra link by sharing vertices to form an $[M\varphi_5]$ chain that is decorated by flanking (PO_4) groups. These chains meld in the *a*-direction by sharing one quarter of the flanking (PO_4) vertices with octahedra of

adjacent chains to form an $[Fe^{3+}_2(PO_4)_2(OH)_2(H_2O)_2]$ sheet (Fig. 4.21a). In the resulting sheet, the (PO_4) tetrahedra are three-connected. Note that there are two distinct octahedra in these sheets, one of which is six-connected within the sheet, and the other of which is only four-connected and has (H_2O) at two vertices. Laueite can also be considered a sheet composed of $[Fe^{3+}(PO_4)_2O_2]$ chains that are linked by $(Fe^{3+}O_6)$ octahedra. These sheets stack in the *b*-direction and are linked by $(Mn^{2+}O_2\{H_2O\}_4)$ octahedra (Fig. 4.21b), and by hydrogen bonds involving the interstitial (H_2O) groups bonded to Mn^{2+} *and* interstitial (H_2O) groups held in the structure solely by hydrogen bonds.

(3) **Brushite**, $Ca(H_2O)_2(PO_3\{OH\})$, is considered as part of the large-cation group. The large cation is [8]-coordinated with the bonded anions that share edges with the $(P\varphi_4)$ tetrahedra to form chains. These chains are a common feature of large-cation structures, and occur in gypsum and other Ca-sulfate minerals. These chains link by sharing edges between $(Ca\varphi_8)$ polyhedra of adjacent chains, and by sharing of vertices between $(P\varphi_4)$ tetrahedra and $(Ca\varphi_8)$ dodecahedra. These are linked solely by hydrogen bonds (Fig. 4.56a,b).

6.2 Polar character of the structural unit

There are numerous structures that have structural units with a neutral charge and, according to the binary structural representation, there would be no way the structural unit could be held together. Schindler et al. (2002) recognized

that this problem needed to be dealt with if this extended bond-valence approach is to be of general utility. Schindler and Hawthorne (2001a, 2001b) considered hydrogen bonds from a structural unit to the interstitial complex as modifying the effective charges (and hence, effective Lewis basicity and acidity) of these components. However, this approach is not *sufficient* to characterize how neutral structural units link together, as there is a spatial characteristic of such hydrogen bonding that must be incorporated into the mechanism.

A good example of a mineral with a neutral structural unit and hydrogen bonding between structural units is lizardite, $[Mg_3Si_2O_5(OH)_4]$. The *t–o* sheets in lizardite are held together by hydrogen bonds between the (OH) groups of the octahedral layer and the bridging O-atoms of the tetrahedral layer in the adjacent *t–o* sheet (Fig. 6.1a). The structural unit (i.e., the *t–o* sheet) has an effective positive charge on the (OH) side and an effective negative charge on the O (bridging) side. Therefore, the *t–o* sheet has *polar* character, which promotes linkage between the formally neutral structural units. This idea of *structural polarity* is very useful when taking into account neutral sulfate and phosphate minerals.

A structural unit of a phosphate mineral may be written as $[M^{2+}(H_2O)_n(OH)_m(PO_4)_k]$. Similar to the lizardite structure, there is an effective positive charge on the $[(M(H_2O)_n(OH)_m)]^{(z-m)+}$ component and an effective negative charge on the O-atoms of the $(PO_4)^{3-}$ group. In the $[M(H_2O)_n(OH)_m]^{(z-m)+}$ component of the structural unit, the constituent (H_2O) and (OH) groups donate hydrogen bonds to the $(PO_4)^{3-}$ component of the structural unit, either directly or

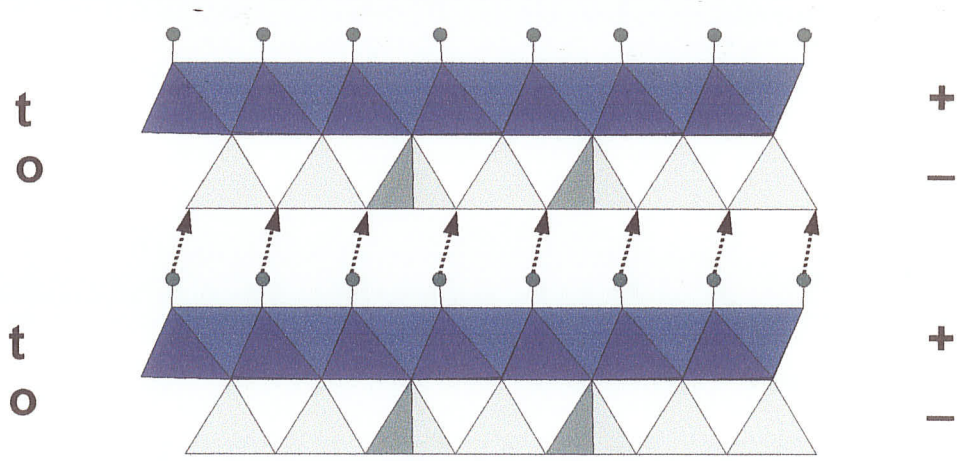

(a)

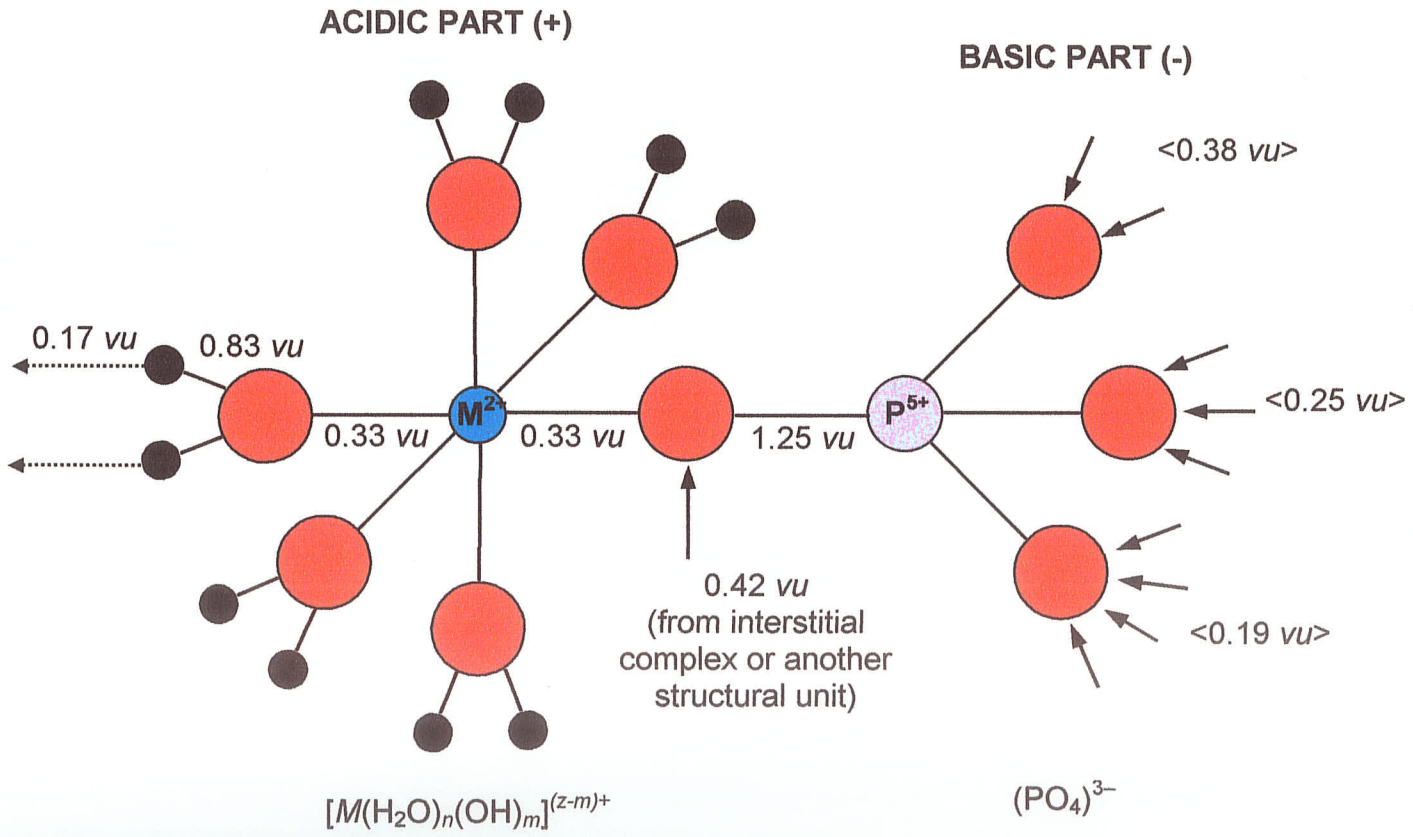

(b)

Figure 6.1. (a) polar character of the structural unit in lizardite, $[Mg_3Si_2O_5(OH)_4]$; (b) acidic and basic parts of the structural unit in a phosphate mineral; H atoms: small dark circles, Oxygen atoms: large red circles (after Schindler et al. 2002).

via the interstitial complex. The $(PO_4)^{3-}$ component of the structural unit accepts bonds only from the interstitial complex and or other structural units. The $[M(H_2O)_n(OH)_m]^{(z-m)+}$ component of the structural unit is *acidic* and the $(PO_4)^{3-}$ component of the structural unit is *basic*. The Lewis acidity of an interstitial complex depends on the average bond-valence of hydrogen bonds emanating from the acidic component of the structural unit. In order to calculate these average bond-valences, we must examine the bonding geometry in the acidic components of structural units.

6.2.1 Example of polarity in phosphate minerals

For a structural unit with divalent cations in the acidic component of the structural unit, the divalent-cations typically occur in octahedral coordination and contribute 0.33 *vu* to the linking O-atoms of the $(PO_4)^{3-}$ group. Such O-atoms receive 1.25 *vu* from the P–O bond and requires an additional 2 – 1.25 – 0.33 = 0.42 *vu* from the interstitial complex (Fig. 6.1b). An O-atom of an $(M^{2+}\varphi_6)$ octahedron which does not link to an $(PO_4)^{3-}$ group requires an additional 2 – 0.33 = 1.67 *vu*. This large additional bond-valence can be supplied either (1) by attaching two H atoms to form an (H_2O) group, or (2) by attaching one H atom to form an (OH) group, combined with polymerization of $(M^{2+}\varphi_6)$ octahedra. If all such (H_2O) groups are transformer (H_2O) groups then, the constituent O-atoms do not receive any bonds from the interstitial complex. Hence, the characteristic bond-valence of the hydrogen bonds emanating from the structural unit in these phosphate minerals is 0.33 / 2 = 0.17 *vu* (Fig. 6.1b).

Example: Leucophosphite, $K(H_2O)[Fe^{3+}_2(OH)(H_2O)_0(H_2O)(PO_4)_2]$ has the structural unit, $[Fe^{3+}_2(OH)(H_2O)_0(H_2O)(PO_4)_2]^-$. There is one non-transformer (H_2O) group and one (OH) group in the acidic component of the structural unit $\{Fe^{3+}_2(OH)(H_2O)_0(H_2O)]^{5+}$ and the basic part of the structural unit is $[(PO_4)_2]^{6-}$. The hydrogen bonds from the (H_2O) and (OH) groups have, on average, bond valences of approximately 0.20 *vu*, An average bond-valence of 0.20 *vu* is used, although Schindler et al. (2002) showed that values of 0.17 and 0.25 *vu* are more appropriate for hydrogen bonds of (H_2O) groups where the structural unit is $[(SO_4)]$. However, the non-transformer (H_2O) groups will not have an effect on Lewis acidity. The formal charge of the structural unit is 1^- and so the effective charge of the structural unit is $1 \times 0.20 + 1 = 1.2^-$.The composition of the interstitial complex is $\{^{[8]}K(H_2O)\}^+$ and there are 8 bonds from the K atom, and 2 bonds from each H atom, which equals 12 bonds emanating from the interstitial complex plus there is the hydrogen bond emanating from the acidic component of the structural unit. Thus, there are thirteen bonds involving primarily the O-atoms of the basic component of the structural unit. The resulting effective Lewis acidity is $1.2 / (8 + 2 \times 2 + 1) = 0.1$ *vu*.

6.3 Lewis acidities of interstitial complexes in phosphate minerals

The phosphate minerals have been divided into the three major groups: (1) those with polymerization of (PO_4) and (TO_4) groups as structural units, (2) those with complex $[M^{z+}(H_2O)_n(OH)_m(PO_4)_k]$ groups as structural units, and (3) those with (PO_4) tetrahedra as the structural unit and > [6]-coordinated polyhedra

as the interstitial complex (Chapter 4). Tables 6.1 and 6.2 list compositions and Lewis acidities of interstitial complexes in selected secondary phosphate minerals with structural units $[(PO_4)]$ and $[M^{z+}(H_2O)_n(OH)_m(PO_4)_k]$, respectively. A number of these minerals are shown in Figure 6.2. This figure shows a 'classical' paragenetic sequence of phosphate minerals. The approximate temperature ranges are shown, where the dashed line at 200°C indicates where in the sequence (H_2O) groups become a stable part of the mineral structure (*i.e.* bonding to transition metal cations). There are many crystal structures of phosphate minerals in which the interstitial hydrogen bonding is not resolved. In these cases, stereochemical constraints were used to determine the probable interstitial hydrogen bonding.

6.4. Calculation of Lewis acidities of interstitial complexes associated with $[M^{z+}(H_2O)_n(OH)_m(PO_4)_k]$ structural units

Hawthorne (1997) described a method for calculating the Lewis acidity for a complex cation (interstitial complex), and Schindler and Hawthorne (2001a) modified this method by including the hydrogen bonds from the structural unit and accounting for the charge-transfer involved. The Lewis acidity of an interstitial complex, $\{^{[m]}M^{+}{}_{a}{}^{[n]}M^{2+}{}_{b}{}^{[l]}M^{3+}{}_{c}(H_2O)_d(H_2O)_e(OH)_f(H_2O)_g\}^{(a+2b+3c-f)+}$, can be defined as the *effective charge* of the complex divided by the number of bonds contributed by the complex, and can be written as

$$(a + 2b + 3c - f + h \times s) / [m \times a + n \times b + l \times c + d - f \times (q - 1) + s]$$

TABLE 6.1. SELECTED PHOSPHATE MINERALS WITH [(PO_4)] STRUCTURAL UNIT WITH AVERAGE BASICITY OF 0.75 *vu*; STRUCTURAL UNIT; INTERSTITIAL COMPLEX; LEWIS ACIDITY (LA); AND AVERAGE O-ATOM COORDINATION OF INTERSTITIAL COMPLEX (CN_{int})

Mineral	Structural Unit	Interstitial Complex	LA [*vu*]	CN_{int}
Pretulite	$[(PO_4)]$	$\{^{[8]}Sc\}^{3+}$	0.375	2
Xenotime-(Y)	$[(PO_4)]$	$\{^{[8]}Y\}^{3+}$	0.375	2
Xenotime-(Yb)	$[(PO_4)]$	$\{^{[8]}Yb\}^{3+}$	0.375	2
Rhabdophane	$[(PO_4)]$	$\{^{[8]}Ce\}^{3+}$	0.375	2
Cheralite-(Ce)	$[(PO_4)]$	$\{^{[8]}Ce\}^{3+}$	0.375	2
Monazite-(Ce)	$[(PO_4)]$	$\{^{[8]}Ce\}^{3+}$	0.375	2
Churchite-(Y)	$[(PO_4)]$	$\{^{[8]}Y(H_2O)_2\}^{3+}$	0.3	2.5
Nabaphite	$[(PO_4)]$	$\{^{[6]}Na^{[9]}Ba(H_2O)_3(H_2O)_6\}^{3+}$	0.167	4.5
Nastrophite	$[(PO_4)]$	$\{^{[6]}Na^{[9]}Sr(H_2O)_3(H_2O)_6\}^{3+}$	0.167	4.5
Lithiophosphate	$[(PO_4)]$	$\{^{[4]}Li_3\}^{3+}$	0.25	3
Nalipoite	$[(PO_4)]$	$\{^{[6]}Na^{[4]}Li_2\}^{3+}$	0.214	3.5
Olgite	$[(PO_4)]$	$\{^{[8,7]}Na^{[12]}Sr\}^{3+}$	0.187	5.2
Vitusite-(Ce)	$[(PO_4)]_2$	$\{^{[6,7]}Na_3^{[8]}Ce\}^{6+}$	0.214	3.5
Buchwaldite	$[(PO_4)]$	$\{^{[7.3]}Na^{[8]}Ca\}^{3+}$	0.196	3.8
Olympite	$[(PO_4)]_2$	$\{^{[4]}Li^{[6]}Na_5\}^{6+}$	0.176	2.8
Alforsite	$[(PO_4)]_3$	$\{^{[8.4]}Ba_5^{[3]}Cl\}$	0.23	3.25
Apatite	$[(PO_4)]_3$	$\{^{[7.8]}Ca_5(OH)\}$	0.24	3.2
Belovite-(Ce)	$[(PO_4)]_3$	$\{^{[7.8]}Sr_3^{[6]}Na^{[9]}Ce(OH)\}$	0.24	3.2
Belovite-(La)	$[(PO_4)]_3$	$\{^{[8]}Sr_3^{[6]}Na^{[9]}La(OH)\}$	0.24	3.2
Chloroapatite	$[(PO_4)]_3$	$\{^{[7.2]}Ca_5^{[3]}Cl\}$	0.27	2.75
Fluorapatite	$[(PO_4)]_3$	$\{^{[7.2]}Ca_5^{[3]}F\}$	0.27	2.75
Fluor-chlor-apatite	$[(PO_4)]_3$	$\{^{[7.2]}Ca_5(^{[3]}F,Cl)\}$	0.27	2.75
Fluorpyromorphite	$[(PO_4)]_3$	$\{^{[7.2]}Pb_5^{[3]}F\}$	0.27	2.75
Hydroxylapatite	$[(PO_4)]_3$	$\{^{[7.6]}Ca_5(OH)\}$	0.25	3
Hydroxyl-	$[(PO_4)]_3$	$\{^{[7.2]}Pb_5(OH)\}$	0.25	3
Oxyapatite	$[(PO_4)]_6$	$\{^{[]}Ca_{10}O\}$	0.25	3
Pyromorphite	$[(PO_4)]_3$	$\{^{[7.2]}Pb_5^{[3]}Cl\}$	0.27	2.75
Stronitumapatite	$[(PO_4)]_3$	$\{^{[7.7]}Sr_3^{[8]}Ca_2^{[3]}F\}$	0.25	3
Strontium-chlorapatite	$[(PO_4)]_3$	$\{^{[7.2]}Sr_5^{[3]}Cl\}$	0.25	3

TABLE 6.2. THE SECONDARY PHOSPHATE MINERALS* (after Moore 1973)

neral	Structural Unit	Interstitial Complex	AB [*vu*]	CN_{su}	CN_{int}	Class
		Phosphate minerals based on ($T\varphi_4$) chains				
braesite	$[Be_2(PO_4)(OH)(H_2O)_2]$	$\{(H_2O)_2\}^0$	0.14	2.6	0.71	subIIb
yrynenite	$[Be(PO_4)(OH)]$	$\{Mn\}^{2+}$	0.44	1.8	1.4	subIIb
scherite	$[Be_4(PO_4)_6(OH)_6]$	$\{^{[7]}Ca_2{}^{[6]}Mn^{2+}{}_5(H_2O)_4(H_2O)_2\}^{16+}$	0.57	1.53	1.8	subIIb
nazziite	$[Be_4(PO_4)_6(OH)_6]$	$\{^{[6]}Ca^{[6]}Mg_5(H_2O)_2\}^{16+}$	0.57	1.53	1.267	subIIb
ansoletite	$[Be_2(PO_4)_2(PO_3\{OH\})_2]$	$\{Ca_3(H_2O)_4\}^{6+}$	0.4		1.625	
rafransoletite	$[Be_2(PO_4)_2(PO_3\{OH\})_2]$	$\{Ca_3(H_2O)_4\}^{6+}$	0.4		1.625	
encerite	$[Zn(PO_4)(OH)(H_2O)]$	$Zn_4(PO_4)_2(OH)_2(H_2O)_3$	0.43		1.67	
		Phosphate minerals based on ($T\varphi_4$) sheets				
rderite	$[Be(PO_4)(OH)]$	$\{^{[8]}Ca\}^{2+}$	0.44	1.8	1.8	subIIb
droxylherderite	$[Be(PO_4)(OH)]$	$\{^{[8]}Ca\}^{2+}$	0.44	1.8	1.8	subIIb
alolite	$[Be_4P_3O_{12}(OH)_3]$	$\{Ca_2(H_2O)_5\}^{4+}$	0.31		1.46	
peite	$[Zn(PO_4)]$	$Zn_3(PO_4)_2(H_2O)_4$	?0.25			
rahopeite	$[Zn(PO_4)]$	$Zn_3(PO_4)_2(H_2O)_4$	?0.25			
		Phosphate minerals based on ($T\varphi_4$) frameworks				
ryllonite	$[BePO_4]$	$\{^{[7]}Na\}^{+}$	0.25	2	1.75	subIIb
rlbutite	$[Be(PO_4)_2]$	$\{^{[7]}Ca\}^{2+}$	0.25	2	0.875	subIIb
inebeneite	$[Be_3(PO_4)_2(OH)_2]$	$\{Ca(H_2O)_4\}^{2+}$	0.24		1.3	
	Phosphate minerals based on isolated tetrahedra and octahedra and finite clusters of tetrahedra and octahedral					
apaite	$[Fe^{2+}(PO_4)_2(H_2O)_4]$	$\{Ca_2\}^{4+}$	0.3666		2	
rinite	$[Al_2(PO_4)_2F_4(OH)(H_2O)_2]$	$\{^{[8]}Ca_2{}^{[5]}Na\}^{5+}$				subIIb
	Phosphate minerals based on infinite chains of tetrahedra and octahedral					
ggildite	$[Al_2(PO_4)F_9]$	$\{^{[9,8]}Sr_2{}^{[9,7]}Na_2\}^{6+}$				subIIb
ssidyite	$[Ni(PO_4)_2(H_2O)_2]$	$\{^{[8]}Ca_2\}^{4+}$	0.48	1.8	2	subIIb
linsite*	$[Mg(PO_4)_2(H_2O)_2]$	$\{^{[7]}Ca_2\}^{4+}$	0.48	1.8	1.8	subIIb
rfieldite*	$[Mn^{2+}(PO_4)_2(H_2O)_2]$	$\{^{[7]}Ca_2\}^{4+}$	0.48	1.8	1.8	subIIb
sselite	$[Fe^{2+}(PO_4)_2(H_2O)_2]$	$\{^{[7]}Ca_2\}^{4+}$	0.48	1.8	1.8	subIIb

ABLE 6.2. continued

neral	Structural Unit	Interstitial Complex	AB [*vu*]	CN_{su}	CN_{int}	Class
ildrenite*	$[Al(PO_4)(OH)_2(H_2O)]$	$\{Mn\}^{2+}$	0.40	2	1.43	subIIb
sphorite	$[Al(PO_4)(OH)_2(H_2O)]$	$\{Fe\}^{2+}$	0.40	2	1.43	subIIb
arthite	$[Al(PO_4)_2(OH)]$	$\{Ca_2\}^{4+}$	0.4888		1.67	
	Phosphate minerals based on infinite sheets of tetrahedra and octahedral					
rdonite	$[Al_2(PO_4)_2(OH)_2(H_2O)_2]$	$\{Mg(H_2O)_4(H_2O)_2\}^{2+}$	0.266	2.167	1.33	subI
ueite*	$[Fe^{3+}{}_2(PO_4)_2(OH)_2(H_2O)_2]$	$\{Mn^{2+}(H_2O)_4(H_2O)_2\}^{2+}$	0.266	2.167	1.33	subI
ngangordonite	$[Al_2(PO_4)_2(OH)_2(H_2O)_2]$	$\{Mn^{2+}(H_2O)_4(H_2O)_2\}^{2+}$	0.266	2.167	1.33	subI
ravauxite	$[Al_2(PO_4)_2(OH)_2(H_2O)_2]$	$\{Fe^{2+}(H_2O)_4(H_2O)_2\}^{2+}$	0.266	2.167	1.33	subI
gloite	$[Al_2(PO_4)_2(OH)_2(H_2O)_2]$	$\{Fe^{3+}(H_2O)_3(OH)(H_2O)_2\}^{2+}$	0.266	2.167	1.25	subI
hkovite	$[Fe^{3+}{}_2(PO_4)_2(OH)_2(H_2O)_2]$	$\{Mg(H_2O)_4(H_2O)_2\}^{2+}$	0.266	2.167	1.33	subI
ewartite*	$[Fe^{3+}{}_2(PO_4)_2(OH)_2(H_2O)_2]$	$\{Mn^{2+}(H_2O)_4(H_2O)_2\}^{2+}$	0.266	2.167	1.33	subI
eudolaueite	$[Fe^{3+}{}_2(PO_4)_2(OH)_2(H_2O)_2]$	$\{Mn^{2+}(H_2O)_4(H_2O)_2\}^{2+}$	0.266	2.167	1.33	subI
unzite*	$[Fe^{3+}{}_2(PO_4)_2(OH)_2(H_2O)_2]$	$\{Mn^{2+}(H_2O)_4\}^{2+}$	0.266	2.167	1.33	subI
rrostrunzite	$[Fe^{3+}{}_2(PO_4)_2(OH)_2(H_2O)_2]$	$\{Fe^{2+}(H_2O)_4\}^{2+}$	0.266	2.167	1.33	subI
ridatite*	$[Fe^{3+}{}_3(PO_4)_3O_2]$	$\{^{[6.5]}Ca_2(H_2O)_3\}^{4+}$	0.286	2.14	0.93	subI
bertsite	$[Mn^{3+}{}_3(PO_4)_3O_2]$	$\{^{[6.5]}Ca_2(H_2O)_3\}^{4+}$	0.286	2.14	0.93	subI
ntgomeryite	$[MgAl_4(PO_4)_6(OH)_4(H_2O)_4]$	$\{^{[8,10,8,6]}Ca_4(H_2O)_2(H_2O)_6\}^{8+}$	0.325	2.06	1.44	subIIb
	Phosphate minerals based on infinite frameworks of tetrahedra and octahedral					
tavariscite*	$[Al(PO_4)(H_2O)_2]$	–	0.133	2.33	0.67	subI
sphosiderite	$[Fe^{3+}(PO_4)(H_2O)_2]$	–	0.133	2.33	0.67	subI
engite	$[Fe^{3+}(PO_4)(H_2O)_2]$	–	0.133	2.33	0.67	subI
iscite*	$[Al(PO_4)(H_2O)_2]$	–	0.133	2.33	0.67	subI
orite	$[Fe^{3+}(PO_4)(OH)]$	$\{^{[6]}Li\}^{+}$	0.24	2.2	1.4	subI
ucophosphite*	$[Fe^{3+}{}_2(PO_4)_2(OH)(H_2O)]$	$\{^{[9]}K(H_2O)_0(H_2O)_2\}^{+}$	0.16	2.3	1.2	subI
sleyite	$[Al_2(PO_4)_2(OH)(H_2O)]$	$\{^{[9]}K(H_2O)\}^{+}$	0.16	2.3	0.8	subI
zhanovskite	$[Mn^{2+}Fe^{3+}{}_2(PO_4)_2(OH)_2(H_2O)]$	–	0.073	2.72	0.4	subI
angaite	$[Fe^{2+}Al_5(PO_4)_4(OH)_6(H_2O)_2]$	$\{^{[8]}Na\}^{+}$	0.125	2.58	0.75	subI
rénite	$[Fe^{2+}Fe^{3+}{}_5(PO_4)_4(OH)_6(H_2O)_2]_2$	$\{^{[8]}Ca\}^{2+}$	0.125	2.58	0.58	subI
rodufrénite	$[Fe^{2+}Fe^{3+}{}_5(PO_4)_4(OH)_6(H_2O)_2]$	$\{^{[8]}Na\}^{+}$	0.125	2.58	0.75	subI
ndellite	$[Mn^{2+}Fe^{3+}{}_4(PO_4)_3(OH)_5]$	–	0.059	2.76	0.3	subI
kbridgeite*	$[Fe^{2+}Fe^{3+}{}_4(PO_4)_3(OH)_5]$	–	0.059	2.76	0.3	subI

ABLE 6.2. continued

ineral	Structural Unit	Interstitial Complex	AB [*vu*]	CN_{su}	CN_{int}	Refs.
arbosalite	$[Fe^{3+}(PO_4)(OH)]_2$	$\{Fe\}^{2+}$	0.24	2.2	0.8	subI
entschelite	$[Fe^{3+}(PO_4)(OH)]_2$	$\{Cu\}^{2+}$	0.24	2.2	0.8	subI
idiamite	$[Fe^{2+}{}_3(PO_4)_2(H_2O)_4]$	–	0.13	2.83	0.67	subIIa
ureaulite	$[Mn^{2+}{}_5(PO_3\{OH\})_2(PO_4)_2(H_2O)_4]$	–	0.10	2.8	0.4	subIIa
iosphoferrite*	$[Fe^{2+}{}_3(PO_4)_2(H_2O)_3]$	–	0.109	2.91	0.55	subIIa
ardite*	$[Al_3(PO_4)_2(OH)_4]$	$\{^{[8]}Na(H_2O)_0(H_2O)_2\}^{+}$	0.15	2.5	1	subIIb
igelite	$[Al_2(PO_4)(OH)_3]$	–	0.086	2.71	0.43	subIIb
azilianite	$[Al_3(PO_4)_2(OH)_4]$	$\{^{[7]}Na\}^{+}$	0.15	2.5	0.917	subIIb
ilermoite	$[Al(PO_4)(OH)]_4$	$\{^{[8]}Sr^{[5]}Li_2\}^{4+}$	0.24	2.2	1.1	subIIb
arebyite*	$[Al_2(PO_4)_3(OH)_3]$	$\{^{[11]}Ba^{[6]}Mn_2\}^{6+}$	0.44	1.8	1.73	subIIb

Subdivision I. Ligand Addition, Alkali-leached Products, Oxidation of some Metals
Subdivision II. Ligand Addition, No Oxidation of Metals
a. Derivatives of primary transition-metal phosphates
b. Hydrothermal products derived from amblygonite-montebrasite, beryl, etc.

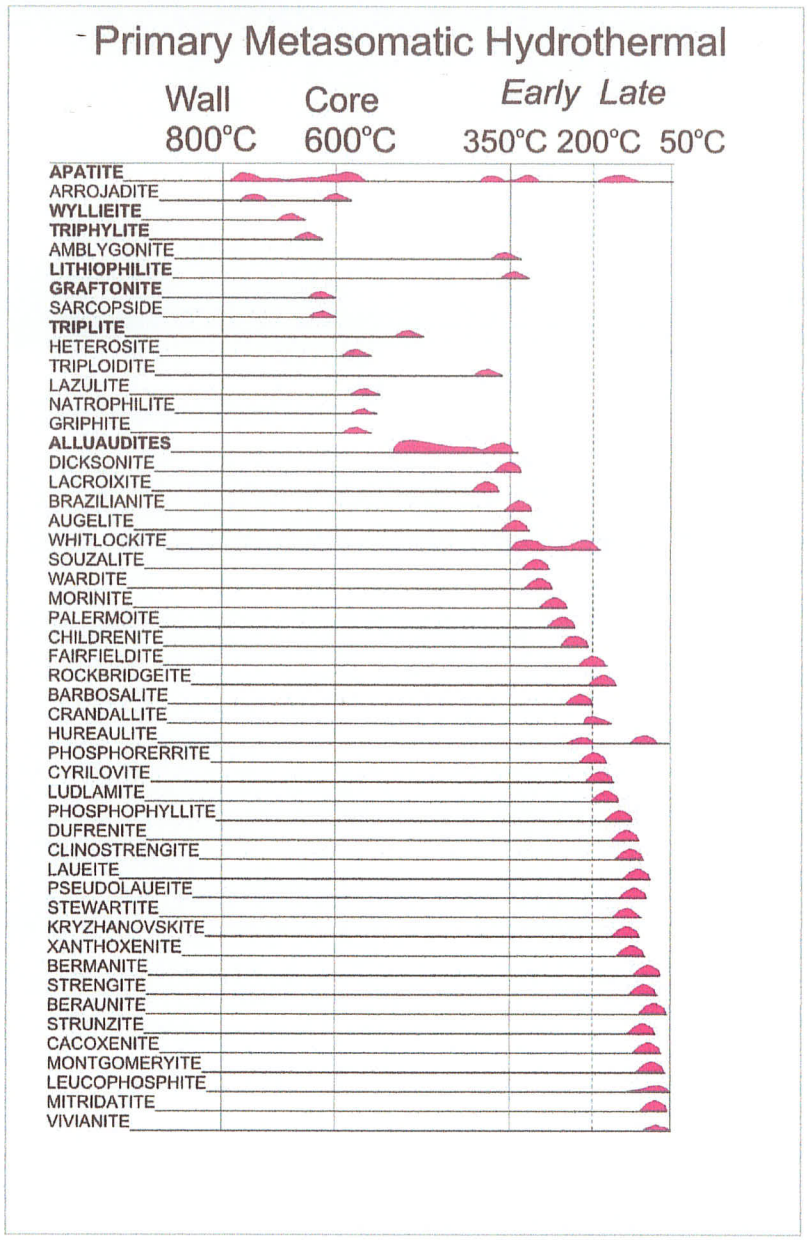

Figure 6.2. A 'classical' paragenetic sequence of phosphate minerals. The approximate temperature ranges are shown in pink. The dashed line at 200°C indicates where water is stable as part of the structure, bonded to transition metal cations (after Moore 1973).

where *h* is the average bond-valence of the hydrogen bonds emanating from the structural unit.

Example: brushite has the interstitial complex $\{^{[8]}Ca(H_2O)_2\}$ and the structural unit $[PO_3(OH)]$; the (OH)-group hydrogen-bonds to the interstitial complex, so $t = 1$ and $s = 1$. There are two transformer (H_2O) groups bonded to Ca of the interstitial complex. There are no non-transformer (H_2O) groups, no (OH) groups and no occluded (H_2O) groups in the interstitial complex. The effective charge of interstitial complex is 2 (the formal charge of the interstitial cations) + 1 x 0.20^+ (the charged transferred by the *s* hydrogen bonds to the interstitial complex) = 2.2^+. The number of bonds from the interstitial complex to the structural unit is 8 (from Ca) + 2 [from transformer (H_2O) groups] + 1 (from the hydrogen bond to the interstitial complex) = 11. Therefore the Lewis acidity of the interstitial complex is 2.2/11 = 0.20 *vu*.

6.5. Lewis acidity of interstitial complexes associated with [(PO_4)] structural units

The average Lewis basicity of the $(PO_4)^{3-}$ oxyanion is considered to 0.25 *vu* assuming an oxygen coordination of [4]. Following the valence-matching principle, the interstitial complexes should have Lewis acidities close to 0.25 vu. Fig. 6.3 shows the frequency of Lewis acidities of interstitial complexes in phosphate minerals with isolated (PO_4) groups as their structural unit (Table 6.1). Here, the Lewis acidities range from 0.167 to 0.375 *vu* with maxima at 0.25, 0.27 and 0.375 *vu*, The highest Lewis acidity (0.375 *vu*) occurs where each O-atom of the (PO_4) group receives, on average, two additional bonds from the interstitial

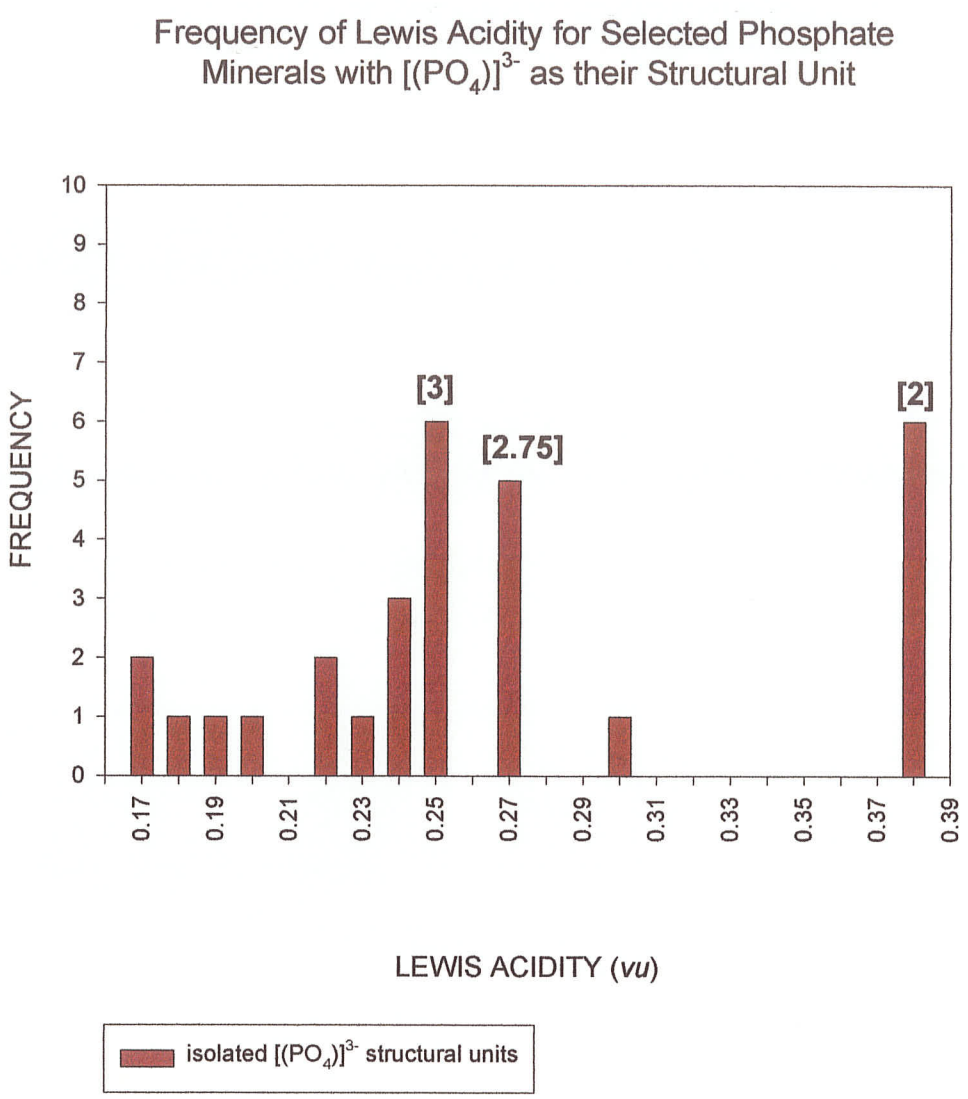

Figure 6.3. The frequency of Lewis acidity for selected phosphate minerals with $[(PO_4)]^{3-}$ as the structural unit.

complex. The minimum Lewis acidity of an interstitial complex (0.167 *vu*) occurs, on average, where two O-atoms of the (PO_4) group receive five additional bonds and two O-atoms receive four additional bonds from the interstitial complex. Interstitial complexes with Lewis acidities of 0.25 and 0.27 *vu* result in average numbers of additional bonds to O of [3] and [2.75], respectively (Fig. 6.2). If Lewis acidities occur between 0.27 and 0.25 *vu*, the corresponding average numbers of additional bonds to O of the (PO_4) group is between 2.75 and 3. There is also a Lewis-acidity maximum at 0.375 *vu*, which corresponds to an average additional number of bonds to O of the $(PO_4)^{3-}$ group of [2]. For example, an interstitial complex with a Lewis acidity of 0.20 vu: there are ten interstitial bonds to four O-atoms of one (PO_4) group, which results in an average O-coordination of (10 + 4) / 4 = [3.5] (Fig. 6.4).

6.6 Average O-coordination numbers in phosphate minerals with $[M^{z+}(H_2O)_n(OH)_m(PO_4)_k]^{(z-m-3k)-}$ structural units

In order to calculate the Lewis basicity of the structural unit, the average O-atom coordination number is required. When considering the correlation between the average basicity and the average O-coordination for the purpose of predicting interstitial complexes, it is the weaker bonds of this complex that are of interest. Considering the bond-valence (average basicity) required for the structural unit, the bonds required can come from either the interstitial complex or from a neighboring structural unit. Thus, it is of interest to determine the average O-coordination from the interstitial complex CN_{int} to the structural unit to examine

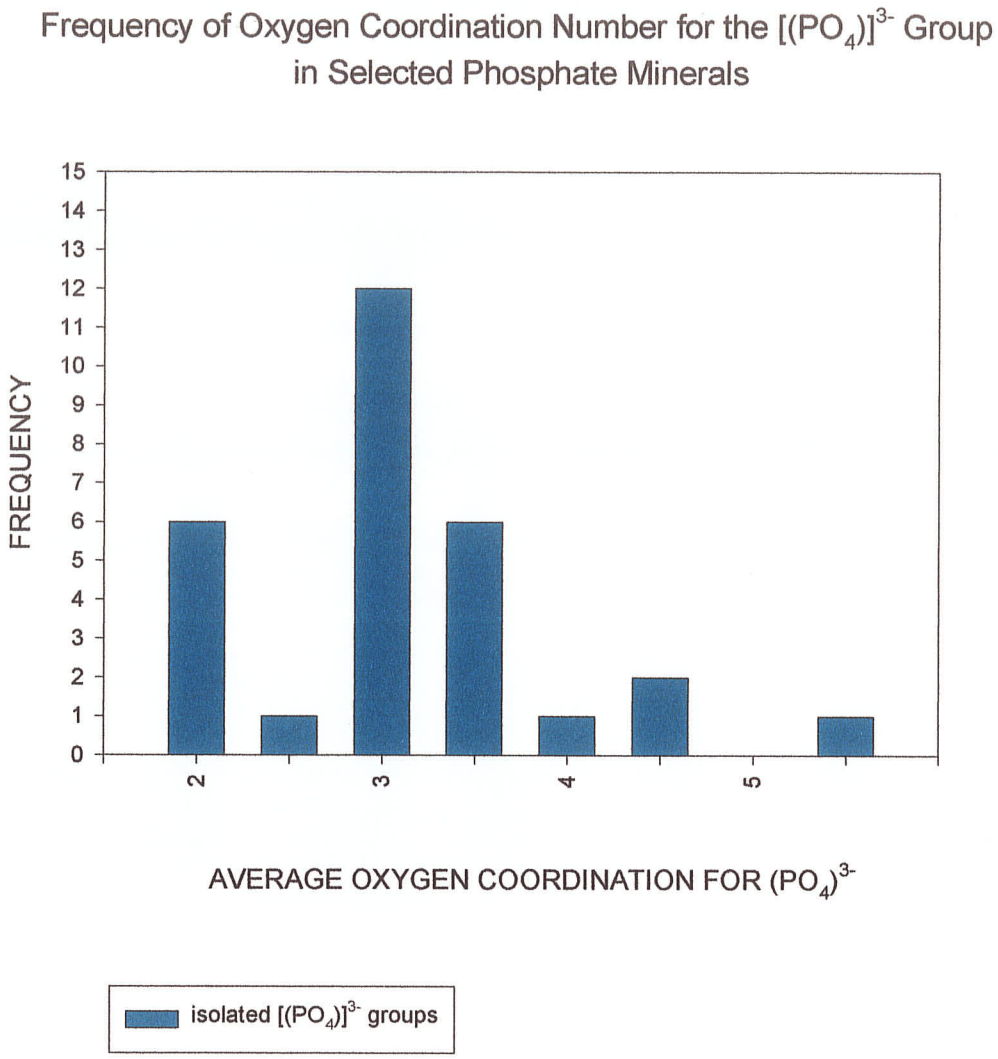

Figure 6.4. Average additional coordination numbers of oxygen in the $(PO_4)^{3-}$ groups of selected phosphate minerals with $[(PO_4)]^{3-}$ as the structural unit.

the correlation for the average CN and average basicity. This correlation is shown for selected phosphates minerals in Figure 6.5 (Table 6.2). The values used for these graphs can be calculated if the number of interstitial transformer (H_2O) groups is known.

Example: laueite, $\{Mn^{2+}(H_2O)_4(H_2O)_2\}[Fe^{3+}{}_2(PO_4)_2(OH)_2(H_2O)_2]$, Mn^{2+} is coordinated by four (H_2O) groups and two O-atoms, providing 4 x 2 + 2 = 10 bonds to the structural unit. There are also 6 weak hydrogen-bonds emanating from the structural unit for a total of 10 + 6 = 16 bonds. There are 12 oxygen atoms in the structural unit, so the interstitial complex donates 16/12 = 1.33 bonds per O-atom of the structural unit.

The average O-coordination of structural unit CN_{su} can be calculated in a similar way. *Example:* The structural unit in laueite is $[Fe^{3+}{}_2(PO_4)_2(OH)_2(H_2O)_2]^{2-}$; there are 2 x 6 bonds from Fe^{3+}, 8 bonds from P, 2 strong bonds involving (OH) and 4 strong bonds involving the (H_2O) groups for a total of 26 bonds in the structural unit. There are 12 oxygen atoms in the structural unit, so the average CN within the structural unit, CN_{su}, is 26/12 = [2.16]. The total average oxygen coordination in laueite is $CN_{int} + CN_{su}$ = [1.33] + [2.16] = [3.49] = CN

The charge on the structural unit is 2^- and there a 2 hydrogen bonds from the (OH) of the structural unit plus 4 additional hydrogen bonds from the 4 transformer (H_2O) groups of the interstitial complex for a total of 6 bonds involving hydrogen with an average bond valence of 0.2 *vu*. Thus the effective

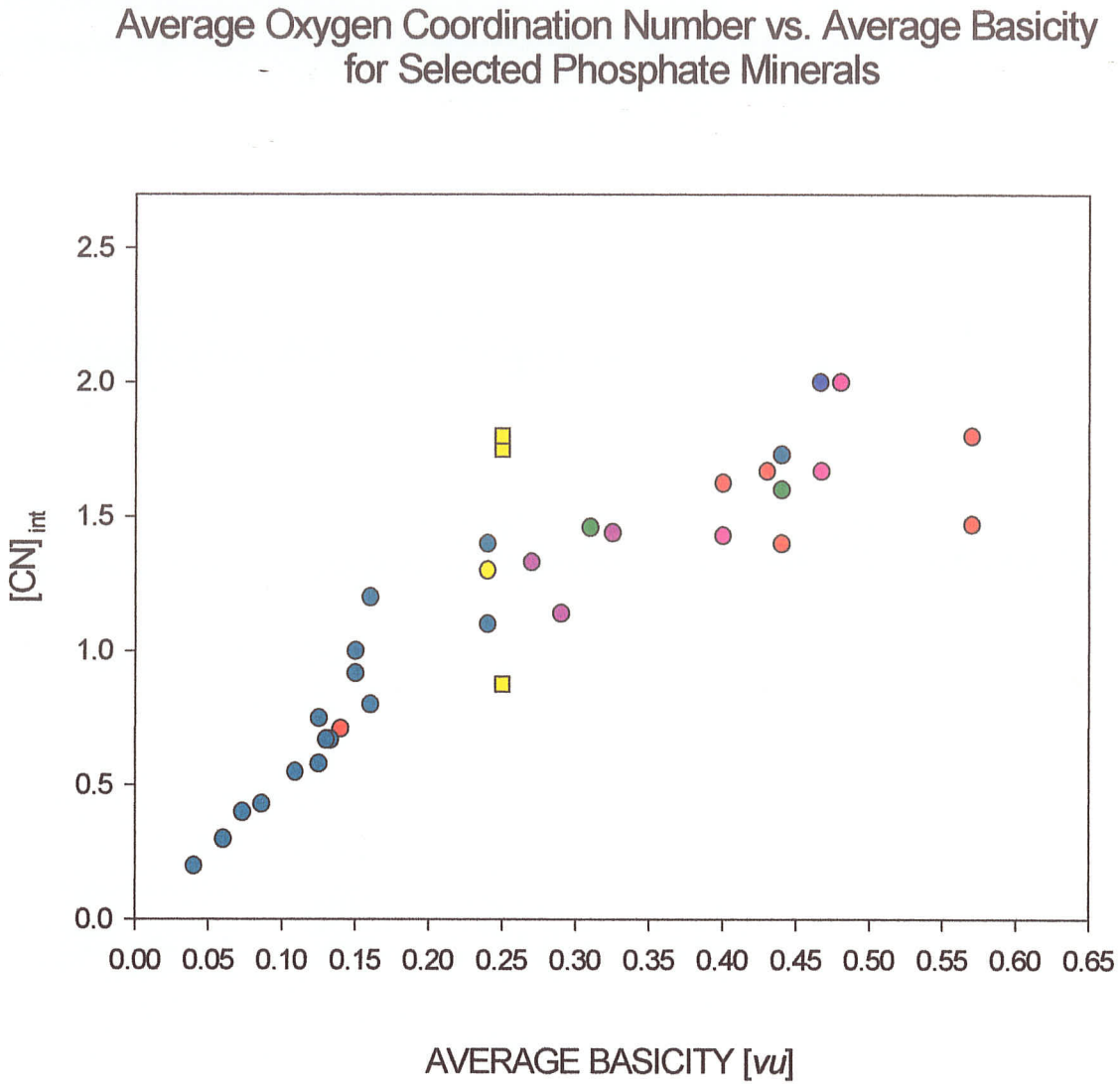

Figure 6.5. Average coordination numbers of the interstitial O-atoms as a function of average basicity in selected phosphate minerals with $[M^{z+}(H_2O)_n(OH)_m(PO_4)_k]$ structural units.

charge is 2^- + (6 x 0.2) = 3.2^-. The average basicity is 3.2 divided by 12 (no. O-atoms in the structural unit) or 0.266 *vu*.

6.7 Average O-coordination numbers in sulfate minerals with $[M^{z+}(H_2O)_n(OH)_m(SO_4)_k]^{(z-m-2k)-}$ structural units

Schindler et al. (2002) showed a similar correlation for the sulfate minerals. Fig. 6.6 shows data for phosphate and sulfate structural units with octahedrally-coordinated trivalent (red triangles) and divalent (green triangles) *M* cations and other sulfate structures (blue triangles). The distribution of data shows that O-atoms in structural units containing M^{3+} cations (mainly Fe^{3+}) have, on average, lower coordination numbers than those in structural units with M^{2+} cations.

These differences in the average O-coordination number of structural units containing trivalent and divalent cations, respectively, can be understood better by considering the average basicity of the structural unit as a function of the average O-coordination number involving bonds *inside* the structural unit, CN_{str}. For structural units of similar average basicity, those containing M^{3+} cations have lower average coordination numbers than those containing M^{2+} cations. Fig. 6.6 shows the average basicity as a function of the average O-coordination number in the structural unit calculated from the interstitial bonds (CN_{int}), *i.e.*, the number of bonds to the structural unit divided by the number of O-atoms in the structural unit (note that $CN = CN_{str} + CN_{int}$). This correlation shows that the number of incident bonds depends on the average basicity not on the degree of

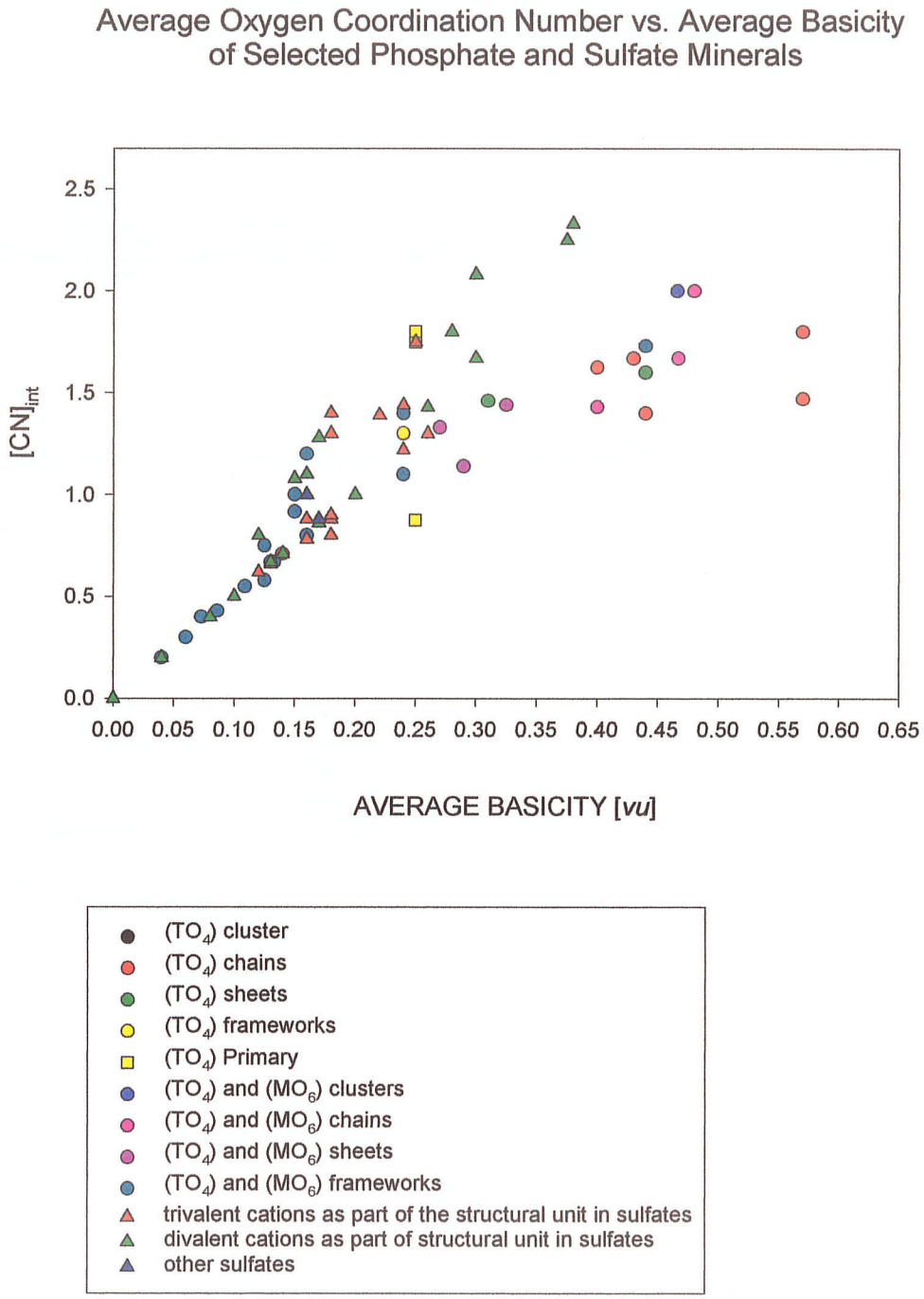

Figure 6.6. The average O-atom coordination number of the interstitial complex as a function of average basicity of selected phosphate and sulfate minerals with a structural unit of the form $[M^{z+}(H_2O)_n(OH)_m(PO_4)_k]$ (sulfate data from Schindler et al. 2002).

polymerization of the ($M^{z+}\varphi_6$) polyhedra. This is to be expected, as the O-atoms of the (SO_4) groups [and not of the ($M^{z+}\varphi_6$) groups] are the principal bond-valence acceptors in $[M^{z+}(H_2O)_n(OH)_m(SO_4)_k]$ structural units.

6.8 Average O-coordination numbers in borate minerals

As already discussed in Chapter 5, Schindler and Hawthorne (2001a, 2001b) showed that there is a correlation between average basicity and average O-coordination number, CN, for structural units in borate minerals (assuming an average hydrogen bond-valence of 0.20 *vu*) (Fig. 5.6). The structural units consisted only of the polymerized ($V^{5+}\varphi_n$), ($V^{4+}\varphi_n$) and ($B\varphi_3$), ($B\varphi_4$) polyhedra. Therefore, in borate minerals, the structural units contain only B cations; these are isovalent but can adopt two coordination numbers, [3] and [4]. This difference in coordination of B causes differences in the average B–O bond-valence: 1.0 to 0.75 *vu*. The value CN_{str} does not change with average basicity in borate structural units; it is almost always [2]. This is surprising, as one might expect that O-atoms in structural units with a higher proportion of $^{[3]}B$ to have lower CN_{str} values than those with a higher proportion of $^{[4]}B$. However, Schindler and Hawthorne (2001b) showed that $^{[4]}B$: $^{[3]}B$ correlates with the average basicity; thus, increasing the average bond-valence of B–O bonds by increasing the proportion of $^{[3]}B$ is balanced by decreasing average basicity. As CN correlates with average basicity and CN_{str} is approximately constant, CN_{int} varies in a similar way to CN as a function of average basicity (Fig. 5.6, and 6.7). In both

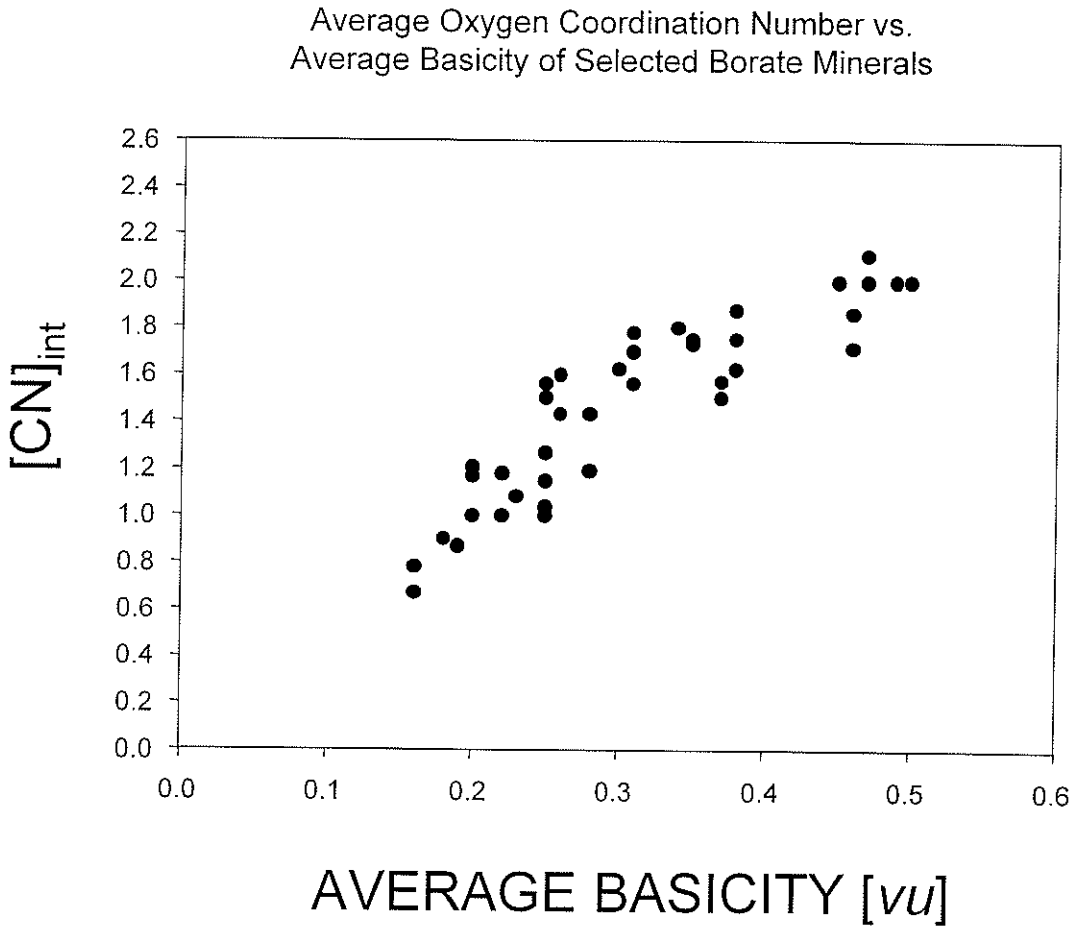

Figure 6.7. The average O-atom coordination number of the interstitial complex as a function of average basicity of selected borate minerals (data from Schindler et al. 2002).

correlations, the bands of data approach the maximum O-coordination numbers [4] and [2], respectively.

6.9 Average basicity versus CN_{int} in phosphate, sulfate and borate structural units

Comparison of Figs. 6.5, 6.6 and 6.7 shows that the bands of data have similar slopes at lower average basicity but different slopes at higher average basicity. Unlike the relation for borate structural units (Fig. 5.6 and 6.7), the band of data points for phosphate and sulfate structural units (Fig. 6.6) does not approach any maximum value of CN_{int}. The reason for this is structural units of phosphates, sulfates and borate minerals with high average basicity have similar average O-coordination numbers, CN; however, CN_{str} is lower in sulfate minerals than in borate minerals. Hence, more interstitial cations bond to O-atoms of structural units in sulfate minerals than is the case in borate minerals. In phosphate minerals the average CN_{int} decreases with increasing average basicity.

6.10 Prediction of interstitial complexes in phosphate minerals

The maximum and minimum Lewis basicities can be calculated if the average basicity is known for a structural unit. Figure 6.5 shows the range in the average oxygen coordination of the interstitial complex (CN_{int}) for structural units with a specific average basicity. Therefore, the maximum and minimum Lewis-bascities can be calculated.

6.10.1 The structural unit $[M^{n+}(PO_4)(OH)(H_2O)]^{(n-4)}$ (M = Al, Fe^{3+})

Example: For the structural unit $[Al(PO_4)(OH)(H_2O)]^-$; the first step in predicting the interstitial complex is to determine the average bascity as already discussed. Average basicity = [(charge + hs) / (no. of O-atoms)] = $(1^- + 0.2 \times 3) / 6 = 0.27$ *vu*. From Figure 6.5 the average oxygen coordination range of the oxygen to the structural unit {$[CN_{int}]_{max}$ and $[CN_{int}]_{min}$} can be determined; $[CN_{int}]_{max} = 1.6$ and $[CN_{int}]_{min} = 1.1$.

The Lewis basicity range for the structural unit $[^{[6]}Al(^{[4]}PO_4)(O^{[2]}H)(^{[2]}H_2O)]_2$ can be calculated from the maximum and minimum oxygen coordination numbers to the structural unit. The Lewis basicity is the effective charge of the structural unit divided by the number of bonds to the structural unit. The effective charge for the structural unit $[^{[6]}Al(^{[4]}PO_4)(O^{[2]}H)(^{[2]}H_2O)]_2$ is $(1^- + 0.2 \times 3) = 1.6^-$. The maximum and minimum number of bonds to the structural unit are: $Bonds_{max} = 1.6 \times 6 = 9.6$; $Bonds_{min} = 1.1 \times 6 = 6.6$. Thus $Lewis\text{-}bascity_{max} = 1.6^- / 6.6 = 0.24$ *vu;* $Lewis\ bascity_{min} = 1.6^- / 9.6 = 0.17$ *vu*. Fig. 6.8 shows the variation in Lewis acidity of a general interstitial complex as a function of cation charge, cation coordination number, and the number of transformer (H_2O) groups, with the range of Lewis basicity of the $[M^{3+}(OH)(PO_4)(H_2O)]^-$ structural unit marked by horizontal broken lines. Where the Lewis-acidity curves intersect the range of Lewis basicity of the structural unit, the valence-matching principle is satisfied and a stable structure can form. For interstitial monovalent cations with coordination numbers [9] and above, the curves do not intersect the range of Lewis-basicity of the structural unit, and monovalent cations cannot occur. For

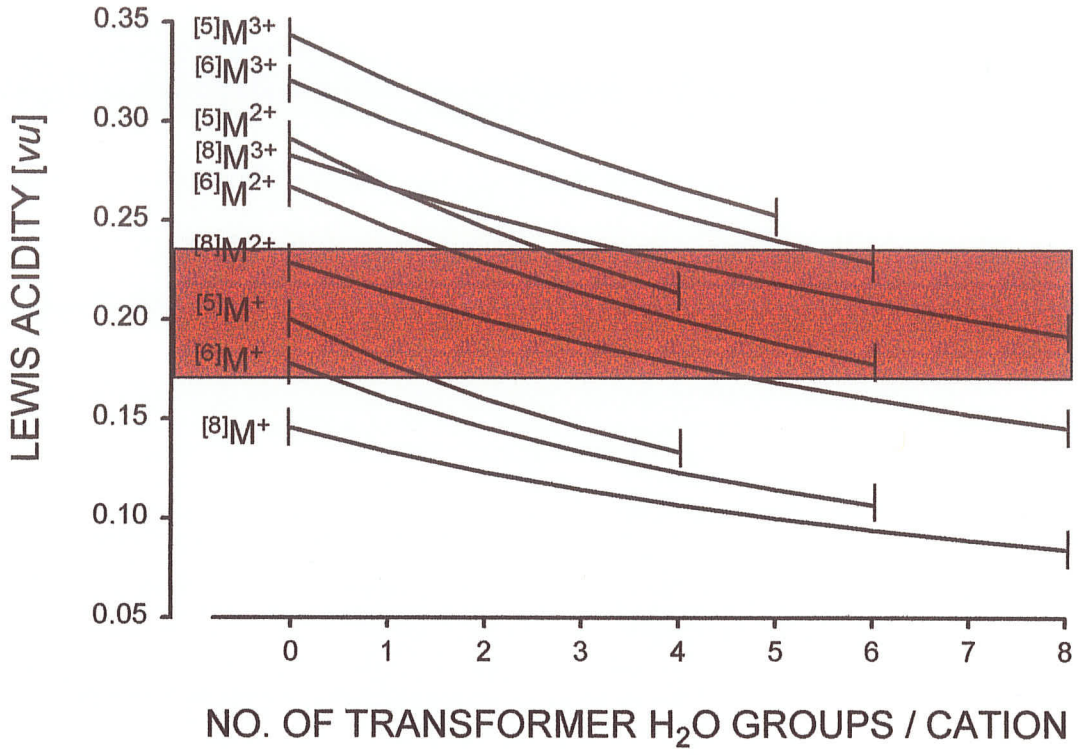

Figure 6.8. The Lewis basicity range for the structural unit $[M^{n+}(OH)(PO_4)(H_2O)]^{(n-4)-}$ plotted on a graph showing the Lewis acidity as a function of coordination number, charge and transformer (H_2O) groups.

coordination numbers [8] to [5], a monovalent cation can occur with 0, 0–1, 0–2 and 0–3 transformer (H_2O) groups present, respectively (Fig. 6.8). Divalent interstitial cations, $^{[8]}M^{2+}$ can occur with 2-6 transformer (H_2O) groups. For divalent interstitial cations, $^{[6]}M^{2+}$ is possible if it does not bond to any anion of the structural unit (*e.g.*, if it occurs as isolated $[^{[6]}M^{2+}(H_2O)_6]$ or $[^{[6]}M^{2+}(H_2O)_n(OH)_m]^{(2-m)+}$ groups), and hence it is possible with 4-6 transformer (H_2O) groups, $^{[8]}M^{3+}$ is possible with 7–8 transformer (H_2O) groups. The following interstitial complexes are found in nature $\{^{[6]}M^{2+}(H_2O)_4(H_2O)_2\}^{2+}$; $\{^{[6]}M^{3+}(H_2O)_3(OH)(H_2O)_2\}^{2+}$; $\{^{[6]}M^{2+}(H_2O)_4\}^{2+}$; $\{^{[6]}M^{2+}(H_2O)_6\}^{2+}$ (Table 6.3).

These predictions show the possible variations in chemical composition of the interstitial complexes.

6.11 Occurrence of interstitial-cation composition

The question of why certain interstitial cations occur in some minerals and not in others can now be addressed with greater confidence. Consider the minerals listed in Table 6.4. Why does $\{Ca_2\}^{4+}$ occur as the interstitial cation for the structural unit $[M(TO_4)_2\varphi_2]^{4-}$ instead of $\{Na_4\}^{4+}$ or $\{K_4\}^{4+}$ (*e.g.* collinsite, $Ca_2[Mg(PO_4)_2(H_2O)_2]$)? Why do $\{Sr_2\}^{4+}$ and $\{Pb_2\}^{4+}$ occur as the interstitial cation for the structural unit $[M(TO_4)_2\varphi]^{4-}$ instead of a four monovalent cations, which would satisfy the electroneutrality principle? These questions can be answered by applying the valence-matching principle such that for a structural arrangement to be stable, the effective Lewis acidity of the interstitial complex must match the Lewis-basicity range of a given structural unit.

TABLE 6.3. PREDICTED AND OBSERVED INTERSTITIAL COMPLEXES FOR THE STRUCTURAL UNIT $[M^{n+}(PO_4)(OH)(H_2O)]^{(n-4)-}$

Predicted Interstitial Complex	Observed Interstitial Complex (mineral)
$\{^{[5]}M^{+}(H_2O)_{0\text{-}1}\}^{+}$	$\{^{[6]}Mg^{2+}(H_2O)_4(H_2O)_2\}^{2+}$ (Gordonite)
$\{^{[8]}M^{2+}(H_2O)_{0\text{-}4}\}^{2+}$	$\{^{[6]}Mn^{2+}(H_2O)_4(H_2O)_2\}^{2+}$ (Laueite)
$\{^{[6]}M^{2+}(H_2O)_{4\text{-}6}(H_2O)_{2\text{-}0}\}^{2+}$	$\{^{[6]}Mn^{2+}(H_2O)_4(H_2O)_2\}^{2+}$ (Mangangordonite)
$\{^{[8]}M^{3+}(H_2O)_{3\text{-}8}\}^{3+}$	$\{^{[6]}Fe^{2+}(H_2O)_4(H_2O)_2\}^{2+}$ (Paravauxite)
$\{^{[5]}M^{2+}(H_2O)_{2\text{-}4}\}^{2+}$	$\{^{[6]}Fe^{3+}(H_2O)_3(OH)(H_2O)_2\}^{2+}$ (Sigloite)
	$\{^{[6]}Mg^{2+}(H_2O)_4(H_2O)_2\}^{2+}$ (Ushkovite)
	$\{^{[6]}Mn^{2+}(H_2O)_4(H_2O)_2\}^{2+}$ (Kastningite)
	$\{^{[6]}Mn^{2+}(H_2O)_4(H_2O)_2\}^{2+}$ (Stewartite)
	$\{^{[6]}Mn^{2+}(H_2O)_4(H_2O)_2\}^{2+}$ (Pseudolaueite)
	$\{^{[6]}Mn^{2+}(H_2O)_4\}^{2+}$ (Strunzite)
	$\{^{[6]}Fe^{2+}(H_2O)_4\}^{2+}$ (Ferrostrunzite)
	$\{^{[6]}Fe^{2+}(H_2O)_6\}^{2+}$ (Metavauxite)

TABLE 6.4. INTERSTITIAL-CATION COMPOSITION OF SELECTED PHOSPHATE AND SULFATE MINERALS

Mineral Name	Interstitial cation	Structural unit
Cassidyite	$\{Ca_2\}^{4+}$	$[Ni(PO_4)_2(H_2O)_2]^{4-}$
Collinsite	$\{Ca_2\}^{4+}$	$[Mg(PO_4)_2(H_2O)_2]^{4-}$
Fairfieldite	$\{Ca_2\}^{4+}$	$[Mn(PO_4)_2(H_2O)_2]^{4-}$
Messelite	$\{Ca_2\}^{4+}$	$[Fe^{2+}(PO_4)_2(H_2O)_2]^{4-}$
Goedkenite	$\{Sr_2\}^{4+}$	$[Al(PO_4)_2(OH)]^{4-}$
Tsumebite	$\{Pb_2\}^{4+}$	$[Cu(PO_4)(SO_4)(OH)]^{4-}$
vauquelinite	$\{Pb_2\}^{4+}$	$[Cu(PO_4)(SO_4)(OH)]^{4-}$

Example: Consider collinsite, $^{[8]}Ca_2[^{[6]}Mg(^{[4]}PO_4)_2(^{[2]}H_2O)_2]$, with a known structure and known hydrogen-bonding scheme. The range in Lewis-basicity is the effective charge of the structural unit divided by the range of bonds from the interstices to the structural unit. As the structure is known, the specific value for the Lewis basicity (rather than the range of Lewis basicity) can be calculated. The average oxygen coordination is 3.4, and the total number of bonds needed for coordination of O-atoms of the structural unit = 3.4 x 10 = 34. The number of bonds within the structural unit $[^{[6]}Mg(^{[4]}PO_4)_2(^{[2]}(H_2O)_2]$ is 6 x 1 + 4 x 2 + 2 x 2 = 18; thus the number of external bonds required = 34 - 18 = 16. The effective charge is 4^- + (0.2 x 4) = 4.8^-. Therefore, the Lewis basicity would be 4.8^- / 16 = 0.3 *vu*.

The Lewis acidity, can also be calculated from the known structure; 4.8^- / (8 + 8) = 0.3 *vu*. Therefore, the Lewis acidity of the interstitial complex matches the Lewis basicity of the structural unit and the structure is stable. From table 2.5 the Lewis basicity is close to the characteristic Lewis acidity of Ca (0.27 *vu*), whereas Na and K have Lewis acidities of 0.16 and 0.13 *vu*, respectively and will not form a stable linkage with the structural unit of collinsite.

CHAPTER 7

Review

7.1 Summary

There have been significant advances toward developing a predictive (*a priori*) method based on the crystal structure of minerals to determine relative mineral stability. An important development is the binary representation of the structures of complex minerals. All complex minerals can be represented in terms of two components. This binary representation allows evaluation of relative mineral stabilities in terms of the interactions of the component parts of the structure. The development of a bond-valence approach to evaluate complex hydroxy-hydrated oxysalt minerals from a crystal-structure perspective uses the combination of a hierarchical ordering scheme based on this binary representation with bond-valence theory and the valence-matching principle to understand the factors that control the chemical compositions of interstitial complexes. This approach provides the ability to predict what chemical compositions tend to be stable in Nature. A framework is then developed in which it becomes possible to predict the chemistry from the structural characteristics of these minerals formed in complex low-temperature environments. These fundamental observations may in the future be applied to all aspects of mineral formation such as paragenetic sequences of minerals.

Some observations that stem from this approach and lead to a better understanding of the factors that control the atomic arrangement, chemical composition and relative stability of complex phosphate minerals are:

(1) The most common polymerizations are based on coordination polyhedra of higher bond-valence in phosphate minerals are between tetrahedra and

tetrahedra, between tetrahedra and octahedra, and between tetrahedra and large-cation polyhedra (i.e. [7]-coordinated and higher). Therefore, the phosphates have been divided into these three principal groups: (a) structures with (PO_4) groups and other ($T\Phi_4$) groups as structural units; (b) structures with complex [$M^{z+}(H_2O)_n(OH)_m(PO_4)_k$] structural units; and (c) structures in which (PO_4) groups as structural units polymerize with > [6]-coordinated polyhedra.

(2) The range in Lewis basicity of any phosphate, sulfate or borate structural unit can be determined *via* a combination of *average basicity* versus CN and average basicity versus CN_{int}.

(3) The calculated range in Lewis basicity for a specific structural unit gives information about the general composition of possible interstitial complexes. Where the Lewis acidity of a generalized interstitial complex overlaps the range of Lewis basicity of a specific structural unit, the valence-matching principle is satisfied and a stable structural arrangement is possible.

(4) Application of this approach to complex minerals shows that there are restrictions on the chemical and structural details of the interstitial complexes. The Lewis basicities of some structural units do not allow certain types of cations to occur as interstitial components. The overlap of Lewis basicity and acidity required for structural stability by the valence-matching principle leads to an explanation and prediction of the number of transformer (H_2O) groups in the interstitial complexes of these minerals.

7.2 Future Work

At this point, it is possible to rationalize and predict the stoichiometry and structural characteristics of paragentic mineral sequences and compare changes of progressive sequences of crystallization for rock-forming minerals to those of non-rock forming minerals in terms of crystal structure.

There are several issues to consider in terms of paragenetic phosphate mineral sequences. It has already been shown that there is a connection between the mode of polymerization of the principal polyhedra and the crystallization sequence for non-rock forming minerals. There is also evidence that this is the case for complex hydroxy-hydrated minerals such as the phosphate minerals. It has been shown that there is correlation between the average basicity and the mean coordination-number of O-atoms in the structural unit for low-temperature chemically complex minerals. This correlation defines a band that allows prediction of the range in average coordination-number of the O-atom. Previous work on sulfate (Schindler et al. 2002) and borate (Schindler and Hawthorne 2001a-c) minerals has also shown that it is within this range that the structural unit responds to changes in pH while remaining stable.

Future work should involve further characterization and classification of complex non-rock-forming mineral groups; the evaluation of mineral-surface reactions/interactions; and determining mechanisms for geometric crystal distortions and substitution of chemical elements in terms of bond-valence requirements for complex hydroxy-hydrated oxysalt minerals. As the phosphate minerals occur in more varied conditions, there are other factors that have to be assessed such as temperature. However, the structural hierarchy that has been developed for phosphate minerals lays the ground work for future work on paragenetic sequences of phosphate minerals based on the details of their crystal structure.

REFERENCES

Abbona F, Calleri M, Ivaldi G (1984) Synthetic struvite, $MgNH_4PO_4 \cdot 6H_2O$: correct polarity and surface features of some complementary forms. Acta Crystallogr B40: 223-227

Abrahams SC (1966) Ferromagnetic and crystal structure of ludlamite, $Fe_3(PO_4)_2(H_2O)_4$ at 4.2 K. J Chem Phys 44: 2230-2237

Adiwidjaja G, Friese K, Klaska K-H, Schlueter J (1999) The crystal structure of kastningite $(Fe_{0.5}Mn_{0.5})(H_2O)_4(Al_2(OH)_2(H_2O)_2(PO_4)_2)(H_2O)_2$ a new hydroxyl aquated orthophosphate hydrate mineral. Z Kristallogr 214: 465-468

Alberti A (1976) Crystal structure of ferrisicklerite, $Li_{<1}(Fe^{(3+)}, Mn^{(2+)})PO_4$. Acta Crystallogr B32: 2761-2764

Alkemper J, Fuess H (1998) The crystal structures of $NaMgPO_4$, $Na_2CaMg(PO_4)_2$ and $Na_{18}Ca_{13}Mg_5(PO_4)_{18}$: new examples for glaserite related structures. Z Kristallogr 213: 282-287

Anderson JB, Shoemaker GL, Kostiner E, Ruszala FA (1977) The crystal structure of synthetic $Cu_5(PO_4)_2(OH)_4$, a polymorph of pseudomalachite. Am Mineral 62: 115-121

Ankinovich EA, Bekanova GK, Shabanova TA, Zazubina IS, Sandomirsakaya SM (1997) Mitryaevaite, $Al_{10}[(PO_4)_{8.7}(SO_3OH)_{1.3}]_{\Sigma 10}AlF_3 \cdot 30H_2O$, a new mineral species from a Cambrian carbonaceous chert formation, Karatau Range and Zhabagly Mountains, southern Kazakhstan. Can Mineral 35: 1415-1419

Antenucci D, Fontan F, Fransolet A-M (1989) X-ray powder diffraction data for wolfeite: $(Fe_{0.59}Mn_{0.40}Mg_{0.01})_2PO_4(OH)$. Powder Diffraction 4: 34-35

Araki T, Moore PB (1981) Fillowite, $Na_2Ca(Mn, Fe)_7(PO_4)_6$: its crystal structure. Am Mineral 66: 827-842

Araki T, Zoltai T (1968) The crystal structure of wavellite. Z Kristallogr 127: 21-33

Araki T, Finney JJ, Zoltai T (1968) The crystal structure of augelite. Am Mineral 53: 1096-1103

Arnold H (1986) Crystal structure of $FePO_4$ at 294 and 20 K. Z Kristallogr 177: 139-142

Atencio D (1988) Chernikovite, a new mineral name for $(H_3O)_2(UO_2)_2(PO_4)_2 \cdot 6H_2O$ superseding "hydorgen autunite". Mineral Rec 19: 249-252

Atencio D, Neumann R, Silva AJGC, Mascarenhas YP (1991) Phurcalite from Perus, Sao Paulo, Brazil, and redetermination of its crystal structure. Can Mineral 29: 95-105

Bakakin VV, Rylov GM, Alekseev VI (1974) Refinement of the crystal structure of hurlbutite $CaBe_2P_2O_8$. Kristallografiya 19: 1283-1285 (in Russ)

Bartl H (1989) Water of crystallization and its hydrogen-bonded cross linking in vivianite $Fe_3(PO_4)_2 \cdot 8(H_2O)$; a neutron diffraction investigation. Z Anal Chem 333: 401-403

Baturin SV, Malinovskii YA, Belov NV (1981) The crystal structure of nastrophite $Na(Sr,Ba)(PO_4)(H_2O)_9$. Dokl Akad Nauk SSSR 261: 619-623

Baturin SV, Malinovskii YA, Belov NV (1982) The crystal structure of nabaphite $NaBa(PO_4)(H_2O)_9$. Dokl Akad Nauk SSSR 266: 624-627

Baur WH (1969a) The crystal structure of paravauxite, $FeAl_2(PO_4)_2(OH)_2(OH_2)_6(H_2O)_2$. N Jahrb Mineral Monatsh 430-433

Baur WH (1969b) A comparison of the crystal structures of pseudolaueite and laueite. Am Mineral 54: 1312-1322

Baur WH (1970) Bond length variation and distorted coordination polyhedra in inorganic crystals. Trans Am Crystallogr Assoc. 6: 129-155

Baur WH (1974) The geometry of polyhedral distortions. Predictive relationships for the phosphate group. Acta Crystallogr B30: 1195-1215

Baur WH (1977) Computer simulation of crystal structures. Phys Chem Minerals 2: 3-20

Baur WH, Rama Rao B (1967) The crystal structure of metavauxite. Naturwiss 54: 561

Baur WH, Rama Rao B (1968) The crystal structure and the chemical composition of vauxite. Am Mineral 53: 1025-1028

Ben Amara M, Vlasse M, le Flem G, Hagenmueller P (1983) Structure of the low-temperature variety of calcium sodium orthophosphate, $NaCaPO_4$. Acta Crystallogr C39: 1483-1485

Bernhard F, Walter F, Ettinger K, Taucher J, Mereiter K (1998) Pretulite, $ScPO_4$, a new scandium mineral from the Styrian and lower Austrian lazulite occurrences, Austria. Am Mineral 83: 625-630

Birch WD, Mumme WG, Segnit ER (1988) Ulrichite: A new copper calcium uranium phosphate from Lake Boga, Victoria, Australia. Aust Mineral 3: 125-131

Birch WD, Pring A, Bevan DJM, Kharisun (1994) Wycheproofite: a new hydrated sodium aluminum zirconium phosphate frmom Wycheproof, Victoria,. Australia, and a new occurrence of kosnarite. Mineral Mag 58: 635-639

Birch WD, Pring A, Foord EE (1995) Selwynite, $NaK(Be,Al)Zr_2(PO_4)_4 \cdot 2H_2O$, a new gainesite-like mineral from Wycheproof, Victoria, Australia. Can Mineral 33: 55-58

Birch WD, Pring A, Self PG, Gibbs RB, Keck E, Jensen MC, Foord EE (1996) Meurigite, a new fibrous iron phosphate resembling kidwellite. Mineral Mag 60: 787-793

Birch WD, Pring A, Kolitsch U (1999) Bleasdaleite $(Ca,Fe^{3+})_2Cu_5(Bi,Cu)(PO_4)_4(H_2O,OH,Cl)_{13}$, a new mineral from Lake Boga, Victoria, Australia. Aust J Mineral 5: 69-75

Bjoerling CO, Westgren A (1938) Minerals of the Varutraesk pegmatite. IX. X-ray studies on triphylite, varulite and their oxidation products. Geolog Foereningen Stockholm Foerhandlingar 412

Blanchard F (1981) ICDD Card # 33-0802 (sicklerite)

Blount AM (1974) The crystal structure of crandallite. Am Mineral 59: 41-47

Borodin LS, Kazakova ME (1954) Belovite-(Ce), a new mineral from an alkaline pegmatite. Dokl Akad Nauk SSSR 96:613-616

Bowen NL (1928) The Evolution of Igneous Rocks. Princeton University Press, Princeton, New Jersey

Bragg WL (1930) The structure of silicates. Z Kristallogr 74: 237-305

Bridge PJ, Clark RM (1983) Mundrabillaite, a new cave mineral from Western Australia. Mineral Mag 47: 80-81

Bridge PJ, Robinson BW (1983) Niahite - a new mineral from Malaysia. Mineral Mag 47: 79-80

Britvin SN, Pakhomovskii YA, Bogdanova AN, Skiba VI (1991) Strontiowhitlockite,

$Sr_9Mg(PO_3OH)(PO_4)_6$, a new mineral species from the Kovdor deposit, Kola Peninsula, U.S.S.R. Can Mineral 29: 87-93

Britvin SN, Pakhomovskii YaA, Bogdanova AN, Khomyakov AP, Krasnova NI (1995) Rimkorolgite $(Mg,Mn)_5(Ba,Sr,Ca)(PO_4)_4 \cdot 8H_2O$ - a new mineral from Kovdor iron deposit, Kola Peninsula. Zap Vser Mineral Obshch 124: 90-95 (in Russian)

Britvin SN, Pakhomovskii YaA, Bogdanova AN (1996) Krasnovite $Ba(Al,Mg)(PO_4,CO_3)(OH)_2 \cdot H_2O$ - a new mineral. Zap Vser Mineral Obshch 125: 110-112

Brotherton PD, Maslen EN, Pryce MW, White AH (1974) Crystal structure of collinsite. Aust J Chem 27: 653-656

Brown ID (1981) The bond-valence method: an empirical approach to chemical structure and bonding. *In* Structure and Bonding in Crystals. O'Keeffe M, Navrotsky A (Eds). Academic Press, New York, 2: 1-30

Brown ID, Shannon RD (1973) Empirical bond strength – bond length curves for oxides. Acta Crystallogr A29: 266-282

Brownfield ME, Foord EE, Sutley SJ, Bottinelly T (1993) Kosnarite, $KZr_2(PO_4)_3$, a new mineral from Mount Mica and Black Mountain, Oxford County, Maine. Am Mineral 78: 653-656

Buchwald VF (1990) A new mineral, arupite, $Ni_3(PO_4)_2 \cdot 8H_2O$, the nickel analogue of vivianite. N Jahrb Mineral Monatsh 76-80

Buck HM, Cooper MA, Černý P, Grice JD, Hawthorne FC (1999) Xenotime-(Yb), $YbPO_4$, a new mineral species from the Shatford Lake pegmatite group, southeastern Manitoba. Can Mineral 37: 1303-1306

Burdett JK, Hawthorne FC (1993) An orbital approach to the theory of bond valence. Am Mineral 78: 884-892

Burns PC (1999) The crystal chemistry of uranium. Rev Mineral 38: 23-91

Burns PC (2000) A new uranyl phosphate chain in the structure of parsonite. Am Mineral 85: 801-805

Burns PC, Hawthorne FC (1995) The crystal structure of sinkankasite, a complex heteropolyhedral sheet mineral. Am Mineral 80: 620-627

Cahill CL, Krivovichev SV, Burns PC, Bekenova GK, Shabanova TA (2001) The crystal structure of mitryaevaite, $Al_5(PO_4)_2[(P,S)O_3(OH,O)]_2F_2(OH)_2(H_2O)_8 \cdot 6.48H_2O$, determined from a microcrystal using synchrotron radiation. Can Mineral 39: 179-186

Calvo C (1968) The crystal structure of graftonite. Am Mineral 53: 742-750

Carling SG, Day P, Visser D (1995) Crystal and magnetic structures of layer transition metal phosphate hydrates. Inorg Chem 34: 3917-3927

Catti M, Franchini-Angela M (1976) Hydrogen bonding in the crystalline state. Structure of $Mg_3(NH_4)_2(HPO_4)_4(H_2O)_8$ (hannayite), and crystal-chemical relationships with schertelite and struvite. Acta Crystallogr B32: 2842-2848

Catti M, Ferraris G, Filhol A (1977a) Hydrogen bonding in the crystalline state. $CaHPO_4$ (monetite), P$\bar{1}$ or P1 ? A novel neutron diffraction study. Acta Crystallogr B33: 1223-1229

Catti M, Ferraris G, Franchini-Angela M (1977b) The crystal structure of $Na_2HPO_4(H_2O)_2$. Competition between coordination and hydrogen bonds. Acta Crystallogr B33: 3449-

3452

Catti M, Ferraris G, Ivaldi G (1977c) Hydrogen bondng in the crystalline state. Structure of talmessite, $Ca_2(Mg,Co)(AsO_4)_2{\cdot}2H_2O$, and crystal chemistry of related minerals. Bull Minéral 100: 230-236

Catti M, Ferraris G, Ivaldi G (1979) Refinement of the crystal structure of anapaite, $Ca_2Fe(PO_4)_2(H_2O)_4$. Hydrogen bonding and relationships with the bihydrated phase. Bull Minéral 102: 314-318

Cavellec M, Riou D, Ferey G (1994) Synthetic spheniscidite. Acta Crystallogr C50: 1379-1381

Cech F, Povondra P (1979) A re-examination of bořickýite. Tschermaks Mineral Petrogr Mitt 26: 79-86

Chao GY (1969) Refinement of the crystal structure of parahopeite. Z Kristallogr 130: 261-266

Chen Z, Huang Y, Gu X (1990) A new uranium mineral-yingjiangite. Acta Mineral Sinica 10: 102-105

Chernorukov N, Karyakin N, Suleimanov E, Belova Yu, Russ J (1997) ICDD Card # 50-1561 (uranocircite)

Chopin C, Brunet F, Gebert W, Medenbach O, Tillmanns E (1993) Bearthite, $Ca_2Al(PO_4)_2(OH)$, a new mineral from high-pressure terranes of the western Alps. Schweiz Mineral Petrogr Mitt 73: 1-9

Chopin C, Ferraris G, Prencipe M, Brunet F, Medenbach O (2001): Raadeite, $Mg_7(PO_4)_2(OH)_8$: a new dense-packed phosphate from Modum (Norway). Eur J Mineral 13: 319-327

Cid-Dresdner H (1965) Determination and refinement of the crystal structure of turquois, $CuAl_6(PO_4)(OH)_8(H_2O)_4$. Z Kristallogr 121: 87-113

Cipriani C, Mellini M, Pratesi G, Viti C (1997) Rodolicoite and grattarolaite, two new phosphate minerals from Santa Barbara mine, Italy. Eur J Mineral 9: 1101-1106

Clark AM, Couper AG, Embrey PG, Fejer EE (1986) Waylandite: New data, from an occurrence in Cornwall, with a note on "agnesite". Mineral Mag 50: 731-733

Cocco G, Fanfani L, Zanzzi PF (1966) The crystal structure of tarbuttite, $Zn_2(OH)PO_4$. Z Kristallogr 123: 321-329

Coda A, Guiseppetti G, Tadini C, Carobbi SG (1967) The crystal structure of wagnerite. Atti Accad Naz Lincei 43: 212-224

Coleman LC, Robertson BT (1981) Nahpoite, Na_2HPO_4, a new mineral from the Big Fish River area, Yukon Territory. Can Mineral 19: 373-376

Cooper M, Hawthorne FC (1994a) Refinement of the crystal structure of kulanite. Can Mineral 32: 15-19

Cooper M, Hawthorne FC (1994b) The crystal structure of curetonite, a complex heteropolyhedral sheet mineral. Am Mineral 79: 545-549

Cooper MA, Hawthorne FC (1999) The crystal structure of wooldridgeite, $Na_2CaCu^{(2+)}_2(P_2O_7)_2(H_2O)_{10}$, a novel copper pyrophosphate mineral. Can Mineral 37: 73-81

Cooper MA, Hawthorne FC, Černý P (2000) Refinement of the crystal structure of cyrilovite from Cyrilov, Western Moravia, Czech Republic. J Czech Geol Soc 45: 95-100

Corbin DR, Abrams L, Jones GA, Harlow RL, Dunn PJ (1991) Flexibility of the zeolite RHO framework: effect of dehydration on the crystal structure of the beryllophosphate mineral, pahasapaite. Zeolites 11: 364-367

Corbridge DEC (1985) Phosphorous. An outline of its chemistry, biochemistry and technology (3rd ed). Elsevier, Amsterdam

Cozzupoli D, Grubessi O, Mottan A, Zanazzi PF (1987) Cyrilovite from Italy: Structure and crystal chemistry. Mineral Petrol 37: 1-14

Curry NA, Jones DW (1971) Crystal structure of brushite, calcium hydrogen orthophosphate dihydrate: A neutron-diffraction investigation. J Chem Soc 3725-3729

Dai Y, Hughes JM (1989) Crystal-structure refinements of vanadinite and pyromorphite. Can Mineral 27: 189-192

de Bruiyn H, Beukes GJ, van der Westhuizen WA, Tordiffe EAW (1989) Unit cell dimensions of the hydrated aluminium phosphate-sulphate minerals sanjuanite, kribergite and hotsonite. Mineral Mag 53: 385-386

Deer WA, Howie RA, Zussman J (1992) An Introduction to the Rock-Forming Minerals. 2nd Edition. Longman Group UK Limited, Harlow, England

Deliens M, Piret P (1981) Les phosphates d'uranyle et d'aluminum de Kobokobo. V. La mundite, nouveau mineral. Bull Minéral 104: 669-671

Deliens M, Piret P (1982) Les phosphates d'uranyle et d'aluminum de Kobokobo. VI. La triangulite, $Al_3(OH)_5[(UO_2)(PO_4)]_4(H_2O)_5$, nouveau mineral. Bull Minéral 105: 611-614

Deliens M, Piret P (1985) Les phosphates d'uranyle et d'aluminum de Kobokobo. V. La moreauite, $Al_3UO_2(PO_4)_3(OH)_2{\cdot}13H_2O$, nouveau mineral. Bull Minéral 108: 9-13

Demartin F, Diella V, Donzelli S, Gramaccioli CM, Pilati T (1991) The importance of accurate crystal structure determination of uranium minerals. I. Phosphuranylite $KCa(H_3O)_3(UO_2)_7(PO_4)_4O_{4.8}H_2O$. Acta Crystallogr B47: 439-446

Demartin F, Pilati T, Gay DD, Gramaccioli CM (1993) The crystal structure of a mineral related to paulkerrite. Z Kristallogr 208: 57-71

Demartin F, Gramaccioli CM, Pilati T, Sciesa E (1996) Sigismundite, $(Ba,K,Pb)Na_3(Ca,Sr)(Fe,Mg,Mn)_{14}Al(OH)_2(PO_4)_{12}$, a new Ba-rich member of the arrojadite group from Spluga Valley, Italy. Can Mineral 34: 827-834

Demartin F, Gay HD, Gramaccioli CM, Pilati T (1997) Benyacarite, a new titanium-bearing phosphate mineral species from Cerro Blanco, Argentina. Can Mineral 35: 707-712

Dempsey MJ, Strens RGJ (1976) Modelling crystal structures. *In* Strens RGJ (Ed) Physics and Chemistry of Rocks and Minerals. Wiley, New York.

Di Cossato YMF, Orlandi P, Pasero M (1989a) Manganese-bearing beraunite from Mangualde, Portugal: Mineral data and structure refinement. Can Mineral 27: 441-446

Di Cossato YMF, Orlandi P, Vezzalini G (1989b) Rittmanite, a new mineral species of the whiteite group from the Mangualde granitic pegmatite, Portugal. Can Mineral 27: 447-449

Dick S (1999) Ueber die Struktur von synthetischem Tinsleyit $K(Al_2(PO_4)_2(OH)(H_2O)) \cdot (H_2O)$. Z Naturforsch Anorg Chem Org Chem 54: 1358-1390

Dick S, Zeiske T (1997) Leucophosphite $K(Fe_2(PO_4)_2(OH)(H_2O)).(H_2O)$; hydrogen bonding and

structural relationships. J Solid State Chem 133: 508-515

Dick S, Zeiske T (1998) Francoanellit $K_3Al_5(HPO_4)_6(PO_4)_2 \cdot 12H_2O$: Struktur und Synthese durch topochemische Entwaesserung von Taranakit. Z Naturforsch Anorg Chem Org Chem 53: 711-719

Dick S, Gossner U, Weis A, Robl C, Grossmann G, Ohms G, Zeiske T (1998) Taranakite - the mineral with the longest crystallographic axis. Inorg Chim Acta 269: 47-57

Dickens B, Brown WE (1971) The crystal structure of $Ca_7Mg_9(Ca, Mg)_2(PO_4)_{12}$. Tschermaks Mineral Petrogr Mitt 16: 79-104

Dooley JR Jr, Hathaway JC (1961) Two occurrences of thorium-bearing minerals with rhabdophane-like structure. US Geol Surv Prof Paper 424C: 339

Dormann J, Gasperin M, Poullen JF (1982) Etude structurale de la sequence d'oxydation de la vivianite $Fe_3(PO_4)_2(H_2O)_8$. Bull Minéral 105: 147-160

Dunn PJ, Rouse RC, Campbell TJ, Roberts WL (1984a) Tinsleyite, the aluminous analogue of leucophosphite, from the Tip Top pegmatite in South Dakota. Am Mineral 69: 374-376

Dunn PJ, Rouse RC, Nelen JA (1984b) Englishite: new chemical data and a second occurrence, from the Tip Top pegmatite, Custer, South Dakota. Can Mineral 22: 469-470

Dunn PJ, Peacor DR, Sturman DB, Ramik RA, Roberts WL, Nelen JA (1986) Johnwalkite, the Mn-analogue of olmsteadite, from South Dakota. N. Jahrb Mineral Monatsh 115-120

Eby RK, Hawthorne FC (1989) Cornetite: Modulated densely-packed Cu^{2+} oxysalt. Mineral Petrol 40: 127-136

Effenberger H, Mereiter K, Pimminger M, Zemann J (1982) Machatschkiite: Crystal structure and revision of the chemical formula. Tschermaks Mineral Petrogr Mitt 30: 145-155

Effenberger H, Krause W, Belendorff K, Bernhardt H–J, Medenbach O, Hybler J, Petricek V (1994) Revision of the crystal structure of mrazekite, $Bi_2Cu_3(OH)_2O_2(PO_4)_{2.2}(H_2O)$. Can Mineral 32: 365-372

Egorov BL, Dara AD, Senderova VM (1969) Melkovite, a new phosphate-molybdate from the zone of oxidation. Zap Vses Mineral Obshch 98: 207-212 (in Russian)

Ercit TS (1991) The crystal structure of nalipoite. Can Mineral 29: 569-573

Ercit TS, Hawthorne FC, Cerny P (1986a) The crystal structure of bobfergusonite. Can Mineral 24:605-614

Ercit TS, Anderson AJ, Cerny P, Hawthorne FC (1986b) Bobfergusonite, a new primary phosphate mineral from Cross Lake, Manitoba. Can Mineral 24:599-604

Ercit TS, Cooper MA, Hawthorne FC (1998) The crystal structure of vuonnemite, $Na_{11}Ti^{(4+)}Nb_2(Si_2O_7)_2(PO_4)_2O_3(F, OH)$, a phosphate-bearing sorosilicate of the lomonosovite group. Can Mineral 36: 1311-1320

Eventoff W, Martin R, Peacor DR (1972) The crystal structure of heterosite. Am Mineral 57: 45-51

Eversheim VP, Kleber W (1953) Morphologie und Struktur des Reddingits, $P_2O_5 \cdot 3FeO \cdot 3H_2O$. Acta Crystallogr 6: 215-216

Fanfani L, Zanazzi PF (1966) La struttura cristallina della metastrengite. Atti Accad Naz Lincei Serie 8 40: 889.

Fanfani L, Zanazzi PF (1967a) The crystal structure of beraunite. Acta Crystallogr 22: 173-181

Fanfani L, Zanazzi PF (1967b) Structural similarities of some secondary lead minerals. Mineral Mag 36: 522-529

Fanfani L, Zanazzi PF (1968) The crystal structure of vauquelinite and the relationships to fornacite. Z Kristallogr 126: 433-443

Fanfani L, Zanazzi PF (1979) Switzerite: its chemical formula and crystal structure. Tschermaks Mineral Petrogr Mitt 26: 255-269

Fanfani L, Nunzi A, Zanazzi PF (1970a) The crystal structure of wardite. Mineral Mag 37: 598-605

Fanfani L, Nunzi A, Zanazzi PF (1970b) The crystal structure of fairfieldite. Acta Crystallogr B26: 640-645

Fanfani L, Nunzi A, Zanazzi PF (1972) Structure and twinninq in spencerite. Mineral Mag 38: 687-692

Fanfani L, Nunzi A, Zanazzi PF, Zanzari AR (1975) The crystal structure of roscherite. Tschermaks Mineral Petrogr Mitt 22: 266-277

Fanfani L, Nunzi A, Zanazzi PF, Zanzari AR (1976) Additional data on the crystal structure of montgomeryite. Am Mineral 61: 12-14

Fanfani L, Zanazzi PF, Zanzari AR (1977) The crystal structure of a triclinic roscherite. Tschermaks Mineral Petrogr Mitt 24: 169-178

Fanfani L, Tomassini M, Zanazzi PF, Zanzari AR (1978) The crystal structure of strunzite, a contribution to the crystal chemistry of basic ferric-manganous hydrated phosphates. Tschermaks Mineral Petrogr Mitt 25: 77-87

Ferraris G, Franchini-Angela M (1973) Hydrogen bonding in the crystalline state. Crystal structure of $MgHAsO_4 \cdot 7H_2O$, rosslerite. Acta Crystallogr B29: 286-292

Ferraris G, Franchini-Angela M (1974) Hydrogen bonding in the crystalline state. Crystal structure and twinning of $NaNH_4HPO_4(H_2O)_4$ (stercorite). Acta Crystallogr B30: 504-510

Ferraris G, Fuess H, Joswig W (1986) Neutron diffraction study of $MgNH_4PO_4(H_2O)_6$ (struvite) and survey of water molecules donating short hydrogen bonds. Acta Crystallogr B42: 253-258

Fisher DJ (1956) Hagendorfite unit cell. Geol Soc Am Bull 67: 1694-1695

Fisher DJ (1965) Dickinsonites, fillowite and alluaudites. Am Mineral 50: 1647-1669

Fisher FG, Meyrowitz R (1962) Brockite, a new calcium thorium phosphate from the Wet Mountains, Colorado. Am Mineral 47: 1346-1355

Fitch AN, Cole M (1991) The structure of $KUO_2PO_{4.3}D_2O$ refined from neutron and synchrotron-radiation powder diffraction data. Material Res Bull 26: 407-414

Fitch AN, Fender BEF (1983) The structure of deuterated ammonium uranyl phosphate trihydrate, $ND_4UO_2PO_4(D_2O)_3$ by powder neutron diffraction. Acta Crystallogr C39: 162-166

Flachsbart I (1963) Zur Kristallstruktur von Phosphoferrit (Fe, Mn)$_3$(PO$_4$)$_2$(H$_2$O)$_3$. Z Kristallogr 118: 327-331

Fontan F, Pillard F, Permingeat F (1982) Natrodufrenite (Na,Fe^{3+},Fe^{2+})(Fe^{3+},Al)$_5$(PO$_4$)$_4$(OH)$_6$·2(H$_2$O), a new mineral species of the dufrenite group. Bull Mineral 105: 321 -326

Foord EE, Taggart JE Jr (1998) A reexamination of the turquoise group, the mineral aheylite, planerite (redefined), turquoise and coeruleolactite. Mineral Mag 62: 93-111

Foord EE, Brownfield ME, Lichte FE, Davis AM, Sutley SJ (1994) McCrillisite, NaCs(Be,Li)Zr$_2$(PO$_4$)$_4$·1–2H$_2$O, a new mineral species from Mount Mica, Oxford County, Maine, and new data for gainesite. Can Mineral 32: 839-842

Fransolet A-M (1989) The problem of Na-Li substitution in primary Li-Al phosphates: New data on lacroixite, a relatively widespread mineral. Can Mineral 27: 211-217

Fransolet A-M (1995) Wyllieite et rosemaryite dans la pegmatite de Buranga, Rwanda. Eur J Mineral 7: 567-575

Fransolet A-M, Cooper MA, Černý P, Hawthorne FC, Chapman R, Grice JD (2000) The Tanco pegmatite at Bernic Lake, southeastern Manitoba. XV. Ercitite, NaMn^{3+}PO$_4$(OH)(H$_2$O)$_2$, a new phosphate mineral species. Can Mineral 38: 893-898

Freeman K, Bayliss P (1991) ICDD card # 44-1429 (natromontebrasite)

Frondel C, Riska DD, Frondel JW (1956) X-ray powder data for uranium and thorium minerals. US Geol Surv Bull B 1036-G: 91-153

Galliski MA, Cooper MA, Hawthorne FC, Cerny P (1999) Bederite, a new pegmatite phosphate mineral from Nevados de Palermo, Argentina: description and crystal structure. Am Mineral 84: 1674-1679

Galliski MA, Hawthorne FC, Cooper MA (2001) Refinement of the crystal structure of ushkovite from Nevados de Palermo, Republica Argentina. Can Mineral (accepted)

García-Guinea J, Chagoyen AM, Nickel EH (1995) A re-investigation of bolivarite and evansite. Can Mineral 33: 59-65

Gatehouse BM, Miskin BK (1974) The crystal structure of brazilianite, NaAl$_3$(PO$_4$)$_2$(OH)$_4$. Acta Crystallogr B30: 1311-1317

Geller S, Durand JL (1960) Refinement of the structure of LiMnPO$_4$. Acta Crystallogr 13: 325-331

Genkina EA, Khomyakov AP (1992) Refinement of the structure of natural sodiumphosphate. Kristallografiya 37: 1559-1560

Genkina EA, Kabalov Yu K, Maksimov BA, Mel'nikov OK (1984) The crystal structure of synthetic tavorite LiFe(PO$_4$)(OH,F). Kristallografiya 29: 50-55

Genkina EA, Maksimov BA, Melnikov OK (1985) Crystal structure of synthetic tarbuttite Zn$_2$(PO$_4$)(OH). Dokl Akad Nauk SSSR 282: 314-317

Gheith MA (1953) Lipscombite: a new synthetic iron lazulite. Am Mineral 38: 612-628

Ghose S, Leo SR, Wan C (1974) Structural chemistry of copper and zinc minerals. Part I. Veszelyite, (Cu$_{0.5}$Zn$_{0.5}$)$_2$ZnPO$_4$NOH)$_3$(H$_2$O)$_3$: a novel type of sheet structure and crystal chemistry of copper-zinc substitution. Am Mineral 59: 573-581

Giuseppetti G, Tadini C (1973) Refinement of the crystal structure of beryllonite, $NaBePO_4$. Tschermaks Mineral Petrogr Mitt 20: 1-12

Giuseppetti G, Tadini C (1983) Lazulite, (Mg,Fe) $Al_2(OH)_2(PO_4)_2$: structure refinement and hydrogen bonding. N Jahrb Mineral Monatsh 410-416

Giuseppetti G, Tadini C (1984) The crystal structure of childrenite from Tavistock (SW England), $Ch_{89}Eo_{11}$ term of childrenite-eosphorite series. N Jahrb Mineral Monatsh 263-271

Giusepetti G, Tadini C (1987) Corkite, $PbFe_3(SO_4)(PO_4)(OH)_6$, its crystal structure and ordered arrangement of the tetrahedral cations. N Jahrb Mineral Monatsh 71-81

Giuseppetti G, Mazzi F, Tadini C (1989) The crystal structure of chalcosiderite $CuFe_6(PO_4)_4(OH)_8(H_2O)_4$. N Jahrb Mineral Monatsh 227-239

Gopal R, Calvo C, Ito J, Sabine WK (1974) Crystal structure of synthetic Mg-whitlockite, $Ca_{18}Mg_2H_2(PO_4)_{14}$. Can J Chem 52: 1152-1164

Grice JD, Dunn PJ (1992) Attakolite new data and crystal-structure determination. Am Mineral 77: 1285-1291

Grice JD, Groat LA (1988) Crystal structure of paulkellerite. Am Mineral 73: 873-875

Grice JD, Roberts AC (1993) Harrisonite, a well-ordered silico-phosphate with a layered crystal structure. Can Mineral 31: 781-785

Grice JD, Peacor DR, Robinson GW, van Velthuizen J, Roberts WL, Campbell TJ, Dunn PJ (1985) Tiptopite (Li,K,Na,Ca,□)$_8Be_6(PO_4)_6(OH)_4$, a new mineral species from the Black Hills, South Dakota. Can Mineral 23: 43-46

Grice JD, Dunn PJ, Ramik RA (1989) Whiteite-(CaMnMg), a new mineral species from the Tip Top pegmatite, Custer, South Dakota. Can Mineral 27: 699-702

Grice JD, Dunn PJ, Ramik RA (1990) Jahnsite-(CaMnMn), a new member of the whiteite group from Mangualde, Beira, Portugal. Am Mineral 75: 401-404

Griffen DT, Ribbe PH (1979) Distortions in the tetrahedral oxyanions of crystalline substances. N Jahrb Mineral Abh 137: 54-73

Groat LA, Hawthorne FC (1990) The crystal structure of nissonite. Am Mineral 75: 1170-1175

Groat LA, Raudsepp M, Hawthorne FC, Ercit TS, Sherriff BL, Hartman JS (1990) The amblygonite-montebrasite series: characterization by single-crystal structure refinement, infrared spectroscopy and multinuclear MAS-NMR spectroscopy. Am Mineral 75: 992-1008

Guy BB, Jeffrey GA (1966) The crystal structure of fluellite, $Al_2PO_4F_2(OH)(H_2O)_7$. Am Mineral 51: 1579-1592

Hanson AW (1960) The crystal structure of eosphorite. Acta Crystallogr 13: 384-387

Harrowfield IR, Segnit ER, Watts JA (1981) Aldermanite, a new magnesium aluminum phosphate. Mineral Mag 44: 59-62

Hata M, Marumo F, Iwai SI (1979) Structure of barium chlorapatite. Acta Crystallogr B35: 2382-2384

Hawthorne FC (1976) Refinement of the crystal structure of adamite. Can Mineral 14: 143-148

Hawthorne FC (1979a) The crystal structure of morinite. Can Mineral 17: 93-102

Hawthorne FC (1979b) Paradamite. Acta Crystallogr B35: 720-722

Hawthorne FC (1982) The crystal structure of bøggildite. Can Mineral 20: 263-270

Hawthorne FC (1983a) Enumeration of polyhedral clusters. Acta Crystallogr A39: 724-736

Hawthorne FC (1983b) The crystal structure of tancoite. Tschermaks Mineral Petrogr Mitt 31: 121-135

Hawthorne FC (1984) The crystal structure of stenonite and the classification of the aluminofluoride minerals. Can Mineral 22: 245-251

Hawthorne FC (1985a) Towards a structural classification of minerals: the $^{VI}M^{IV}T_2O_n$ minerals. Am Mineral 70: 455-473

Hawthorne FC (1985b) Refinement of the crystal structure of bloedite: structural similarities in the $[^{VI}M(^{IV}T\phi_4)_2\phi_n]$ finite-cluster minerals. Can Mineral 23: 669-674

Hawthorne FC (1988) Sigloite: The oxidation mechanism in $[(M_2^{3+}(PO_4)_2(OH)_2(H_2O)_2)]^{2-}$ structures. Mineral Petrol 38: 201-211

Hawthorne FC (1990) Structural hierarchy in $M^{[6]}T^{[4]}\Phi_n$ minerals. Z Kristallogr 192: 1-52

Hawthorne FC (1992) The role of OH and H_2O in oxide and oxysalt minerals. Z Kristallogr 201: 183-206

Hawthorne FC (1993) Minerals, Mineralogy and Mineralogists: Past, Present and Future. Can Mineral 31: 253-296

Hawthorne FC (1994) Structural aspects of oxide and oxysalt crystals. Acta Crystallogr B50: 481-510

Hawthorne FC (1997) Structural aspects of oxide and oxysalt minerals. *In* European Mineralogical Union Notes in Mineralogy, Vol.1, "Modular Aspects of Minerals". Merlino S (Ed). Eötvös University Press, 373-429

Hawthorne FC (1998) Structure and chemistry of phosphate minerals. Mineral Mag 62: 141-164

Hawthorne FC (2002) The use of end-member charge-arrangements in defining new minerals and heterovalent substitutions in complex minerals. Can Mineral (accepted)

Hawthorne FC, Ferguson RB (1975) Anhydrous sulphates. II Refinement of the crystal structure of anhydrite. Can Mineral 13: 289-292

Hawthorne FC, Grice JD (1987) The crystal structure of ehrleite, a tetrahedral sheet structure. Can Mineral 25: 767-774

Hawthorne FC, Schindler MS (2000) Topological enumeration of decorated $[Cu^{2+}\phi_2]_N$ sheets in hydroxy-hydrated copper-oxysalt minerals. Can Mineral 38: 751-761

Hawthorne FC, Sokolova EV (2002) Simonkolleite, $Zn_5(OH)_8Cl_2(H_2O)$, a decorated interrupted-sheet structure of the form $[M\phi_2]_4$. Can Mineral (submitted)

Hawthorne FC, Groat LA, Raudsepp M, Ercit TS (1987) Kieserite, a titanite-group mineral. N Jahrb Mineral Abh 157: 121-132

Hawthorne FC, Cooper MA, Green DI, Starkey RE, Roberts AC, Grice JD (1999) Wooldridgeite, $Na_2CaCu^{2+}{}_2(P_2O_7)_2(H_2O)_{10}$: a new mineral from Judkins quarry, Warwickshire, England. Mineral Mag 63: 13-16

Hawthorne FC, Krivovichev SV, Burns PC (2000) The crystal chemistry of sulfate minerals. Rev

Mineral 40: 1-112

Hey MH, Milton C, Dwornik WJ (1982) Eggonite (kolbeckite, sterrettite), $ScPO_4 \cdot 2H_2O$. Mineral Mag 46: 493-497

Hill RG (1977) The crystal structure of phosphophyllite. Am Mineral 63: 812-817

Hill RG, Jones JB (1976) The crystal structure of hopeite. Am Mineral 61: 987-995

Hoyos MA, Calderon T, Vergara I, Garcia-Sole J (1993) New structural and spectroscopic data for eosphorite. Mineral Mag 57: 329-336

Hughes JM, Drexler JW (1991) Cation substitution in the apatite tetrahedral site: crystal structures of type hydroxylellestadtite and type fermorite. N Jahrb Mineral Monatsh 327-336

Hughes JM, Cameron M, Crowley KD (1990) Crystal structures of natural ternary apatites: solid solution in the $Ca_5(PO_4)_3X$ (X= F, OH, Cl) system. Am Mineral 75: 295-304

Hughes JM, Foord EE, Hubbard MA, Ni YX (1995) The crystal structure of cheralite - (Ce), (LREE, Ca, Th, U)(P, Si)O_4, a monazite-group mineral. N Jahrb Mineral Monatsh 344-350

Huminicki DMC, Hawthorne FC (2000) Refinement of the crystal structure of väyrynenite. Can Mineral 38: 1425-1432

Huminicki DMC, Hawthorne FC (2002) Hydrogen bonding in the crystal structure of seamanite. Can Mineral (submitted)

Huminicki DMC, Hawthorne FC (2002) The crystal chemistry of the phosphate minerals.Rev Mineral (accepted)

Hurlbut CS (1942) Sampleite, a new mineral from Chuquicamata, Chile. Am Mineral 27: 586-589

Ilyukhin AB, Katser SB, Levin AA (1995) Structure refinement of two crystals from the KDP family $(ND_4)D_2PO_4$ and KH_2AsO_4 in the paraphase. Z Neorg Khim 40: 1599-1600

Isaaks AM, Peacor DR (1981) Panasquieratite, a new mineral: The OH-equivalent of isokite. Can Mineral 19: 389-392

Isaaks AM, Peacor DR (1982) The crystal structure of thadeuite, Mg(Ca,Mn)(Mg, Fe, $Mn)_2(PO_4)_2(OH, F)_2$. Am Mineral 67: 120-125

Johan Z, Slansky E, Povondra P (1983) Vashegyite, a sheet aluminum phosphate: new data. Can Mineral 21: 489-498

Kabalov YuK, Sokolova EV, Pekov IV (1997) Crystal structure of belovite-(La). Phys Dokl 42: 344-348

Kampf AR (1977a) Schoonerite: its atomic arrangement. Am Mineral 62: 250-255

Kampf AR (1977b) Minyulite : its atomic arrangement. Am Mineral 62: 256-262

Kampf AR (1977c) A new mineral: perloffite, the Fe^{3+} analogue of bjarebyite. Mineral Rec 8: 112-114

Kampf AR (1992) Beryllophosphate chains in the structures of fransoletite, parafransoletite, and ehrleite and some general comments on beryllophosphate linkages. Am Mineral 77: 848-856

Kampf AR, Moore PB (1976) The crystal structure of bermanite, a hydrated manganese phosphate. Am Mineral 61: 1241-1248

Kampf AR, Moore PB (1977) Melonjosephite, calcium iron hydroxy phosphate: its crystal structure. Am Mineral 62: 60-66

Kampf AR, Dunn PJ, Foord EE (1992) Parafransoletite, a new dimorph of fransoletite from the Tip Top Pegmatite, Custer, South Dakota. Am Mineral 77: 843-847

Kato T (1970) Cell dimensions of the hydrated phosphate, kingite. Am Mineral 55: 515-517

Kato T (1971) The crystal structures of goyazite and woodhouseite. N Jahrb Mineral Monatsh 241-247

Kato T (1987) Further refinement of the goyazite structure. Mineral J 13: 390-396

Kato T (1990) The crystal structure of florencite. N Jahrb Mineral Monatsh 227-231

Kato T, Miura Y (1977) The crystal structures of jarosite and svanbergite. Mineral J 8: 418-430

Katz L, Lipscomb WN (1951) The crystal structure of iron lazulite, a synthetic mineral related to lazulite. Acta Crystallogr 4: 345-348

Keegan TD, Araki T, Moore PB (1979) Senegalite, $Al_2(OH)_3(H_2O)(PO_4)$, a novel structure type. Am Mineral 64: 1243-1247

Keller P, Fontan F, Velasco Roldan F, Melgarejo I Draper JC (1997) Staněkite, $Fe^{3+}(Mn,Fe^{2+},Mg)(PO_4)O$: a new phosphate mineral in pegmatites at Karibib (Namibia) and French Pyrénées (France). Eur J Mineral 9: 475-482

Khan AA, Baur WH (1972) Salt hydrates. VIII. The crystal structures of sodium ammonium orthochromate dihydrate and magnesium diammonium bis(hydrogen ortho phosphate) tetrahydrate and a discussion of the ammonium ion. Acta Crystallogr B28: 683-693

Khan AA, Roux JP, James WJ (1972) The crystal structure of diammonium hydrogen phosphate, $(NH_4)_2HPO_4$. Acta Crystallogr B28: 2065-2069

Kharisun, Taylor MR, Bevan DJM, Pring A (1997) The crystal structure of kintoreite, $PbFe_3(PO_4)_2(OH,H_2O)_6$. Mineral Mag 61: 123-129

Khomyakov AP, Aleksandrov VV, Krasnova NI, Ermilov VV, Smolyaninova (1982) Bonshtedtite, $Na_3Fe(PO_4)(CO_3)$, a new mineral. Zap Vses Mineral Obshch 111: 486-490 (in Russian)

Khomyakov AP, Polezhaeva LI, Sokolova EV (1994) Crawfordite $Na_3Sr(PO_4)(CO_3)$-a new mineral from the bradleyite. Zap Vser Mineral Obshch 123: 107-111

Khomyakov AP, Lisitsin DV, Kulikova IM, Rastsvetsaeva RK (1996) Deloneite-(Ce) $NaCa_2SrCe(PO_4)_3F$ - a new mineral with a belovite-like structure. Zap Vser Mineral Obshch 125: 83-94 (in Russian)

Khomyakov AP, Kulikova IM, Rastsvetaeva RK (1997) Fluorcaphite $Ca(Sr,Na,Ca)(Ca,Sr,Ce)_3(PO_4)_3F$ - a new mineral with the apatite structural motif. Zap Vser Mineral Obshch 126: 87-97

Khosrawan-Sazedj F (1982a) The crystal structure of meta-uranocircite II, $Ba(UO_2)_2(PO_4)_2(H_2O)_6$. Tschermaks Mineral Petrogr Mitt 29: 193-204

Khosrawan-Sazedj F (1982b) On the space group of threadgoldite. Tschermaks Mineral Petrogr Mitt 30: 111-115

Kim Y, Kirkpatrick RJ (1996) Application of MAS NMR spectroscopy to poorly crystalline materials: viséite. Mineral Mag 60:957-962

King GSD, Sengier Roberts L (1988) Drugmanite, $Pb_2(Fe_{0.78}Al_{0.22})H(PO_4)_2(OH)_2$: Its crystal structure and place in the datolite group. Bull Minéral 111: 431-437

Klein C, Hurlbut CS Jr. (1985) Manual of Mineralogy. John Wiley & Sons, Inc., New York.

Klevtsova RF (1964) About the crystal structure of strontiumapatite. Z Strukt Khim 5: 318-320

Kniep R, Mootz D (1973) Metavariscite - a redetermination of its crystal structure. Acta Crystallogr B29: 2292-2294

Kniep R, Mootz D, Vegas A (1977) Variscite. Acta Crystallogr B33: 263-265

Kohlmann M, Sowa H, Reithmayer K, Schulz H, Krueger R–R, Abriel W (1994) Structure of $[Y_{(1-x)}(Gd,Dy,Er)_x]PO_4 \cdot 2H_2O$ microcrystal using synchrotron radiation. Acta Crystallogr C50: 1651-1652

Kolitsch U, Giester G (2000) The crystal structure of faustite and its copper analogue turquoise. Mineral Mag 64: 905-913

Kolitsch U, Taylor MR, Fallon GD, Pring A (1999a) Springcreekite, $BaV^{3+}_3(PO_4)_2(OH,H_2O)_6$, a new member of the crandalite group, from the Spring Creek mine, South Australia: the first natural V^{3+}-member of the alunite family and its crystal structure. N Jahrb Mineral Monatsh 529-544

Kolitsch U, Tiekink ERT, Slade PG, Taylor MR, Pring A (1999b) Hinsdalite and plumbogummite, their atomic arrangements and disordered lead sites. Eur J Mineral 11: 513-520

Kolitsch U, Pring A, Tiekink ERT (2000) Johntomaite, a new member of the bjarebyite group of barium phosphates: description and structure refinement. Mineral Petrol 70: 1-14

Kolkovski B (1971) ICDD card # 29-0756 (orpheite)

Khomyakov AP, Nechelyustov GN, Sokolova EV, Dorokhova GI (1992) Quadruphite, $Na_{14}CaMgTi_4[Si_2O_7]_2[PO_4]_4O_4F_2$ and polyphite $Na_{17}Ca_3Mg(Ti,Mn)_4[Si_2O_7]_2[PO_4]_6O_2F_6$ - new minerals of the lomonovosite family. Zap Vser Mineral Obshch 121:105-112 (in Russian)

Krause W, Belendorff K, Bernhardt H-J (1993) Petitjeanite, $Bi_3O(OH)(PO_4)_2$, a new mineral, and additional data for the corresponding arsenate and vanadate, preisingerite and schumacherite. Neues Jahrb Mineral Monatsh 487-503

Krause W, Belendorff K, Bernhardt H-J, Petitjean K (1998a) Phosphogartrellite, $PbCuFe^{3+}(PO_4)_2(OH) \cdot H_2O$, a new member of the tsumcorite group. N Jahrb Mineral Monatsh 111-118

Krause W, Belendorff K, Bernhardt H-J, McCammon C, Effenberger H, Mikenda W (1998b) Crystal chemistry of the tsumcorite-group minerals. New data on ferrilotharmeyerite, tsumcorite, thometzekite, mounanaite, helmutwinklerite, and a redefinition of gartrellite. Eur J Mineral 10: 179-206

Krause W, Bernhardt H-J, McCammon C, Effenberger H (1998c) Brendelite, $(Bi,Pb)_2Fe^{(3+,2+)}O_2(OH)(PO_4)$, a new mineral from Schneeberg, Germany: description and crystal structure. Mineral Petrol 63: 263-277

Krutik VM, Pushcharovskii DYu, Khomyakov AP, Pobedimskaya EA, Belov NV (1980) Anion radical of mixed type (four (S_4O_{12}) rings and P orthotetrahedral) in the structure of monoclinic phosinaite. Kristallografiya 25: 240-247

Kumbasar I, Finney JJ (1968) The crystal structure of parahopeite. Mineral Mag 36: 621-624

Kurova TA, Shumyatskaya NG, Voronkov AA, Pyatenko YA (1980) Crystal structure of sidorenkite $Na_3Mn(PO_4)(CO_3)$. Dokl Akad Nauk SSSR 251: 605-607

Lager GA, Gibbs GV (1974) A refinement of the crystal structure of herderite, $CaBePO_4OH$. Am Mineral 59: 919-925

Lahti SI (1981) The granite pegmatites of the Eräjärevi area in Orivesi, southern Finland. Geol Surv Finland Bull 314: 1-82

Lahti SI, Pajunen A (1985) New data on lacroixite, $NaAlFPO_4$. I. Occurrence, physical properties and chemical composition. Am Mineral 70: 849-855

Leavens PB, Rheingold AL (1988) Crystal structures of gordonite, $MgAl_2(PO_4)_2(OH)_2(H_2O)_6(H_2O)_2$, and its Mn analog. N Jahrb Mineral Monatsh 265-270

Leavens PB, White JS, Nelen JA (1990) Zanazziite, a new mineral from Minas Gerais, Brazil. Mineral Rec 21: 413-417

Lefebvre J-J, Gasparrini C (1980) Florencite, an occurrence in the Zairian copperbelt. Can Mineral 18: 301-311

Le Page Y, Donnay G (1977) The crystal structure of the new mineral maricite $NaFePO_4$. Can Mineral 15: 518-521

Liebau F (1985) Structural Chemistry of Silicates. Springer-Verlag, Berlin

Liferovich RP, Yakovenchuk VN, Pakhomovsky YaA, Bogdanova AN, Britvin SN (1997) Juonniite, a new mineral of scandium from dolomitic carbonatites of the Kovdor massif. Zap Vser Mineral Obshch 126: 80-88

Liferovich RP, Sokolova EV, Hawthorne FC, Laajoki K, Gehör S, Pakhomovsky YuA, Sorokhtina NV (2000a) Gladiusite, $Fe^{3+}{}_2(Fe^{2+},Mg_4)(PO_4)(OH)_{11}(H_2O)$, a new hydrothermal mineral from the phoscorite-carbonatite unit, Kovdor Complex, Kola Peninsula, Russia. Can Mineral 38: 1477-1485

Liferovich RP, Pakhomovsky YaA, Yakubovich OV, Massa W, Laajoki K, Gehör S, Bogdanova AN, Sorokhtina NV (2000b) Bakhchisaraitsevite, $Na_2Mg_5[PO_4]_4{\cdot}7H_2O$, a new mineral from hydrothermal assemblages related to phoscorite-carbonatite complex of the Kovdor massif, Russia. N Jahrb Mineral Monatsh. (in press)

Lightfoot P, Cheetham AK, Sleight AW (1987) Structure of $MnPO_4{\cdot}H_2O$ by synchrotron X-ray powder diffraction. Inorg Chem 26: 3544-3547

Lindberg ML (1949) Frondelite and the frondelite-rockbridgeite series. Am Mineral 34: 541-549

Lindberg ML (1958) The beryllium content of roscherite from the Sapucaia pegmatite mine, Minas Gerais, Brazil and from other localities. Am Mineral 43: 824-838

Lindberg (1962) Manganoan lipscombite from the Sapucaia pegmatite mine, Minas Gerais,

Brazil. First occurrence of lipscombite in nature. Am Mineral 47: 353-359

Lindberg ML, Christ CL (1959) Crystal structures of the isostructural minerals lazulite, scorzalite and barbosalite. Acta Crystallogr 12: 695-697

Livingstone A (1980) Johnsomervilleite, a new transition-metal phosphate mineral from the Loch Quoich area, Scotland. Mineral Mag 43: 833-836

Makarov YS, Ivanov VI (1960) The crystal structure of meta-autunite, $Ca(UO_2)_2(PO_4)_2 \square 6H_2O$. Dokl Akad Nauk SSSR 132:601-603

Makarov ES, Tobelko KI (1960) The crystal structure of metatorbernite. Dokl Akad Nauk SSSR 131: 87-89

Malinovskii YuA, Genkina EA (1992) Crystal structure of olympite $LiNa_5[PO_4]_2$. Sov Phys Crystallogr 37: 772-782

Mandarino JA, Sturman BD (1976) Kulanite, a new barium iron aluminum phosphate from the Yukon territory, Canada. Can Mineral 14: 127-131

Mandarino JA, Sturman BD, Corlett MI (1977) Penikisite, the magnesium analogue of kulanite, from Yukon Territory. Can Mineral 15: 393-395

Mandarino JA, Sturman BD, Corlett MI (1978) Satterlyite, a new hydroxyl-bearing ferrous phosphate from the Big Fish area, Yukon Territory. Can Mineral 16: 411-413

Martini JEJ (1978) Sasaite, a new phosphate mineral from West Driefontein Cave, Transvaal, South Africa. Mineral Mag 42: 401-404

Martini JEJ (1991) Swaknoite [$Ca(NH_4)_2(HPO_4)_2 \cdot H_2O$, orthorhombic]: a new mineral from Arnheim Cave, Namibia. Bull S African Speleol Assoc 32: 72-74

Martini JEJ (1993) ICDD Card # 45-1411 (swaknoite)

Matsubara S (2000) Vivianite nodules and secondary phosphates in Pliocene-Pleistocene clay deposits from Hime-Shima, Oita Prefecture and Kobe, Hyogo Prefecture, eastern Japan. Mem National Sci Mus, Tokyo 33:15-27

Mazzi F, Ungaretti L (1994) The crystal structure of vitusite from Illimaussaq (South Greenland): $Na_3REE(PO_4)_2$. N Jahrb Mineral Monatsh 49-66

McConnell D (1952) Viséite, a zeolite with the analcime structure and containing linked SiO_4, PO_4 and H_xO_4 groups. Am Mineral 37: 609-617

McConnell D (1963) Thermocrystallization of richellite to produce a lazulite structure (calcium lipscombite). Am Mineral 48: 300-307

McCoy TJ, Steele IM, Keil K, Leonard BF, Endres M (1994) Chladniite, $Na_2CaMg_7(PO_4)_6$: a new mineral from the Carlton (IIICD) iron meteorite. Am Mineral 79: 375-380

McDonald AM, Chao GY, Grice JD (1994) Abenakiite-(Ce), a new silicophosphate carbonate mineral from Mont Saint-Hilaire, Quebec: description and structure determination. Can Mineral 32: 843-854

McDonald AM, Chao GY, Grice JD (1996) Phosinaite-(Ce) from Mont Saint-Hilaire, Quebec: new data and structure refinement. Can Mineral 34: 107-114

McDonald AM, Grice JD, Chao GY (2000) The crystal structure of yoshimuraite, a layered Ba-Mn-Ti silicophosphate, with comments on five-coordinated Ti^{4+}. Can Mineral 38: 649-656

Meagher EP, Gibbons CS, Trotter J (1974) The crystal structure of jagowerite. $BaAl_2P_2O_8(OH)_2$. Am Mineral 59: 291-295

Medrano MD, Evans HTJr, Wenk H-R, Piper DZ (1998) Phosphovanadylite: a new vanadium phosphate mineral with a zeolite-type structure. Am Mineral 83: 889-895

Mereiter K, Niedermayr G, Walter F (1994) Uralolite, $Ca_2Be_4(PO_4)_3(OH) \cdot 3.5(H_2O)$: new data and crystal structure. Eur J Mineral 6: 887-896

Merlino S, Pasero M (1992) Crystal chemistry of beryllophosphates: The crystal structure of moraesite, $Be_2(PO_4)(OH)\cdot 4H_2O$. Z Kristallogr 201: 253-262

Merlino S, Mellini M, Zanazzi PF (1981) Structure of arrojadite, $KNa_4CaMn_4Fe_{10}Al(PO_4)_{12}(OH)_2$. Acta Crystallogr B37: 1733-1736

Miller SA, Taylor JC (1986) The crystal structure of saleeite, $Mg(UO_2PO_4)_2\cdot 10\ H_2O$. Z Kristallogr 177: 247-253

Milton DJ, Bastron H (1971) Churchite and florencite (Nd) from Sausalito, California. Mineral Rec 2: 166-168

Milton C, McGee JJ, Evans HT Jr (1993) Mahlmoodite, $FeZr(PO_4)_2\cdot 4H_2O$, a new iron zirconium phosphate mineral from Wilson Springs, Arkansas. Am Mineral 78: 437-440

Moëlo Y, Lasnier B, Palvadeau P, Léone P, Fontan F (2000) Lulzacite, $Sr_2Fe^{2+}(Fe^{2+},Mg)_2Al_4(PO_4)_4(OH)_{10}$, a new strontium phosphte (Saint Aubin-des-Châteaux, Loire-Atlantique, France). CR Acad Sci Paris, Earth Planet Sci 330: 317-324

Mooney RCL (1948) Crystal structure of a series of rare earth phosphates. J Chem Phys 16: 1003

Mooney RCL (1950) X-ray diffraction study of cerous phosphate and related crystals. I. Hexagonal modification. Acta Crystallogr 3: 337-340

Moore PB (1965a) The crystal structure of laueite, $MnFe_2(OH)_2(PO_4)_2(H_2O)_6(H_2O)_2$. Am Mineral 50: 1884-1892

Moore PB (1965b) A structural classification of Fe–Mn orthophosphate hydrates. Am Mineral 50: 2052-2062

Moore PB (1966) The crystal structure of metastrengite and its relationship to strengite and phosphophyllite. Am Mineral 51: 168-176

Moore PB (1970) Crystal chemistry of the basic iron phosphates. Am Mineral 55: 135-169

Moore PB (1971a) The $Fe_3^{2+}(H_2O)_n(PO_4)_2$ homologous series: Crystal-chemical relationships and oxidized equivalents. Am Mineral 56: 1-16

Moore PB (1971b) Crystal chemistry of the alluaudite structure type: Contribution to the paragenesis of pegmatite phosphate giant crystals. Am Mineral 56: 1955-1975

Moore PB (1972a) Natrophilite, $NaMn(PO_4)$, has ordered cations. Am Mineral 57: 1333-1344

Moore PB (1972b) Octahedral tetramer in the crystal structure of leucophosphite, $K_2[Fe^{3+}_4(OH)_2(H_2O)_2(PO_4)_4]\cdot 2H_2O$. Am Mineral 57: 397-410

Moore PB (1973a) Pegmatite phosphates. Descriptive mineralogy and crystal chemistry. Mineral Rec 4: 103-130

Moore PB (1973b) Bracelets and pinwheels: A topological-geometrical approach to the calcium

orthosilicate and alkali sulfate structures. Am Mineral 58: 32-42

Moore PB (1974) I. Jahnsite, segelerite, and robertsite, three new transition metal phosphate species. II. Redefinition of overite, an isotype of segelerite. III. Isotypy of robertsite, mitridatite, and arseniosiderite. Am Mineral 59: 48–59, 640

Moore PB (1975a) Brianite, $Na_2CaMg[PO_4]_2$: a phosphate analog of merwinite, $Ca_2CaMg[SiO_4]_2$. Am Mineral 60: 717-718

Moore PB (1975b) Laueite, pseudolaueite, stewartite and metavauxite: a study in combinatorial polymorphism. N Jahrb Mineral Abh 123:148-59

Moore PB (1976) Derivative structures based on the alunite octahedral sheet: mitridatite and englishite. Mineral Mag 40: 863-866

Moore PB (1982) Pegmatite minerals of P(V) and B(III). MAC Short course handbook 8, 267-291.

Moore PB (1984) Crystallochemical aspects of the phosphate minerals. *In* Phosphate Minerals. Nriagu JO, Moore PB (Eds). Springer-Verlag, Berlin, 155-170.

Moore PB, Araki T (1973) Hureaulite, $(Mn^{2+})_5(H_2O)_4(PO_3(OH))_2(PO_4)_2$: Its atomic arrangement. Am Mineral 58: 302-307

Moore PB, Araki T (1974a) Jahnsite, $CaMnMg_2(H_2O)_8Fe_2(OH)_2(PO_4)_4$. A novel stereoisomerism of ligands about octahedral corner-chains. Am Mineral 59: 964-973

Moore PB, Araki T (1974b) Trolleite, $Al_4(OH)_3(PO_4)_3$. A very dense structure with octahedral face-sharing dimers. Am Mineral 59: 974-984

Moore PB, Araki T (1974c) Bjarebyite, $Ba(Mn,Fe)_2Al_3(OH)_3(PO_4)_3$. Its atomic arrangement. Am Mineral 59: 567-572

Moore PB, Araki T (1974d) Stewartite, $Mn^{2+}Fe_2^{3+}(OH)_2(H_2O)_6(PO_4)_2(H_2O)_2$. Its atomic arrangement. Am Mineral 59: 1272-1276

Moore PB, Araki T (1974e) Montgomeryite, $Ca_4Mg(H_2O)_{12}[Al_4(OH)_4(PO_4)_6]$: Its crystal structure and relaton to vauxite, $Fe^{2+}{}_2(H_2O)_4[Al_4(OH)_4(H_2O)_4(PO_4)_4]\cdot 4H_2O$. Am Mineral 59: 843-850

Moore PB, Araki T (1975) Palermoite, $SrLi_2(Al_4(OH)_4(PO_4)$. Its atomic arrangement and relationship to carminite, $Pb_2(Fe_4(OH)_4(AsO_4)_4)$. Am Mineral 60: 460-465

Moore PB, Araki T (1976) A mixed-valence solid solution series: Crystal structures of phosphoferrite and kryzhanovskite. Inorg Chem 15: 316-321

Moore PB, Araki T (1977a) Samuelsonite: its crystal structure and relation to apatite and octacalcium phosphate. Am Mineral 62: 229-245

Moore PB, Araki T (1977b) Mitridatite, $Ca_6(H_2O)_6(Fe_9O_6(PO_4)_9)(H_2O)_3$. A noteworthy octahedral sheet structure. Mineral Mag 41: 527-528

Moore PB, Araki T (1977c) Overite, segelerite, and jahnsite: a study in combinatorial polymorphism. Am Mineral 62: 692-702

Moore PB, Ghose S (1971) A novel face-sharing octahedral trimer in the crystal structure of seamanite. Am Mineral 56: 1527-1538

Moore PB, Ito J (1978) I. Whiteite, a new species, and a proposed nomenclature for the

jahnsite-whiteite complex series. II. New data on xanthoxenite. Mineral Mag 42: 309-316

Moore PB, Ito J (1979) Alluaudites, wyllieites, arrojadites: crystal chemistry and nomenclature. Mineral Mag 43: 227-35

Moore PB, Kampf AR (1977) Schoonerite, a new zinc-manganese-iron-phosphate mineral. Am Mineral 62: 246-249

Moore PB, Molin-Case J (1974) Contribution to pegmatite phosphate giant crystal paragenesis. II. The crystal chemistry of wyllieite, $Na_2Fe(II)_2Al(PO_4)_3$, a primary phase. Am Mineral 59: 280-290

Moore PB, Shen J (1983a) An X-Ray structural study of cacoxenite, a mineral phosphate. Nature 306: 356-358

Moore Pb, Shen J (1983b) Crystal structure of steenstrupine: a rod structure of unusual complexity. Tschermaks Mineral Petrogr Mitt 31: 47-67

Moore PB, Kampf AR, Irving AJ (1974) Whitmoreite, $Fe(II)Fe(III)_2(OH)_2(H_2O)_4(PO_4)_2$, a new species. Its description and atomic arrangement. Am Mineral 59: 900-905

Moore PB, Irving AJ, Kampf AR (1975a) Foggite, $CaAl(OH)_2(H_2O)[PO_4]$; goedkenite, $(Sr,Ca)_2Al(OH)[PO_4]_2$; and samuelsonite, $(Ca,Ba)Fe^{2+}{}_2Mn^{2+}{}_2Ca_8Al_2(OH)_2[PO_4]_{10}$: Three new species from the Palermo No. 1 Pegmatite, North Groton, New Hampshire. Am Mineral 60: 957-964

Moore PB, Kampf AR, Araki T (1975b) Foggite, $(CaH_2O)_2(CaAl_2(OH)_4(PO_4)_2)$. Its atomic arrangement and relationship to calcium Tschermak's pyroxene. Am Mineral 60: 965-971

Moore PB, Araki T, Kampf AR, Steele IM (1976) Olmsteadite, $K_2(Fe^{2+})_2((Fe^{2+})_2((Nb^{6+})(Ta^{6+}))_2O_4(H_2O)_4(PO_4)_4)$, a new species, its crystal structure and relation to vauxite and montgomeryite. Am Mineral 61: 5-11

Moore PB, Araki T, Kampf AR (1980) Nomenclature of the phosphoferrite structure type: refinements of landesite and kryzhanovskite. Mineral Mag 43: 789-795

Moore PB, Araki T, Merlino S, Mellini M, Zanazzi PF (1981) The arrojadite-dickinsonite series, $KNa_4Ca(Fe,Mn)^{2+}{}_{14}Al(OH)_2(PO_4)_{12}$: crystal structure and crystal chemistry. Am Mineral 66: 1034-1049

Moore PB, Araki T, Steele IM, Swihart GH, Kampf AR (1983) Gainesite, sodium zirkonium beryllophosphate: a new mineral and its crystal structure. Am Mineral 68: 1022-1028

Moring J, Kostiner E (1986) The crystal structure of $NaMnPO_4$. J Sol State Chem 61: 379-383

Mrose ME (1971) Dittmarite. US Geol Surv Prof Pap 750-A: A115

Mücke A (1979) Keckit, $(Ca,Mg)(Mn,Zn)_2Fe^{3+}{}_3[(OH)_3(PO_4)_4]\cdot 2H_2O$, ein neues Mineral von Hagendorf/Opf, und seine genetische Stellung. N Jahrb Mineral Abh 134: 183-192

Mücke A (1983) Wilhelmvierlingite, $(Ca,Zn)MnFe^{3+}[OH(PO_4)_2]\cdot 2H_2O$, a new mineral from Hagendorf/Oberpfalz. Aufschluss 34: 267-274

Mücke A (1988) Lehnerit, $Mn[UO_2/PO_4]_2\cdot 8H_2O$, ein neues Mineral aus dem Pegmatit von Hagendorf/Oberpfalz. Aufschluss 39: 209-217

Muto T, Meyrowitz R, Pommer AM, Murano T (1959) Ningyoite, a new uranous phosphate

mineral from Japan. Am Mineral 44: 633-650

Ng HN, Calvo C (1976) X-ray study of the alpha-beta transformation of berlinite AlPO4. Can J Phys 54: 638-647

Ni YX, Hughes JM, Mariano AN (1995) Crystal chemistry of the monazite and xenotime structures. Am Mineral 80: 21-26

Nord AG, Kierkegaard P (1968) The crystal structure of $Mg_3(PO_4)_2$. Acta Chem Scand 22: 1466-1474

Nriagu JO (1984) Phosphate minerals: Their properties and general modes of occurrence. *In* Phosphate Minerals. Nriagu JO, Moore PB (Eds). Springer-Verlag, Berlin, 1-136

Olsen EJ, Steele IM (1997) Galileiite: a new meteoritic phosphate mineral. Meteor Planet Sci 32: A155-A156

Ono Y, Yamada N (1991) A structural study of the mixed crystal $K_{0.77}(NH_4)_{0.23}H_2PO_4$. J Phys Soc Japan 60: 533-538

Ovchinnikov VE, Solov'eva LP, Pudovkina ZV, Kapustin YuL, Belov NV (1980) The crystal structure of kovdorskite $Mg_2(PO_4)(OH)(H_2O)_3$. Dokl Akad Nauk SSSR 255: 351-354

Owens JP, Altschuler ZS, Berman R (1960) Millisite in phosphorite from Homeland, Florida. Am Mineral 45: 547-561

Pajunen A, Lahti SI (1984) The crystal structure of viitaniemiite. Am Mineral 69: 961-966

Pajunen A, Lahti SI (1985) New data on lacroixite, $NaAlFPO_4$. II. Crystal structure. Am Mineral 70: 849-855

Pauling LS (1929) The principles determining the structure of complex ionic crystals. J Am Chem Soc 51: 1010-1026

Pauling L (1960) The nature of the chemical bond. 3rd ed. Cornell University Press, Ithaca, New York

Pavlov PV, Belov NV (1957) The crystal structures of herderite, datolite and gadolinite. Dokl Akad Nauk SSSR 114: 884-887

Peacor DR, Dunn PJ (1982) Petersite, a REE and phospahte analogue of mixite. Am Mineral 67:1039-1042

Peacor DR, Dunn PJ, Simmons WB (1983) Ferrostrunzite, the ferrous iron analogue of strunzite from Mullica Hill, New Jersey N Jahrb Mineral Monatsh 524-528

Peacor DR, Dunn PJ, Simmons WB (1984) Earlshannonite, the Mn analogue of whitmoreite, from North Carolina. Can Mineral 22: 471-474

Peacor DR, Rouse RC, Ahn T-H (1987) Crystal structure of tiptopite, a framework beryllophosphate isotypic with basic cancrinite. Am Mineral 72: 816-820

Peacor DR, Rouse RC, Coskren TD, Essene EJ (1999) Destinezite ("diadochite"), $Fe_2(PO_4)(SO_4)(OH) \cdot 6(H_2O)$: its crystal structure and role as a soil mineral at Alum Cave Bluff,Tennessee. Clays Clay Mineral 47: 1-11

Pekov IV, Kulikova IM, Kabalov YuK, Eletskaya OV, Chukanov NV, Menshikov YuP, Khomyakov AP (1996) Belovite-(La), $Sr_3Na(La,Ce)[PO_4]_3(F,OH)$ - a new rare earth mineral in the apatite group. Zap Vser Mineral Obshch 125: 101-109 (in Russian)

Piret P, Declercq J-P (1983) Structure cristalline de l'upalite $Al((UO_2)_3O(OH)(PO_4)_2 \cdot 7(H_2O)$. Un exemple de macle mimetique. Bull Minéral 106: 383-389

Piret P, Deliens M (1981) New data on holotype bergenite. Bull Mineral 104: 16-18

Piret P, Deliens M (1982) La Vanmeersscheite, $U(UO_2)_3(PO_4)_2(OH)_6 \cdot 4H_2O$ et la meta-vanmeersscheite, $U(UO_2)_3(PO_4)_2(OH)_6 \cdot 2H_2O$, nouveaux mineraux. Bull Minéral 105: 125-128

Piret P, Deliens M (1987) Les phosphates d'uranyle et d'aluminium de Kobokobo IX. L'althupite $AlTh(UO_2)((UO_2)_3O(OH)(PO_4)_2)_2(OH)_3(H_2O)_{15}$, nouveau mineral; proprietes et structure crystalline. Bull Minéral 110: 65-72

Piret P, Deliens M (1988) Description of ludjibaite, a polymorph of pseudomalachite, $Cu_5(PO_4)_2(OH)_4$. Bull Minéral 111:167-171

Piret P, Piret-Meunier J (1988) Nouvelle determination de la structure cristalline de la dumontite $Pb_2((UO_2)_3O_2(PO_4)_3)(H_2O)5)$ Bull Minéral 111: 439-442

Piret P, Piret-Meunier J, Declercq JP (1979) Structure of phuralumite. Acta Crystallogr B35: 1880-1882

Piret P, Deliens M, Piret-Meunier J (1985) Occurrence and crystal structure of kipushite, a new copper-zinc phosphate from Kipushi, Zaire. Can Mineral 23: 35-42

Piret P, Deliens M, Piret-Meunier J (1988) La francoisite-(Nd), nouveau phosphate d'uranyle et de terres rares; proprietes et structure crystalline. Bull Minéral 111: 443-449

Piret P, Piret-Meunier J, Deliens M (1990) Composition chimique et structure cristalline de la dewindtite $Pb_3(H(UO_2)_3O_2(PO_4)_2)_2 \cdot 12H_2O$. Eur J Mineral 2: 399-405

Popova VI, Popov VA, Sokolova EV, Ferraris G, Chukanov NV (2001) Kanonerovite $MnNa_3P_3O_{10} \cdot 12H_2O$, first triphosphate mineral (Kazennitsa, Middle Urals, Russia). N Jahrb Mineral Monatsh (accepted)

Potenza MF (1958) Autunite e metatorbernite nella Sienite di Biella. Rend Soc Mineral Ital 14: 215-223

Pring A, Birch WD (1993) Gatehouseite, a new manganese hydroxy phosphate from Iron Monarch, South Australia. 57: 309-313

Pring A, Birch WD, Dawe J, Taylor M, Deliens M, Walenta K (1995) Kintoreite, $PbFe_2(PO_4)_2(OH,H_2O)_6$, a new mineral of the jarosite-alunite family, and lusungite discredited. Mineral Mag 59: 143-148

Pring A, Kolitsch U, Birch WD, Beyer BD, Elliott P, Ayyappan P, Ramanan A (1999) Bariosincosite, a new hydrated barium vanadium phosphate, from the Spring Creek mine, South Australia. Mineral Mag 63: 735-741

Raade G, Roemming C, Medenbach O (1998) Carbonate-substituted phosphoellenbergerite from Modum, Norway: description and crystal structure. Mineral Petrol 62: 89-101

Radoslovich EW, Slade PG (1980) Pseudo-trigonal symmetry and the structure of gorceixite. N Jahrb Mineral Monatsh 157-170

Rastsvetaeva RK (1971) Kristallicheskaya struktura lomonosovita $Na_5Ti_2(Si_2O_7)(PO_4)O_2$. Dokl Akad Nauk SSSR 197: 81-84

Rastsvetsaeva RK, Khomyakov AP (1996) Crystal structure of deloneite-(Ce), the highly

ordered Ca analogue of belovite. Dokl Ross Akad Nauk 349: 354-357 (in Russian)

Richardson JM, Roberts AC, Grice JD, Ramik RA (1988) Mcauslanite, a supergene hydrated iron aluminum fluorophosphate from the East Kemptville tin mine, Yarmouth County, Nova Scotia. Can Mineral 26: 917-921

Řídkošil T, Sejkora J, Šrein VL (1996) Smrkovecite, monoclinic $Bi_2O(OH)(PO_4)$, a new mineral of the atelesite group. N Jahrb Mineral Monatsh 97-102

Rinaldi R (1978) The crystal structure of griphite, a complex phosphate, not a garnetoid. Bull Minéral 101: 543-547

Rius J, Louër D, Mouër M, Galí S, Melgarejo JC (2000) Structure solution from powder data of the phosphate hydrate tinticite. Eur J Mineral 12: 581-588

Roberts AC, Dunn PJ, Grice JD, Newbury DE, Roberts WL (1988) The X-ray crystallography of tavorite from the Tip Top pegmatite, Custer, South Dakota. Powder Diffraction 3: 93-95

Roberts AC, Sturman BD, Dunn PJ, Roberts WL (1989) Pararobertsite, $Ca_2Mn^{3+}{}_3(PO_4)_3O_2{\cdot}3H_2O$, a new mineral species form the Tip Top pegmatite, Custer Country, South Dakota, and its relationship to robertsite. Can Mineral 27: 451-455

Roca M, Marcos MD, Amorós P, Alamo J, Beltrán-Porter A, Beltrán-Porter D (1997) Synthesis and crystal structure of a novel lamellar barium derivative: $Ba(VOPO_4)_2{\cdot}4H_2O$. Synthetic pathways for layered oxovanadium phosphate hydrates $M(VOPO_4)_2{\cdot}nH_2O$. Inorg Chem 36: 3414-3421

Romming C, Raade G (1980) The crystal structure of althausite, $Mg_4(PO_4)_2(OH,O)F$. Am Mineral 65: 488-498

Romming C, Raade G (1986) The crystal structure of heneuite, $CaMg_5(CO_3)(PO_4)_3(OH)$. N Jahrb Mineral Monatsh 351-359

Romming C, Raade G (1989) The crystal structure of natural and synthetic holtedahlite. Mineral Petrol 40: 91-100

Rose D (1980) Brabantite, $CaTh[PO_4]_2$, a new mineral of the monazite group. N Jahrb Mineral Monatsh 247-257

Ross V (1956) Studies of uranium minerals XXII: Synthetic calcium and lead uranyl phosphate minerals. Am Mineral 41: 915-926

Rouse RC, Peacor DR, Freed RL (1988) Pyrophosphate groups in the structure of canaphite, $CaNa_2P_2O_7 \cdot 4(H_2O)$: The first occurrence of a condensed phosphate as a mineral. Am Mineral 73: 168-171

Rouse RC, Peacor DR, Merlino S (1989) Crystal structure of pahasapaite, a beryllophosphate mineral with a distorted zeolite rho framework. Am Mineral 74: 1195-1202

Sakae T, Nagata H, Sudo T (1978) The crystal structure of synthetic calcium phosphate sulfate hydrate, $Ca_2(HPO_4)(SO_4)(H_2O)_4$, and its relation to brushite and gypsum. Am Mineral 63: 520-527

Sales BC, Chakoumakos BC, Boatner LA, Ramey JO (1993) Structural properties of the amorphous phases produced by heating crystalline $MgHPO_4{\cdot}3H_2O$. J Non-Crystalline Solids 159: 121-139

Schindler M, Hawthorne FC (2001a) A bond-valence approach to the structure, chemistry and paragenesis of hydroxy-hydrated oxysalt minerals: I. Theory. Can Mineral 39: 1225-1242

Schindler M, Hawthorne FC (2001b) A bond-valence approach to the structure, chemistry and paragenesis of hydroxy-hydrated oxysalt minerals: II. Crystal structure and chemical composition of borate minerals. Can Mineral 39: 1243-1256

Schindler M, Hawthorne FC (2001c) A bond-valence approach to the structure, chemistry and paragenesis of hydroxy-hydrated oxysalt minerals: III. Paragenesis of borate minerals. Can Mineral 39: 1257-1274

Schindler M, Huminicki DMC, Hawthorne FC (2002) A bond-valence approach to the chemical composition and occurrence of sulfate minerals. Chem Geol (submitted)

Schlüter J, Klaska K-H, Friese K, Adiwidjaja G (1999) Kastningite, $(Mn,Fe,Mg)Al_2(PO_4)_2(OH)_2 \cdot 8H_2O$, a new phosphate mineral from Waidhaus, Bavaria, Germany. N Jahrb Mineral Monatsh 40-48

Sebais M, Dorokhova GI, Pobedimskaya EA, Khomyakov AP (1984) The crystal structure of nefedovite and its typomorphism. Dokl Akad Nauk SSSR 278: 353-357

Selway JB, Cooper MA, Hawthorne FC (1997) Refinement of the crystal structure of burangaite. Can Mineral 35: 1515-1522

Sen Gupta PK, Swihart GH, Dimitrijevic R, Hossain MB (1991) The crystal structure of lueneburgite, $Mg_3(H_2O)_6(B_2(OH)_6(PO_4)_2)$. Am Mineral 76: 1400-1407

Sergeev AS (1964) Pseudo-autunite, a new hydrous calcium phosphate. Mineral Geokhim 1: 31-39 (in Russian)

Shannon RD (1976) Revised effective ionic radii and systematic studies of interatomic distances in halides and chalcogenides. Acta Crystallogr A32: 751-767

Shen J, Peng Z (1981) The crystal structure of furongite. Acta Crystallogr A37: supp C-186

Shoemaker GL, Anderson JB, Kostiner E (1977) Refinement of the crystal structure of pseudomalachite. Am Mineral 62: 1042-1048

Shoemaker GL, Anderson JB, Kostiner E (1981) The crystal structure of a third polymorph of $Cu_5(PO_4)_3(OH)_4$. Am Mineral 66: 169-181

Sieber NHW, Tillmanns E, Medenbach O (1987) Hentschelite, $CuFe_2(PO_4)_2(OH)_2$, a new member of the lazulite group, and reichenbachite, $Cu_5(PO_4)_2(OH)_4$, a polymorph of pseudomalachite, two new copper phosphate minerals from Reichenbach, Germany. Am Mineral 72: 404-408

Simonov MA, Egorov-Tismenko YK, Belov NV (1980) Use of modern X-ray equipment to solve fine problems of structural mineralogy by the example of the crystal RE of structure of babefphite $BaBe(PO_4)F$. Kristallografiya 25: 55-59 (in Russ)

Slavik F (1914) Neue Phosphate vom Greifenstein bei Ehrenfriedersdorf. Ak Ceská, Bull intern ac sc Bohême 19: 108-123

Sljukic M, Matkovic B, Prodic B, Anderson D (1969) The crystal structure of $KZr_2(PO_4)_3$. Z Kristallogr 130: 148-161

Soboleva MV, Pudovkina IA (1957) Mineralogy of Uranium Handbook. Moscow: Dept Tech Lit USSR

Sokolova EV, Egorov-Tismenko YuK (1990) Crystal structure of girvasite. Dokl Akad Nauk SSSR 311: 1372-1376

Sokolova EV, Hawthorne FC (2001) The crystal chemistry of the $[M_3\phi_{11-14}]$ trimeric structures: from hyperagpaitic complexes to saline lakes. Can Mineral (accepted)

Sokolova EV, Khomyakov AP (1992) Crystal structure of a new mineral $Na_3Sr(PO_4)(CO_3)$ from bredliit group. Dokl Akad Nauk SSSR 322: 531-535

Sokolova EV, Yamnova NA, Egorov-Tismenko YK, Khomyakov AP (1984a) The crystal structure of a new phosphate of Na, Ca and $Ba(Na_5Ca)Ca_6Ba(PO_4)_6F_3$. Dokl Akad Nauk SSSR 274: 78-83

Sokolova EV, Egorov-Tismenko YK, Yamnova NA, Simonov MA (1984b) The crystal structure of olgite $Na(Sr_{0.52}Ba_{0.48})(Sr_{0.58}Na_{0.42})(Na_{0.81}Sr_{0.19})(PO_{3.40})(P_{0.76}O_{3.88})$. Kristallografiya 29: 1079-1083

Sokolova EV, Egorov-Tismenko YuK, Khomyakov AP (1987a) Crystal structure of lomonosovite and sulfohalite as a homolog of the structures of $Na_{14}CaMgTi_4(Si_2O_7)_2(PO_4)_4O_4F_2$. Mineral Z 9: 28-35

Sokolova EV, Egorov-Tismenko YK, Khomyakov AP (1987b) Crystal structure of $Na_{17}Ca_3Mg(Ti, Mn)_4(Si_2O_7)_2(PO_4)_3O_2F_6$, a new representative of the family of layered titanium silicates. Dokl Akad Nauk SSSR 294: 357-362

Sokolova EV, Egorov-Tismenko YuK, Khomyakov AP (1988) Crystal structure of sobolevite, Sov Phys Dokl 33: 711-714

Sokolova EV, Hawthorne FC, McCammon C, Liferovich RP (2001) The crystal structure of gladiusite, $(Fe^{2+},Mg)_4Fe^{3+}{}_2(PO_4)(OH)_{11}(H_2O)$. Can Mineral 39: 1121-1130

Steele IM, Olsen E, Pluth J, Davis AM (1991) Occurrence and crystal structure of Ca-free beusite in the El Sampal IIIA iron meteorite. Am Mineral 76: 1985-1989

Stergiou AC, Rentzeperis PJ, Sklavounos S (1993) Refinement of the crystal structure of metatorbernite. Z Kristallogr 205: 1-7

Street RLT, Whitaker A (1973) The isostructurality of rosslerite and phosphorosslerite. Z Kristallgr 137: 246-255

Sturman BD, Mandarino JA, Mrose ME, Dunn PJ (1981a) Gormanite, $Fe^{2+}{}_3Al_4(PO_4)_4(OH)_6{\cdot}2H_2O$, the ferrous analogue of souzalite, and new data for souzalite. Can Mineral 19: 381-387

Sturman BD, Peacor DR, Dunn PJ (1981b) Wicksite, a new mineral from northeastern Yukon Territory. Can Mineral 19: 377-380

Sutor DJ (1967) The crystal and molecular structure of newberyite, $MgHPO_4(H_2O)_3$. Acta Crystallogr 23: 418-422

Szymanski JT, Roberts AC (1990) The crystal structure of voggite, a new hydrated Na-Zr hydroxide-phosphate-carbonate mineral. Mineral Mag 54: 495-500

Tadini C (1981) Magniotriplite: its crystal structure and relation to the triplite-triploidite group. Bull Minéral 104: 677-680

Takagi S, Mathew M, Brown WE (1986) Crystal structures of bobierrite and synthetic $Mg_3(PO_4)_2(H_2O)_8$. Am Mineral 71: 1229-1233

Taxer KJ (1975) Structural investigations on scholzite. Am Mineral 60: 1019-1022

Taxer KJ, Bartl H (1997) Die "geordnete gemittelte" Kristallstruktur von Parascholzit. Zur

Dimorphie von $CaZn_2(PO_4)_2 \cdot 2(H_2O)$, Parascholzit-Scholzit. Z Kristallogr 212: 197-202

van der Westhuizen WA, deBruiyn H, Beukes GJ, Strydom D (1990) Dufrenite in iron-formation on the Kangnas farm, Aggeneys district, Bushmanland, South Africa. Mineral Mag 54: 419-424

van Tassel R (1968) Données cristallographiques sur la koninckite. Bull Minéral 91: 487-489

van Wambeke L (1972) Eylettersite, un nouveau phosphate de thorium appartenant à la série de la crandallite. Bull Mineral 95: 98-105

van Wambeke L (1975) La zairite, un nouveau minéral appartenant à la serie de la crandallite. Bull Minéral 98: 351-353

Vencato I, Mattievich E, Mascarenhas YP (1989) Crystal structure of synthetic lipscombite: A redetermination. Am Mineral 74: 456-460

Vochten RD, De Grave E (1981) Crystallographic, Mössbauer, and electrokinetic study of synthetic lipscombite. Phys Chem Minerals 7: 197-203

Vochten R, Pelsmaekers J (1983) Synthesis, solubility, electrokinetic properties and refined crystallographic data of sabugalite. Phys Chem Mineral 9: 23-29

Vochten RF, van Acker P, De Grave E (1983) Mössbauer, electrokinetic and refine parameters study of synthetic manganoan lipscombite. Phys Chem Minerals 9: 263-268

Vochten R, de Grave E, Pelsmaekers J (1984) Mineralogical study of bassetite in relation to its oxidation. Am Mineral 69: 967-978

Voloshin AV, Pakhomovskiy YuA, Tyusheva FN (1983) Lun'okite; a new phosphate, the manganese analog of overite from granitic pegmatites of the Kola Peninsula. Int Geol Rev 25: 1131-1136

Voloshin AV, Pakhomovskii YaA, Tyusheva EN (1992) Manganosegelerite $(Mn,Ca)(Mn,Fe,Mg)Fe^{3+}(PO_4)_2(OH)\cdot 4H_2O$-a new phosphate of the overite group from granitic pegmatites of the Kola Peninsula. Zap Vser Mineral Obshch 121: 95-103

von Knorring O, Fransolet A-M (1977) Gatumbaite, $CaAl_2(PO_4)_2(OH)_2\cdot H_2O$: a new species from Buranga pegmatite, Rwanda. N Jahrb Mineral Monatsh: 561-568

von Knorring O, Mrose ME (1966) Bertossaite, $(Li,Na)_2(Ca,Fe,Mn)Al_4(PO_4)_4(OH,F)_4$, a new mineral from Rwanda (Africa). Can Mineral 8: 668

Waldrop L (1968a) Crystal structure of triplite. Naturwiss 55: 178

Waldrop L (1968b) Crystal structure of triploidite. Naturwiss 55: 296-297

Waldrop L (1970) The crystal structure of tripoidite and its relations to the structures of other minerals of the triplite-triploidite group. Z Kristallogr 131: 1-20

Walenta K (1978) Uranospathite and arsenuranospathite. Mineral Mag 42: 117-28

Walenta K, Dunn PJ (1984) Phosphofibrite, ein neues Eisenphosphat aus der Grube Clara im mittleren Schwarzwald (BRD) Chem Erde 43: 11-16

Walenta K, Theye T (1999) Haigerachit, ein neues Phosphatmineral von der Grube Silberbrünnle bei Gengenbach im mittleren Schwarzwald. Aufschluss 50: 1-7

Walenta K, Birch WD, Dunn PJ (1996) Benauite, a new mineral of the crandallite group from the Clara mine in the central Black Forest, Germany. Chem Erde 56: 171-176

Walter F (1992) Weinebeneite, $CaBe_3(PO_4)_2(OH)_2 \cdot 4(H_2O)$, a new mineral species: mineral data and crystal structure. Eur J Mineral 4: 1275-1283

Warner JK, Cheetham AK, Nord AG, von Dreele RB, Yethiraj M (1992) Magnetic structure of iron(II) phosphate, sarcopside, $Fe_3(PO_4)_2$. J Mater Chem 2: 191-196

White JS Jr, Henderson EP, Mason B (1967) Secondary minerals produced by weathering of the Wolf Creek meteorite. Am Mineral 52: 1190-1197

White JS Jr, Leavens PB, Zanazzi PF (1986) Switzerite redefined as $Mn_3(PO_4)_2 \cdot 7H_2O$, and metaswitzerite, $Mn_3(PO_4)_2 \cdot 4H_2O$. Am Mineral 71: 1221-1223

Wiench DM, Jansen M (1983) Kristallstruktur von wasserfreiem Na_2HPO_4. Z Anorg Allg Chem 501: 95-101

Wise MA, Hawthorne FC, Černý PC (1990) Crystal structure of a Ca-rich beusite from the Yellowknife pegmatite field, Northwest Territories. Can Mineral 28: 141-146

Witzke T, Wegner R, Doering T, Pöllmann H, Schuckmann W (2000) Serrabrancaite, $MnPO_4 \cdot H_2O$, a new mineral from the Alto Serra Branca pegmatite, Pedra Lavrada, Paraiba, Brazil. Am Mineral 85: 847-849

Yakubovich OV, Mel'nikov OK (1993) Libethenite $Cu_2(PO_4)(OH)$: Synthesis, crystal structure refinement, comparative crystal chemistry. Kristallografiya 38: 63-70

Yakubovich OV, Urusov VS (1996) The genetic crystal chemistry of pegmatite phosphates. Moscow University Geology Bulletin 51: 18-40.

Yakubovich OV, Urusov VS (1997) Electron density distribution in lithiophosphatite Li_3PO_4: Crystallochemical features of orthophosphates with hexagonal close packing. Kristallografiya 42: 301-308

Yakubovich OV, Simonov MA, Belov NV (1977) The crystal structure of a synthetic triphylite $LiFe(PO_4)$. Dokl Akad Nauk SSSR 235: 93-95

Yakubovich OV, Simonov MA, Matvienko EN, Belov NV (1978) The crystal structure of the synthetic finite Fe-term of the series triplite – zwieselite $Fe_2(PO_4)$ F. Dokl Akad Nauk SSSR 238: 576-579

Yakubovich OV, Massa W, Liferovich RP, Pakhomovsky YA (2000) The crystal structure of bakhchisaraitsevite, $[Na_2(H_2O)_2]$ $\{(Mg_{4.5}Fe_{0.5})(PO_4)_4(H_2O)_5\}$, a new mineral species of hydrothermal origin from the Kovdor phoscorite-carbonatite complex, Russia. Can Mineral 38: 831-838

Yakubovich OV, Massa W, Liferovich RP, McCammon CA (2001) The crystal structure of barićite, $(Mg_{1.70}Fe_{1.30})(PO_4)_2 \cdot 8H_2O$, the magnesium-dominant member of the vivianite group. Can Mineral 39: 1317-1324

Young EJ, Weeks AD, Meyrowitz R (1966) Coconinoite, a new uranium mineral from Utah and Arizona. Am Mineral 51: 651-663

Zanazzi PF, Leavens PB, White JS (1986) Crystal structure of switzerite, $Mn_3(PO_4)_2(H_2O)_7$ and its relationship to metaswitzerite, $Mn_3(PO_4)_2(H_2O)_4$. Am Mineral 71: 1224-1228

Zhang J, Wan A, Gong W (1992) New data on yingjiangite. Acta Petrol Mineral 11: 178-184

Zhesheng M, Nicheng S, Zhizhong P (1983) Crystal structure of a new phosphatic mineral—qingheiite. Scientia Sinica (Series B) 25: 876-884

Zolensky ME (1985) New data on sincosite. Am Mineral 70: 409-410

Zoltai T (1960) Classification of silicates and other minerals with tetrahedral structures. Am Mineral 45: 960-973

Zwaan PC, Arps CES, de Grave E (1989) Vochtenite, $(Fe^{2+},Mg)(Fe^{3+}[UO_2/PO_4]_4(OH)\cdot 12–13H_2O$, a new uranyl phosphate mineral from Wheal Basset, Redruth, Cornwall, England. Mineral Mag 53: 473-478

APPENDIX A. DATA AND REFERENCES FOR SELECTED PHOSPHATE MINERALS

Mineral Name	Formula	*a* (Å)	*b* (Å)	*c* (Å)	α (°)	β (°)	γ (Å)	Space Group	Ref.
Abenakiite-(Ce)	$Na_{26}(Ce_3Nd_2La)(SO_2)(SiO_3)_6(PO_4)_6(CO_3)_6$	16.018(2)	*a*	19.761(4)	90	90	120	$R\bar{3}$	(1)
Aheylite	$Fe^{2+}Al_6(PO_4)_4(OH)_8(H_2O)_4$	7.400(1)	9.896(1)	7.627(1)	110.87	115.00	69.96	$P\bar{1}$	(2)
Aldermanite	$Mg_5Al_{12}(PO_4)_8(OH)_{22}(H_2O)_{32}$	15.000(7)	8.330(6)	2.660(1)	90	90	90	*P*– – –	(3)
Alforsite	$Ba_5(PO_4)_3Cl$	10.284(2)	*a*	7.651(3)	90	90	120	$P6_3/m$	(4)
Alluaudite	$(Na,Ca)[Fe^{2+}(Mn^{2+},Fe^{2+},Fe^{3+},Mg)_2(PO_4)_3]$	12.004(2)	12.533(4)	6.404(1)	90	114.4(1)	90	*C*2/*c*	(5)
Althausite	$Mg_4(PO_4)_2(OH)F$	8.258(2)	6.054(2)	14.383(5)	90	90	90	*Pnma*	(6)
Althupite	$AlTh(UO_2)[(UO_2)_3(PO_4)_2O(OH)]_2(OH)_3(H_2O)_{15}$	10.953(3)	18.567(4)	13.504(3)	72.6(0)	68.2(0)	84.2(0)	$P\bar{1}$	(7)
Amblygonite	$Li[Al(PO_4)F]$	5.060	5.160	7.080	109.9	107.5	97.9	$P\bar{1}$	(8)
Anapaite	$Ca_2[Fe^{2+}(PO_4)_2(H_2O)_4]$	6.477(1)	6.816(1)	5.898(1)	101.64(3)	104.24(3)	70.76(4)	$P\bar{1}$	(9)
Archerite	$K[H_2(PO_4)]$	7.427(2)	*a*	7.046(2)	90	90	90	$I\bar{4}2d$	(10)
Arctite	$(Na_5Ca)Ca_6Ba(PO_4)_6F_3$	14.366(9)	*a*	14.366(9)	28.6(0)	28.6(0)	28.6(0)	$R\bar{3}m$	(11)
Ardealite	$Ca_2(PO_3\{OH\})(SO_4)(H_2O)_4$	5.721(5)	30.992(5)	6.250(4)	90	117.3(1)	90	*Cc*	(12)
Arrojadite	$KNa_4CaMn^{2+}{}_4Fe^{2+}{}_{10}Al(PO_4)_{12}(OH)_2$	16.526(4)	10.057(3)	24.730(5)	90	105.8	90	*C*2/*c*	(13)
Arupite	$Ni_3(PO_4)_2(H_2O)_8$	9.889	13.225	4.645	90	102.41	90	*I*2/*m*	(14)
Attakolite	$CaMn^{2+}Al_4(SiO_3\{OH\})(PO_4)_3(OH)_4$	17.188(4)	11.477(8)	7.322(5)	90	113.8(0)	90	*C*2/*m*	(15)
Augelite	$[Al_2PO_4(OH)_3]$	13.124(6)	7.988(5)	5.066(3)	90	112.3(0)	90	*C*2/*m*	(16)
Autunite	$Ca[(UO_2)(PO_4)]_2(H_2O)_{10\text{-}12}$	7.027	*a*	20.790	90	90	90	*I*4/*mmm*	(17)
Babefphite	$Ba[BePO_4F]$	6.889(3)	16.814(7)	6.902(3)	90.0(0)	90.0(0)	90.3(0)	*F*1	(18)
Bakhchisaraitsevite	$Na_2Mg_5(PO_4)_4(H_2O)_7$	8.3086(8)	12.906(1)	17.486(2)	90	102.01(1)	90	$P2_1/c$	(19)
Barbosalite	$Fe^{2+}[Fe^{3+}(PO_4)(OH)]_2$	7.250(20)	7.460(20)	7.490(20)	90	120.2(85)	90	$P2_1/c$	(20)
Baričite	$Mg_3(PO_4)_2(H_2O)_8$	10.085(2)	13.390(3)	4.6713(9)	90	104.96(3)	90	*C*2/*m*	(21)
Bariosincosite	$Ba(V^{4+}OPO_4)_2(H_2O)_4$	9.031(6)	*a*	12.755(8)	90	90	90	*P*4/*nmm*	(22)
Bassetite	$Fe^{2+}[(UO_2)(PO_4)]_2(H_2O)_8$	6.98(4)	17.07(4)	7.01(7)	90	90.53(1)	90	$P2_1/m$	(23)
Bearthite	$Ca_2Al(PO_4)_2(OH)$	7.231(3)	5.734(2)	8.263(4)	90	112.6(1)	90	$P2_1/m$	(24)
Bederite	$Ca_2(Mn^{2+}{}_2Fe^{3+}{}_2Mn^{3+}{}_2)(PO_4)_6(H_2O)_2$	12.559(2)	12.834(1)	11.714(2)	90	90	90	*Pcab*	(25)
Belovite-(Ce)	$Sr_3NaCe(PO_4)_3(OH)$	9.664(0)	*a*	7.182(0)	90	90	120	$P\bar{3}$	(26)
Belovite-(La)	$Sr_3NaLa(PO_4)_3F$	9.647	*a*	7.170	90	90	120	$P\bar{3}$	(27)

APPENDIX A continued

Mineral Name	Formula	*a* (Å)	*b* (Å)	*c* (Å)	α (°)	β (°)	γ (Å)	Space Group	Ref.
Benauite	$HSrFe^{3+}_3(PO_4)_2(OH)_6$	7.28	*a*	16.85	90	90	120	$R\bar{3}m$	(28)
Benyacarite	$(H_2O,K)_2TiMn^{2+}_2(Fe^{3+},Ti)_2(PO_4)_4(OH)_2(H_2O)_{14}$	10.561(5)	20.585(8)	12.516(2)	90	90	90	*Pbca*	(29)
Beraunite	$Fe^{2+}Fe^{3+}_5(PO_4)_4(OH)_5(H_2O)_6$	20.646(5)	5.129(7)	19.213(5)	90	93.62(7)	90	*C2/c*	(30)
Bergenite	$Ba[(UO_2)_3O_2(PO_4)_2](H_2O)_{6.5}$	22.32	17.19	20.63	90	93.0	90	$P2_1/c$	(31)
Berlinite	$[Al(PO_4)]$	4.943(0)	*a*	10.948(0)	90	90	120	$P3_12$	(32)
Bermanite	$Mn^{2+}[Mn^{3+}(PO_4)(OH)]_2(H_2O)_4$	5.446(3)	19.250(10)	5.428(3)	90	110.3(0)	90	$P2_1$	(33)
Bertossaite	$CaLi_2[Al(PO_4)(OH)]_4$	11.48(1)	15.73(2)	7.23(1)	90	90	90	*I*aa*	(34)
Beryllonite	$Na[BePO_4]$	8.178(3)	7.818(2)	14.114(6)	90	90	90	$P2_1/n$	(35)
Beusite	$(Mn^{2+},Fe^{2+})_3(PO_4)_2$	8.757(3)	11.381(4)	6.136(1)	90	99.1(0)	90	$P2_1/c$	(36)
Biphosphammite	$(NH_4)H_2PO_4$	7.514(0)	*a*	7.539(1)	90	90	90	$I\bar{4}2d$	(37)
Bjarebyite	$BaMn_2Al_2(OH)_3(PO_4)_3$	8.930(14)	12.073(24)	4.917(9)	90	100.2(1)	90	$P2_1/m$	(38)
Bleasdaleite	$(Ca,Fe^{3+})_2Cu^{2+}_5(Bi,Cu^{2+})(PO_4)_4(H_2O,OH,Cl)_{13}$	14.200(7)	13.832(7)	14.971(10)	90	102.08(8)	90	*C2/m*	(39)
Bobfergusonite	$Na_2Mn^{2+}_5Fe^{3+}Al(PO_4)_6$	12.776(2)	12.488(2)	11.035(2)	90	97.2(0)	90	$P2_1/n$	(40)
Bobierrite	$Mg_3(PO_4)_2(H_2O)_8$	4.667(1)	27.926(8)	10.067(3)	90	105.0(0)	90	*C2/c*	(41)
Böggildite	$Sr_2Na_2Al_2(PO_4)F_9$	5.251(3)	10.464(5)	18.577(9)	90	107.5(0)	90	$P2_1/c$	(42)
Bolivarite	$Al_2(PO_4)(OH)_3(H_2O)_4$	Amorphous	–	–	–	–	–	–	(43)
Bonshtedtite	$Na_3Fe^{2+}(PO_4)(CO_3)$	8.921	6.631	5.151	90	90.42	90	$P2_1/m$	(44)
Brabantite	$CaTh(PO_4)_2$	6.726(6)	6.933(5)	6.447(12)	90	103.89(3)	90	$P2_1$	(45)
Bradleyite	$Na_3Sr(PO_4)(CO_3)$	9.187(3)	5.279(1)	6.707(2)	90	90	90	$P2_1$	(46)
Brazilianite	$NaAl_3(PO_4)_2(OH)_4$	11.233(6)	10.142(5)	7.097(4)	90	97.4(0)	90	$P2_1/n$	(47)
Brendelite	$Bi^{3+}Fe^{3+}O_2(OH)(PO_4)$	12.278(2)	3.185(1)	6.899(1)	90	111.0(0)	90	*C2/m*	(48)
Brianite	$Na_2Ca[Mg(PO_4)_2]$	9.120(3)	5.198(2)	13.370(4)	90	90.8(0)	90	$P2_1/c$	(49)
Brockite	$(Ca,Th,REE)(PO_4)(H_2O)$	6.98(3)	6.98(3)	6.40(3)	90	90	90	*Aa*	(50)
Brushite	$Ca(PO_3\{OH\})(H_2O)_2$	5.812(2)	15.180(3)	6.239(2)	90	116.4(0)	90	*Ia*	(51)
Buchwaldite	$NaCa(PO_4)$	20.397(10)	5.412(4)	9.161(5)	90	90	90	$Pn2_1a$	(52)
Burangaite	$Na_2Fe^{2+}_2Al_{10}(PO_4)_8(OH)_{12}(H_2O)_4$	25.099(2)	5.049(1)	13.438(1)	90	110.9(0)	90	*C2/c*	(53)
Cacoxenite	$Fe^{3+}_{25}(PO_4)_{17}O_6(OH)_{12}(H_2O)_{75}$	27.559(1)	*a*	10.550(1)	90	90	120	$P6_3/m$	(54)

APPENDIX A continued

Mineral Name	Formula	*a* (Å)	*b* (Å)	*c* (Å)	α (°)	β (°)	γ (Å)	Space Group	Ref.
Canaphite	$CaNa_2P_2O_7(H_2O)_4$	5.673(4)	8.480(10)	10.529(5)	90	106.13(6)	90	*Pc*	(55)
Cassidyite	$Ca_2[Ni(PO_4)_2(H_2O)_2]$	5.71	6.73	5.41	96.83	107.36	104.58	$P\bar{1}$	(56)
Chalcosiderite	$Cu^{2+}Fe^{3+}{}_6(PO_4)_4(OH)_8(H_2O)_4$	7.653(4)	7.873(4)	10.190(4)	67.6(0)	69.2(0)	64.9(0)	$P\bar{1}$	(57)
Cheralite-(Ce)	$Ce(PO_4)$	6.747(2)	6.960(2)	6.453(1)	90	103.7(0)	90	$P2_1/n$	(58)
Chernikovite	$(H_3O)[(UO_2)(PO_4)]_2(H_2O)_8$	7.030(6)	*a*	9.034(8)	90	90	90	*P4/nmm*	(59)
Childrenite	$Mn^{2+}[Al(PO_4)(OH)_2(H_2O)]$	10.395(1)	13.394(1)	6.918(1)	90	90	90	*Bba2*	(60)
Chladniite	$Na_2CaMg_7(PO_4)_6$	14.967(2)	*a*	42.595(4)	90	90	120	$R\bar{3}$	(61)
Chlorapatite	$Ca_5(PO_4)_3Cl$	9.620(1)	*a*	6.776(1)	90	90	120	$P6_3/m$	(62)
Churchite-(Y)	$Y(PO_4)(H_2O)_2$	5.578(1)	15.006(3)	6.275(2)	90	117.8(0)	90	*I2/a*	(63)
Clinophosinaite	$Na_3Ca(SiO_3)(PO_4)$	7.303(2)	12.201(5)	14.715(4)	90	91.9	90	*P2/c*	(64)
Coconinoite	$Fe^{3+}{}_2Al_2(UO_2)_6(PO_4)_4(SO_4)(OH)_2(H_2O)_{20}$	12.50	12.97	23.00	90	106.6	90	*C2/c*	(65)
Coeruleolactite	$CaAl_6(PO_4)_4(OH)_8(H_2O)_{4\text{-}5}$	Existence dubious		–	–	–	–	–	(2)
Collinsite	$Ca_2[Mg(PO_4)_2(H_2O)_2]$	5.734(1)	6.780(1)	5.441(1)	97.3(0)	108.6(0)	107.3(0)	$P\bar{1}$	(66)
Corkite	$PbFe^{3+}{}_3(SO_4)(PO_4)(OH)_6$	7.280(1)	*a*	16.821(1)	90	90	120	*R3m*	(67)
Cornetite	$Cu^{2+}{}_3PO_4(OH)_3$	10.854(1)	14.053(3)	7.086(2)	90	90	90	*Pbca*	(68)
Crandallite	$CaAl_3(PO_4)_2(OH)_5(H_2O)$	7.006(15)	*a*	16.192(32)	90	90	120	$R\bar{3}m$	(69)
Crawfordite	$Na_3Sr(PO_4)(CO_3)$	9.187	6.707	5.279	90	90	90	$P2_1$	(70)
Curetonite	$BaAl(PO_4)(OH)F$	6.977(2)	12.564(4)	5.223(1)	90	102.2(0)	90	$P2_1/n$	(71)
Cyrilovite	$NaFe^{3+}{}_3(OH)_4(PO_4)_2(H_2O)_2$	7.3255(4)	*a*	19.328(2)	90	90	90	$P4_12_12$	(72)
Deloneite-(Ce)	$NaCr_2SrCe(PO_4)_3F$	9.51	*a*	7.01	90	90	120	*P3*	(73)
Delvauxite	$CaFe^{3+}{}_4(PO_4)_2(OH)_8(H_2O)_{4\text{-}6}$	Amorphous	–	–	–	–	–	–	(74)
Destinezite	$Fe^{3+}{}_2(PO_4)(SO_4)(OH)(H_2O)_6$	9.570(1)	9.716(1)	7.313(1)	98.7(0)	107.9(0)	63.9(0)	$P\bar{1}$	(75)
Dewindtite	$Pb^{2+}{}_3[H(UO_2)_3O_2(PO_4)_2]_2(H_2O)_{12}$	16.031(6)	17.264(6)	13.605(2)	90	90	90	*Bmmb*	(76)
Dickinsonite	$(Na,Ca)_5(Mn,Fe,Mg)_{14}Al(PO_4)_{12}(OH)_2$	24.940(6)	10.131(4)	16.722(2)	90	105.6(0)	90	*A2/a*	(77)
Dittmarite	$(NH_4)Mg(PO_4)(H_2O)$	5.606	8.758	4.788	90	90	90	$Pmn2_1$	(78)
Dorfmanite	$Na_2(PO_3\{OH\})(H_2O)_2$	16.872(9)	10.359(4)	6.599(3)	90	90	90	*Pbca*	(79)
Drugmanite	$Pb^{2+}{}_2Fe^{3+}H(PO_4)_2(OH)_2$	11.111(5)	7.986(5)	4.643(3)	90	90.4(0)	90	$P2_1/a$	(80)

APPENDIX A continued

Mineral Name	Formula	*a* (Å)	*b* (Å)	*c* (Å)	α (°)	β (°)	γ (Å)	Space Group	Ref.
Dufrénite	$Fe^{2+}Fe^{3+}_5(PO_4)_3(OH)_5(H_2O)_2$	25.840(20)	5.126(3)	13.780(10)	90	111.2(1)	90	*C*2/*c*	(81)
Dumontite	$Pb^{2+}_2[(UO_2)_3(PO_4)_2O_2](H_2O)_5$	8.118(6)	16.819(8)	6.983(3)	90	109.0(0)	90	$P2_1/m$	(82)
Earlshannonite	$Mn^{2+}[Fe^{3+}(PO_4)(OH)]_2(H_2O)_4$	9.910(13)	9.669(8)	5.455(9)	90	93.95(9)	90	$P2_1/c$	(83)
Ehrleite	$Ca_2ZnBe(PO_4)_2(PO_3OH)(H_2O)_4$	7.130(4)	7.430(4)	12.479(9)	94.31(5)	102.07(4)	82.65(4)	$P\bar{1}$	(84)
Englishite	$Na_2K_3Ca_{10}Al_{15}(PO_4)_{21}(OH)_7(H_2O)_{26}$	38.43(2)	11.86	20.67	90	111.27	90	*A*2/*a*	(85)
Eosphorite	$Fe^{2+}[Al(PO_4)(OH)_2(H_2O)]$	10.445(1)	13.501(2)	6.970(30)	90	90	90	*Bba*2	(86)
Ercitite	$Na[Mn^{3+}(PO_4)(OH)](H_2O)_2$	5.362(5)	19.89(1)	5.362(5)	90	108.97(8)	90	$P2_1/n$	(87)
Evansite	$Al_3(PO_4)(OH)_6(H_2O)_8$	Amorphous	–	–	–	–	–	–	(43)
Eylettersite	$(Th,Pb)_{1-x}Al_3(PO_4,SiO_4)_2(OH)_6$	6.99	*a*	16.70	90	90	90	$R\bar{3}m$	(88)
Fairfieldite	$Ca_2[Mn^{2+}(PO_4)_2(H_2O)_2]$	5.790(10)	6.570(10)	5.510(10)	102.3(2)	108.7(2)	90.3(2)	$P\bar{1}$	(89)
Farringtonite	$Mg_3(PO_4)_2$	7.596(1)	8.231(1)	5.077(1)	90	94.1(0)	90	$P2_1/n$	(90)
Faustite	$ZnAl_6(PO_4)_4(OH)_8(H_2O)_4$	7.419(2)	7.629(3)	9.905(3)	69.17(2)	69.88(2)	64.98(2)	$P\bar{1}$	(91)
Fermorite	$Ca_4Sr(PO_4)_3(OH)$	9.594(2)	9.597(2)	6.975(2)	90	90	120(0)	$P2_1/m$	(92)
Ferrisicklerite	$Li(Fe^{3+},Mn^{2+})(PO_4)$	5.918	10.037	4.798	90	90	90	*Pmnb*	(93)
Ferrostrunzite	$Fe^{2+}[Fe^{3+}(PO_4)(OH)(H_2O)]_2(H_2O)_4$	10.23(2)	9.77(3)	7.37(1)	89.65(16)	98.28(12)	117.26(16)	$P\bar{1}$	(94)
Fillowite	$Na_2CaMn^{2+}_7(PO_4)_6$	15.282(2)	*a*	43.507(3)	90	90	120	$R\bar{3}$	(95)
Florencite-(Ce)	$CeAl_3(PO_4)_2(OH)_6$	6.972(2)	*a*	16.261(6)	90	90	120	$R\bar{3}m$	(96)
Florencite-(La)	$LaAl_3(PO_4)_2(OH)_6$	6.987(2)	*a*	16.248(6)	90	90	120	$R\bar{3}m$	(97)
Florencite-(Nd)	$NdAl_3(PO_4)_2(OH)_6$	–	–	–	–	–	–	–	(98)
Fluellite	$Al_2(PO_4)F_2(OH)(H_2O)_7$	8.546(8)	11.222(5)	21.158(5)	90	90	90	*Fddd*	(99)
Fluorapatite	$Ca_5(PO_4)_3F$	9.367	*a*	6.884	90	90	90	$P6_3/m$	(62)
Fluorcaphite	$CaSrCa_3(PO_4)_3F$	9.485	*a*	7.000	90	90	120	$P6_3$	(100)
Foggite	$Ca[Al(PO_4)(OH)_2](H_2O)$	9.270(2)	21.324(7)	5.190(2)	90	90	90	$A2_122$	(101)
Francoanellite	$K_3Al_5(PO_3\{OH\})_6(PO_4)_2(H_2O)_{12}$	8.690(2)	*a*	82.271(13)	90	90	120	$R\bar{3}c$	(102)
Françoisite-(Nd)	$Nd[(UO_2)_3(PO_4)_2O(OH)](H_2O)_6$	9.298(2)	15.605(4)	13.668(2)	90	112.8(0)	90	$P2_1/c$	(103)
Fransoletite	$Ca_3[Be_2(PO_4)_2(PO_3\{OH\})_2](H_2O)_4$	7.348(1)	15.052(3)	7.068(1)	90	96.5(0)	90	$P2_1/a$	(104)
Frondellite	$Mn^{2+}Fe^{3+}_4(PO_4)_3(OH)_5$	13.89	17.01	5.21	90	90	90	$B22_12$	(105)

APPENDIX A continued

Mineral Name	Formula	*a* (Å)	*b* (Å)	*c* (Å)	α (°)	β (°)	γ (Å)	Space Group	Ref.
Furongite	$Al_2(OH)_2[(UO_2)(PO_4)_2](H_2O)_8$	17.87	14.18	12.18	67.8	77.5	79.9	$P\bar{1}$	(106)
Gainesite	$NaKZr_2[Be(P_4O_{15}]$	6.567(3)	*a*	17.119(5)	90	90	90	$I4_1/amd$	(107)
Galileiite	$NaFe^{2+}{}_4(PO_4)_3$	14.98	*a*	41.66	90	90	120	$R\bar{3}$	(108)
Gatehouseite	$Mn^{2+}{}_5(OH)_4(PO_4)_2$	9.097(2)	5.693(2)	18.002(10)	90	90	90	$P2_12_12_1$	(109)
Gatumbaite	$CaAl_2(PO_4)_2(OH)_2$	6.907(2)	5.095(2)	10.764(3)	90.68(8)	99.17(8)	90.17(8)	$P2/m$	(110)
Girvasite	$NaCa_2Mg_3(PO_4)_2[PO_2(OH)_2](CO_3)(OH)_2(H_2O)_4$	6.522(3)	12.250(30)	21.560(20)	90	89.5(0)	90	$P2_1/c$	(111)
Gladiusite	$Fe^{2+}{}_4Fe^{3+}{}_2(PO_4)(OH)_{11}(H_2O)$	16.950(2)	11.650(1)	6.2660(6)		90.000(4)		$P2_1/m$	(112)
Goedkenite	$Sr_2[Al(PO_4)_2(OH)]$	8.45(2)	5.74(2)	7.26(2)	90	113.7(1)	90	$P2_1/m$	(113)
Gorceixite	$BaAl_3(PO_4)(PO_3OH)(OH)_6$	7.036(0)	*a*	17.282(0)	90	90	120	$R3m$	(114)
Gordonite	$Mg[Al_2(PO_4)_2(OH)_2(H_2O)_2](H_2O)_4(H_2O)_2$	5.246(2)	10.532(5)	6.975(3)	107.5(0)	111.0(0)	72.2(0)	$P\bar{1}$	(115)
Gormanite	$Fe^{2+}{}_3Al_4(PO_4)_4(OH)_6(H_2O)_2$	11.76(1)	5.10(1)	13.57(1)	90.68(8)	99.17(8)	90.17(8)	$P\bar{1}$	(116)
Goyazite	$SrAl_3(PO_4)_2(OH)_5(H_2O)$	7.021(3)	*a*	16.505(15)	90	90	120	$R\bar{3}m$	(117)
Graftonite	$(Fe^{2+},Mn^{2+},Ca)_3(PO_4)_2$	8.910(10)	11.580(10)	6.239(8)	90	98.9(1)	90	$P2_1/c$	(118)
Grattarolaite	$Fe^{3+}{}_3O_3(PO_4)$	7.994(4)	*a*	6.855(4)	90	90	120	$R3m$	(119)
Grayite	$ThCa(PO_4)_2(H_2O)_2$	6.957	*a*	6.396	90	90	120	$P6_222$	(120)
Griphite	$Na_4Ca_6(Mn,Fe^{2+},Mg)_{19}Li_2Al_8(PO_4)_{24}F_8$	12.205(8)	*a*	*a*	90	90	90	$Pa\bar{3}$	(121)
Hagendorfite	$(Na,Ca)[Mn^{2+}(Fe^{2+},Mg,Fe^{3+})_2(PO_4)_3]$	11.92	12.59	6.52	90	114.7	90	$C2/c$	(122)
Haigerachite	$KFe^{3+}{}_3(PO_2\{OH\}_2)_6(PO_3\{OH\})_2(H_2O)_4$	16.95	9.59	17.57	90	90.85	90	$C2/c$	(123)
Hannayite	$Mg_3(NH_4)_2(PO_3\{OH\})_4(H_2O)_8$	10.728	7.670	6.702	97.87	96.97	104.74	$P\bar{1}$	(124)
Harrisonite	$CaFe^{2+}{}_6(SiO_4)_2(PO_4)_2$	6.248(1)	*a*	26.802(7)	90	90	120	$R\bar{3}m$	(125)
Heneuite	$CaMg_5(CO_3)(PO_4)_3(OH)$	6.311(1)	10.843(1)	8.676(1)	95.0(0)	93.4(0)	101.0(0)	$P\bar{1}$	(126)
Hentschelite	$Cu^{2+}Fe^{3+}{}_2(OH)_2(PO_4)_2$	6.984(3)	7.786(3)	7.266(3)	90	117.68(2)	90	$P2_1/n$	(127)
Herderite	$Ca[BePO_4F]$	9.800	7.680	4.800	90	90	90	$P2_1/a$	(128)
Heterosite	$Fe^{3+}(PO_4)$	5.830(10)	9.760(10)	4.769(5)	90	90	90	$Pmnb$	(129)
Hinsdalite	$Pb^{2+}[Al_3(OH)_6(PO_4)(SO_4)]$	7.029	*a*	16.789	90	90	120	$R\bar{3}m$	(130)
Holtedahlite	$Mg_{12}(PO_3\{OH\})(PO_4)_5(OH)_6$	11.203(3)	*a*	4.977(1)	90	90	90	$P31m$	(131)
Hopeite	$Zn_3(PO_4)_2(H_2O)_4$	10.597(3)	18.318(8)	5.031(1)	90	90	90	$Pnma$	(132)

APPENDIX A continued

Mineral Name	Formula	*a* (Å)	*b* (Å)	*c* (Å)	α (°)	β (°)	γ (Å)	Space Group	Ref.
Hotsonite	$Al_5(PO_4)(SO_4)(OH)_{10}$	11.29(6)	11.66(6)	10.55(7)	112.54(5)	107.52(5)	64.45(5)	$P\bar{1}$	(133)
Hureaulite	$Mn^{2+}{}_5(PO_3\{OH\})_2(PO_4)_2(H_2O)_4$	17.594(10)	9.086(5)	9.404(5)	90	96.67(8)	90	*C2/c*	(134)
Hurlbutite	$Ca[Be_2P_2O_8]$	8.306(1)	8.790(1)	7.804(1)	90	89.5(0)	90	$P2_1/a$	(135)
Hydroxylapatite	$Ca_5(PO_4)_3(OH)$	9.418	*a*	6.875	90	90	120	$P6_3/m$	(62)
Hydroxylherderite	$Ca[BePO_4(OH)]$	9.789(2)	7.661(1)	4.804(1)	90	90.02(1)	90	$P2_1/a$	(136)
Isokite	$Ca[Mg(PO_4)F]$	6.909	8.746	6.518	90	112.2	90	*A2/a*	(137)
Jagowerite	$Ba[Al(PO_4)(OH)]_2$	6.049(2)	6.964(3)	4.971(2)	116.51(4)	86.06(4)	112.59(3)	$P\bar{1}$	(138)
Jahnsite	$CaMnMg_2[Fe^{3+}(PO_4)_2(OH)]_2(H_2O)_8$	14.940(20)	7.140(10)	9.930(10)	90	110.16(8)	90	*P2/a*	(139)
Jahnsite-(CaMnMn)	$CaMn^{2+}Mn^{2+}{}_2Fe^{3+}{}_2(PO_4)_4(OH)_2(H_2O)_8$	14.887(8)	7.152(7)	9.966(6)	90	109.77(5)	90	*P2/a*	(140)
Johnsomervilleite	$Na_{10}Ca_6Mg_{18}(Fe^{2+},Mn^{2+})_{25}(PO_4)_{36}$	15.00	*a*	42.75	90	90	120	Hex	(141)
Johntomaite	$BaFe^{2+}{}_2Fe^{3+}{}_2(PO_4)_3(OH)_3$	9.199(9)	12.359(8)	5.004(2)	90	100.19(6)	90	$P2_1/m$	(142)
Johnwalkite	$KMn^{2+}{}_2[Nb(PO_4)_2O_2](H_2O)_2$	7.516(4)	10.023(8)	6.502(4)	90	90	90	$Pb2_1m$	(143)
Juonniite	$CaMgSc(PO_4)_2(OH)(H_2O)_4$	15.03	18.95	7.59	90	90	90	*Pbca*	(144)
Kanonerovite	$MnNa_3P_3O_{10}(H_2O)_{12}$	14.71(1)	9.33(1)	15.13(2)	90	89.8(1)	90	$P2_1/n$	(145)
Kastningite	$Mn(H_2O)_4[Al_2(OH)_2(H_2O)_2(PO_4)_2](H_2O)_2$	10.205(1)	10.504(1)	7.010(1)	90.38(1)	110.10(1)	71.82(1)	$P\bar{1}$	(146)
Keckite	$CaMn^{2+}{}_2Fe^{3+}{}_3(PO_4)_4(OH)_3(H_2O)_2$	15.02	7.19	19.74	90	110.5	90	$P2_1/a$	(147)
Kingite	$Al_3(PO_4)_2(OH)_3(H_2O)_9$	9.15(1)	10.00(1)	7.24(2)	98.6	93.6	93.2	$P\bar{1}$	(148)
Kintoreite	$Pb^{2+}Fe^{3+}{}_3(PO_4)_2(OH)_5(H_2O)$	7.331(1)	*a*	16.885(2)	90	90	120	$R\bar{3}m$	(149)
Kipushite	$[Cu^{2+}{}_5Zn(PO_4)_2](OH)_6(H_2O)$	12.197(2)	9.156(2)	10.667(2)	90	96.8(0)	90	$P2_1/c$	(150)
Kolbeckite	$[Sc(PO_4)(H_2O)_2]$	5.418	10.25	8.893	90	90.7	90	$P2_1/n$	(151)
Koninckite	$Fe^{3+}(PO_4)(H_2O)_3$	11.95	*a*	14.52	90	90	90	Tetragonal	(152)
Kosnarite	$KZr_2(PO_4)_3$	8.687(2)	*a*	23.877(7)	90	90	120	$R\bar{3}c$	(153)
Kovdorskite	$Mg_2(PO_4)(OH)(H_2O)_3$	10.350(40)	12.900(40)	4.730(20)	90	102.0(5)	90	$P2_1/a$	(154)
Krasnovite	$BaAl(PO_4)(OH)_2(H_2O)$	8.939	5.669	11.073	90	90	90	*Pnna*/*Pnnn*	(155)
Kribergite	$Al_5(PO_4)_3(SO_4)(OH)_4(H_2O)_4$	18.13(3)	13.5(2)	7.50(1)	70.50	117.87	136.58	$P\bar{1}$	(133)
Kryzhanovskite	$Mn^{2+}Fe^{3+}{}_2(PO_4)_2(OH)_2(H_2O)$	9.450(2)	10.013(2)	8.179(2)	90	90	90	*Pbna*	(156)
Kulanite	$BaFe^{2+}{}_2Al_2(PO_4)_3(OH)_3$	9.014(1)	12.074(1)	4.926(1)	90	100.48(1)	90	$P2_1/m$	(157)

APPENDIX A continued

Mineral Name	Formula	*a* (Å)	*b* (Å)	*c* (Å)	α (°)	β (°)	γ (Å)	Space Group	Ref.
Lacroixite	$Na[Al(PO_4)F]$	6.414(2)	8.207(2)	6.885(2)	90	115.5	90	*C2/c*	(158)
Landesite	$Fe^{3+}Mn^{2+}{}_2(PO_4)_2(OH)(H_2O)_2$	9.458(3)	10.185(2)	8.543(2)	90	90	90	*Pbna*	(159)
Laueite	$Mn^{2+}[Fe^{3+}{}_2(PO_4)_2(OH)_2(H_2O)_2](H_2O)_4(H_2O)_2$	5.280	10.660	7.140	107.9	111.0	71.1	$P\bar{1}$	(160)
Lazulite	$Mg[Al(PO_4)(OH)]_2$	7.144(1)	7.278(1)	7.228(1)	90	120.5(0)	90	$P2_1/c$	(161)
Lehnerite	$Mn^{2+}[(UO_2)(PO_4)]_2(H_2O)_8$	7.04(2)	17.16(4)	6.95(2)	90	90.18	90	$P2_1/n$	(162)
Leucophosphite	$K[Fe^{3+}{}_2(PO_4)_2(OH)(H_2O)](H_2O)_2$	9.782	9.658	9.751	90	102.24	90	$P2_1/n$	(163)
Libethenite	$Cu^{2+}{}_2(PO_4)(OH)$	8.071(2)	8.403(4)	5.898(3)	90	90	90	*Pnnm*	(164)
Lipscombite	$Fe^{2+}Fe^{3+}{}_2(PO_4)_2(OH)_2$	7.310	*a*	13.212	90	90	90	$P4_32_12_1$	(165)
Lithiophosphate	$Li_3(PO_4)$	10.490(3)	6.120(2)	4.9266(7)	90	90	90	*Pnma*	(166)
Lithiophyllite	$LiMn^{2+}(PO_4)$	6.100(20)	10.460(30)	4.744(10)	90	90	90	*Pmnb*	(167)
Lomonosovite	$Na_5Ti^{4+}{}_2(Si_2O_7)(PO_4)O_2$	5.440	7.163	14.830	99.0	106.0	90	$P\bar{1}$	(168)
Ludjibaite	$Cu^{2+}{}_5(PO_4)_2(OH)_4$	4.445(1)	5.873(1)	8.668(3)	103.6(0)	90.3(0)	93.0(0)	$P\bar{1}$	(169)
Ludlamite	$Fe^{2+}{}_3(PO_4)_2(H_2O)_4$	10.541(10)	4.638(8)	9.285(10)	90	100.7(1)	90	$P2_1/a$	(170)
Lulzacite	$Sr_2Fe^{2+}Fe^{2+}{}_2Al_4(PO_4)_4(OH)_{10}$	5.457(1)	9.131(2)	9.769(2)	108.47(3)	91.72(3)	97.44(3)	$P\bar{1}$	(171)
Lüneburgite	$Mg_3B_2(OH)_6(PO_4)_2(H_2O)_6$	6.347(1)	9.803(1)	6.298(1)	84.5(0)	106.4(0)	96.4(0)	$P\bar{1}$	(172)
Lun'okite	$Mn^{2+}{}_2Mg_2[Al(PO_4)_2(OH)]_2(H_2O)_8$	14.95	18.71	6.96	90	90	90	*Pbca*	(173)
Machatschkiite	$Ca_6(AsO_4)(AsO_3\{OH\})_3(PO_4)(H_2O)_{15}$	15.127(2)	*a*	22.471(3)	90	90	120	*R3c*	(174)
Maghagendorfite	$Na[Mn^{2+}MgFe^{2+}{}_2(PO_4)_3]$	–	–	–	–	–	–	–	(175)
Magniotriplite	$Mg_2(PO_4)F$	12.035(5)	6.432(4)	9.799(2)	90	108.1(0)	90	*I2/a*	(176)
Mahlmoodite	$FeZr(PO_4)_2(H_2O)_4$	9.12(2)	5.42(1)	19.17(2)	90	94.8(1)	90	$P2_1/c$	(177)
Mangangordonite	$Mn^{2+}[Al_2(PO_4)_2(OH)_2(H_2O)_6](H_2O)_2$	5.257(3)	10.363(4)	7.040(3)	105.4(0)	113.1(0)	78.7(0)	$P\bar{1}$	(115)
Manganosegelerite	$Mn^{2+}Mn^{2+}Fe^{3+}(PO_4)_2(OH)(H_2O)_4$	14.89	18.79	7.408	90	90	90	*Pbca*	(178)
Marićite	$NaFe^{2+}(PO_4)$	6.861(1)	8.987(1)	5.045(1)	90	90	90	*Pmnb*	(179)
Mcauslanite	$Fe^{2+}{}_3Al_2H(PO_4)_4F(H_2O)_{18}$	10.055(5)	11.568(5)	6.888(5)	105.84(6)	93.66(6)	106.47(5)	$P\bar{1}$	(180)
Mccrillisite	$NaCs[BeZr_2(PO_4)_4](H_2O)_{1\text{-}2}$	6.573(2)	*a*	17.28(2)	90	90	90	$I4_1/amd$	(181)
Melkovite	$CaFe^{3+}H_6(MoO_4)_4(PO_4)(H_2O)_6$	17.46	18.48	10.93	90	94.5	90	Mono	(182)
Mélonjosephite	$Ca[Fe^{2+}\ Fe^{3+}(PO_4)_2(OH)]$	9.542(1)	10.834(1)	6.374(2)	90	90	90	*Pbam*	(183)

APPENDIX A continued

Mineral Name	Formula	*a* (Å)	*b* (Å)	*c* (Å)	α (°)	β (°)	γ (Å)	Space Group	Ref.
Messelite	$Ca_2[Fe^{2+}(PO_4)_2(H_2O)_2]$	5.95(2)	6.52(2)	5.45(2)	102.3(4)	107.5(4)	90.8(2)	$P\bar{1}$	(184)
Meta-ankoleite	$K(UO_2)(PO_4)(H_2O)_3$	6.994(0)	*a*	17.784(0)	90	90	90	*P4/ncc*	(185)
Meta-autunite	$Ca[(UO_2)(PO_4)]_2(H_2O)_5$	6.960(10)	*a*	8.400(20)	90	90	90	*P4/nmm*	(186)
Metaswitzerite	$Mn^{2+}{}_3(PO_4)_2(H_2O)_4$	8.496(3)	13.173(3)	17.214(4)	90	96.7(0)	90	$P2_1/c$	(187)
Metatorbernite	$Cu^{2+}[(UO_2)(PO_4)]_2(H_2O)_8$	6.972(1)	*a*	17.277	90	90	90	*P4/n*	(188)
Meta-uranocircite	$Ba[(UO_2)(PO_4)]_2(H_2O)_6$	9.789(3)	9.882(3)	16.868(3)	90	90	89.9(0)	$P2_1/a$	(189)
Metavanmeerscheite	$U(OH)_4[(UO_2)_3(PO_4)(OH)_2](H_2O)_2$	34.18	33.88	14.074	90	90	90	*Fddd*	(190)
Metavariscite	$[Al(PO_4)(H_2O)_2]$	5.178(2)	9.514(2)	8.454(2)	90	90.35(2)	90	$P2_1/n$	(191)
Metavauxite	$Fe^{2+}(H_2O)_6[Al(PO_4)(OH)(H_2O)]_2(H_2O)_6$	10.220	9.560	6.940	90	97.9	90	$P2_1/c$	(192)
Metavivianite	$Fe^{2+}{}_3(PO_4)_2(H_2O)_8$	7.840(10)	9.110(10)	4.670(10)	95.0(0)	96.9(0)	107.7(0)	$P\bar{1}$	(193)
Meurigite	$KFe^{3+}{}_7(PO_4)_5(OH)_7(H_2O)_8$	29.52(4)	5.249(6)	18.26(1)	90	109.27(7)	90	*C2/m*	(194)
Millisite	$NaCaAl_6(PO_4)_4(OH)_9(H_2O)_3$	7.00	*a*	19.07	90	90	90	$P4_12_12$	(195)
Minyulite	$K[Al_2(PO_4)_2F(H_2O)_4]$	9.337(5)	9.740(5)	5.522(3)	90	90	90	*Pba2*	(196)
Mitridatite	$Ca_2[Fe^{3+}{}_3(PO_4)_3O_2](H_2O)_3$	17.553(2)	19.354(3)	11.248(2)	90	95.84(1)	90	*Aa*	(197)
Mitryaevaite	$Al_5(PO_4)_2(PO_3\{OH\})_2F_2(OH)_2(H_2O)_8(H_2O)_{6.5}$	6.918(1)	10.127(2)	10.296(2)	77.036(3)	73.989(4)	76.272(4)	$P\bar{1}$	(198)
Monazite-(Ce)	$Ce(PO_4)$	6.7902(10)	7.0203(6)	6.4674(7)	90	103.38(1)	90	$P2_1/n$	(199)
Monetite	$CaH[PO_4]$	6.910(1)	6.627(2)	6.998(2)	96.34(2)	103.82(2)	88.33(2)	$P\bar{1}$	(200)
Montebrasite	$Li[Al(PO_4)(OH)]$	6.713(1)	7.708(1)	7.019(1)	91.31(1)	117.93(1)	91.77(1)	$C\bar{1}$	(8)
Montgomeryite	$Ca_4MgAl_4(PO_4)_6(OH)_4(H_2O)_{12}$	10.023(1)	24.121(3)	6.243(1)	90	91.55(1)	90	*C2/c*	(201)
Moraesite	$[Be_2(PO_4)(OH)](H_2O)_4$	8.553(6)	12.319(6)	7.155(8)	90	97.9(1)	90	*C2/c*	(202)
Moreauite	$Al_3(UO_2)(PO_4)_3(OH)_2(H_2O)_{13}$	23.41	21.44	18.34	90	92.0	90	$P2_1/c$	(203)
Morinite	$Ca_2Na[Al_2(PO_4)_2F_4(OH)(H_2O)_2]$	9.454(3)	10.692(4)	5.444(2)	90	105.46(2)	90	$P2_1/m$	(204)
Mrázekite	$Bi^{3+}{}_2Cu^{2+}{}_3(OH)_2O_2(PO_4)_2(H_2O)_2$	9.065(1)	6.340(1)	21.239(3)	90	101.6(0)	90	$P2_1/n$	(205)
Mundite	$Al(OH)[(UO_2)_3(OH)_2(PO_4)_2](H_2O)_{5.5}$	17.08	30.98	13.76	90	90	90	*Pmcn*	(206)
Mundrabillaite	$(NH_4)_2Ca(PO_3\{OH\})_2(H_2O)$	8.643	8.184	6.411	90	98.0	90	*P2/m*	(207)
Nabaphite	$NaBa(PO_4)(H_2O)_9$	10.712(1)	*a*	*a*	90	90	90	$P2_13$	(208)
Nacaphite	$Na(Na\ Ca)(PO_4)F$	5.3232(2)	12.2103(4)	7.0961(2)	90.002(1)	89.998(1)	89.965(1)	$P\bar{1}$	(209)

APPENDIX A continued

Mineral Name	Formula	*a* (Å)	*b* (Å)	*c* (Å)	α (°)	β (°)	γ (Å)	Space Group	Ref.
Nahpoite	$Na_2H[PO_4]$	5.451(1)	6.847(2)	5.473(1)	90	116.33(8)	90	$P2_1/m$	(210)
Nalipoite	$NaLi_2(PO_4)$	6.884(2)	9.976(4)	4.927(2)	90	90	90	*Pmnb*	(211)
Nastrophite	$NaSr(PO_4)(H_2O)_9$	10.559(1)	*a*	*a*	90	90	90	$P2_13$	(212)
Natrodufrénite	$NaFe^{2+}Fe^{3+}{}_5(PO_4)_4(OH)_6(H_2O)_2$	25.83	5.150	13.772	90	111.53	90	*C2/c*	(213)
Natromontebrasite	$Na[Al(PO_4)(OH)]$	5.266	7.174	5.042	112.3	97.70	67.13	$P\bar{1}$	(214)
Natrophilite	$NaMn^{2+}(PO_4)$	10.523(5)	4.987(2)	6.312(3)	90	90	90	*Pnam*	(215)
Natrophosphate	$Na_7(PO_4)_2F(H_2O)_{19}$	27.712(2)	*a*	*a*	90	90	90	$Fd\bar{3}c2$	(216)
Nefedovite	$Na_5Ca_4(PO_4)_4F$	11.644(2)	*a*	5.396(1)	90	90	90	$I\bar{4}$	(217)
Newberyite	$[Mg(PO_3\{OH\})(H_2O)_3]$	10.215(2)	10.681(2)	10.014(2)	90	90	90	*Pbca*	(218)
Niahite	$(NH_4)Mn^{2+}(PO_4)(H_2O)$	5.68	8.78	4.88	90	90	90	$Pmn2_1$	(219)
Ningyoite	$(U,Ca,Ce,Fe)_2(PO_4)_2(H_2O)_{1-2}$	6.78	12.10	6.38	90	90	90	*P222*	(220)
Nissonite	$Cu^{2+}{}_2Mg_2(PO_4)_2(OH)_2(H_2O)_5$	22.523(5)	5.015(2)	10.506(3)	90	99.62(2)	90	*C2/c*	(221)
Olgite	$NaSr(PO_4)$	5.565(2)	*a*	7.050(3)	90	90	120	*P3*	(222)
Olmsteadite	$KFe^{2+}{}_2(H_2O)_2[Nb(PO_4)_2O_2]$	7.512(1)	10.000(3)	6.492(2)	90	90	90	$Pb2_1m$	(223)
Olympite	$LiNa_5(PO_4)_2$	10.143(1)	14.819(3)	10.154(5)	90	90	90	*Pcmn*	(224)
Orpheite	$H_6Pb^{2+}{}_{10}Al_{20}(PO_4)_{12}(SO_4)_5(OH)_{40}(H_2O)_{11}$	7.016	*a*	16.730	90	90	120	$R\bar{3}m$	(225)
Overite	$Ca_2Mg_2[Al(PO_4)_2(OH)]_2(H_2O)_8$	14.723(14)	18.746(16)	7.107(4)	90	90	90	*Pbca*	(226)
Pahasapaite	$Ca_8Li_8[Be_{24}P_{24}O_{96}](H_2O)_{38}$	13.781(4)	*a*	13.783(1)	90	90	90	*I23*	(227)
Palermoite	$SrLi_2[Al(PO_4)(OH)]_4$	11.556(5)	15.847(7)	7.315(4)	90	90	90	*Imcb*	(228)
Panasqueiraite	$Ca[Mg(PO_4)(OH)]$	6.535(3)	8.753(4)	6.919(4)	90	112.33(4)	90	*C2/c*	(137)
Parafransoletite	$Ca_3[Be_2(PO_4)_2(PO_3\{OH\})_2](H_2O)_4$	7.327(1)	7.696(1)	7.061(1)	94.9(0)	96.8(0)	101.9(0)	$P\bar{1}$	(104)
Parahopeite	$Zn_3(PO_4)_2(H_2O)_4$	5.768(5)	7.550(5)	5.276(5)	93.42	91.18	91.37	$P\bar{1}$	(229)
Pararobertsite	$Ca_2Mn^{3+}{}_3(PO_4)_3O_2(H_2O)_3$	8.825(3)	13.258(4)	11.087(3)	90	101.19(4)	90	$P2_1/c$	(230)
Paraschoizite	$CaZn_2(PO_4)_2(H_2O)_2$	17.186(6)	7.413(3)	6.663(2)	90	95.4(0)	90	*I2/c*	(231)
Paravauxite	$Fe^{2+}[Al_2(PO_4)_2(OH)_2(H_2O)_2](H_2O)_4(H_2O)_2$	5.233	10.541	6.962	106.9	110.8	72.1	$P\bar{1}$	(232)
Parsonsite	$Pb^{2+}{}_2[(UO_2)(PO_4)_2]$	6.842(4)	10.383(6)	6.670(4)	101.26(7)	98.17(7)	86.38(7)	$P\bar{1}$	(233)
Paulkellerite	$Bi^{3+}{}_2Fe^{3+}(PO_4)O_2(OH)_2$	11.380(3)	6.660(3)	9.653(3)	90	115.3(0)	90	*C2/c*	(234)

APPENDIX A continued

Mineral Name	Formula	*a* (Å)	*b* (Å)	*c* (Å)	α (°)	β (°)	γ (Å)	Space Group	Ref.
Penikisite	$BaMg_2Al_2(PO_4)_3(OH)_3$	8.999	12.069	4.921	90	100.52	90	$P2_1/m$	(235)
Perloffite	$BaMg_2Fe^{3+}{}_2(PO_4)_3(OH)_3$	9.223(5)	12.422(8)	4.995(7)	90	100.39(4)	90	$P2_1/m$	(236)
Petersite-(Y)	$YCu^{2+}{}_6(PO_4)_3(OH)_6(H_2O)_3$	13.288(5)	*a*	5.877(5)	90	90	120	$P6_3/m$	(237)
Petitjeanite	$Bi^{3+}{}_3(PO_4)_2O(OH)$	9.798	7.250	6.866	88.28	115.27	110.70	$P\bar{1}$	(238)
Phosinaite-(Ce)	$Na_{13}Ca_2Ce[Si_4O_{12}](PO_4)_4$	12.297(2)	14.660(3)	7.245(1)	90	90	90	$P22_12_1$	(239)
Phosphammite	$(NH_4)_2(PO_3\{OH\})$	11.043(6)	6.700(3)	8.031(4)	90	113.4(0)	90	$P2_1/c$	(240)
Phosphoellenbergite	$Mg_{14}(PO_4)_6(PO_3\{OH\})_2(OH)_6$	12.467(2)	*a*	5.044(0)	90	90	120	$P6_3mc$	(241)
Phosphoferrite	$Fe^{2+}{}_3(PO_4)_2(H_2O)_3$	8.660(30)	10.060(30)	9.410(30)	90	90	90	$Pcn2$	(242)
Phosphofibrite	$KCu^{2+}Fe^{3+}{}_{15}(PO_4)_{12}(OH)_{12}(H_2O)_{12}$	14.40	18.76	10.40	90	90	90	$Pbnm$	(243)
Phosphogartrellite	$Pb^{2+}Cu^{2+}Fe^{3+}(PO_4)_2(OH,H_2O)_2$	5.320	5.528	7.434	67.61	69.68	70.65	$P\bar{1}$	(244)
Phosphophyllite	$Zn_2Fe^{2+}(PO_4)_2(H_2O)_4$	10.378(3)	5.084(1)	10.553(3)	90	121.14(2)	90	$P2_1/c$	(245)
Phosphorrösslerite	$\{Mg(H_2O)_6\}(PO_3\{OH\})(H_2O)$	6.60	25.36	11.35	90	95	90	$C2/c$	(246)
Phosphosiderite	$[Fe^{3+}(PO_4)(H_2O)_2]$	5.330(3)	9.809(4)	8.714(5)	90	90.6(1)	90	$P2_1/n$	(247)
Phosphovanadylite	$V^{4+}{}_4P_2O_{10}(OH)_6(H_2O)_{12}$	15.470(4)	*a*	15.470(4)	90	90	90	$I\bar{4}3m$	(248)
Phosphuranylite	$KCa(H_3O)_3(UO_2)[(UO_2)_3(PO_4)_2O_2]_2(H_2O)_8$	15.899(2)	13.740(2)	17.300(3)	90	90	90	$Cmcm$	(249)
Phuralumite	$Al_2[(UO_2)_3(PO_4)_2(OH)_2](OH)_4(H_2O)_{10}$	13.836(6)	20.918(6)	9.428(3)	90	112.44	90	$P2_1/a$	(250)
Phurcalite	$Ca_2[(UO_2)_3O_2(PO_4)_2](H_2O)_7$	17.415(2)	16.035(3)	13.598(3)	90	90	90	$Pbca$	(251)
Planerite	$Al_6(PO_4)_2(PO_3\{OH\})_2(OH)_8(H_2O)_4$	7.505(2)	9.723(3)	7.814(2)	111.43	115.56	68.69	$P\bar{1}$	(2)
Plumbogummite	$Pb^{2+}Al_3(PO_4)_2(OH)_5(H_2O)$	7.039(5)	*a*	16.761(3)	90	90	120	$R\bar{3}m$	(130)
Polyphite	$Na_{17}Ca_3MgTi^{4+}{}_4(Si_2O_7)_2(PO_4)_6O_3F_5$	5.412(2)	7.079(3)	26.560(10)	95.2(0)	93.5(0)	90.1(0)	$P1$	(252)
Pretulite	$Sc(PO_4)$	6.589(1)	*a*	5.806(1)	90	90	90	$I4/amd$	(253)
Przhevalskite	$Pb[(UO_2)(PO_4)]_2(H_2O)_4$	7.24	*a*	18.22	90	90	90	Tetra	(254)
Pseudo-autunite	$Ca_2[(UO_2)_2(PO_4)_4](H_2O)_9$	6.964	*a*	12.85	90	90	120	Hexa	(255)
Pseudolaueite	$Mn^{2+}[Fe^{3+}(PO_4)(OH)(H_2O)]_2(H_2O)_4(H_2O)_2$	9.647	7.428	10.194	90	104.63	90	$P2_1/a$	(256)
Pseudomalachite	$Cu^{2+}{}_5(PO_4)_2(OH)_4$	4.4728(4)	5.7469(5)	17.032(3)	90	91.043(7)	90	$P2_1/c$	(257)
Purpurite	$Mn^{3+}(PO_4)$	4.760	9.680	5.819	90	90	90	$Pbnm$	(258)
Pyromorphite	$Pb_5(PO_4)_3Cl$	9.977(1)	9.976(1)	7.351(2)	90	90	120	$P6_3/m$	(259)

APPENDIX A continued

Mineral Name	Formula	*a* (Å)	*b* (Å)	*c* (Å)	α (°)	β (°)	γ (Å)	Space Group	Ref.
Qingheiite	$Na_2NaMn^{2+}{}_2Mg_2Al_2(PO_4)_6$	11.856(3)	12.411(3)	6.421(1)	90	114.45(2)	90	$P2_1/n$	(260)
Quadruphite	$Na_{14}CaMgTi^{4+}{}_4(Si_2O_7)_2(PO_4)_4O_4F_2$	5.4206(2)	7.0846(2)	20.364(1)	86.89(1)	94.42(1)	89.94(1)	$P1$	(209)
Raadeite	$Mg_7(PO_4)_2(OH)_8$	5.250(1)	11.647(2)	9.655(2)	90	95.94(1)	90	$P2_1/n$	(261)
Reddingite	$Mn^{2+}{}_3(PO_4)_2(H_2O)_3$	8.750(20)	10.173(8)	9.590(20)	90	90	90	$Pcmb$	(262)
Reichenbachite	$Cu^{2+}{}_5(PO_4)_2(OH)_4$	9.186(2)	10.684(2)	4.461(1)	90	92.31(1)	90	$P2_1/a$	(263)
Renardite	$Pb^{2+}(UO_2)[(UO_2)_3O_2(PO_4)_2](H_2O)_9$	15.9	17.6	13.8	90	90	90	$Bmmb$	(264)
Rhabdophane	$Ce(PO_4)(H_2O)$	7.055(3)	*a*	6.439(5)	90	90	120	$P6_222$	(265)
Richellite	$Ca_3Fe^{3+}{}_{10}(PO_4)_8(OH)_{12}(H_2O)_n$	Amorphous	–	–	–	–	–	–	(266)
Rimkorolgite	$Mg_5Ba(PO_4)_4(H_2O)_8$	12.829	8.335	18.312	90	90	90	$Pcmm$	(267)
Rittmanite	$Mn^{2+}Mn^{2+}Fe^{2+}{}_2[Al(PO_4)_2(OH)]_2(H_2O)_8$	15.01(4)	6.89(3)	10.16(3)	90	112.82(25)	90	$P2_1/a$	(268)
Robertsite	$Ca_2[Mn^{3+}{}_3(PO_4)_3O_2](H_2O)_3$	17.36(2)	19.53(5)	11.30(3)	90	96.0	90	Aa	(269)
Rockbridgeite	$Fe^{2+}Fe^{3+}{}_4(PO_4)_3(OH)_5$	13.873(12)	16.805(9)	5.172(4)	90	90	90	$Bbmm$	(81)
Rodolicoite	$Fe^{3+}(PO_4)$	5.048(3)	*a*	11.215(8)	90	90	120	$R3_121$	(270)
Roscherite	$Ca_2Mn^{2+}{}_5[Be_4P_6O_{24}(OH)_4](H_2O)_6$	15.874(4)	11.854(3)	6.605(1)	90	95.35(3)	90	$C2/c$	(271)
Rosemaryite	$NaMn^{2+}Fe^{3+}Al(PO_4)_3$	11.977(2)	12.388(2)	6.320(1)	90	114.45(2)	90	$P2_1/n$	(272)
Sabugalite	$Al[(UO_2)_4(PO_3\{OH\})(PO_4)_3](H_2O)_{16}$	19.426	9.843	9.850	90	96.16	90	$C2/m$	(273)
Saléeite	$Mg[(UO_2)(PO_4)]_2(H_2O)_{10}$	6.951(3)	19.947(8)	9.896(4)	90	135.17	90	$P2_1/c$	(274)
Sampleite	$NaCaCu^{2+}{}_5(PO_4)_4Cl(H_2O)_5$	9.70	38.40	9.65	90	90	90	Orth	(275)
Samuelsonite	$BaCa_8Fe^{2+}Al_2(OH)_2(PO_4)_{10}$	18.495(10)	6.804(4)	14.000(8)	90	112.8(1)	90	$C2/m$	(276)
Sanjuanite	$Al_2(PO_4)(SO_4)(OH)(H_2O)_9$	11.314(11)	9.018(9)	7.376(7)	93.07(1)	95.77(7)	105.66(7)	$P\bar{1}$	(133)
Sarcopside	$(Fe^{2+},Mn^{2+},Mg)_3(PO_4)_2$	6.019(0)	4.777(0)	10.419(1)	90	91.0(0)	90	$P2_1/c$	(277)
Sasaite	$Al_6(PO_4)_5(OH)_3(H_2O)_{35\text{-}36}$	10.75	15.02	46.03	90	90	90	$P---$	(278)
Satterlyite	$Fe^{2+}{}_2(PO_4)(OH)$	11.361	*a*	5.041	90	90	120	$P\bar{3}1m$	(279)
Schertelite	$(NH_4)_2[Mg(PO_3\{OH\})_2(H_2O)_4]$	11.49(2)	23.66(6)	8.62(1)	90	90	90	$Pbca$	(280)
Scholzite	$CaZn_2(PO_4)_2(H_2O)_2$	17.149(3)	22.236(2)	6.667(1)	90	90	90	$Pbc2_1$	(281)
Schoonerite	$Fe^{2+}{}_2ZnMn^{2+}(PO_4)_3(OH)_2(H_2O)_9$	11.119(4)	25.546(11)	6.437(3)	90	90	90	$Pmab$	(282)
Scorzalite	$Fe^{2+}[Al(PO_4)(OH)]_2$	7.15(2)	7.31(2)	7.25(2)	90	120.7(1)	90	$P2_1/c$	(20)

APPENDIX A continued

Mineral Name	Formula	*a* (Å)	*b* (Å)	*c* (Å)	α (°)	β (°)	γ (Å)	Space Group	Ref.
Seamanite	$[Mn^{2+}_3(B\{OH\}_4)(PO_4)(OH)_2]$	7.8231(9)	15.1405(14)	6.6999(7)	90	90	90	*Pbnm*	(283)
Segelerite	$Ca_2Mg_2[Fe^{3+}(PO_4)_2(OH)]_2(H_2O)_8$	14.826(5)	18.751(4)	7.307(1)	90	90	90	*Pbca*	(226)
Selwynite	$NaK[BeZr_2(PO_4)_4](H_2O)_2$	6.570(3)	*a*	17.142(6)	90	90	90	$I4_1/amd$	(284)
Senegalite	$Al_2(OH)_3(PO_4)(H_2O)$	7.675(4)	9.711(4)	7.635(4)	90	90	90	$P2_1nb$	(285)
Serrabrancaite	$Mn^{3+}(PO_4)(H_2O)$	6.914(2)	7.468(2)	7.364(2)	90	112.29(3)	90	*C2/c*	(286)
Sicklerite	$LiMn^{2+}(PO_4)$	4.794	10.063	5.947	90	90	90	*Pbnm*	(287)
Sidorenkite	$Na_3Mn^{2+}(PO_4)(CO_3)$	8.997(4)	6.741(2)	5.163(2)	90	90.16(4)	90	$P2_1/m$	(288)
Sigismundite	$BaNa_3CaFe^{2+}{}_{14}Al(PO_4)_{12}(OH)_2$	16.406(5)	9.945(3)	24.470(5)	90	105.73(2)	90	*C2/c*	(289)
Sigloite	$Fe^{3+}[Al_2(PO_4)_2(OH)_2(H_2O)_2](H_2O)_3(OH)(H_2O)_2$	5.190(2)	10.419(4)	7.033(3)	105.00(3)	111.31(3)	70.87(3)	$P\bar{1}$	(290)
Sincosite	$Ca(V^{4+}O)_2(PO_4)_2(OH)_4(H_2O)_3$	8.895(3)	*a*	12.747(2)	90	90	90	*P4/nmm*	(291)
Sinkankasite	$(Mn^{2+}(H_2O)_4)(Al(PO_3\{OH\})_2(OH))(H_2O)_2$	9.590(2)	9.818(2)	6.860(1)	108.0(0)	99.6(0)	98.9(0)	$P\bar{1}$	(292)
Smrkovecite	$Bi^{3+}{}_2O(PO_4)(OH)$	6.954	7.494	10.869	90	107.00	90	$P2_1/c$	(293)
Sobolevite	$Na_{11}Na_4MgTi^{4+}{}_4(Si_2O_7)_2(PO_4)_4O_3F_3$	7.078(1)	5.411(1)	40.618(10)	90	93.2(0)	90	*P1*	(294)
Souzalite	$Mg_3Al_4(PO_4)_4(OH)_6(H_2O)_2$	11.74(1)	5.11(1)	13.58(1)	90.83(8)	99.08(8)	90.33(8)	$P\bar{1}$	(116)
Spencerite	$Zn_4(PO_4)_2(OH)_2(H_2O)_3$	10.448(3)	5.282(1)	11.208(3)	90	116.73(3)	90	$P2_1/c$	(295)
Spheniscidite	$(NH_4)Fe^{3+}{}_2(OH)(PO_4)_2(H_2O)_2$	9.75	9.63	9.70	90	102.57	90	$P2_1/n$	(296)
Springcreekite	$BaV^{3+}{}_3(PO_4)_2(OH)_5(H_2O)$	7.258(1)	*a*	17.361(9)	90	90	120	$R\bar{3}m$	(297)
Staněkite	$Fe^{3+}Mn^{2+}(PO_4)O$	11.844(3)	12.662(3)	9.989(3)	90	105.93(2)	90	$P2_1/a$	(298)
Stanfieldite	$Mg_3Ca_3(PO_4)_4$	22.841(3)	9.994(1)	17.088(5)	90	99.6(0)	90	*C2/c*	(299)
Steenstrupine-(Ce)	$Na_{14}Ce_6Mn^{2+}Mn^{3+}Fe^{2+}{}_2Zr(Si_6O_{18})_2(PO_4)_7(H_2O)_3$	10.460(4)	*a*	45.479(15)	90	90	120	$R\bar{3}m$	(300)
Stercorite	$Na(NH_4)H[PO_4](H_2O)_4$	10.636(2)	6.919(1)	6.436(1)	90.46(3)	97.87(3)	109.20(3)	$P\bar{1}$	(301)
Stewartite	$Mn^{2+}[Fe^{3+}{}_2(PO_4)_2(OH)_2(H_2O)_2](H_2O)_4(H_2O)_2$	10.398(2)	10.672(3)	7.223(3)	90.10(3)	109.10(2)	71.83(2)	$P\bar{1}$	(302)
Strengite	$[Fe^{3+}(PO_4)(H_2O)_2]$	10.05	9.80	8.65	90	90	90	*Pcab*	(303)
Strontiowhitlockite	$Sr_9Mg(PO_4)_6(PO_3\{OH\})$	10.644(9)	*a*	39.54(6)	90	90	120	*R3c*	(304)
Strontium-apatite	$Sr_6Ca_4(PO_4)_6F_2$	9.630	*a*	7.220	90	90	120	$P6_3$	(305)
Strunzite	$Mn^{2+}[Fe^{3+}(PO_4)(OH)(H_2O)]_2(H_2O)_4$	10.228(5)	9.837(3)	7.284(5)	90.17(5)	98.44(5)	117.44(2)	$P\bar{1}$	(306)
Strüvite	$(NH_4)[Mg(H_2O)_6][PO_4]$	6.941(2)	6.941(2)	11.199(4)	90	90	90	$Pmn2_1$	(307)

APPENDIX A continued

Mineral Name	Formula	*a* (Å)	*b* (Å)	*c* (Å)	α (°)	β (°)	γ (Å)	Space Group	Ref.
Svanbergite	$Sr[Al_3(SO_4)(PO_4)(OH)_6]$	6.890	*a*	*a*	60.6	60.6	60.6	$R\bar{3}m$	(308)
Swaknoite	$Ca(NH_4)_2(PO_3\{OH\})_2(H_2O)$	20.959	7.403	6.478	90	90	90	*C– – –*	(309)
Switzerite	$Mn^{2+}{}_3(PO_4)_2(H_2O)_7$	8.528(4)	13.166(5)	11.812(4)	90	110.05(3)	90	$P2_1/a$	(310)
Tancoite	$Na_2Li[Al(PO_4)_2(OH)]H$	6.948(2)	14.089(4)	14.065(3)	90	90	90	*Pbcb*	(311)
Taranakite	$K_3Al_5(PO_3\{OH\})_6(PO_4)_2(H_2O)_{18}$	8.703(1)	*a*	95.050(10)	90	90	120	$R\bar{3}c$	(312)
Tarbuttite	$Zn_2(PO_4)(OH)$	5.499	5.654	6.465	102.85	102.77	86.83	$P\bar{1}$	(313)
Tavorite	$Li[Fe^{3+}(PO_4)(OH)]$	5.340(2)	7.283(2)	5.110(2)	109.29(2)	97.86(3)	106.32(3)	$P\bar{1}$	(314)
Thadeuite	$CaMg_3(PO_4)_2(OH)_2$	6.412(3)	13.563(8)	8.545(5)	90	90	90	$C222_1$	(315)
Threadgoldite	$Al[(UO_2)(PO_4)]_2(OH)(H_2O)_8$	20.168(8)	9.847(2)	19.719(4)	90	110.7(0)	90	*C2/c*	(316)
Tinsleyite	$K[Al_2(PO_4)_2(OH)(H_2O)](H_2O)$	9.499(2)	9.503(2)	9.535(2)	90	103.3(0)	90	$P2_1/n$	(317)
Tinticite	$Fe^{3+}{}_4(PO_4)_3(H_2O)_5$	7.965(2)	9.999(2)	7.644(2)	103.94(2)	115.91(2)	67.86(2)	$P\bar{1}$	(318)
Tiptopite	$K_2NaCaLi_3[Be_6P_6O_{24}(OH)_2](H_2O)_4$	11.655(5)	*a*	4.692(2)	90	90	120	$P6_3$	(319)
Torbernite	$Cu^{2+}[(UO_2)(PO_4)]_2(H_2O)_8$	7.06	*a*	20.5	90	90	90	*I4/mmm*	(320)
Triangulite	$Al_3(OH)_5[(UO_2(PO_4)]_4(H_2O)_5$	10.39	10.56	8.82	101.25	109.58	113.4	$P\bar{1}$	(321)
Triphylite	$LiFe^{2+}(PO_4)$	4.704	10.347	6.0189	90	90	90	*Pbnm*	(322)
Triplite	$Mn^{2+}{}_2(PO_4)F$	12.065	6.454	9.937	90	107.1	90	*I2/c*	(323)
Triploidite	$Mn^{2+}{}_2(PO_4)(OH)$	12.366(1)	13.276(2)	9.943(2)	90	108.2(0)	90	$P2_1/a$	(324)
Trolleite	$Al_4(OH)_3(PO_4)_3$	18.894(5)	7.161(1)	7.162(2)	90	99.99(2)	90	*I2/c*	(325)
Tsumebite	$Pb^{2+}{}_2[Cu^{2+}(PO_4)(SO_4)(OH)]$	7.85	5.80	8.70	90	111.5	90	$P2_1/m$	(326)
Turquoise	$Cu^{2+}Al_6(PO_4)_4(OH)_8(H_2O)_4$	7.410(1)	7.633(1)	9.904(1)	68.42(1)	69.65(1)	65.05(1)	$P\bar{1}$	(327)
Ulrichite	$Cu^{2+}[Ca(UO_2)(PO_4)_2](H_2O)_4$	12.790(30)	6.850(20)	13.020(30)	90	91.0(1)	90	*C2/m*	(328)
Upalite	$Al[(UO_2)_3O(OH)(PO_4)_2](H_2O)_7$	13.704	16.82	9.332	90	111.5	90	$P2_1/a$	(329)
Uralolite	$Ca_2[Be_4(PO_4)_3(OH)_3](H_2O)_5$	6.550(1)	16.005(3)	15.969(4)	90	101.64(2)	90	$P2_1/n$	(330)
Uramphite	$(NH_4)(UO_2)(PO_4)(H_2O)_3$	7.022(0)	*a*	18.091(0)	90	90	90	*P4/ncc*	(331)
Uranocircite	$Ba[(UO_2)(PO_4)]_2(H_2O)_{10}$	7.02	*a*	20.58	90	90	90	*P4/ncc*	(332)
Uranospathite	$AlH[(UO_2)(PO_4)]_4(H_2O)_{40}$	7.00	*a*	30.02	90	90	90	$P4_2/n$	(333)
Ushkovite	$Mg[Fe^{3+}{}_2(PO_4)_2(OH)_2(H_2O)_2](H_2O)_4(H_2O)_2$	5.3468(4)	10.592(1)	7.2251(7)	108.278(7)	111.739(7)	71.626(7)	$P\bar{1}$	(334)

APPENDIX A continued

Mineral Name	Formula	*a* (Å)	*b* (Å)	*c* (Å)	α (°)	β (°)	γ (Å)	Space Group	Ref.
Vanmeerscheite	$U(OH)_4[(UO_2)_3(PO_4)_2(OH)_2](H_2O)_4$	17.060(50)	16.760(30)	7.023(3)	90	90	90	$P2_1mn$	(190)
Variscite	$[Al(PO_4)(H_2O)_2]$	9.822(3)	8.561(3)	9.630(3)	90	90	90	*Pbca*	(335)
Varulite	$(Na,Ca)[Mn^{2+}(Mn,Fe^{2+},Fe^{3+})_2(PO_4)_3]$	11.99	12.64	6.51	90	114.64	90	*C2/c*	(336)
Vashegyite	$Pb^{2+}{}_2Cu^{2+}(CrO_4)(PO_4)(OH)$	10.773(3)	14.971(5)	20.626(6)	90	90	90	$Pna2_1$	(337)
Vauquelinite	$Pb^{2+}{}_2[Cu^{2+}(PO_4)(CrO_4)(OH)]$	13.754(5)	5.808(6)	9.563(3)	90	94.56(3)	90	$P2_1/n$	(338)
Vauxite	$Fe^{2+}Al_2(PO_4)_2(OH)_2(H_2O)_6$	9.13	11.59	6.14	98.3	92.0	108.4	$P\bar{1}$	(339)
Väyrynenite	$Mn^{2+}[Be(PO_4)(OH)]$	5.4044(6)	14.5145(12)	4.7052(6)	90	102.798(9)	90	$P2_1/a$	(340)
Veszelyite	$Cu^{2+}{}_3(PO_4)(OH)_3(H_2O)_2$	9.828(3)	10.224(3)	7.532(2)	90	103.18(2)	90	$P2_1/a$	(341)
Viitaniemiite	$NaCaAl(PO_4)(OH)F_2$	5.457(2)	7.151(2)	6.836(2)	90	109.36(3)	90	$P2_1/n$	(342)
Viséite	$Ca_{10}Al_{24}(SiO_4)_6(PO_4)_7O_{22}F_3(H_2O)_{72}$	6.89	*a*	18.065	90	90	120	$R\bar{3}m$	(343)
Vitusite-(Ce)	$Na_3Ce(PO_4)_2$	14.091(4)	5.357(1)	18.740(3)	90	90	90	$Pca2_1$	(344)
Vivianite	$Fe^{2+}{}_3(PO_4)_2(H_2O)_8$	10.021(5)	13.441(6)	4.721(3)	90	102.8(0)	90	*I2/m*	(345)
Vochtenite	$Fe^{2+}Fe^{3+}[(UO_2)(PO_4)]_4(OH)(H_2O)_{12\text{-}13}$	12.606	19.990	9.990	90	102.52	90	Mono	(346)
Voggite	$Na_2Zr(PO_4)(CO_3)(OH)(H_2O)_2$	12.261(2)	6.561(1)	11.757(2)	90	116.2(0)	90	*I2/m*	(347)
Vuonnemite	$Na_{11}Ti^{4+}Nb_2(Si_2O_7)_2(PO_4)_2O_3(OH)$	5.4984(6)	7.161(1)	14.450(2)	92.60(1)	95.30(1)	90.60(1)	$P\bar{1}$	(348)
Wagnerite	$Mg_2(PO_4)F$	11.957(8)	12.679(8)	9.644(7)	90	108.3(2)	90	$P2_1/a$	(349)
Wardite	$NaAl_3(OH)_4(PO_4)_2(H_2O)_2$	7.030(10)	*a*	19.040(10)	90	90	90	$P4_12_12$	(350)
Wavellite	$Al_3(OH)_3(PO_4)_2(H_2O)_5$	9.621(2)	17.363(4)	6.994(3)	90	90	90	*Pcmn*	(351)
Waylandite	$(Bi,Ca)Al_3(PO_4,SiO_4)_2(OH)_6$	6.983(3)	*a*	16.175(1)	90	90	120	$R\bar{3}m$	(352)
Weinbeneite	$Ca[Be_3(PO_4)_2(OH)_2](H_2O)_4$	11.897(2)	9.707(1)	9.633(1)	90	95.76(1)	90	*Cc*	(353)
Whiteite-(CaFeMg)	$CaFe^{2+}Mg_2[Fe^{3+}(PO_4)_2(OH)]_2(H_2O)_8$	14.90(4)	6.98(2)	10.13(2)	90	113.11(9)	90	*P2/a*	(354)
Whiteite-(CaMnMg)	$CaMn^{2+}Mg_2Al_2(PO_4)_4(OH)_2(H_2O)_8$	14.842(9)	6.976(1)	10.109(4)	90	112.59(5)	90	*P2/a*	(355)
Whitlockite	$Ca_9Mg(PO_4)_6(PO_3\{OH\})$	10.350(5)	*a*	37.085(12)	90	90	120	*R3c*	(356)
Whitmoreite	$Fe^{2+}[Fe^{3+}(PO_4)(OH)]_2(H_2O)_4$	10.00(2)	9.73(2)	5.471(8)	90	93.8(1)	90	$P2_1/c$	(357)
Wicksite	$NaCa_2Fe^{2+}{}_4MgFe^{3+}(PO_4)_6$	12.896(3)	12.511(3)	11.634(3)	90	90	90	*Pbca*	(358)
Wilhelmvierlingite	$Ca_2Mn_2[Fe^{3+}(PO_4)_2(OH)]_2(H_2O)_8$	14.80(5)	18.50(5)	7.31(2)	90	90	90	*Pbca*	(359)
Wolfeite	$Fe^{2+}{}_2(PO_4)(OH)$	12.319	13.230	9.840	90	108.40	90	$P2_1/a$	(360)

APPENDIX A continued

Mineral Name	Formula	*a* (Å)	*b* (Å)	*c* (Å)	α (°)	β (°)	γ (Å)	Space Group	Ref.
Woodhouseite	$CaAl_3(PO_4)(SO_4)(OH)_6$	6.976(2)	*a*	16.235(8)	90	90	120	$R\bar{3}m$	(361)
Wooldridgeite	$Na_2CaCu^{2+}{}_2(P_2O_7)_2(H_2O)_{10}$	11.938(1)	32.854(2)	11.017(1)	90	90	90	*Fdd2*	(362)
Wycheproofite	$NaAlZr(PO_4)_2(OH)_2(H_2O)$	10.926(5)	10.986(5)	12.479(9)	71.37(4)	77.39(4)	87.54(3)	*P*1 or $P\bar{1}$	(363)
Wyllieite	$Na(Mn^{2+},Fe^{2+})(Fe^{2+},Fe^{3+},Mg)Al(PO_4)_3$	11.868(15)	12.382(12)	6.354(9)	90	114.52(8)	90	$P2_1/n$	(364)
Xanthoxenite	$Ca_4Fe^{3+}{}_2(PO_4)_4(OH)_2(H_2O)_5$	6.70(4)	8.65(4)	6.54(3)	92.1(2)	110.2(2)	93.2(3)	$P\bar{1}$	(354)
Xenotime-(Y)	$Y(PO_4)$	6.895(1)	*a*	6.0276(6)	90	90	90	$I4_1/amd$	(199)
Xenotime-(Yb)	$YbPO_4$	6.866(2)	*a*	6.004(3)	90	90	90	$I4_1/amd$	(365)
Yingjiangite	$K_2Ca(UO_2)_7(PO_4)_4(OH)_6(H_2O)_6$	15.707	17.424	13.692	90	90	90	*Bmmb*	(366)
Yoshimuraite	$Ba_2Mn_2TiO(Si_2O_7)(PO_4)(OH)$	5.386(1)	6.999(1)	14.748(3)	89.98(1)	93.62(2)	95.50(2)	$P\bar{1}$	(367)
Zairite	$Bi(Fe^{3+},Al)_3(PO_4)_2(OH)_6$	7.015(5)	*a*	16.365(15)	90	90	120	$R\bar{3}m$	(368)
Zanazziite	$CaMg_5[Be_4P_6O_{24}(OH)_4](H_2O)_6$	15.874(4)	11.854(3)	6.605(1)	90	95.3(0)	90	*C2/c*	(369)
Zwieselite	$Fe_2(PO_4)F$	11.999(3)	9.890(3)	6.489(1)	90	90	107.7(0)	*I2/a*	(370)

References: (1) McDonald et al. (1994), (2) Foord and Taggart (1998), (3) Harrowfield et al. (1981), (4) Hata et al. (1979), (5) Moore (1971b), (6) Romming and Raade (1980), (7) Piret and Deliens (1987), (8) Groat et al. (1990), (9) Catti et al. (1979), (10) Ono and Yamada (1991), (11) Sokolova et al. (1984a), (12) Sakae et al. (1978), (13) Moore et al. (1981), Merlino et al. (1981), (14) Buchwald (1990), (15) Grice and Dunn (1992), (16) Araki et al. (1968), (17) Potenza (1958), (18) Simonov et al. (1980), (19) Yakubovich et al. (2000), Liferovich et al. (2000b), (20) Lindberg and Christ (1959), (21) Yakubovich et al. (2001), (22) Roca et al. (1997), Pring et al. (1999), (23) Vochten et al. (1984), (24) Chopin et al. (1993), (25) Galliski et al. (1999), (26) Borodin and Kazakova (1954), (27) Pekov et al. (1996), Kabalov et al. (1997), (28) Walenta et al. (1996), (29) Demartin et al. (1993), Demartin et al. (1997), (30) di Cossato et al. (1989a), Fanfani and Zanazzi (1967a), (31) Piret and Deliens (1981), (32) Ng and Calvo (1976), (33) Kampf and Moore (1976), (34) von Knorring and Mrose (1966), (35) Giuseppetti and Tadini (1973), (36) Steele et al. (1991), Wise et al. (1990), (37) Ilyukhin et al. (1995), (38) Moore and Araki (1974c), (39) Birch et al. (1999), (40) Ercit et al. (1986a), (41) Takagi et al. (1986), (42) Hawthorne (1982), (43) Garcia-Guinea et al. (1995), (44) Khomyakov et al. (1982), (45) Rose (1980), (46) Sokolova and Khomyakov (1992), (47) Gatehouse and Miskin (1974), (48) Krause et al. (1998c), (49) Moore (1975a), Alkemper and Fuess (1998), (50) Fisher and Meyrowitz (1962), (51) Curry and Jones (1971), (52) Ben Amara et al. (1983), (53) Selway et al. (1997), (54) Moore and Shen (1983a), (55) Rouse et al. (1988), (56) White et al. (1967), (57) Giuseppetti et al. (1989), (58) Hughes et al. (1995), (59) Atencio (1988), (60) Giuseppetti and Tadini (1984), (61) McCoy et al. (1994), (62) Hughes et al. (1990), (63) Kohlmann et al. (1994), (64) Krutik et al. (1980), (65) Young et al. (1966), (66) Brotherton et al. (1974), (67) Giuseppetti and Tadini (1987), (68) Eby and Hawthorne (1989), (69) Blount (1974), (70) Khomyakov et al. (1994), (71) Cooper and Hawthorne (1994b), (72) Cozzupoli et al. (1987), Cooper et al. (2000), (73) Khomyakov et al. (1996), Rastsvetaeva and Khomyakov (1996), (74) Cech and Povondra (1979), (75) Peacor et al. (1999), (76) Piret et al. (1990), (77) Moore et al. (1981), (78) Mrose (1971), Carling et al. (1995), (79) Catti et al. (1977b), (80) King and Sengier Roberts (1988), (81) Moore (1970), (82) Piret and Piret-Meunier (1988), (83) Peacor et al. (1984), (84) Hawthorne and Grice (1987), (85) Dunn et al. (1984b), Moore (1976), (86) Hansen (1960), Hoyos et al. (1993), (87) Fransolet et al. (2000), (88) van Wambeke (1972), (89) Fanfani et al. (1970b), (90) Nord and Kierkegaard (1968), (91) Kolitsch and Giester (2000), (92) Hughes and Drexler (1991), (93) Alberti (1976), (94) Peacor et al. (1983), (95) Araki and Moore (1981), (96) Kato (1990), (97) Lefebvre and Gasparrini (1980), (98) Milton and Bastron (1971), (99) Guy and Jeffrey (1966), (100) Khomyakov et al. (1997), (101) Moore et al. (1975b), (102) Dick and Zeiske (1998), (103) Piret et al. (1988), (104) Kampf (1992), Kampf

et al. (1992), (105) Lindberg (1949), (106) Shen and Peng (1981), (107) Moore et al. (1983), (108) Olsen and Steele (1997), (109) Pring and Birch (1993), (110) von Knorring and Fransolet (1977), (111) Sokolova and Egorov-Tismenko (1990), (112) Liferovich et al. (2000a), Sokolova et al. (2001), (113) Moore et al. (1975a), (114) Radoslovich and Slade (1980), (115) Leavens and Rheingold (1988), (116) Sturman et al. (1981a), (117) Kato (1971), Kato (1987), (118) Calvo (1968), (119) Cipriani et al. (1997), (120 Dooley and Hathaway (1961), (121) Rinaldi (1978), (122) Fisher (1956), (123) Walenta and Theye (1999), (124) Catti and Franchini-Angela (1976), (125) Grice and Roberts (1993), (126) Romming and Raade (1986), (127) Sieber et al. (1987), (128) Pavlov and Belov (1957), (129) Eventoff et al. (1972), (130) Kolitsch et al. (1999b), (131) Romming and Raade (1989), (132) Hill and Jones (1976), (133) de Bruiyn et al. (1989), (134) Moore and Araki (1973), (135) Bakakin et al. (1974), (136) Lager and Gibbs (1974), (137 Isaaks and Peacor (1981), (138) Meagher et al. (1974), (139) Moore (1974), Moore and Araki (1974a), (140) Grice et al. (1990), (141) Livingstone (1980), (142) Kolitsch et al. (2000), (143) Dunn et al. (1986), (144) Liferovich et al. (1997), (145) Popova et al. (2001), (146) Adiwidjaja et al. (1999), Schluter et al. (1999), (147) Mücke (1979) (148) Kato (1970), (149) Kharisun et al. (1997), Pring et al. (1995), (150) Piret et al. (1985), (151) Hey et al. (1982), (152) van Tassel (1968), (153) Brownfield et al. (1993) Sljukic et al. (1969), (154) Ovchinnikov et al. (1980), (155) Britvin et al. (1996), (156) Moore (1971a), Moore and Araki (1976), Moore et al. (1980), (157) Cooper and Hawthorne (1994a), (158) Lahti and Pajunen (1985), Pajunen and Lahti (1985), Fransolet (1989), (159) Moore et al. (1980), (160) Moore (1965a), (161) Giuseppetti and Tadini (1983), (162) Mucke (1988), (163) Dick and Zeiske (1997), (164) Yakubovich and Mel'nikov (1993), (165) Vencato et al. (1989), (166) Yakubovich and Urusov (1997) (167) Geller and Durand (1960), (168) Rastvetaeva (1971), Sokolova et al. (1987a), (169) Piret and Deliens (1988), Shoemaker et al. (1981), (170) Abrahams (1966), (171 Moelo et al. (2000), (172) Sen Gupta et al. (1991), (173) Voloshin et al. (1983), (174) Effenberger et al. (1982), (175) Moore and Ito (1979), (176) Tadini (1981), (177) Miltoi et al. (1993), (178) Voloshin et al. (1992), (179) Le Page and Donnay (1977), (180) Richardson et al. (1988), (181) Foord et al. (1994), (182) Egorov et al. (1969), (183) Kamp and Moore (1977), (184) Catti et al. (1977c), (185) Fitch and Cole (1991), (186) Makarov and Ivanov (1960), (187) Zanazzi et al. (1986), Fanfani and Zanazzi (1979), White et al. (1986), (188) Stergiou et al. (1993), Makarov and Tobelko (1960), (189) Khosrawan-Sazedj (1982a), (190) Piret and Deliens (1982), (191) Kniep and Mootz (1973) (192) Baur and Rama Rao (1967), (193) Dormann et al. (1982), (194) Birch et al. (1996), (195) Owens et al. (1960), (196) Kampf (1977b), (197) Moore and Araki (1977b) Moore (1976), (198) Cahill et al. (2001), Ankinovich et al. (1997), (199) Ni et al. (1995), (200) Catti et al. (1977a), (201) Fanfani et al. (1976), Moore and Araki (1974e), (202 Merlino and Pasero (1992), (203) Deliens and Piret (1985), (204) Hawthorne (1979a), (205) Effenberger et al. (1994), (206) Deliens and Piret (1981), (207) Bridge and Clark (1983), (208) Baturin et al. (1982), (209) Sokolova and Hawthorne (2001), (210) Coleman and Robertson (1981), Wiench and Jansen (1983), (211) Ercit (1991), (212) Baturin et al. (1981), (213) Fontan et al. (1982), (214) Freeman and Bayliss (1991), (215) Moore (1972a), Moring and Kostiner (1986), (216) Genkina and Khomyakov (1992), (217 Sebais et al. (1984), (218) Sutor (1967), Sales et al. (1993), (219) Bridge and Robinson (1983), (220) Muto et al. (1959), (221) Groat and Hawthorne (1990), (222) Sokolova et al. (1984b), (223) Moore et al. (1976), (224) Malinovskii and Genkina (1992), (225) Kolkovski (1971), (226) Moore and Araki (1977c), (227) Corbin et al. (1991), Rouse et al. (1989), (228) Moore and Araki (1975), (229) Chao (1969), Kumbasar and Finney (1968), (230) Roberts et al. (1989), (231) Taxer and Bartl (1997), (232) Baur (1969a) (233) Burns (2000), (234) Grice and Groat (1988), (235) Mandarino et al. (1977 (see text)), (236) Kampf (1977c), (237) Peacor and Dunn (1982), (238) Krause et al. (1993) (239) McDonald et al. (1996), (240) Khan et al. (1972), (241) Raade et al. (1998), (242) Flachsbart (1963), Moore and Araki (1976), (243) Walenta and Dunn (1984), (244 Krause et al. (1998a), Krause et al. (1998b), (245) Hill (1977), (246) Ferraris and Franchini-Angela (1973), Street and Whitaker (1973), (247) Moore (1966), Fanfani and Zanazzi (1966), (248) Medrano et al. (1998), (249) Demartin et al. (1991), (250) Piret et al. (1979), (251) Atencio et al. (1991), (252) Sokolova et al. (1987b), Khomyakov et al. (1992), (253) Bernhard et al. (1998), (254) Soboleva and Pudovkina (1957), (255) Sergeev (1964), (256) Baur (1969b), (257) Shoemaker et al. (1977), (258) Bjoerling and Westgren (1938), (259) Dai and Hughes (1989), (260) Zhesheng et al. (1983), (261) Chopin et al. (2001), (262) Eversheim and Kleber (1953), (263) Anderson et al (1977), Sieber et al. (1987), (264) Ross (1956), (265) Mooney (1948), (1950), (266) McConnell (1963), (267) Britvin et al. (1995), (268) di Cossato et al. (1989b), (269) Moore (1974), (270) Cipriani et al. (1997), Arnold (1986), (271) Fanfani et al. (1975), (1977), (272) Fransolet (1995), (273) Vochten and Pelsmaekers (1983), (274) Miller and Taylo (1986), (275) Hurlbut (1942), (276) Moore and Araki (1977a), Moore et al. (1975a), (277) Warner et al. (1992), (278) Martini (1978), Johan et al. (1983), (279) Mandarino et al. (1978), (280) Khan and Baur (1972), (281) Taxer (1975), (282) Kampf (1977a), Moore and Kampf (1977), (283) Huminicki and Hawthorne (2002), (284) Birch et al (1995), (285) Keegan et al. (1979), (286) Lightfoot et al. (1987), Witzke et al. (2000), (287) Blanchard (1981), (288) Kurova et al. (1980), (289) Demartin et al. (1996), (290 Hawthorne (1988), (291) Zolensky (1985), (292) Burns and Hawthorne (1995), (293) Rídkošil et al. (1996), (294) Sokolova et al. (1988), (295) Fanfani et al. (1972), (296 Cavellec et al. (1994), (297) Kolitsch et al. (1999a), (298) Keller et al. (1997), (299) Dickens and Brown (1971), (300) Moore and Shen (1983b), (301) Ferraris and Franchini-Angela (1974), (302) Moore and Araki (1974d), (303) Moore (1966), (304) Britvin et al. (1991), (305) Klevtsova (1964), (306) Fanfani et al. (1978), (307) Abbona et al. (1984), Ferraris et al. (1986), (308) Kato and Miura (1977), (309) Martini (1991), (1993), (310) Fanfani and Zanazzi (1979), Zanazzi et al. (1986), White et al. (1986) (311) Hawthorne (1983b), (312) Dick et al. (1998), (313) Cocco et al. (1966), Genkina et al. (1985), (314) Roberts et al. (1988), Genkina et al. (1984), (315) Isaacs and Peacor (1982), (316) Khosrawan-Sazedj (1982b), (317) Dick (1999), Dunn et al. (1984a), (318) Rius et al. (2000), (319) Peacor et al. (1987), Grice et al. (1985), (320) Frondel et al. (1956), (321) Deliens and Piret (1982), (322) Yakubovich et al. (1977), (323) Waldrop (1968a), (324) Waldrop (1968b), Waldrop (1970), (325) Moore and Araki (1974b)

(326) Fanfani and Zanazzi (1967b), (327) Cid-Dresner (1965), Kolitsch and Geister (2000), (328) Birch et al. (1988), (329) Piret and Declerq (1983), (330) Mereiter et al. (1994),(331)FitchandFender(1983),(332)Chernorukovetal.(1997),(333)Walenta(1978),(334)Galliskietal.(2001),(335)Kniepetal.(1977),(336)Fisher(1965),(337) Johan et al. (1983), (338) Fanfani and Zanazzi (1968), (339) Baur and Rama Rao (1968), (340) Huminicki and Hawthorne (2000), (341) Ghose et al. (1974), (342) Pajunen and Lahti (1984), Lahti (1981), (343) McConnell (1952), Kim and Kirkpatrick (1996), (344) Mazzi and Ungaretti (1994), (345) Bartl (1989), (346) Zwaan et al. (1989), (347) Szymanski and Roberts (1990), (348) Ercit et al. (1998), (349) Coda et al. (1967), (350) Fanfani et al. (1970a), (351) Araki and Zoltai (1968), (352) Clark et al. (1986), (353) Walter (1992), (354) Moore and Ito (1978), (355) Grice et al. (1989), (356) Gopal et al. (1974), (357) Moore et al. (1974), (358) Sturman et al. (1981b), (359) Mücke (1983), (360)Antenuccietal.(1989),(361)Kato(1971),(362)CooperandHawthorne(1999),Hawthorneetal.(1999),(363)Birchetal.(1994),(364)MooreandMolin-Case(1974), Fransolet (1995), (365) Buck et al. (1999), (366) Zhang et al. (1992), (367) McDonald et al. (2000), (368) van Wambeke (1975), (369) Leavens et al. (1990), Fanfani et al. (1975), (370) Yakubovich et al. (1978)

APPENDIX B. DEFINITIONS

Bond valence: a measure of the strength of a bond which varies with the corresponding bond length. The bond valence, s, may be expressed as a function of bond length, R, in the following way: $s = \exp\{(R_0 - R) / b\}$, where R_0 and b are constant characteristic of cation-anion pairs.

Characteristic bond-valence: the formal valence of a cation or an anion divided by its mean coordination-number. The characteristic bond-valence of an oxyanion is its formal charge divided by the mean number of bonds to the oxyanion. For example, an O-atom of an (SO_4) group is, on average, [4]-coordinated, which means it receives three bonds in addition to that from the central S atom; thus, there are, on average, twelve bonds to the oxyanion, and its characteristic bond-valence is 2 / 12 = 0.17 vu.

Lewis acid strength (Lewis acidity): the characteristic bond-valence of a cation; the Lewis acidity of a cation correlates with its electronegativity.

Lewis base strength (Lewis basicity): the characteristic bond-valence of an anion or an oxyanion.

Valence-matching principle: The most stable structures will form when the Lewis acidity of the cation closely matches the Lewis basicity of the anion or oxyanion.

Structural unit: the strongly bonded part of the structure; it is usually anionic, but can be neutral or cationic.

Interstitial complex: the weakly bonded part of the structure, consisting of large low-valence alkali and alkaline-earth cations, (H_2O) groups and monovalent anions such as $(OH)^-$ and Cl^-.

Binary structural representation: Interstitial complex and structural unit are each considered as single components, whose interaction can be examined using the valence-matching principle.

Transformer (H_2O) groups: (H_2O) groups in which the O-atoms accept only one bond from a cation (inclusive of hydrogen bonds). Hence, they receive only one bond but propagate two hydrogen bonds, i.e., they split one bond into two bonds. This effect transforms the higher bond-valence of one cation-(H_2O) bond into the lower bond-valences of two hydrogen bonds.

Non-transformer (H_2O) groups: (H_2O) groups in which the O-atoms accept two additional bonds from cations (inclusive of hydrogen bonds). Hence, they receive two bonds and also propagate two bonds (i.e., they do not transform bonds). Non-transformer (H_2O) groups propagate bond-valence

to acceptor O-atoms of the structural unit.

General interstitial complex:

$$\{^{[m]}M^{+}_{a}\ ^{[n]}M^{2+}_{b}\ ^{[l]}M^{3+}_{c}\ (H_2O)_d\ (H_2O)_e\ ^{[q]}(OH)_f\}^{(a+2b+3c-f)+}\ (H_2O)_g$$

where *d* is the number of interstitial transformer (H_2O) groups, *e* is the number of interstitial non-transformer (H_2O) groups, *f* is the number of interstitial (OH) groups, and *g* is the number of interstitial (H_2O) groups which do not bond to interstitial cations.

General structural unit:

$$[M^{z+}_{x}\ (H_2O)_i\ (OH)_j\ (PO_4)_k]^{(x+3k-l)-}$$

where *x* is the number of cations in the structural unit, *i* is the number of transformer (H_2O) groups in the structural unit, and *j* is the number of (OH) groups in the structural unit

Effective charge of a structural unit: the formal charge plus the amount of bond-valence contributed to the interstitial complex from hydrogen bonds of (H_2O) and (OH) groups in the structural unit. For example, the formal charge of the structural unit $[Fe^{2+}(H_2O)_4(SO_4)_2]^{2-}$ is 2^- and there are eight hydrogen bonds emanating from the structural unit; thus, the effective charge of the structural unit is $(2 + 8h)^-$, where h is the bond valence of the hydrogen bond. The corresponding interstitial complex must have the same effective charge with an opposite sign.

Average basicity of the structural unit: the effective charge of the structural unit divided by the number of O-atoms in the structural unit.

Effective Lewis basicity (Lewis basicity) of the structural unit: the effective charge of the structural unit divided by the number of bonds from the structural unit.

Effective Lewis acidity (Lewis acidity) of an interstitial complex: the effective charge of the interstitial complex divided by the number of bonds emanating from the interstitial complex.